Universidade de Aveiro Departamento de Electrónica, Telecomunicações e Informática
2011

Claunir Pavan

Dimensionamento de Redes Ópticas Multicamada

Dimensioning of Multilayer Optical Networks

Universidade de Aveiro Departamento de Electrónica, Telecomunicações e Informática
2011

Claunir Pavan

Dimensionamento de Redes Ópticas Multicamada
Dimensioning of Multilayer Optical Networks

Tese apresentada à Universidade de Aveiro para cumprimento dos requisitos necessários à obtenção do grau de Doutor em Engenharia Electrotécnica, realizada sob a orientação científica do Doutor Armando Humberto Moreira Nolasco Pinto, professor auxiliar do Departamento de Electrónica, Telecomunicações e Informática da Universidade de Aveiro e do Doutor José Rodrigues Ferreira da Rocha, professor catedrático do Departamento de Electrónica, Telecomunicações e Informática da Universidade de Aveiro.

Apoio financeiro da Fundação para a Ciência e a Tecnologia através da bolsa SFRH/BD/27545/2006.

FCT Fundação para a Ciência e a Tecnologia
MINISTÉRIO DA CIÊNCIA, TECNOLOGIA E ENSINO SUPERIOR Portugal

o júri / the jury

presidente / president	**Doutor António Carlos Matias Correia** Professor Catedrático da Universidade de Aveiro
vogais / examiners committee	**Doutor José Rodrigues Ferreira da Rocha** Professor Catedrático da Universidade de Aveiro
	Doutor Mário Marques Freire Professor Catedrático da Universidade da Beira Interior
	Doutor João José de Oliveira Pires Professor Auxiliar da Universidade Técnica de Lisboa
	Doutor Armando Humberto Moreira Nolasco Pinto Professor Auxiliar da Universidade de Aveiro
	Doutora Maria do Carmo Raposo de Medeiros Professora Auxiliar da Universidade do Algarve

agradecimentos / acknowledgements

First and foremost, I would like to extend my thanks and gratitude to my thesis advisor, Professor Armando Nolasco Pinto, and my co-advisor, Professor José Ferreira da Rocha, for their guidance and advice throughout the entire execution of this thesis. I feel honored and privileged for having had the opportunity of working and learning from both.

My sincere thanks to the Universidade de Aveiro and Instituto de Telecomunicações and all administrative staff, for the excellent equipments and facilities offered during the course of this research.

Pursuing the PhD abroad would not be possible without the financial support from Fundação para a Ciência e a Tecnologia - FCT, so thank you.

My sincere thanks also go to all my colleagues at Instituto de Telecomunicações, for the helpful scientific discussions and for a warm human contact. I would like to separately acknowledge the help and support of my colleagues Rui Manuel Morais and Abel Correia.

I am very grateful for having collaborated on the following projects: IP over WDM, DROM and PANORAMA.

To my family, specially my father and mother, for their blessing and support which is really invaluable.

Finally, to my wife, for her dedication and for being a great partner.

To my wife, Márcia Andréia.

Palavras-chave

Dimensionamento de redes ópticas, redes ópticas de transporte, gerador de topologias, redes sobreviventes.

Resumo

Este trabalho apresenta um estudo sobre o dimensionamento de redes ópticas, com vistas a obter um modelo de dimensionamento para redes de transporte sobreviventes. No estudo utilizou-se uma abordagem estatística em detrimento à determinística.

Inicialmente, apresentam-se as principais tecnologias e diferentes arquitecturas utilizadas nas redes ópticas de transporte. Bem como os principais esquemas de sobrevivência e modos de transporte.

São identificadas variáveis necessárias e apresenta-se um modelo dimensionamento para redes de transporte, tendo-se dado ênfase às redes com topologia em malha e considerando os modos de transporte opaco, transparente e translúcido.

É feita uma análise rigorosa das características das topologias de redes de transporte reais, e desenvolve-se um gerador de topologias de redes de transporte, para testar a validade dos modelos desenvolvidos. Também é implementado um algoritmo genético para a obtenção de uma topologia optimizada para um dado tráfego.

São propostas expressões para o cálculo de variáveis não determinísticas, nomeadamente, para o número médio de saltos de um pedido, coeficiente de protecção e coeficiente de restauro. Para as duas últimas, também é analisado o impacto do modelo de tráfego. Verifica-se que os resultados obtidos pelas expressões propostas são similares às obtidas por cálculo numérico, e que o modelo de tráfego não influencia significativamente os valores obtidos para os coeficientes.

Finalmente, é demonstrado que o modelo proposto é útil para o dimensionamento e cálculo dos custos de capital de redes com informação incompleta.

Keywords Dimensioning of optical networks, optical transport networks, topology generator, survivable networks.

Abstract

This work presents a study on the dimensioning of optical networks, aiming to obtain a dimensioning model for survivable optical transport networks. The study relies on a statistical approach rather than a deterministic approach.

Initially, enabling technologies and different architectures usually employed in optical transport networks are presented. The main survivability schemes and transport modes are also presented.

Useful variables are identified and a transport network dimensioning model is presented, with emphasis on mesh-based network topologies, and considering opaque, transparent and translucent transport modes.

A rigorous analysis on the characteristics of real-world transport networks is done, and a topology generator is developed. The topology generator is used for testing and validating the developed models. A genetic algorithm for obtaining an optimized topology for a given traffic load is implemented as well.

Expressions for calculating non-deterministic variables are proposed, namely for the average number of hops per demand, protection and restoration coefficient. For the last two, the impact of the traffic model was analyzed. It is shown that results obtained from the proposed expressions are quite similar to the ones obtained from numeric calculation. Moreover, the traffic model does not influence significantly the values obtained for the coefficients.

Finally, it is shown that the proposed model is useful for the dimensioning and calculation of capital expenditures of networks in absence of complete information.

Contents

List of Acronyms

Notation	Description
ADM	Add-Drop Multiplexer.
ATM	Asynchronous Transfer Mode.
BER	Bit Error Rate.
CAPEX	Capital Expenditures.
CWDM	Coarse Wavelength Division Multiplexing.
DWDM	Dense Wavelength Division Multiplexing.
DXC	Digital Cross Connect.
EDFA	Erbium Doped Fiber Amplifier.
EXC	Electrical Cross Connect.
FEC	Forward Error Correction.
ILP	Integer Linear Programming.
IP	Internet Protocol.
ITU	International Telecommunication Union.
ITU-T	International Telecommunication Union - Telecommunication Standardization Sector.
MTL	Maximum Transparency Length.
OA	Optical Amplifier.

Notation	**Description**
OADM	Optical Add/Drop Multiplexer.
OAM	Operation, Administration and Maintenance.
OCh	Optical Channel.
OE	Optical-Electrical.
OEO	Optical-Electrical-Optical.
OLT	Optical Line Terminal.
OMS	Optical Multiplex Section.
OOO	Optical-Optical-Optical.
OPEX	Operational Expenditures.
OSC	Optical Supervisory Channel.
OTN	Optical Transport Network.
OTS	Optical Transmission Section.
OXC	Optical Cross Connect.
PDH	Plesiochronous Digital Hierarchy.
PON	Passive Optical Network.
ROADM	Reconfigurable Optical Add/Drop Multiplexer.
SOA	Semiconductor Optical Amplifier.
SONET/SDH	Synchronous Optical Network/Synchronous Digital Hierarchy.
TCO	Total Cost of Ownership.
WDM	Wavelength Division Multiplexing.
WWDM	Wide Wavelength Division Multiplexing.

List of Symbols

Symbol	Description
A	area of a plane.
χ_r	a routing solution.
$\langle c \rangle$	average clustering coefficient.
$\langle c_{tl}^{OXC} \rangle$	average cost of a translucent OXC.
$\langle c_{op}^{OXC} \rangle$	average cost of an opaque OXC.
$\langle c^{EXC} \rangle$	average cost of EXCs per node.
$\langle c^{EXC} \rangle$	average cost of EXCs.
$\langle c^{F} \rangle$	average cost of fiber per link.
$\langle c_l \rangle$	average cost of links.
$\langle c_n \rangle$	average cost of nodes.
$\langle c_n \rangle$	average cost of nodes.
$\langle c^{A} \rangle$	average cost of OAs per link.
$\langle c^{OLT} \rangle$	average cost of OLTs per link.
$\langle c^{OXC} \rangle$	average cost of OXCs.
$\langle c^{REG} \rangle$	average cost of regenerators per node.
$\langle c_{tr}^{OXC} \rangle$	average cost of transparent OXCs.
$\langle c_{op}^{TSP} \rangle$	average cost of transponders per node, in opaque networks.
$\langle c_{tl}^{TSP} \rangle$	average cost of transponders per node, in translucent networks.
$\langle c_{tr}^{TSP} \rangle$	average cost of transponders per node, in transparent networks.
$\langle c^{TSP} \rangle$	average cost of transponders per node.
$\langle \nu \rangle$	average link length.
$\langle \omega \rangle$	average link-disjoint-pairwise connectivity.
$\langle \delta \rangle$	average nodal degree.
$\langle \theta \rangle$	average node-disjoint-pairwise connectivity.
$\langle w_l \rangle$	average number of channels in the link l.

Symbol	Description
$\langle w \rangle$	average number of channels per link.
$\langle n_{tl,n}^{CH} \rangle$	average number of channels processed in the translucent OXC n.
n_{tl}^{CH}	number of channels processed in translucent OXCs.
$\langle d \rangle$	average number of demands.
$\langle n_{exc}^{TP} \rangle$	average number of EXC trunk ports per node.
$\langle h' \rangle$	average number of hops for the backup paths.
$\langle h \rangle$	average number of hops.
$\langle n_{op}^{LR} \rangle$	average number of long-reach transponders per opaque node.
$\langle n_{tl}^{LR} \rangle$	average number of long-reach transponders per translucent node.
$\langle n_{tr}^{LR} \rangle$	average number of long-reach transponders per transparent node.
$\langle n^{A} \rangle$	average number of OAs per links.
$\langle n^{OLT} \rangle$	average number of OLTs per link.
$\langle n^{R} \rangle$	average number of regenerators per node.
$\langle n^{SR} \rangle$	average number of short-reach transponders per node.
$\langle n^{S} \rangle$	average number of transmission systems per link.
$\langle n^{F} \rangle$	average quantity of fiber per link.
γ^{EXC}	base cost of an EXC.
γ^{OXC}	base cost of an OXC.
γ^{LR}	cost of a long-reach transponder.
γ^{TP}	cost of an EXC trunk port.
γ^{SR}	cost of a short-reach transponder.
γ^{SW}	cost of switching a channel.
γ^{F}	cost of 1 km of optical fiber.
c_l^F	cost of a pair of fibers for the link l.
c_l	cost of a single link l.
c_n	cost of a single node n.
c_n^{EXC}	cost of EXC in the node n.
c_l^{A}	cost of OAs in the link l.
c_l^{OLT}	cost of OLTs for a link l.
$c_{op,n}^{OXC}$	cost of opaque OXC in the node n.
c_n^{OXC}	cost of OXC in the node n.
c_n^{REG}	cost of regenerators for a node n.
c_n^{REG}	cost of regenerators in the node n.

Symbol	Description
$c_{tl,n}^{OXC}$	cost of the translucent OXC in node n.
$c_{tr,n}^{OXC}$	cost of the transparent OXC in the node n.
$c_{op,n}^{TSP}$	cost of transponders for the opaque node n.
$c_{tr,n}^{TSP}$	cost of transponders for the transparent node n.
$c_{tl,n}^{TSP}$	cost of transponders for the translucent node n.
S	capacity of transmission systems.
c	clustering coefficient.
ν_l	length of the link l.
ω	link-disjoint-pairwise connectivity.
ι	minimum distance between two nodes.
$\langle\phi\rangle$	network resource sharing.
δ	nodal degree.
θ	node-disjoint-pairwise connectivity.
$n_{op,n}^{CH}$	number of bidirectional channels processed in the opaque OXC n.
$n_{tr,n}^{CH}$	number of bidirectional channels processed in the transparent node n.
D	number of bidirectional demands.
$w_{n,j}$	number of channels transported in each link connected to node n.
n_n^{DR}	number of demands that need regeneration in the node n.
n_n^{D}	number of demands that originate or terminate in the node n.
R	number of different routing solutions.
h	number of hops.
$n_{op,n}^{LR}$	number of long-reach transponder for the opaque node n.
$n_{tl,n}^{LR}$	number of long-reach transponders for the translucent node n.
$n_{tr,n}^{LR}$	number of long-reach transponders for the transparent node n.
n_n^{LR}	number of long-reach transponders in the node n.
n_l^{A}	number of OAs in the link l.
n_d^{R}	number of regenerations that a demand d has to suffer.
$\mathring{R}$	number of regions.
n_n^{SR}	number of short-reach transponders in the node n.
φ	number of simulations.
T	number of topologies generated during the algorithm run.
n_l^{S}	number of transmission systems in the link l.
$n_{exc,n}^{TP}$	number of trunk ports in the EXC node n.

Symbol	Description
D_1	number of unidirectional demands.
α	parameter of Waxman function.
β	parameter of Waxman function.
$\langle k_p \rangle$	protection coefficient.
$\langle k_r \rangle$	restoration coefficient.
∂	span. i.e., the distance between OAs.
ψ_l	spare capacity of a link.
Λ	maximum transparency length, MTL.
P_d	path length of demand d.
C_T	total cost of a network.
C_L	total cost of links.
C_N	total cost of nodes.
W	total number of channels on links.
N_{op}^{CH}	total number of channels processed in the opaque OXCs.
N_{tl}^{CH}	total number of channels processed in the translucent OXCs.
N_{tr}^{CH}	total number of channels processed in the transparent OXCs.
N_{exc}^{TP}	total number of EXC trunk ports in the network.
L	total number of links.
N_{op}^{LR}	total number of long-reach transponders in the opaque network.
N_{tl}^{LR}	total number of long-reach transponders in the translucent network.
N_{tr}^{LR}	total number of long-reach transponders in the transparent network.
N	total number of nodes.
N^A	total number of OAs in the network.
N^{OLT}	total number of OLTs in the network.
N^R	total number of regenerators in the network.
N^{SR}	total number of short-reach transponders in the network.
N^F	total quantity of fiber in the network.
Ψ	total spare capacity of a network.

List of Figures

List of Tables

Chapter 1

Introduction

TELECOMMUNICATION networks play an important role in the today's society. They connect business and end users across the world, and they support services of voice, video and data together with mobile services. This blend of services is known as quad-play. As Internet traffic grows and new services are introduced, network operators continually face the increasing of bandwidth requirements [1]. Hence, the network dimensioning task becomes critical and the goal of operators is to be able to dimension their networks to offer the bandwidth requirements in the most cost effective manner.

The network Total Cost of Ownership (TCO) can be divided into Capital Expenditures (CAPEX) and Operational Expenditures (OPEX) [2]. CAPEX contributes to the required infrastructure. This includes buildings (to host equipment and staff), network infrastructure (such as routers, switches, fiber) and software (network management systems). OPEX contributes to the costs to keep the network working, including maintenance, the provisioning of services, service management, pricing, billing, rents (such as buildings or fibers), ongoing network planning and marketing.

Optical transport network problems may be classified into three categories: traffic engineering, network engineering and network planning. Traffic engineering consists of allocating the traffic on the existing network resources in order to meet traffic performance objectives. It is essentially a routing problem, where the traffic to be routed could be packets, packet flows, or lightpaths. Traffic engineering is a dynamic problem whose decision-making time may be in the order of milliseconds to seconds [3]. Network engineering concerns on efficient allocation of network resources to a traffic demand and deal with network exhaustion due to traffic growth or variation. Commonly the goal is to find a network configuration and resource allocation that makes a cost-efficient use of resources, i.e., minimizing CAPEX. The decision-make time of network engineering is on the order of weeks or months. The network planning description is similar to the network engineering, except that in this category the

network topology may not be known and traffic is forecasted. Network planning corresponds to the dimensioning of a network from scratch, with a decision-making timescale of perhaps a few years [3]. In this thesis we study problems mainly in the network planning category. The dimensioning problems are mathematically hard and generally beyond formal optimization techniques (e.g., linear programming) for realistic sized problems [4]. The tools for that task usually rely on iterative heuristics that reflect an acceptable degree of accuracy and may be applicable to a large class of problems.

In the classical network dimensioning, which uses a numerical dimensioning tool, a set of information (called input parameters) must be given before designing a network. Then the tool processes those information and generates a variety of outputs (such as reports and configuration files). Figure 1.1 illustrates the dimensioning process.

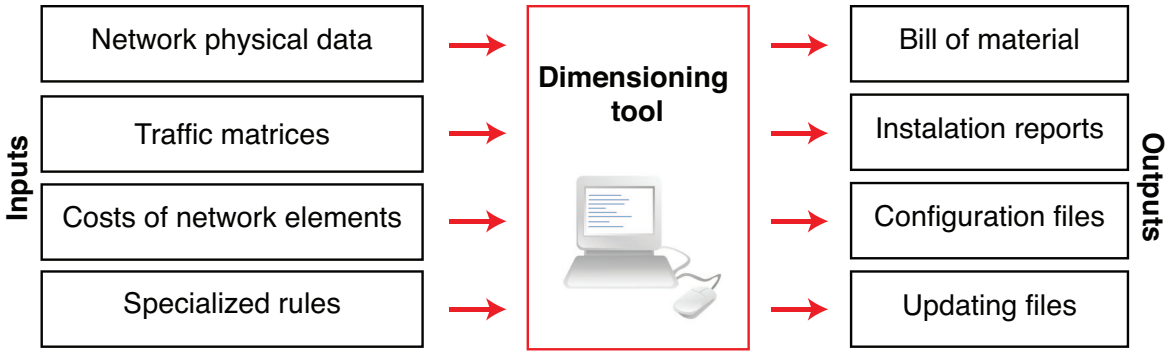

Figure 1.1: Classical dimensioning phases.

As shown in Figure 1.1, input parameters generally include: a physical network topology. A set of traffic matrices that the network must accommodate. The costs of each component, and a set of configurations (specialized rules) such as transport mode, routing, survivability, and grooming schemes.

The output data include the bill of materials, in which is reported the links and nodes equipment such as port cards, Digital Cross Connects (DXCs) and Optical Cross Connects (OXCs), transponders, Optical Amplifiers (OAs) and regenerators. Installation reports, files for configurations and updates, and reports with overall performance analyses and for the total cost of the network. After a set of scenarios are dimensioned, the designers (or the software tool) must compare each other and then chose the one that better meets the objective. Usually the objective is to dimension a network with a minimum CAPEX, given a set of constraints.

1.1 Related Work

In this section, a brief review of the state-of-art for dimensioning optical networks without complete information is presented. The problem of dimensioning optical networks is an active research area. In order to determine the amount of resources that must be employed on the network, operators make use of software tools such as OPNET Transport Planner [5], but detailed information about the network is required. Furthermore, especially for larger networks, this task may require a lot of time and effort. However, sometimes network designers need to evaluate the feasibility of a network (e.g., in terms of costs) in less time and without having complete information about the network. For that reason, some researchers are devoting efforts to obtain models allowing a preliminary evaluation and verification of the network feasibility. This would be particularly useful for comparisons between different solutions before considering a full numerical analysis.

In this context, a semi-empirical formulation for calculating CAPEX of optical networks is described in [6, 7]. The authors present a model which includes the calculation of the mean value of key network quantities which may be applied to a wide range of topologies and architectures. In the study, the authors considered heuristics favoring quasi-regular network topologies (i.e., networks with small difference between the number of hops of working and backup paths). In [8], the authors present a collection of approximation formulas to estimate the size of mesh optical networks with limited inputs. In particular, it provides a set of equations that relate number of sites, average fiber connectivity, demand load and capacity for mesh protection architectures. The aim of their work is to quickly estimate the amount of traffic that can be carried over a given network, or, conversely, given the traffic to be supported, to assess the characteristics of the topology required. In [9], the author describes a model to dimension optical transport networks and present new expressions to calculate the restoration coefficient and the average number of hops per demand. The proposed expressions were obtained from statistical methods.

These approaches usually perform simulations and analysis considering computer generated topologies. Network topology generators are extensively available in the literature. In [10], the author presents a model for generating random graphs in which the nodes are distributed over a plane, and links are added to the graph using a probability function based on the Euclidean distance between the nodes. In [11]

and [12], the multi-level hierarchy found in the Internet is used to generate Internet-like topologies. In [13], the authors extract the autonomous system and router level topologies from the Internet and from that realistic core, topologies are generated. In [14], the authors show that the nodal degree distribution of the autonomous system level topologies follow a power-law. From that, several topology generators have been built based on power laws [15–18]. These efforts have been focused on topologies resembling the Internet, which is a scale-free network [19].

Another problem that has attracted the attention of researcher is the topological design problem, which consists of determining the least-cost topology for a given traffic load. In this context, many studies have addressed this problem through Integer Linear Programming models [20, 21]. In [22–24], genetic algorithms are used in the design of telecommunication networks. In [22], a genetic algorithm is presented to route and dimension dynamic optical networks, without considering the network survivability. In [23], a genetic algorithm is used to design survivable networks. It is assumed that the topology is given. The genetic algorithm presented in [24] minimizes the CAPEX of an all-optical network, considering physical impairments.

1.2 Motivation and Objectives

In the early planning phase of a network, designers must make some predictions such as the traffic demand and the suitable architecture. These predictions will be useful to forecast the total cost of the network which is usually a restriction. Usually total costs will determine the overall feasibility of the network and it is a very important issue. Many studies of the economics of network structures focus on numerical simulation methods. However, this approach requires a detailed knowledge of the network to be build, and it is a time consuming task (in the order of days or months). In this context, the possibility to provide fast approximated results for the preliminary evaluation and design of such networks is very helpful in the dimensioning process because alternative approaches can easily be compared, hence it could speed up the decision-making.

In this context, the main objective of this thesis is to contribute to the field of optical network dimensioning, with incomplete information. We are not concerned with every single network element, but rather into obtain the expected network cost without the requirements of detailed information about the network and traffic demand. Therefore,

the strategy that we follow is to investigate the dimensioning problem considering also statistical models instead of purely deterministic ones. This approach is not supposed to be a substitute for the current numerical approaches (which leads to exact results), but a complement to speed up the decision-making when a variety of possibilities are on the table, e.g., the use of alternative types of network elements or transport modes.

To achieve this goal, we firstly analyze the relationship between key variables of the dimensioning problem, aiming at obtaining expressions to fast calculate the quantities and costs of network elements required to transport a traffic demand. In the lack of complete information, such as network topology and traffic pattern, we develop useful expressions to forecast those quantities and costs. We are aware that a statistical approach depends on high quality data base about real/realistic optical transport network topologies. Therefore, another target is to investigate the characteristics of real transport networks and how to represent them in a simulation environment.

1.3 Contributions

In the opinion of the author, the most important results of thesis are the following:

- Development of expressions to calculate the quantities and costs of network elements for opaque, transparent and translucent transport modes, in survivable optical transport networks [25–29].
- Identification of key variables of real transport networks and development of a reliable network topology generator [30].
- Improved approximations for the average number of hops, restoration and protection coefficient for optical transport networks [26, 27, 31–33].
- Proposal of a genetic algorithm that can be used to determine the least cost network topology [34–36].
- Determination of robustness of CAPEX calculations in relation to network topology [28, 37, 38].
- Proposal of a model for the dimensioning and calculation of cost of networks, without requiring complete information [28, 29, 32, 37–41].

1.4 Thesis Outline

This thesis is structured as follows. Chapter 2 consists of a literature review about optical transport networks. We first describe some architectures and enabling technologies, then we present a few survivability techniques, based on protection and restoration strategies. Thereafter we present the main characteristics relative to the opaque, transparent and translucent transport modes.

Then, the problem of dimensioning optical transport networks is analyzed in Chapter 3. The problem consists in determining the key variables and the quantities of network elements required to transport the traffic demand. We first present expressions to calculate the network costs, which are further divided into costs of links and costs of nodes. A small network topology is used to illustrate the model. Thereafter we show how to obtain the number of channels per link, the number of hops per demand, and survivability coefficients, which are essential for obtaining the network costs. We also present the variables that are affected when survivability is considered, and a case study for calculating the capital expenditures of a network, considering different transport modes and survivability schemes.

In order for obtaining a meaningful data set to perform statistic analysis we present in Chapter 4 a method to generate realistic optical transport networks. We first present an extensive analysis of real-world transport networks and their relevant characteristics. Then we present the proposed model and its validation by comparing the variables of real-world and computer generated networks.

A genetic algorithm that can be used to obtain the most cost efficient network topology is also presented in this Chapter. As the convergence of the genetic algorithms depends on the used genetic operators, we analyze their impact on the quality of the obtained solutions. We also compare the performance of different generators of initial population, selection methods, crossover operators and population sizes. The performance of the proposed heuristic is evaluates using an ILP model, and a set of real-world transport networks.

As the exact values of some key variables are not deterministic, we have to rely on approximations. Thus, in Chapter 5 we first generate an appropriate set of networks using the proposed topology generator. Next, we present a study on estimating the average number of hops for working and protection paths. Moreover, we present a similar study for the survivability coefficients. We also compare our proposed

expressions with previous works. Since the traffic demand in optical transport networks exhibit a non-uniform statistical behavior, we investigate the impact of traffic model on survivability coefficient. Then, we study the impact of approximations for calculating CAPEX in optical networks. Finally, the main conclusions and suggestions for future directions are presented in Chapter 6.

1.5 List of Publications

The major results obtained during this work were submitted to the scientific international community through the following papers.

1.5.1 Papers in Journals

1. C. Pavan, R. M. Morais, J. R. F. da Rocha, and A. N. Pinto, "Generating realistic optical transport network topologies," *IEEE/OSA Journal of Optical Communications and Networking*, vol. 2, no. 1, pp. 80–90, 2010.

2. R. M. Morais, C. Pavan, A. N. Pinto, and C. Requejo, "Genetic Algorithm for the Topological Design of Survivable Optical Transport Networks", *IEEE/OSA Journal of Optical Communications and Networking* vol. 3, no. 1, pp. 17–26, 2011.

3. R. M. Morais, C. Pavan, J. R. F. da Rocha, and A. N. Pinto, "Estimating Extra Capacity for Protection in Optical Transport Networks", *IEEE/OSA Journal of Optical Communications and Networking*, (submitted).

4. C. Pavan, R. M. Morais, J. R. F. da Rocha, and A. N. Pinto, "Capacity Provisioning for Random Traffic in Optical Networks", *IEEE/OSA Journal of Optical Communications and Networking*, (to be submitted).

1.5.2 Papers in Conferences

1. C. Pavan, A. Correia, and A. Pinto, "A graph problem in the context of optical networks dimensioning," in *Proceedings of the 3rd International Workshop on Mathematical Techniques and Problems in Telecommunications, MTPT'06*, vol. 1, Leiria, Portugal, September 2006, pp. 22–25.

2. A. R. Correia, C. Pavan, and A. N. Pinto, "A probabilistic model for the demands on link on mesh optical networks," in *Proceedings of the 4th Symposium on Enabling Optical Networks and Sensors, SEON'06*, Porto, Portugal, Jun. 2006, pp. 43–44.

3. C. Pavan, A. R. Correia, and A. N. Pinto, "A statistical model for the average number of hops in optical networks," in *Proceedings of the 6th Conference on Telecommunications, ConfTele'07*, Peniche, Portugal, May 2007, pp. 465–467.

4. C. Pavan, R. Morais, A. Correia, and A. Pinto, "Assessment of an expectation model for the dimensioning problem in optical networks," in *Proceedings of the 4th Symposium on Enabling Optical Networks, SEON'08*, Porto, Portugal, June 2008, pp. 91–93.

5. C. Pavan, R. M. Morais, A. R. Correia, and A. N. Pinto, "Impact of the mean nodal degree on optical networks," in *Photonics North 2008*, vol. 7099, no. 1. Montreal, QC, Canada: SPIE, June 2008, p. 709910.

6. C. Pavan, R. Morais, A. Correia, and A. Pinto, "Dimensioning of optical networks with incomplete information," in *Proceedings of the 6th Advanced International Conference on Telecommunications, AICT'08*. Athens, Greece: IEEE, June 2008, pp. 261–264.

7. M. Guerreiro, C. Pavan, A. L. Barradas, A. N. Pinto, and M. C. Medeiros, "Path selection strategy for consumer grid over obs networks," in *Proceedings of the 10th International Conference on Transparent Optical Networks, ICTON'08*, vol. 3. Athens, Greece: IEEE, June 2008, pp. 138–141.

8. C. Pavan, R. M. Morais, and A. N. Pinto., "Estimating capex in optical multilayer networks," in *Proceedings of the 7th Conference on Telecommunications, ConfTele'09*, Santa Maria da Feira, Portugal, May 2009, pp. 335–338.

9. R. M. Morais, C. Pavan, C. Requejo, and A. N. Pinto., "Design of survivable optical networks with minimum capex," in *Proceedings of the 7th Conference on Telecommunications, ConfTele'09*, Santa Maria da Feira, Portugal, May 2009, pp. 307–310.

10. C. Pavan, R. Morais, and A. Pinto, "Quantifying the restoration capacity in optical mesh networks," in *Proceedings of the Next Generation Internet Networks, NGI '09*. Aveiro, Portugal: IEEE, July 2009, pp. 1–5.

11. R. M. Morais, C. Pavan, A. N. Pinto, and C. Agra, "Genetic algorithm for the design of survivable optical transport networks: Operators comparison," in *Proceedings of the 14th Congresso da APDIO'09*, Lisbon, Portugal, September 2009, pp. 123–130.

12. C. Pavan, R. M. Morais, and A. N. Pinto, "Impact of the traffic model on the restoration coefficient in optical transport networks," in *Proceedings of the 8th International Conference on Decision Support for Telecommunications and Information Society, DSTIS'09*, Coimbra, Portugal, September 2009.

13. C. Pavan, R. M. Morais, and A. N. Pinto, "Fast calculation of capex in optical multilayer networks," in *Proceedings of the 14th European Conference on Networks and Optical Communications, NOC/OC&I'09*, Valladolid, Spain, June 2009, pp. 325–332.

14. A. Pinto, C. Pavan, and R. Morais, "A statistical model for capex fast calculation in optical transport networks," in *Proceedings of the 11th International Conference on Transparent Optical Networks, ICTON'09*. Island of São Miguel, Azores, Portugal: IEEE, July 2009, pp. 1–4.

15. C. Pavan, R. M. Morais, and A. N. Pinto, "Estimation of capex in survivable optical transport networks," in *Proceedings of the 15th European Conference on Networks and Optical Communcations, NOC/OC&I'10*. Faro-Algarve, Portugal: IEEE, June 2010, pp. 1–6.

16. R. M. Morais, C. Pavan, and A. N. Pinto, "Equipment and energy related costs in survivable optical transport networks," in *Proceedings of the 15th European Conference on Networks and Optical Communcations, NOC/OC&I'10*. Faro-Algarve, Portugal: IEEE, June 2010, pp. 1–6.

17. A. N. Pinto, C. Pavan, and R. M. Morais, "Dimensioning optical networks: A practical approach," in *Proceedings of the 12th International Conference on Transparent Optical Networks, ICTON'10*. Munich, Germany: IEEE, June 2010, pp. 1–4.

18. R. M. Morais, C. Pavan, and A. N. Pinto, "Estimating the Energy Consumption in Survivable Optical Transport Networks," in *Proceedings of the 8th Conference on Telecommunications, ConfTele'11*, Lisbon, Portugal, April 2011. (accepted)

References

[1] C. Machuca, "Expenditures study for network operators," in *Proceedings of the 8th International Conference on Transparent Optical Networks, ICTON'06*, vol. 1. Nottingham, UK: IEEE, June 2006, pp. 18–22.

[2] R. Huelsermann, M. Gunkel, C. Meusburger, and D. A. Schupke, "Cost modeling and evaluation of capital expenditures in optical multilayer networks," *J. Opt. Netw.*, vol. 7, no. 9, pp. 814–833, Aug. 2008.

[3] B. Mukherjee, *Optical WDM Networks*. New York, NY, USA: Springer, 2006.

[4] C. P. Botham, N. Hayman, A. Tsiaparas, and P. Gaynord, "Advanced modelling techniques for designing telecommunications networks," *BT Technology Journal*, vol. 21, no. 2, pp. 37–47, April 2003.

[5] Opnet Technologies Inc., "OPNET SP Guru Transport Planner," 2009.

[6] S. K. Korotky, "Network global expectation model: A statistical formalism for quickly quantifying network needs and costs," *IEEE Journal of Lightwave Technology*, vol. 22, no. 3, pp. 703–722, Mar. 2004.

[7] ——, "Analysis and optimization of two-tier networks with application to optical transport backbones," *J. Opt. Netw.*, vol. 4, no. 1, pp. 45–63, 2005.

[8] J. F. Labourdette, E. Bouillet, R. Ramamurthy, and A. A. Akyama, "Fast approximate dimensioning and performance analysis of mesh optical networks," *IEEE/ACM Journal of Transactions on Networking*, vol. 3, no. 4, pp. 906–917, Aug. 2005.

[9] A. R. Correia, "Planeamento e dimensionamento de redes ópticas com encaminhamento ao nível da camada óptica," Master thesis, Universidade de Aveiro, Aveiro, Portugal, 2008.

[10] B. Waxman, "Routing of multipoint connections," *IEEE Journal on Selected Areas in Communications*, vol. 6, no. 9, pp. 1617–1622, Dec. 1988.

[11] M. Doar, "A better model for generating test networks," in *Proceedings of the IEEE Global Telecommunications Conference, GLOBECOM '96*. IEEE, November 1996, pp. 86–93.

[12] E. Zegura, K. Calvert, and S. Bhattacharjee, "How to model an internetwork," in *Proceedings of the 15th Annual Joint Conference of the IEEE Computer Societies. Networking the Next Generation. INFOCOM '96*, vol. 2, March 1996, pp. 594–602.

[13] L. Cheng, N. Hutchinson, and M. Ito, "Realnet: A topology generator based on real internet topology," in *Proceedings of the 22nd International Conference on Advanced Information Networking and Applications, AINAW '08*, March 2008, pp. 526–532.

[14] M. Faloutsos, P. Faloutsos, and C. Faloutsos, "On power-law relationships of the internet topology," in *Proceedings of the Conference on Applications, Technologies, Architectures, and Protocols for Computer Communication, SIGCOMM '99*. New York, NY, USA: ACM, 1999, pp. 251–262.

[15] C. Jin, C. J. Qian, and S. Jamin, "Inet: Internet topology generator," Technical Report CSE-TR-433-00, EECS Department, University of Michigan, 2000.

[16] D. Magoni, "Nem: A software for network topology analysis and modeling," in *Proceedings of the 10th IEEE International Symposium on Modeling, Analysis and Simulation of Computer and Telecommunications Systems, MASCOTS '02*. IEEE Computer Society, October 2002, pp. 364–371.

[17] C. Palmer and J. Steffan, "Generating network topologies that obey power laws," in *Proceedings of the Global Telecommunications Conference, GLOBECOM '00*, vol. 1. IEEE, November 2000, pp. 434–438.

[18] A. Medina, A. Lakhina, I. Matta, and J. Byers, "Brite: An approach to universal topology generation," in *Proceedings of the 9th International Symposium on Modeling, Analysis and Simulation of Computer and Telecommunication Systems, MASCOTS '01*. IEEE Computer Society, August 2001, pp. 346–353.

[19] A.-L. Barabasi and E. Bonabeau, "Scale-free networks," *Scientific American Magazine*, pp. 60–69, May 2003.

[20] H. Kerivin and A. R. Mahjoub, "Design of survivable networks: A survey," *Journal of Network*, vol. 46, no. 1, pp. 1–21, June 2005.

[21] C. Pluntke, M. Menth, and M. Duelli, "Capex-aware design of survivable dwdm mesh networks," in *Proceedings of the International Conference on Communications, 2009. ICC '09*. Dresden, Germany: IEEE, June 2009, pp. 1–6.

[22] I. de Miguel, R. Vallejos, A. Beghelli, and R. J. Durán, "Genetic algorithm for joint routing and dimensioning of dynamic wdm networks," *IEEE/OSA Journal of Optical Communications and Networking*, vol. 1, no. 7, pp. 608 –621, December 2009.

[23] L. S. Buriol, M. G. C. Resende, and M. Thorup, "Survivable ip network design with ospf routing," *Journal of Networks*, vol. 49, pp. 51–64, January 2007.

[24] D. Chaves, C. Bastos-Filho, and J. Martins-Filho, "Multiobjective physical topology design of all-optical networks considering qos and capex," in *Proceedings of the Optical Fiber Communications, OFC'10*. San Diego, CA, USA: IEEE, March 2010, pp. 1–3.

[25] A. R. Correia, C. Pavan, and A. N. Pinto, "A probabilistic model for the demands on link on mesh optical networks," in *Proceedings of the 4th Symposium on Enabling Optical Networks and Sensors, SEON'06*, Porto, Portugal, Jun. 2006, pp. 43–44.

[26] C. Pavan, A. R. Correia, and A. N. Pinto, "A statistical model for the average number of hops in optical networks," in *Proceedings of the 6th Conference on Telecommunications, ConfTele'07*, Peniche, Portugal, May 2007, pp. 465–467.

[27] C. Pavan, R. Morais, A. Correia, and A. Pinto, "Assessment of an expectation model for the dimensioning problem in optical networks," in *Proceedings of the 4th Symposium on Enabling Optical Networks, SEON'08*, Porto, Portugal, June 2008, pp. 91–93.

[28] C. Pavan, R. M. Morais, A. R. Correia, and A. N. Pinto, "Impact of the mean nodal degree on optical networks," in *Proceedings of Photonics North 2008*, vol. 7099, no. 1. Montreal, QC, Canada: SPIE, June 2008, p. 709910. [Online]. Available: http://link.aip.org/link/?PSI/7099/709910/1

[29] C. Pavan, R. M. Morais, and A. N. Pinto, "Estimation of capex in survivable optical transport networks," in *Proceedings of the 15th European Conference on Networks and Optical Communcations, NOC/OC&I'10*. Faro-Algarve, Portugal: IEEE, June 2010, pp. 1–6.

[30] C. Pavan, R. M. Morais, J. R. F. da Rocha, and A. N. Pinto, "Generating realistic optical transport network topologies," *IEEE/OSA Journal of Optical Communications and Networking*, vol. 2, no. 1, pp. 80–90, January 2010.

[31] R. M. Morais, C. Pavan, J. R. F. da Rocha, and A. N. Pinto, "Estimating extra capacity for protection in optical transport networks," *IEEE/OSA Journal of Optical Communications and Networking (submitted)*, 2010.

[32] C. Pavan, R. Morais, and A. Pinto, "Quantifying the restoration capacity in optical mesh networks," in *Proceedings of the Next Generation Internet Networks, NGI '09*. Aveiro, Portugal: IEEE, July 2009, pp. 1–5.

[33] C. Pavan, R. M. Morais, and A. N. Pinto, "Impact of the traffic model on the restoration coefficient in optical transport networks," in *Proceedings of the 8th International Conference on Decision Support for Telecommunications and Information Society, DSTIS'09*, Coimbra, Portugal, September 2009.

[34] R. M. Morais, C. Pavan, A. N. Pinto, and C. Requejo, "Genetic algorithm for the topological design of survivable optical transport networks," *IEEE/OSA Journal of Optical Communications and Networking*, vol. 3, no. 1, pp. 17–26, January 2011.

[35] R. M. Morais, C. Pavan, C. Requejo, and A. N. Pinto., "Design of survivable optical networks with minimum capex," in *Proceedings of the 7th Conference on Telecommunications, ConfTele'09*, Santa Maria da Feira, Portugal, May 2009, pp. 307–310.

[36] R. M. Morais, C. Pavan, A. N. Pinto, and C. Agra, "Genetic algorithm for the design of survivable optical transport networks: Operators comparison," in *Proceedings of the 14th Congresso da APDIO'09*, Lisbon, Portugal, September 2009, pp. 123–130.

[37] C. Pavan, R. Morais, A. Correia, and A. Pinto, "Dimensioning of optical networks with incomplete information," in *Proceedings of the 6th Advanced International Conference on Telecommunications, AICT'08*. Athens, Greece: IEEE, June 2008, pp. 261–264.

[38] C. Pavan, R. M. Morais, and A. N. Pinto., "Estimating capex in optical multilayer networks," in *Proceedings of the 7th Conference on Telecommunications, ConfTele'09*, Santa Maria da Feira, Portugal, May 2009, pp. 335–338.

[39] A. Pinto, C. Pavan, and R. Morais, "A statistical model for capex fast calculation in optical transport networks," in *Proceedings of the 11th International Conference on Transparent Optical Networks, ICTON'09*. Island of São Miguel, Azores, Portugal: IEEE, July 2009, pp. 1–4.

[40] R. M. Morais, C. Pavan, and A. N. Pinto, "Equipment and energy related costs in survivable optical transport networks," in *Proceedings of the 15th European Conference on Networks and Optical Communcations, NOC/OC&I'10*. Faro-Algarve, Portugal: IEEE, June 2010, pp. 1–6.

[41] A. N. Pinto, C. Pavan, and R. M. Morais, “Dimensioning optical networks: A practical approach,” in *Proceedings of the 12th International Conference on Transparent Optical Networks, ICTON’10*. Munich, Germany: IEEE, June 2010, pp. 1–4.

Chapter 2

Optical Core Transport Networks

In this Chapter we offer a brief introduction to optical core transport networks, also known as backbone networks. This class of network aggregates the traffic of metro and access networks and transport it to longer distances.

2.1 Introduction

Current optical transport networks comprise a set of network elements, connected by optical fiber links, with the functionality necessary to provide transport, multiplexing, routing, supervision, and survivability of service layer signals.

From 90's, after the first generation of Synchronous Optical Network/Synchronous Digital Hierarchy (SONET/SDH) was standardized, the Plesiochronous Digital Hierarchy (PDH) based transport networks were replaced by SONET/SDH. This latter technology allowed transporting voice and data traffic over the same fiber and fulfilled synchronization and Operation, Administration and Maintenance (OA&M) requirements. With the emergence of optical amplifiers and Wavelength Division Multiplexing (WDM) technology for optical transport, in which several channels are combined and transmitted over a single fiber, SONET/SDH networks took advantage of this technology to provide economic higher capacities. Thus, operators began to deploy WDM transmission systems to mitigate capacity exhaustion in transport networks. Notice that SONET/SDH systems are today limited to 40 Gbps [1], and WDM systems allow hundreds of Gbps to be carried per fiber (which means that multiple SONET/SDH channels may be transported into a single fiber). Nevertheless, most of the transport network functionality was maintained as a responsibility of the SONET/SDH layer.

Due to the growing bandwidth demand for different types of services, operators were forced to converge their networks in order to support both data and wavelength

services, along with traditional circuit services. Thus, operators introduced a new type of multiplexer in the network (called Reconfigurable Optical Add/Drop Multiplexer (ROADM)), which enables the support for a variety of network topologies and provide protocol transparency. For instance, SONET/SDH, Ethernet and other services may coexist in the same WDM network.

Despite the high efficiency increase provided by WDM, operators are under pressure to lower the cost per bit transported [2]. Future directions of transport networks include reducing Optical-Electrical-Optical (OEO) conversions in the networks, which reduce the number of costly OEO converters (e.g., transponders). Actually the technology that is driving the evolution to improve network performance and to deal with the next generation of fixed line telecommunication networks is the Optical Transport Network (OTN) standard (an International Telecommunication Union - Telecommunication Standardization Sector (ITU-T) standard). ITU-T developed the OTN with the intention of combining the benefits of SONET/SDH technology with the bandwidth expansion capabilities offered by WDM technology. Additionally, it has provided a standardized way for managing the optical channels in the optical layer. Thus, transport, multiplexing, routing, supervision, and survivability are supported predominantly at optical layer [3, 4]. Another key advantage of OTN include stronger Forward Error Correction (FEC) to improve error performance and enable longer optical spans.

Current optical networks may stack a variety of technologies such as SONET/SDH, ATM, OTN, Ethernet, IP. One problem of stacking layers is the resulting lower efficiency in bandwidth utilization [5]. This occurs because the grooming of the traffic of each layer into the adjacent lower layer may not fit perfectly, so the more layers we stack the less efficiency in bandwidth utilization we obtain. Operators create multilayer structures because they do not want to replace the legacy infrastructures (due to the costs) when new network capabilities are implemented. However, as networks become more Internet Protocol (IP) data centric and IP and WDM evolve, the SONET/SDH layer may be eventually removed [2, 5].

As the number of channels multiplexed into higher-rate signal increases, failures which occur may cause huge losses of data and great influence on a large number of users. Therefore, the survivability of networks become increasingly important. In this thesis we are concerned with the dimensioning of survivable optical core transport networks. The work presented here does not depend on a specific implementation

technology so it should be valid for any network that follows the generic functional architecture presented in the ITU-T Recommendation G.805 [6], such as SDH-based transport networks, which is described in ITU-T Recommendation G.803 [7] and OTN as in ITU-T Recommendation G.872 [8]. Nevertheless we use the OTN terminology in the majority or our examples, and make reference to other terminology when appropriate.

2.2 Enabling Technologies

In order to make this thesis more "self-sufficient", in this section we present a brief description of the network elements, that will be considered throughout this work, and their use in optical transport networks.

2.2.1 WDM

In optical communications, WDM is an enabling technology that allows multiple optical signals to be combined (multiplexed) and transmitted simultaneously into a single fiber. In a WDM system, as illustrated in Figure 2.1, a transponder accepts an

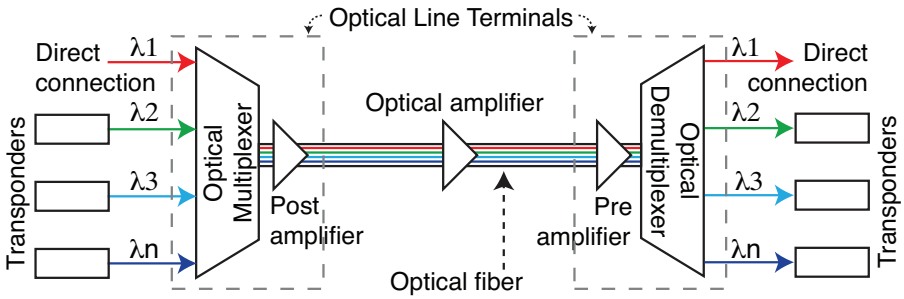

Figure 2.1: A point-to-point WDM transmission system (adapted from [9]).

input from different physical media, protocols, and traffic types. Then the input signal is mapped to a WDM wavelength, which supports a single communication channel operating at a given bit rate (10, 40 or 100 Gbps today). The WDM non-overlapping wavelengths from the transponders are then multiplexed into a single optical signal and launched into an optical fiber. The system might include the ability to accept direct optical signals to the multiplexer [9]. In the source Optical Line Terminal (OLT) a post-amplifier may be employed to strengthen the optical signal as it leaves the system.

Depending on the length of the optical fiber, optical amplifiers may be periodically installed along the fiber to compensate for signal losses. At the receiving OLT a pre-amplifier may be employed to boost the signal before it enters the end system. Then the multiplexed signals are demultiplexed to allow individual utilization of the transported wavelengths. Next, each individual wavelength is mapped to the required output type, using a transponder. As a result WDM increases the used bandwidth of the fiber proportionally to the number of wavelengths multiplexed into the fiber, allowing several orders of magnitude increase when compared with current electronic networks.

Currently, WDM systems are divided in different wavelength patterns, that differ on capabilities and costs: Wide Wavelength Division Multiplexing (WWDM), Coarse Wavelength Division Multiplexing (CWDM) and Dense Wavelength Division Multiplexing (DWDM) [10,11]. WWDM supports a channel wavelength spacing greater than or equal to 50 nm, which is suitable for use in Passive Optical Networks (PONs). Devices operating in this pattern typically separate a channel in one conventional transmission window (e.g., 1310 nm) from another (e.g., 1550 nm), also known as O-band and C-band, respectively.

CWDM supports multiple wavelengths spaced at 20 nm from each other. According to ITU-T Recommendation G.694.2 [12], eighteen CWDM wavelengths are specified for the spectral range of 1271 nm to 1611 nm, so it uses O, E, S, C and L-band. Transmitters, optical multiplexers and demultiplexers are at defined wavelengths, but they do not need to be tightly controlled, which translates into lower costs when compared to DWDM. CWDM systems can realize cost-effective applications and are suitable for use in transport networks in metropolitan areas for a variety of clients, services and protocols.

DWDM is characterized by narrower channel spacing than CWDM as defined in the ITU-T Recommendation G.671 [10]. ITU-T Recommendation G.694.1 [13] provides a frequency grid for DWDM applications. The reference set of frequencies support a variety of channel spacings ranging from 12.5 GHz to 100 GHz and wider for C and L-band. Therefore, hundreds of channels are possible. The frequencies of today's practical DWDM systems are spaced at 100 GHz (approximately 8 nm) which allow about 40 wavelengths in C-band [11]. In general the transmitters employed in DWDM applications require a control mechanism to enable them to meet the application's frequency stability requirements, in contrast to CWDM transmitters which are generally uncontrolled in this respect. DWDM is suitable for long-haul applications.

For ease of explanation, from now on we use the term WDM independently of the number of wavelengths or optical range supported.

According to ITU-T recommendation G.872 [4], an OTN using the WDM technology is defined as a layered structure that comprises four sublayers: Optical Channel (OCh), Optical Multiplex Section (OMS), Optical Transmission Section (OTS), and Physical Media, also presented in Figure 2.2. These layers and their functions are distributed along the network and their termination points are illustrated in Figure 2.2b.

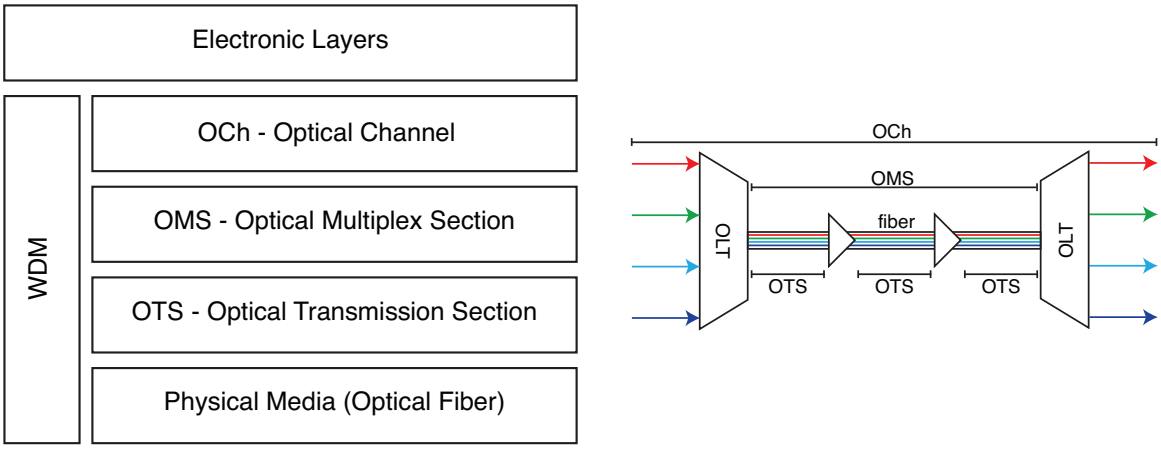

(a) (b)

Figure 2.2: Sublayers of the WDM layer (adapted from [14]).

The lowest layer is the Physical Media that works as a server of the OTS and is a defined optical fiber. The highest sublayer is the OCh (also referred to as a path sublayer), which deals with individual connections or lightpaths in an end-to-end basis across the network. It is used, for instance, for adding/dropping wavelengths and for routing the optical channels [15]. Optical channels, i.e., lightpaths, are therefore the main entities that are managed in this sublayer. An optical channel may span multiple fiber links to interconnect a pair of nodes. Each intermediate node in the optical channel provides an optical bypass facility to support the optical channel [16]. Notice that some literature have referred to an optical channel as an all-optical entity. However, nowadays we can refer to an optical channel even when intermediate nodes perform OEO conversion. An optical channel may traverses many links in the network, wherein it may be multiplexed with many other optical channels, since their wavelengths differ from one another [14]. End-to-end networking functionality is provided to the optical channels transparently transporting client signals of varying formats (e.g., SONET/SDH, Asynchronous Transfer Mode (ATM), etc.) between 3R

regeneration (re-amplification, reshaping and retiming) sites in the network.

The sublayer OMS controls the multiplexing of all the optical channels that traverse a single optical fiber, each one carried by a distinct wavelength. Therefore, it provides the networking functionality for a multi-wavelength optical signal. Each OMS in turn consists of several link segments, being each segment the span between optical amplifiers, or between an optical amplifier and an optical line terminal. Each of these portions is an OTS. Optical amplifiers are periodically introduced for compensating the loss in optical power, while the signal travels along the fiber. The OTS consists of the OMS along with an additional Optical Supervisory Channel [15]. Moreover, the OTS sublayer is the lowest section sublayer. The managed entity is the same of the OMS, but here it provides functionality for transmission of optical signals on optical media of various types (e.g., G.652, G.653 and G.655 fiber), and manage and supervise the optical transmission devices, such as OAs and transponders [4].

2.2.2 Optical Transponder

An optical transponder is typically a plug-in card or module that integrates a receiver, an electronic regenerator and an optical transmitter. Transponders may be characterized by their different capabilities and goals. For instance, short-reach transponders (also called gray or non-WDM interfaces) provide an interface to signals from the client equipment (e.g., SONET/SDH signals) [17]. Long-reach transponders (also called colored interfaces) convert a gray optical signal to a specific WDM wavelength. They provide an interface to the WDM transmission systems [18, 19].

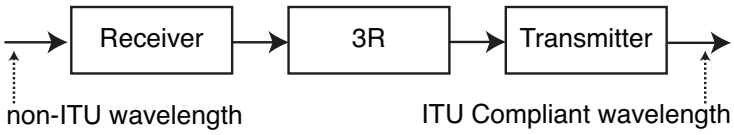

Figure 2.3: Transponder functions (adapted from [9]).

An optical transponder may also receive an optical signal at an arbitrary wavelength, such as a short-reach SONET/SDH signal at 1310 nm, and convert it to an electrical form, then it regenerates the signal and transmits it at a suitable International Telecommunication Union (ITU) WDM wavelength [2] (commonly known as the ITU grid), see Figure 2.3. Likewise, the reverse process is also possible, i.e., the transponder receives a signal from a WDM link and outputs it at another format, such as short-

reach SONET/SDH at 1310 nm. It commonly has flexibility in terms of data rates, protocols and WDM options (e.g., CWDM or DWDM) through pluggable optics for both client and trunk sides [20]. Besides the adaptation of wavelength, most transponders are equipped with 3R (regeneration, reshaping, and retiming) and FEC functionality. Actually transponders are designed to interface with a variety of signals, such as SONET/SDH, Ethernet and GbEthernet.

2.2.3 Optical Amplifier

In optical networks, the signal attenuates as it traverses the fiber links, then OAs are incorporated in optical fiber at periodic intervals to boost optical signals and reach longer distances [21]. An OA counteracts fiber attenuation over a complete spectral range at once, so several channels can be amplified at the same time. This is one of the major advantages of optical amplifiers.

Before the emergence of the optical amplifiers the standard method to compensate the power loss in optical fiber was to periodically regenerate the signal in the electrical domain along the transmission link. The use of regeneration has the advantage that the transmission impairments such as noise, dispersion and nonlinearities effects do not accumulate along the link [22]. However, system upgrades, such as bit rates and modulation formats are expensive and difficult to implement because all the regenerators of the link have to be replaced. Furthermore, the huge bandwidth of the optical fiber cannot be exploited properly. Optical amplifiers are transparent to modulation and bit rate. This means that the modulation scheme and bit rate of each channel can be changed without replacing the OAs.

Today, the most deployed amplifier is the Erbium Doped Fiber Amplifier (EDFA), of which a possible configuration consists of an erbium-doped silica fiber, one optical isolator at each end point of the erbium doped fiber, a fiber coupler and an optical pump, which is in most cases a semiconductor laser. Figure 2.4 illustrates an EDFA diagram. EDFAs can amplify signals in the conventional band, or C-band, from approximately 1525 nm to 1565 nm, and the Long band, or L-band, from approximately 1570 nm to 1610 nm, independently on the number of channels. The main difference between C- and L-band amplifiers is that a longer length of doped fiber is used in L-band amplifiers.

Other types of amplifiers can also be used, such as Semiconductor Optical Amplifier

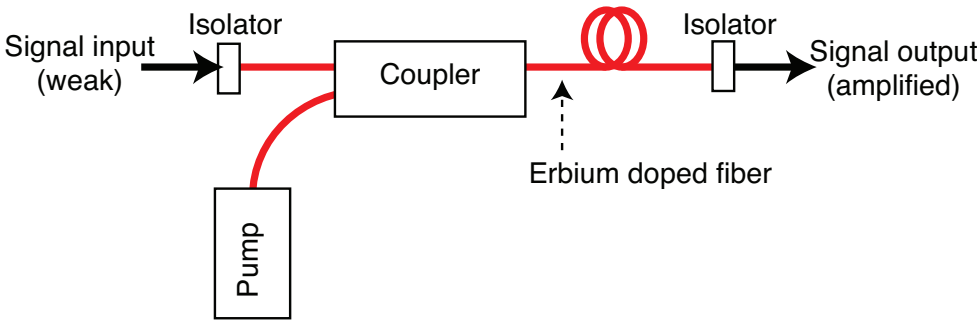

Figure 2.4: Schematic diagram of a possible configuration of an erbium-doped fiber amplifier (EDFA) (adapted from [20]).

(SOA) and Raman Amplifiers [21]. An SOA is an optical amplifier that is built on a single chip and can be integrated into multifunction optical chips. It can be less expensive than EDFAs, but the performance is still not comparable with the EDFA because of a higher noise. However, SOAs are attractive for optical signal processing (e.g., all-optical switching, wavelength conversion) and because the possibility for gain in different wavelength regions from the EDFA.

A Raman amplifier uses a powerful laser source to boost the signal power in standard optical fiber [21]. The signal is intensified based on the stimulated Raman scattering phenomenon. Differently from EDFA and SOA the amplification effect is obtained by a nonlinear interaction between the signal and a pump laser within the optical fiber. The pump power required for Raman amplification is higher than the required on EDFAs, but the main advantage of Raman amplification is its ability to provide gain in any transmission window.

Notice that OAs amplify the signals and add noise, but they do not perform the 3R regeneration as a regenerator does. Thus, the signals may still need to be regenerated periodically [9].

2.2.4 Optical Line Terminal

OLTs are devices used at the ends of a point-to-point WDM link. In case of opaque optical networks, they can be composed of transponders, wavelength multiplexers and optical amplifiers [15]. However, in this thesis we consider the transponders as components of nodes. Figure 2.5 shows the possible functional elements inside an OLT. At the transmission side the signal coming out from a transponder is multiplexed with signals of other transponders at different wavelengths using a wavelength multiplexer.

Then the bundle of multiplexed wavelengths is fed into an optical fiber. Besides that, an optical amplifier may be used to boost the signal power if needed. At the receiving side, the signal is amplified again before it is sent through a demultiplexer where individual wavelengths are extracted. The wavelengths are again terminated at a transponder or connected directly to the client equipment. This structure is generally used when client nodes are SONET/SDH, Add-Drop Multiplexers (ADMs), DXCs or IP routers and the traffic has to be processed at the electric domain [23]. Transponders are not

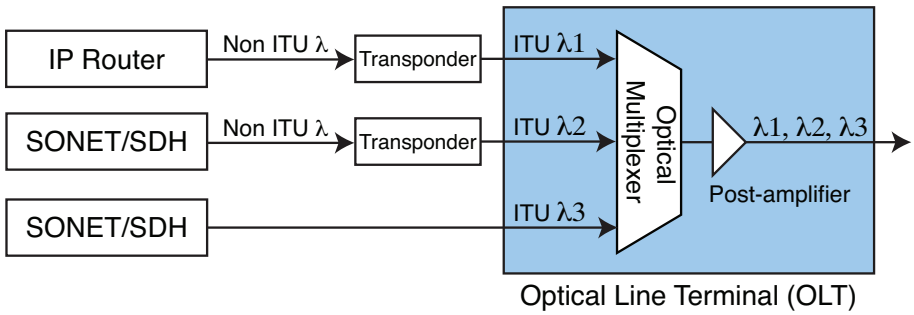

Figure 2.5: Functional elements of an Optical Line Terminal (adapted from [15]).

needed if the client equipment can directly send and receive signals compatible with the WDM link. Moreover, the interface between the client and the transponder may vary depending on the client, bit rate, and distance between client and transponder.

2.2.5 Optical Add/Drop Multiplexer

An Optical Add/Drop Multiplexer (OADM) is used at locations where some fraction of the wavelengths need to be terminated locally and others need to be routed to other destinations [24]. The device drops one or more pre-selected wavelengths from an input signal, and adds one or more pre-selected wavelengths into the outgoing signal. In todays' networks, the traffic that is to be passed through a node, i.e., the transit traffic, can be large at many of the network nodes. In this context, OADMs perform an important function of passing through this traffic in a cost-effective manner, since the number of conversions between the electrical and optical domains and frame processing time are reduced [20].

A traditional OADM consists of an optical demultiplexer, an optical multiplexer, a method of reconfiguring the paths between the optical demultiplexers, and a set of ports for adding and dropping signals. They are typically deployed in linear or ring topologies, and supports a variety of client types, such as IP routers, Ethernet switches

and SONET terminals. OXCs perform a similar function but on a much larger scale in terms of number of ports and wavelengths involved.

A very desirable attribute in an OADM is reconfigurability, which is the ability to drop and add the desired wavelengths on the fly, as opposed to having to plan ahead and deploy appropriate equipment [24]. This attribute allows lightpaths to be set up and taken down dynamically as needed in the network. An OADM with this attribute is called Reconfigurable Optical Add/Drop Multiplexer (ROADM). Moreover, this type of device may be employed in a variety of topologies, such as ring and mesh topologies.

The switching or reconfiguration functions of an ROADM can be achieved using a variety of switching technologies including MEMS and tunable optical filter technologies.

2.2.6 Optical Cross Connect

OADMs can be used to handle a relative modest number of wavelengths [24]. In order to handle more complex mesh topologies and a large number of wavelengths, an OXC is required. This device is used to build mesh wide-area networks [25] and it can terminate several fiber links, each carrying a large number of wavelengths. The provisioning of lightpaths is performed in an automated manner, without depending on manual patch panel connections. The role of an OXC in an optical network includes to switch individual optical signals, based on a routing matrix, arriving from an input fiber to output fibers, and perform regeneration and wavelength conversion when needed (the latter two actions are usually performed by transponders). Additionally, multiplexing and grooming capabilities may also be incorporated into an OXC to deal with finer granularities [26].

Although the term “optical” is used, an OXC may be internally equipped with a pure optical or an electrical switch fabric. Then, depending on the switching technology and the use of Optical-Electrical (OE) and OEO conversions, OXCs are commonly implemented into three main configurations: opaque, transparent, and translucent. The OXCs are installed between the client equipment (e.g., SONET/SDH equipment, IP router, ATM switches) and the OLTs, or between OLTs in transit nodes. Thus, since some OXC ports are connected to OLTs and other ports to client equipment, the OXC provides cost-effective passthrough for transit traffic, i.e., wavelengths that do not need to be terminated in that location but rather passed through to another destination, as

well as collecting traffic from client equipment into the network.

If the OXC is implemented as opaque, the optical signal is converted to the electrical domain as it passes through the node. An advantage is that the optical signals are regenerated, so they leave the node free of dispersion and attenuation. The switching module can be based either on electrical or optical technology surrounded by OEO components (e.g., transponders).

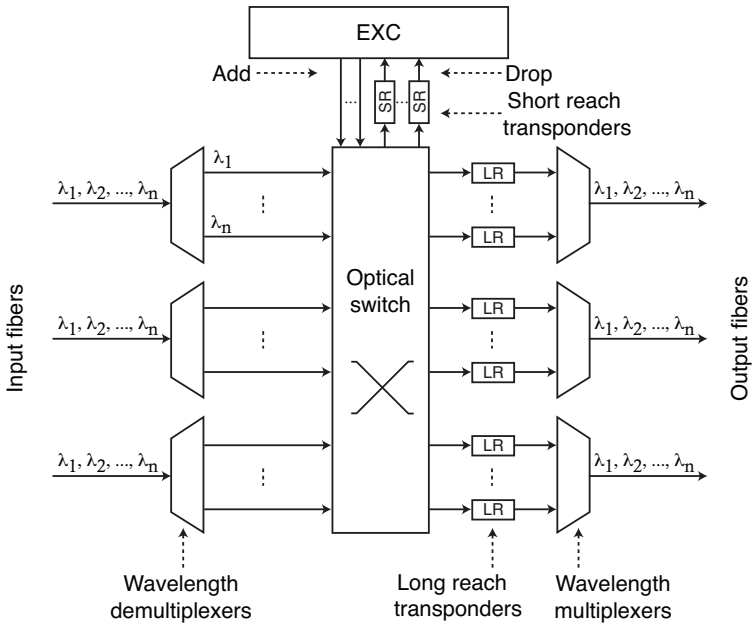

Figure 2.6: Functional diagram of an opaque OXC with an optical switching matrix (adapted from [5] and [15]).

If an electrical switching module is used, the input signals coming out of a demultiplexer are first converted into electronic signals before switching. Thereafter, the electronic signals are converted again into optical signals and multiplexed into output optical fibers. In this case sub-wavelength switching granularities can be supported, by providing grooming capabilities, for more efficient bandwidth utilization. Nonetheless, the cost of a port on an electrical switch increases with the bit rate and is dependent on interface type (e.g., 10 Gbps Ethernet or 10 Gbps SONET/SDH), and at higher bit rates the use of optical switch becomes more cost-effective.

If an optical switching module is used, the input signals coming out of a demultiplexer are optically switched and then go through OEO conversion before multiplexing into output optical fibers. In contrast to electrical switching, optical switch does not care whether it is switching a 10 Gbps Ethernet or a 10 Gbps SONET/SDH

signal. Moreover, for optical switching of 10 or 40 Gbps we can consider the optical switch is independent on bit-rate, which allows switching both signals at the same cost. In this thesis we consider all OXCs are equipped with optical switching matrices, as illustrated in Figure 2.6.

Transparent OXCs are implemented in the optical domain, so it can also be characterized as an Optical-Optical-Optical (OOO) component. In this design after the signals are demultiplexed they are switched by optical switch modules. Thereafter, the optical signals are multiplexed onto output fibers by optical multiplexers. Since signals are kept in the optical format, this design offers transparency to a variety of bit rates and protocols, but optical signal quality monitoring is harder. A functional diagram of a transparent OXC is illustrated in Figure 2.7.

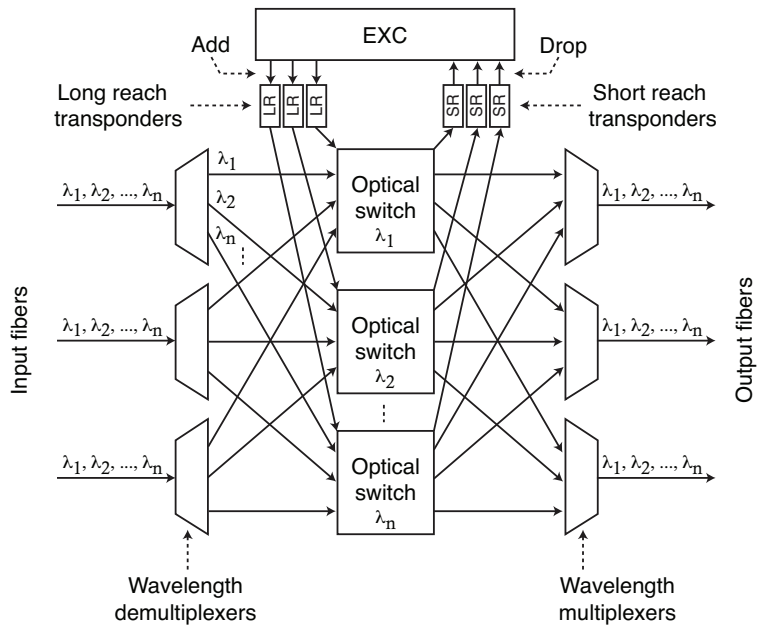

Figure 2.7: Functional diagram of a transparent OXC (adapted from [5] and [15]).

Because OAs add noise as well as boost any incoming noise with the signal, and other fiber and amplifier related impairments accumulate in the lightpath, a regeneration process is required after a number of amplifications. The needed regeneration limits the transparency in optical networks [5]. A regeneration is performed before the Maximum Transparency Length (MTL) is exceeded. Therefore, as a compromise between opaque and totally transparent, there exists a hybrid OXC that can function as both opaque and transparent, which is called a translucent OXC. Essentially, as illustrated in Figure 2.8, this OXC is implemented with an

optical switch module and a pool of transponders to perform the wavelength conversion or regeneration. Notice that regeneration is usually performed by back-to-back transponders. In this thesis we do not consider wavelength conversion and represent a regenerator as a triangular shape. In this case, after the optical signals are

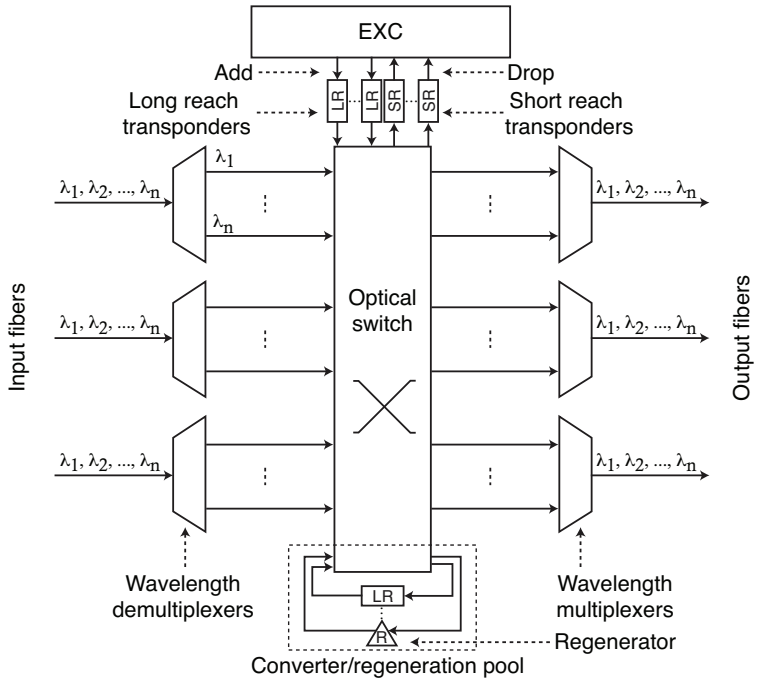

Figure 2.8: Functional diagram of a translucent OXC (adapted from [5] and [15]).

demultiplexed they are switched through the transponders pool and then multiplexed to the next appropriate fiber, or they are switched directly (transparently) to the output fibers. If wavelength conversions for the local channels are needed they can also be performed this way, eliminating the need for separate transponders between the OXC and Eletrical Cross Connect (EXC). As an alternative, the OXC might be implemented with two switch modules, one optical and one electronic. Then, optical signals traversing the device can be switched either optically or electronically. Generally the optical switch is preferred due to transparency, but in case the optical switch is all busy or an optical signal needs to be regenerated the electronic switch is then used.

2.3 Survivability in Optical Core Transport Networks

Society relies more and more on telecommunications services. Current optical transport networks carry a huge amount of data, and the demand continues to

increase. Thus, an interruption of a high-bit-rate link, even for a few seconds, means a considerable loss of data, which in turn may affect the work and revenue of both users and operators. For these reasons, network survivability is a critical aspect of transport networks, that reflects the ability of a network to maintain the services working in the presence of failures. There exist a variety of network elements along the lightpath connections that are susceptible to failures (e.g., transponders, OXCs, OAs, fibers), and survivability mechanisms are engineered to protect the networks against different types of failures, such as single link, multiple link or node failures. In this thesis we are concerned with single link failures, since the probability of a multiple link failure or a node failure is much smaller than single link failures [14].

Most of the actual transport networks are implemented with SONET/SDH as a client layer of the WDM layer. Before WDM recovery was defined SONET/SDH recovery mechanisms were mainly adopted to guarantee optical network survivability. However, when failures occur at the optical network layer, the recovery is preferably performed in the optical layer because it may recover the affected connections in group. The recovery action is also fast and easier to manage than recovering each affected connection individually in the client layer [23]. Furthermore, managing survivability at a lower protocol layer allows the control system to have a direct knowledge of the physical topology and behavior of the network. For example, information about optical circuit performance (such as Bit Error Rate (BER), optical power and wavelength value) does not need to be mediated by many layers. As a consequence, the bandwidth consumed by control system overhead is reduced and the signaling-data format is simplified. These benefits contribute to increase the speed and effectiveness of the survivability, and justify the efforts to employ survivability at the optical layer.

A distinction that can be made in survivability techniques for mesh-based networks is between protection and restoration, as illustrated in Figure 2.9.

In a survivable network we call working paths the ones that carry traffic under normal operation, and backup paths the ones that provide an alternate route to carry the traffic in case of failures (or network maintenance). Working and backup paths are usually disjointly routed so that both paths are not affected in case of a single failure [15]. The survivability techniques for the WDM layer can operate at two different sublayers: OMS or OCh. If survivability is implemented in the OMS sublayer, the entire group of lightpaths on a transmission system is recovered at once (i.e., the multiplexed collection of WDM channels), in case of failures, and individual lightpaths

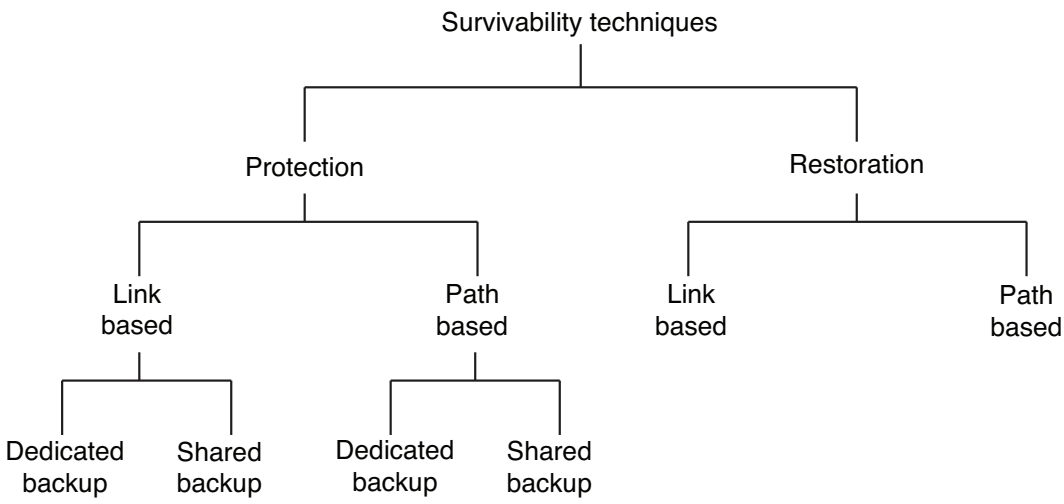

Figure 2.9: Different schemes for surviving single-link failures (adapted from [27]).

cannot be recovered separately. On the other hand, if survivability is implemented in the OCh sublayer, the lightpath is the entity to be protected, so one lightpath is recovered at a time [24]. Figure 2.10 illustrates the two implementation modes considering dedicated protection. In case of a failure, the receiving end-point of the OMS switch

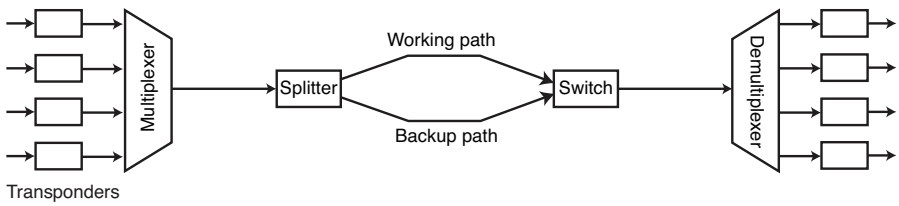

(a) OMS based survivability

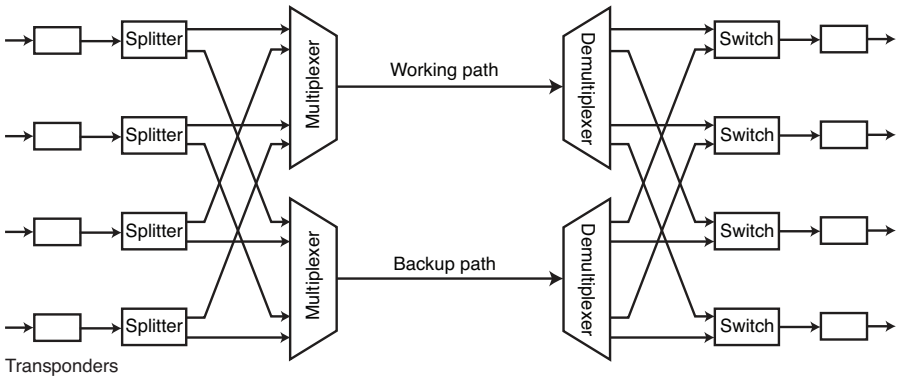

(b) OCh based survivability

Figure 2.10: Survivability techniques for: (a) 1+1 at OMS layer (link based recovery) and (b) 1+1 at OCh layer (path based recovery). In order to consider shared protection (1:1), splitters are replaced by switches.

selects the backup path around the failed link. Notice that in this case only the affected part of the working path is replaced and all the lightpaths crossing a failed link are re-routed together. In case of survivability at OCh layer, each single affected lightpath is individually switched to its backup path.

Since optical cross connects can also provide both OCh and OMS layer survivability [24], in this thesis we use simple unprotected WDM point-to-point systems and rely on the OXCs to perform the survivability functions.

Survivability techniques implemented at OMS layer are classified as link based recovery schemes, whereas the ones implemented at OCh layer are classified as path based recovery schemes. It has been shown that path based recovery typically requires less spare capacity when compared to link based recovery because backup paths in link based recovery are in general longer [23]. Furthermore, survivability at the OCh level allows recovery from node failures (notice that OMS does not cross the nodes).

2.3.1 Protection

Protection is a proactive technique in which spare capacity is reserved during connection setup [28], i.e., recovery paths are preplanned and fully signaled before a failure occurs. Hence, when a failure occurs, no additional signaling is needed to establish the protection path [23, 29]. This is essential for rapid reconfiguration and to assure a time limit to recovering from faults.

The protection technique can be applied in both OMS and OCh sublayers (which is also known as link-based protection and path-based protection), and it can be implemented as dedicated backup protection or shared backup protection. In dedicated backup protection spare resources are reserved exclusively to each working entity, (e.g., a link for survivability implemented at the OMS sublayer or a lightpath for OCh). There exist a few variants for dedicated protection: 1+1 and 1:1. In 1+1 the backup path is reserved and the cross connection matrices at intermediate nodes are fully configured before a failure occurs. Thus, the optical signal is simultaneously transmitted through both the working and the backup path. The destination node selects the stronger one from both received signals and, in the case of a link failure, only the destination node needs to perform the switching from the failing to the active signal. The advantage of 1+1 protection is that the switching time is fast and easy, but a disadvantage is that the backup resources are permanently occupied. Regarding 1:1

protection, the resources for backup path are reserved only to ensure recovery when a failure occurs. In a failure-free condition the spare resources can even be used to transport low priority traffic (that are dropped when recovery is needed). However, switching has to be done at both source and destination nodes, which takes more time when compared with 1+1 protection. As an example, Figure 2.11a illustrates a dedicated protection over a six-node network with two lightpaths, one interconnecting the nodes (1-6) having the nodes 2 and 4 as intermediate, and another lightpath interconnecting the nodes (4-5) having no intermediate nodes (see the bold solid lines). In the case a link failure along the lightpath (1-6), the lightpath is switched to its dedicated backup path, which follows the route (1-3-5-6). In the case of a failure in the link (4-5), the lightpath (4-5) is switched to its dedicated backup path, which follows the route (4-6-5). Notice that the two represented lightpaths are not affected by the same failure, even though the link (5-6) holds spare capacity to support failure on both lightpaths.

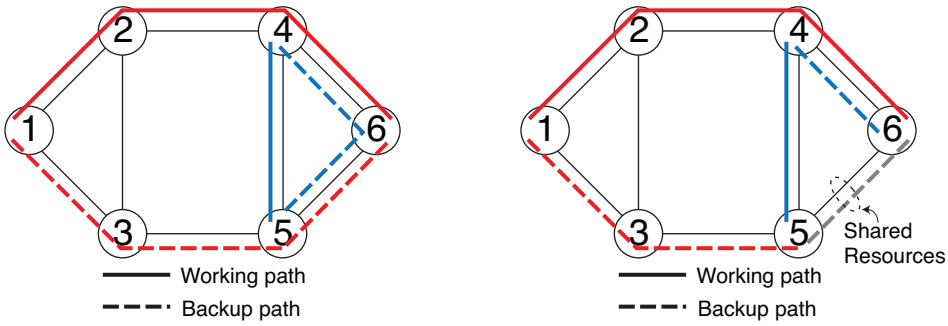

(a) Dedicated protection (b) Shared protection

Figure 2.11: Protection techniques: (a) dedicated backup protection and (b) shared backup protection.

In contrast, in shared backup protection the spare resources are shared among multiple backup paths for a number of working entities, since they are not affected by the same failure. Notice that the backup paths are established only after the failure has occurred. There exist also two variants for shared protection: 1:N and M:N (with M < N). In 1:N protection each backup path is shared between N working paths. In M:N, M backup paths are shared between N working paths, being this scheme more complex than 1:N. Figure 2.11b shows an example of shared protection over a six-node network with two lightpaths. Notice that the spare capacity reserved on the link (5-6) can be used to recover from a failure along the lightpath between the nodes (1-6) or from a failure along the lightpath between the nodes (4-5).

Dedicated backup protection is computationally simpler than shared backup protection, but less efficient in terms of resource utilization, which depends on the extent to which extra resources can be shared. Shared methods increase switching times because the switches on the backup path must be configured after the failure.

2.3.2 Restoration

Restoration is a reactive scheme which implies either preplanning or dynamic discovery of spare capacity in the network to restore the lightpaths affected by a failure [23]. Restoration can be applied to both link and path recovery, depending on the layer in which it is implemented. It is called link based restoration and path based restoration for implementations at OMS and OCh sublayers, respectively.

The resources used for recovery are not reserved at the time of connection set up but are chosen from available shared resources after a failure occurs, i.e., the backup path is provided only when a failure has occurred, thus additional signaling will be needed [30]. This scheme is typically more efficient than protection, in terms of spare capacity requirements, but the recovery time takes longer due to the intense activity of the network management system to set up new connections [31].

In preplanning restoration the computation of backup routes is done before a failure occurs, while in dynamic restoration is done after. Additionally, with dynamic restoration, the restoration route resulting from the calculation scheme may be different from the one that was supposed to be during the network design process. As a consequence, even if enough spare capacity is provided to the network overall, some failures may not be recovered. On the other hand, dynamic restoration will allow recovering from unexpected failures, which is not the case with preplanned restoration [23]. Because a preplanned restoration scheme does not spend time for route calculation, it usually recover faster than dynamic restoration.

2.4 Transport Modes

An optical transport network can operate in three different transport modes, depending on the number of all-optical fragments in a single lightpath, i.e., a transport mode is identified in function of its utilization of OEO conversions. The modes are known as opaque, transparent and translucent [32]. In the following we briefly describe the main characteristics of them.

2.4.1 Opaque Transport Mode

A network configured in opaque transport mode performs OEO conversion of the signals at the end of each transmission system [32]. It is also called an opaque network. In this kind of networks the signals are regenerated at every node since they have to be converted to the electronic domain. An advantage of this mode it that it eliminates cascading of physical impairments, allows multi-vendor interoperability and full flexibility in signal routing [33]. Furthermore, it provides good performance monitoring capability because the details of the frames are accessible at nodes, and it can improve capacity utilization of wavelength channels by providing subwavelength traffic grooming.

However, because every node needs to carry out OEO conversion, a pair of transponders are required for each single WDM channel, which increases the CAPEX of the network. In addition, because the transponders are not transparent to the data rate of optical channels, the network upgrade is costly. New electronic switch nodes and higher-bit-rate optical transponders need to be deployed when the network has to support higher-bit-rates. Figure 2.12 illustrates an example of opaque mode configuration, with and without survivability.

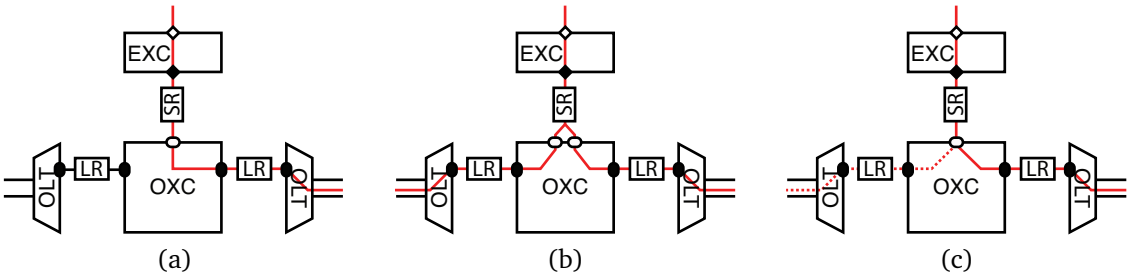

Figure 2.12: Nodes in opaque transport mode. (a) without survivability, (b) with dedicated protection, and (c) with shared restoration.

Each node comprises a non-blocking OXC equipped with an optical switch and an EXC as the access station. The OXC switches wavelengths whereas the EXC switches client traffic such as SONET/SDH or IP, and performs traffic grooming. Short-reach transponders (SR) interconnect the OXCs tributary ports with the EXCs trunk ports. Long-reach transponders (LR) make the interface between OLTs and OXC trunk ports.

The client traffic enters from the tributary ports of EXCs and is groomed before being routed through the network. Add and drop traffic have to go through both the EXC and OXC, whereas transit traffic is kept in the transport domain, i.e., transit traffic

is not processed on EXCs. Alternative opaque mode configurations can be realized. For instance, using a fixed patch panel in the node to connect WDM transmission systems equipped with optical transponders; or using an opaque switching node with electrical switch fabrics. More details can be found in [33, 34].

In order to provide dedicated protection at the optical layer, we may use a short-reach protection transponder outside the OXC, see Figure 2.12b. Since the OXC cannot broadcast an input signal through two output ports, the protection transponder takes one signal as input and splits the signal into a working and a backup signal. Each signal is then fed into a tributary port of the OXC. The OXC switches the working and the protection paths to the appropriate trunk ports, which are connected to different transmission systems. This method is known as single-ended switching since only the destination node does switching, while the source node duplicates the traffic.

For the case of shared protection or shared restoration at the optical layer, the protection transponder is not required, see Figure 2.12c. A regular short-reach transponder takes one client signal as input and feeds the signal into a tributary port of the OXC. The OXC drives the signal toward the trunk port of the working path. In case of a failure, the OXC switches the signal toward the trunk port of the backup path. This method is known as dual-ended switching because both source and destination nodes have to perform switching in case of failures. Notice that the OXC trunk port used for the backup path can be shared with other backup paths.

2.4.2 Transparent Transport Mode

A network operating in a fully transparent mode keeps the signal of a source-destination connection in the optical domain at every intermediate nodes, i.e., except in the end nodes the signal does not undergo OEO conversion. Regeneration capacity is not present as well. Networks operating in this mode are also called transparent networks [33]. As the signal must remain on the same wavelength until it reaches the destination node, this architecture implies end-to-end bit rate and protocol transparency. Additionally, it is easy to upgrade the network to higher-bit-rates since only a transmitter and a receiver per end-to-end connection need to be replaced.

However, because the absence of OEO conversion, the quality of the optical signals degrade as they traverse the optical components along the route between the source-destination nodes. In addition, longer lightpaths are sensitive to various nonlinear

optical impairments, especially when considering high-bit-rates (> 10 Gbps) [35]. The MTL of a system, which is the maximum distance that light can travel without 3R regeneration, puts a limit on the size of a completely transparent network.

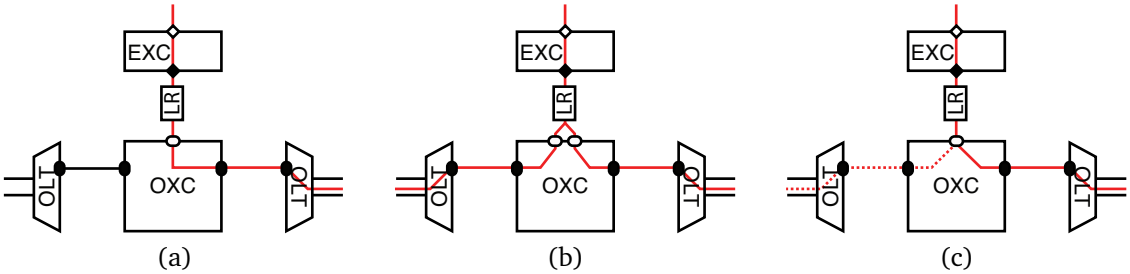

Figure 2.13: Nodes in transparent transport mode. (a) without survivability, (b) with dedicated protection, and (c) with shared restoration.

Figure 2.13 illustrates a possible transparent configuration. The OXCs are equipped with transparent optical switches and its interface with WDM transmission systems do not contain transponders. The EXCs that are attached to OXCs function as access stations. Long-reach transponders make the interface between the OXCs and EXCs, but they are used only for local add-drop traffic. Dedicated protection at the optical layer is provided by long-reach protection transponders, see Figure 2.13b. Whereas shared protection or restoration is provided by the OXC, which switches the client signal toward the appropriate trunk port, see Figure 2.13c.

2.4.3 Translucent Transport Mode

In order to take the advantages of the two above mentioned types of networks, an alternative to fully opaque networks and fully transparent networks was first proposed in [32] and termed translucent networks. In this architecture the signals travel through the network “as far as possible” in the optical domain.

The signals are regenerated only when the lightpaths reach their MTL, or when a different wavelength must be assigned. OEO signal regeneration may be performed to provide just 3R regeneration, but may include subwavelength traffic grooming. Notice that the signal can be regenerated several times in the network before it reaches its destination. Furthermore, a lightpath in a translucent network could span one or more fiber links and may even span the entire source-destination path. This case is similar to the transparent one in that the BER is first estimated on an available lightpath. However, if that lightpath is unavailable (either because of unavailable resources or

because the BER turns out to be above the acceptable limit), then the lightpath is broken into smaller fragments. At each fragment the signal is regenerated [32].

Translucent networks can be configured into a number or ways. For example, a) it can be equipped with sparsely opaque switch nodes among transparent switch nodes; b) equipped with all translucent switch nodes, in which each node is equipped with electronic and optical switches; c) equipped with sets of opaque nodes, translucent nodes, and transparent nodes.

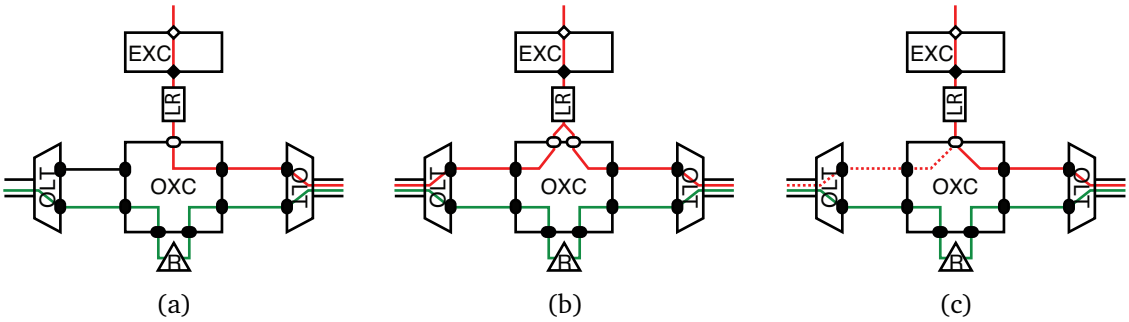

Figure 2.14: Nodes in translucent transport mode. (a) without survivability, (b) with dedicated protection, and (c) with shared restoration.

In this thesis we consider the setup presented in Figure 2.14. The network is based on translucent OXCs, equipped with an all optical non-blocking switching fabric together with a number of transponders.

Long-reach transponders are installed at the OXC tributary ports for local traffic. Additionally, a pool of regenerators is attached to the OXC for regeneration and wavelength conversion purposes, see the triangular shape in Figure 2.14. Alternatively, regeneration could be performed through the attached EXC, then the tributary ports can be assigned to either local or transit traffic that requires regeneration.

Similarly to the transparent mode, dedicated protection survivability at the optical layer is provided by long-reach protection transponders, see Figure 2.14b. Whereas shared protection or restoration is provided by the OXC, see Figure 2.14c.

Knowing the three network transport modes, Table 2.1 summarizes the main characteristics relative to opaque, transparent and translucent networks [36].

Table 2.1: Features related to the opaque, transparent and translucent networks.

	Opaque	Transparent	Translucent
	OEO at each node	No OEO at intermediary nodes	Possible OEO at intermediary nodes
Flexibility to bit rate	No	Partial	Partial
Flexibility to reconfiguration	Yes	Possible	Possible
OEO regeneration devices	Yes	No	Possible
OEO wavelength conversion devices	Yes	No	Possible
Physical impairment consideration in routing tools	No	Yes	Yes
Impairment compensation devices	Simple	Complex	Complex
Network upgradeability	Complex	Easy	Easy
Network extension	Unlimited	Limited	Unlimited
Network monitoring	Simple	Complex	Complex
Optimization of electronics	No	Yes	Yes

2.5 Chapter Summary

This chapter provides an overview of the optical core transport networks. We started by presenting a description of enabling technologies. Then we presented a few survivability techniques, based on protection and restoration strategies. Finally, we presented the three transport modes in which a network may operate, which are opaque, transparent and translucent modes.

References

[1] ITU-T Recommendation G.707, "Architecture of optical transport networks," International Telecommunication Union, Tech. Rep., January 2007. [Online]. Available: http://www.itu.int/rec/T-REC-G.707/en

[2] A. Gladisch, R.-P. Braun, D. Breuer, A. Ehrhardt, H.-M. Foisel, M. Jaeger, R. Leppla, M. Schneiders, S. Vorbeck, W. Weiershausen, and F.-J. Westphal, "Evolution of terrestrial optical system and core network architecture," *Proceedings of the IEEE*, vol. 94, no. 5, pp. 869 –891, may 2006.

[3] J. Manchester, P. Bonenfant, and C. Newton, "The evolution of transport network survivability," *Communications Magazine, IEEE*, vol. 37, no. 8, pp. 44 –51, Aug. 1999.

[4] ITU-T Recommendation G.872, "Architecture of optical transport networks," International Telecommunication Union, Tech. Rep., November 2001. [Online]. Available: http://www.itu.int/rec/T-REC-G/e

[5] W. D. Grover, *Mesh-Based Survivable Networks: options and strategies for optical, MPLS, SONET, and ATM networking*. NJ: Prentice Hall, 2004.

[6] ITU-T Recommendation G.805, "Generic functional architecture of transport networks," International Telecommunication Union, Tech. Rep., March 2000. [Online]. Available: http://www.itu.int/rec/T-REC-G.805-200003-I/en

[7] ITU-T Recommendation G.803, "Architecture of transport networks based on the synchronous digital hierarchy (SDH) (revised)," International Telecommunication Union, Tech. Rep., March 2000. [Online]. Available: http://www.itu.int/rec/T-REC-G.803/e

[8] ITU-T Recommendation G.872, "Amendment 2 of g.872 architecture of optical transport networks," International Telecommunication Union, Tech. Rep., June 2010. [Online]. Available: http://www.itu.int/rec/T-REC-G/e

[9] *Introduction to DWDM Technology (manual)*, Cisco Cystems, Inc., San Jose, CA, USA, June 2001. [Online]. Available: http://www.cisco.com/en/US/products/hw/optical/ps2011/

[10] ITU-T Recommendation G.671, "Transmission characteristics of optical components and subsystems," International Telecommunication Union, Tech. Rep., January 2009. [Online]. Available: http://www.itu.int/rec/T-REC-G.671/en

[11] S. M. Esser, "WDM/CWDM/DWDM: Segmentation primer - maximizing capacity for revenue," Motorola, Inc., White Paper, June 2008.

[12] ITU-T Recommendation G.694.2, "Spectral grids for WDM applications: CWDM wavelength grid," International Telecommunication Union, Tech. Rep., December 2003. [Online]. Available: http://www.itu.int/rec/T-REC-G/e

[13] ITU-T Recommendation G.694.1, "Spectral grids for WDM applications: DWDM wavelength grid," International Telecommunication Union, Tech. Rep., June 2002. [Online]. Available: http://www.itu.int/rec/T-REC-G/e

[14] G. Maier, A. Pattavina, S. de Patre, and M. Martinelli, "Optical network survivability: Protection techniques in the WDM layer," *Photonic Network Communications*, vol. 4, no. 3-4, pp. 252–269, July 2002.

[15] R. Ramaswami and K. N. Sivarajan, *Optical networks: A practical perspective*. San Francisco, CA, USA: Morgan Kaufmann Publishers Inc., 2002.

[16] B. Mukherjee, *Optical WDM Networks*. New York, NY, USA: Springer, 2006.

[17] *SP Guru Transport Planner Documentation Set*, 16th ed., OPNET Technologies, Bethesda, MD, USA, February 2010.

[18] F. Yu, S. Jutamulia, and S. Yin, Eds., *Introduction to information optics*, ser. Optics and Photonics. San Diego, CA, USA: Academic Press, 2001.

[19] J. Simmons, "On determining the optimal optical reach for a long-haul network," *Journal of Lightwave Technology*, vol. 23, no. 3, pp. 1039–1048, March 2005.

[20] I. P. Kaminow, T. Li, and A. E. Willner, Eds., *Optical Fiber Telecommunications*, 5th ed., ser. Systems and netwotks. Burlington, USA: Elsevier, February 2008, vol. B.

[21] L. Goleniewski and K. W. Jarrett, *Telecommunications Essentials: The Complete Global Source*, 2nd ed. Addison Wesley Professional, 2006.

[22] C. F. Lam, *Passive optical networks : principles and practice*, 1st ed. Burlington, USA: Elsevier, 2007.

[23] J.-P. Vasseur, M. Pickavet, and P. Demeester, *Network Recovery: Protection and Restoration of Optical, SONET-SDH, IP, and MPLS*. San Francisco, CA, USA: Morgan Kaufmann, 2004.

[24] R. Ramaswami, K. Sivarajan, and G. Sasaki, *Optical Networks: A Practical Perspective*, 3rd ed. Morgan Kaufmann, 2009.

[25] B. Mukherjee, "Wdm optical communication networks: progress and challenges," *IEEE Journal on Selected Areas in Communications*, vol. 18, no. 10, pp. 1810 – 1824, October 2000.

[26] N. S. C. Correia, J. Coimbra, and M. C. R. Medeiros, "Sparse traffic grooming in WDM networks using coarse granularity OXCs," *Photonic Network Communications*, vol. 17, no. 1, pp. 49–62, February 2009.

[27] S. Ramamurthy and B. Mukherjee, "Survivable wdm mesh networks, part i - protection," in *Proceedings of the Conference on Computer Communications, INFOCOM'99*. New York, USA: IEEE, Mar. 1999, pp. 744–751.

[28] S. Ramamurthy, L. Sahasrabuddhe, and B. Mukherjee, "Survivable WDM mesh networks," *IEEE/OSA Journal of Lightwave Technology*, vol. 21, no. 4, pp. 870–883, April 2003.

[29] K. J. Warbrick, X. Lu, R. Friskney, and K. Durrani, "Shortest-cycle photonic network restoration," in *Proceedings of the London Communications Symposium, LCS'01*, London, UK, September 2001.

[30] A. Somani, *Survivability and Traffic Grooming in WDM Optical Networks*. New York, NY, USA: Cambridge University Press, 2005.

[31] N. Correia, "Survivable WDM mesh networks," PhD thesis, Faculty of Science and Technology, University of Algarve, Faro-Algarve, Portugal, 2004.

[32] B. Ramamurthy, H. Feng, D. Datta, J. Heritage, and B. Mukherjee, "Transparent vs. opaque vs. translucent wavelength-routed optical networks," *Optical Fiber Communication Conference, 1999, and the International Conference on Integrated Optics and Optical Fiber Communication. OFC/IOOC '99. Technical Digest*, vol. 1, pp. 59–61 vol.1, 1999.

[33] E. Bouillet, G. Ellinas, J.-F. Labourdette, and R. Ramamurthy, *Path Routing in Mesh Optical Networks*. Chichester, England; Hoboken, NJ: John Wiley & Sons, 2007.

[34] G. Ellinas, J.-F. Labourdette, J. Walker, S. Chaudhuri, L. Lin, E. Goldstein, and K. Bala, "Network control and management challenges in opaque networks utilizing transparent optical switches," *Communications Magazine*, vol. 42, no. 2, pp. S16 – S24, February 2004.

[35] D. Staessens, D. Colle, M. Pickavet, and P. Demeester, "Cost efficiency of protection in future transparent networks," in *11th International Conference on Transparent Optical Networks, 2009. ICTON '09.*, July 2009, pp. 1 –4.

[36] A. Morea, F. Leplingard, T. Zami, N. Brogard, C. Simonneau, B. Lavigne, L. Lorcy, and D. Bayart, "New transmission systems enabling transparent network perspectives," *Comptes Rendus Physique*, vol. 9, no. 9–10, pp. 985–1001, 2008.

Chapter 3

Network Cost Model

3.1 Introduction

The dimensioning of optical networks involves identifying the needed resources, their quantities, and Capital Expenditures. Since most decisions are taken based on costs, CAPEX is a key factor for the evaluation of alternative solutions. Therefore, a network model is important to identify the most cost-efficient network design that meets the operator's necessity. A model to calculate the exact CAPEX depends on detailed information such as the network architecture, topology, traffic load, transport mode, routing and survivability schemes. Moreover, we have to know how those inputs relate to each other. In this Chapter we focus on the installation cost of survivable networks. We present a cost model for CAPEX in optical transport networks. We start from the work presented in [1], which can be used for networks in opaque transport mode with restoration survivability schemes. As our main contribution to that effort we extended the model by considering transparent and translucent transport modes, and protection survivability schemes.

In section 3.2, we present a network and traffic representation. Then, we present expressions to calculate the network costs, in section 3.3, which are further divided into cost of links, in section 3.4, and cost of nodes, in section 3.5. To illustrate the use of the model we consider a four-node mesh network with five links. Since the costs are dependent on the number of channels in the network, we show how to calculate the number of channels per link in section 3.6. Furthermore, the calculation of the number of channels on links require information about the number of hops per demand. Then, we present how to obtain the number of hops in section 3.7. We also present how to obtain survivability coefficients, section 3.8, which are used to calculate the costs of networks operating with capacity for survivability. Finally we present the variables that

are affected when survivability is considered, for links in section 3.9 and for nodes in section 3.10. In section 3.11 we calculate CAPEX of a network, considering survivability and opaque, translucent, and transparent transport mode.

3.2 Network and Traffic Representation

A network topology is generally represented as a graph $G(N, L)$, where N and L are the number of nodes and links in the network, respectively [2]. Each node corresponds to a number of physical modules and links to the transmission systems between the nodes. Figure 3.1 shows a physical topology of a four-node and five-link network.

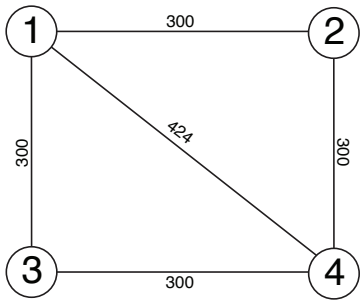

Figure 3.1: The physical network as a weighted graph. The numbers close to links represent the fiber length (e.g. in km).

The network topology can also be represented as an $N \times N$ adjacency matrix $[g]$ in which the elements $(g_{i,j})$ hold the number 1 or 0 to indicate whether the source-destination node pair (i, j) is adjacent or not, respectively. The adjacency matrix for the network in Figure 3.1 is given by

$$[g] = \begin{bmatrix} 0 & 1 & 1 & 1 \\ 1 & 0 & 0 & 1 \\ 1 & 0 & 0 & 1 \\ 1 & 1 & 1 & 0 \end{bmatrix}. \tag{3.1}$$

The number of nodes and links are not independent quantities. In fact, according to the graph theory a complete graph, i.e., a graph in which there exists one link between each pair of nodes, has exactly $N(N-1)/2$ links (assuming no parallel links). On the other hand, for having a connected graph it is required at least $N-1$ links [3]. If disjoint path between node pairs is required, the graph must have at least N links.

Notice, however, that this condition is necessary but not sufficient for path disjointness. Although some networks may implement, in this thesis we do not consider parallel links (i.e., multiple links between the same pair of nodes), nor self-loops (links with $i = j$).

3.2.1 Nodal Degree

The degree of a node, δ_n, is defined as the number of physical connections or links that the node has to other nodes. The nodes may have two different degrees if the links are considered to be unidirectional (the incoming and outgoing degrees). However, in this thesis we consider that all links are bidirectional. Therefore, using a matrix $[g]$ the degree of a node n can be calculated with

$$\delta_n = \sum_{j=1}^{N} g_{i,j}. \tag{3.2}$$

Considering the adjacency matrix of the network presented in (3.1), the nodal degree of node 1 is $\delta_1 = 3$. Considering all nodes we can calculate the average nodal degree, which is the summation over all node degrees divided by the number of nodes,

$$\langle \delta \rangle = \frac{1}{N} \sum_{n=1}^{N} \delta_n. \tag{3.3}$$

Since one node is attached at each endpoint of a link, each link contributes twice to the nodal degree. Then, another way to calculate the same average is

$$\langle \delta \rangle = \frac{2L}{N}. \tag{3.4}$$

Notice that the expression (3.4) is exact and does not depend on the network topology and demand model (e.g., uniform or random). Considering our example network, Figure 3.1, and the expression (3.4), we obtain $\langle \delta \rangle = 2.5$.

3.2.2 Traffic Model

A demand $d_{i,j}$ is the capacity, in units of transmission (e.g., one STM-1), that a pair of nodes (i, j) require to transport data from node i to node j. The traffic

demand between the network nodes can be represented as a matrix $[d]$ in which the elements $d_{i,j}$ represent the number of demands between the source node i to the destination node j. Traffic matrices reflect the volume of traffic that flows between all possible pairs of sources and destinations in a network [4]. We consider the assumption that the currently deployed transport core networks contain bidirectional optical line systems [5] and the traffic is symmetric. Hence, in this work we consider that all demands are bidirectional, then $d_{i,j} = d_{j,i}$ and $[d]$ is a symmetric matrix. A possible traffic matrix for the network in Figure 3.1 is

$$[d] = \begin{bmatrix} 0 & 1 & 1 & 1 \\ 1 & 0 & 2 & 1 \\ 1 & 2 & 0 & 1 \\ 1 & 1 & 1 & 0 \end{bmatrix}. \tag{3.5}$$

The summation over the elements in $[d]$ yields the number of unidirectional demands D_1, which can be written as

$$D_1 = \sum_{i=1}^{N} \sum_{j=1}^{N} d_{i,j}. \tag{3.6}$$

Assuming $[d]$ as a symmetric matrix, the summation of all elements of the upper (or lower) triangular part of the matrix yields the number of bidirectional demands D which can be written as

$$D = \sum_{i=1}^{N-1} \sum_{j=i+1}^{N} d_{i,j} = \frac{D_1}{2}. \tag{3.7}$$

Dividing the number of unidirectional demands by the number of nodes we obtain the average number of bidirectional demands per node, which can be written as

$$\langle d \rangle = \frac{D_1}{N} = \frac{2D}{N}. \tag{3.8}$$

We should note that for a uniform and unitary traffic model the average number of demands that is originated in a given node is

$$\langle d \rangle = N - 1. \tag{3.9}$$

Using (3.8) we obtain

$$D_1 = N\langle d \rangle, \tag{3.10}$$

and

$$D = \frac{N\langle d \rangle}{2}. \tag{3.11}$$

Considering the network presented in Figure 3.1, in which $N = 4$, and the traffic load presented in (3.5) we obtain $D = 7$ and $\langle d \rangle = 3.5$.

3.3 Network Costs

The total cost of a network (C_T) can be calculated as the summation of the costs of all constituent components. In this thesis we divide the costs into two major groups. The cost of links (C_L) that is related to the transmission systems, and the cost of nodes (C_N) that is related to the bandwidth management. Considering this statement we can write the total cost of a network as

$$C_T = C_L + C_N. \tag{3.12}$$

The total costs with links is the summation of the costs of every links in the network, which can be written as

$$C_L = \sum_{l=1}^{L} c_l, \tag{3.13}$$

where L is the number of links in the network and c_l the cost of a single link l. Similarly, the cost of nodes is the summation of the costs of all nodes in the network, which can be written as

$$C_N = \sum_{n=1}^{N} c_n, \tag{3.14}$$

where N is the number of nodes in the network and c_n the cost of a single node n. From (3.12), (3.13) and (3.14) we obtain

$$C_T = \sum_{l=1}^{L} c_l + \sum_{n=1}^{N} c_n. \tag{3.15}$$

We can also calculate the costs considering the average values, without loss of accuracy. Notice that we can rewrite (3.15) as

$$C_T = \frac{L}{L}\sum_{l=1}^{L} c_l + \frac{N}{N}\sum_{n=1}^{N} c_n. \tag{3.16}$$

Considering the definition of average

$$\langle q \rangle = \frac{1}{M}\sum_{m=1}^{M} q_m, \tag{3.17}$$

we obtain

$$C_T = L\langle c_l \rangle + N\langle c_n \rangle, \tag{3.18}$$

where

$$\langle c_l \rangle = \frac{1}{L}\sum_{l=1}^{L} c_l, \tag{3.19}$$

and

$$\langle c_n \rangle = \frac{1}{N}\sum_{n=1}^{N} c_n, \tag{3.20}$$

are the average cost of links and nodes, respectively. Equations (3.15) and (3.18) are equivalent and no approximations are involved.

3.4 Cost of Links

Each link is composed of one or more transmission systems. Each transmission system is composed of two bidirectional Optical Line Terminals (OLTs), a bidirectional optical fiber and a number of bidirectional Optical Amplifiers (OAs). Therefore, the cost of a link l is given by

$$c_l = c_l^{OLT} + c_l^{A} + c_l^{F}, \tag{3.21}$$

where c_l^{OLT} is the cost of OLTs for all transmission system in the link l, c_l^{A} is the cost of OAs for all transmission system in the link l, and c_l^{F} is the cost of optical fibers for all transmission system in the link l.

3.4.1 Cost of OLTs per Link

We consider that the cost of an OLT is fixed and includes a WDM multiplexer/demultiplexer and a pre- and post-amplifier. Therefore, the cost of OLTs per link is given by,

$$c_l^{OLT} = 2n_l^S \gamma^{OLT}, \tag{3.22}$$

where n_l^S is the number of transmission systems in the link l, and γ^{OLT} is the cost of an OLT. The number of transmission systems in a link depends on the traffic demand and the maximum capacity of the WDM terminal multiplexer, and can be written as

$$n_l^S = \left\lceil \frac{w_l}{S} \right\rceil, \tag{3.23}$$

where w_l is the number of optical channels (or demands) that traverse the link l, and S is the maximum capacity of the WDM terminal multiplexer used in the transmission systems, e.g., 40 channels. The calculation of w_l is further discussed in section 3.6.

The number of OLTs in the network is obtained with

$$N^{OLT} = \sum_{l=1}^{L} 2n_l^S, \tag{3.24}$$

and the average number of OLTs per link with

$$\langle n^{OLT} \rangle = \frac{N^{OLT}}{L} = 2\langle n^S \rangle, \tag{3.25}$$

where $\langle n^S \rangle$ is the average number of transmission system per link, which can be written as

$$\langle n^S \rangle = \frac{1}{L} \sum_{l=1}^{L} n_l^S. \tag{3.26}$$

The term $\langle n^S \rangle$ in (3.25) is multiplied by two because each transmission system uses two OLTs (one on each end). From (3.25) we can obtain the average cost of OLTs per link with

$$\langle c^{OLT} \rangle = \langle n^{OLT} \rangle \gamma^{OLT}. \tag{3.27}$$

3.4.2 Cost of Optical Amplifiers per Link

The costs of optical amplifiers in a transmission system is a function of the link length and the span between amplifiers. Considering this cost per link we have,

$$c_l^A = n_l^A \gamma^A, \tag{3.28}$$

where n_l^A is the number of OAs in the link l and γ^A is the cost of an OA. We can obtain the number of OAs per link as

$$n_l^A = \left(\left\lceil \frac{\nu_l}{\partial} \right\rceil - 1 \right) n_l^S, \tag{3.29}$$

where ν_l is the length of the link l and ∂ is the span, i.e., the distance between optical amplifiers (or between an OA and an OLT). Summing over all links we obtain the total number of amplifiers,

$$N^A = \sum_{l=1}^{L} n_l^A. \tag{3.30}$$

Dividing (3.30) by the number of links we obtain the average number of optical amplifiers per link, which can be written as

$$\langle n^A \rangle = \frac{N^A}{L}. \tag{3.31}$$

The average cost of OAs per link is, therefore,

$$\langle c^A \rangle = \langle n^A \rangle \gamma^A. \tag{3.32}$$

Considering our example network, and $\partial = 100$, we obtain $\langle n^A \rangle = 2.4$ per link.

3.4.3 Cost of Optical Fiber per Link

The cost of a pair of optical fibers in a link is a function of the link length, ν_l, which can be written as

$$c_l^F = 2\nu_l n_l^S \gamma^F, \tag{3.33}$$

where γ^F is the cost of a unit of length of optical fiber. Notice that we multiply the first term by two because a transmission system uses a pair of optical fibers. Summing over all links we obtain the total quantity of optical fiber in the network, which is

$$N^F = \sum_{l=1}^{L} 2\nu_l n_l^S, \tag{3.34}$$

and dividing (3.34) by L we obtain the average quantity of optical fiber per link,

$$\langle n^F \rangle = \frac{N^F}{L}. \tag{3.35}$$

Using (3.35) we can obtain the average cost of optical fiber per link with

$$\langle c^F \rangle = \langle n^F \rangle \gamma^F. \tag{3.36}$$

Considering our example network, in Figure 3.1, and assuming just one transmission system per link, we have $\langle n^F \rangle = 649.6$, which is twice the average link length.

Considering (3.27), (3.32), (3.36) we can write,

$$C_L = L\left(\langle c^{OLT} \rangle + \langle c^A \rangle + \langle c^F \rangle\right), \tag{3.37}$$

and

$$\langle c_l \rangle = \langle c^{OLT} \rangle + \langle c^A \rangle + \langle c^F \rangle. \tag{3.38}$$

Nowadays, a number of entities own optical cables. For instance, besides the telecom operators, operators of railways lay optical fiber cables along the railway tracks. Electrical power companies use the existing electrical power infrastructure to lay optical fiber cables along the power lines. In this scenario, telecom operators tend to lease fiber optical cables instead of installing or expand their infrastructures. Therefore, in this thesis we do not consider the cost of optical fibers since we assume that a sufficient amount of dark fibers is already available, and the costs of leasing cables are OPEX.

3.5 Cost of Nodes

The nodes of a transport network may be implemented in a variety of manners. Usually, the nodes receive traffic coming from the metro/access networks via their tributary ports, and traffic coming from adjacent core nodes via their trunk ports. In this thesis we assume the node architectures presented in Chapter 2. We assume that client traffic is added from an EXC where it is groomed and sent to the tributary ports of an OXC. The OXC switches the local traffic wavelengths between the OXC tributary ports and the WDM links and the transit traffic between different WDM links. Moreover, the nodes are implemented in three ways: opaque OXC, using OEO conversion and optical switch core; totally transparent OXC, using optical switch and no OEO conversion; and translucent core OXC, using optical switch core and some OEO conversions.

Therefore, the cost of nodes depends on the costs of EXCs, OXCs, transponders, and regenerators, which can be written as

$$c_n = c_n^{EXC} + c_n^{OXC} + c_n^{TSP} + c_n^{REG}, \tag{3.39}$$

where c_n^{EXC} is the cost of the EXC, c_n^{OXC} the cost of the OXC, c_n^{TSP} the cost of transponders, and c_n^{REG} is the cost of regenerators, at node n. Using the averages we can write

$$\langle c_n \rangle = \langle c^{EXC} \rangle + \langle c^{OXC} \rangle + \langle c^{TSP} \rangle + \langle c^{REG} \rangle, \tag{3.40}$$

to obtain the average cost of nodes. Multiplying (3.40) by the number of nodes we obtain the total cost of nodes,

$$C_N = N \langle c_n \rangle. \tag{3.41}$$

3.5.1 Cost of EXCs

We assume that the cost of an EXC consists of a fixed cost and a cost that grows linearly on the number of trunk ports. Therefore we can write,

$$c_n^{EXC} = \gamma^{EXC} + n_{exc,n}^{TP} \gamma_{exc}^{TP}. \tag{3.42}$$

where γ^{EXC} is the base cost of an EXC, $n_{exc,n}^{TP}$ is the number of trunk ports in the EXC n, and γ_{exc}^{TP} is the cost of a trunk port.

The number of trunk ports depends on client traffic and the multiplexing factor. However, we consider that the given traffic demand is already groomed from client layer to optical layer. Each demand occupies a trunk port. Therefore, the number of trunk ports in an EXC node n can be written as

$$n_{exc,n}^{TP} = n_n^D, \tag{3.43}$$

where n_n^D is the number of demands that originate or terminate at the node n. Considering all nodes we obtain the number of EXC trunk ports in the network with

$$N_{exc}^{TP} = \sum_{n=1}^{N} n_n^D = D_1, \tag{3.44}$$

and the average number of EXC trunk ports per node is

$$\langle n_{exc}^{TP} \rangle = \frac{D_1}{N} = \langle d \rangle. \tag{3.45}$$

Considering our example network and traffic presented in (3.5) we have $\langle n_{exc}^{TP} \rangle = 3.5$. From (3.42) and (3.45) we obtain the average cost of an EXC with

$$\langle c^{EXC} \rangle = \gamma^{EXC} + \langle n_{exc}^{TP} \rangle \gamma_{exc}^{TP}. \tag{3.46}$$

3.5.2 Cost of OXCs

We assume that the cost of an OXC consists of a fixed base cost and a cost dependent on the number of channels it has to switch. This number of channels determines size of the switching matrix, and is dependent on the traffic and transport mode. In the following we show how to obtain cost of equipped OXCs considering opaque, transparent and translucent transport modes.

3.5.2.1 Cost of OXCs in Opaque Transport Mode

In order to obtain the cost of an OXC, we start with the cost of OXC at node n:

$$c_{op,n}^{OXC} = \gamma^{OXC} + n_{op,n}^{CH} \gamma^{SW}. \tag{3.47}$$

where γ^{OXC} is the base cost of an OXC, $n_{op,n}^{CH}$ the number of bidirectional channels that are processed in the opaque node n, and γ^{SW} is the cost of switching a channel. The "op" index indicates opaque mode. We can obtain $n_{op,n}^{CH}$ with:

$$n_{op,n}^{CH} = \frac{1}{2}\left(n_n^D + \sum_{j=1}^{N} w_{n,j}\right), \tag{3.48}$$

where n_n^D is the number of demands that originate or terminate at node n, $w_{n,j}$ is the number of channels transported in each link connected to node n, being $w_{n,j} = 0$ when the pair of nodes n, j is not directly connected. Notice that the expression (3.48) is divided by two because each channel always enters and exit the OXC. In order to illustrate the calculation of (3.48), let's consider our example network, in Figure 3.1, and three bidirectional demands: one demand interconnecting nodes 1-2, one interconnecting nodes 1-3, and one interconnecting nodes 2-3. Figure 3.2 illustrates the routing of the three demands. The demand {1-2} is represented as a blue line; demand {1-3} as a green line and demand {2-3} as a red line. Notice the demand {2-3} traverses the node 1.

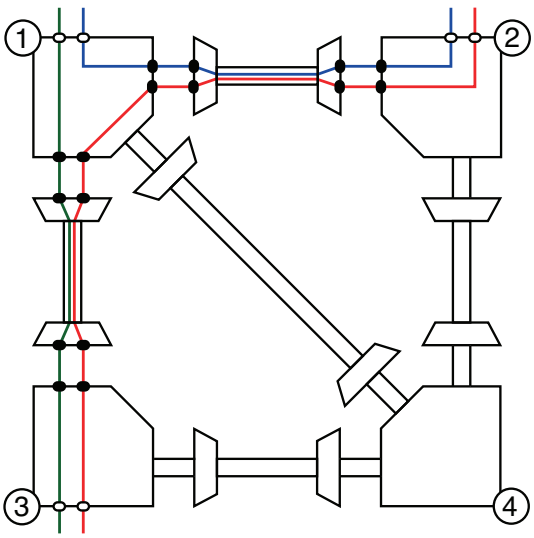

Figure 3.2: The example network in opaque mode and with three demands. Routing performed through the shortest path (in number of hops).

Now let's calculate the number of channels in node 1, with (3.48). We have $n_1^D = 2$ and $w_{1,1} = 0$, $w_{1,2} = 2$, $w_{1,3} = 2$, and $w_{1,4} = 0$. Thus, can write

$$n_{op,1}^{CH} = \frac{1}{2}\left(2 + (0 + 2 + 2 + 0)\right) = 3.$$

This result can also be obtained by counting the number of channels directly in the node 1 of Figure 3.2. Considering all nodes we obtain the total number of channels in opaque OXCs, which can be written as

$$\begin{aligned} N_{op}^{CH} = \sum_{n=1}^{N} n_{op,n}^{CH} &= \frac{1}{2}\sum_{n=1}^{N}\left(n_n^D + \sum_{j=1}^{N} w_{n,j}\right) \\ &= \frac{1}{2}\left(\sum_{n=1}^{N} n_n^D + \sum_{n=1}^{N}\sum_{j=1}^{N} w_{n,j}\right) \\ &= \frac{D_1 + 2W}{2}, \end{aligned} \tag{3.49}$$

where W is the total number of channels on links. Notice that the term $2W$ in (3.49) appears because each channel contributes twice in the summation of the number of channels transported in each link. Dividing (3.49) by the number of nodes we obtain the average number of channels per node, which is

$$\begin{aligned} \langle n_{op}^{CH} \rangle = \frac{N_{op}^{CH}}{N} &= \frac{D_1 + 2W}{2N} \\ &= \frac{D_1}{2N} + \frac{L}{L}\frac{2W}{2N} \\ &= \frac{\langle d \rangle}{2} + \langle \delta \rangle \frac{W}{2L}, \end{aligned} \tag{3.50}$$

where W/L is the average number of channels per link, $\langle w \rangle$. In the last expression, (3.50), we have taken into account the equation (3.4) and (3.8). Then we have,

$$\langle n_{op}^{CH} \rangle = \frac{\langle d \rangle + \langle \delta \rangle \langle w \rangle}{2}. \tag{3.51}$$

Considering our example network, Figure 3.1, with the demand matrix (3.5), we obtain $\langle n_{op}^{CH} \rangle = 4$. From (3.47) and (3.51) we obtain the average cost per OXC with

$$\langle c_{op}^{OXC} \rangle = \gamma^{OXC} + \langle n_{op}^{CH} \rangle \gamma^{SW}. \tag{3.52}$$

3.5.2.2 Cost of OXCs in Transparent Transport Mode

In transparent mode the OXC requires the same capabilities of opaque mode. In fact, the difference between the transport modes is the placement of transponders. Therefore, we can rewrite the expressions used for opaque mode, but only changing the index "op" to "tr" to indicate the transparent mode. Thus, we have

$$c_{tr,n}^{OXC} = \gamma^{OXC} + n_{tr,n}^{CH}\gamma^{SW}, \tag{3.53}$$

$$n_{tr,n}^{CH} = \frac{1}{2}\left(n_n^D + \sum_{j=1}^{N} w_{n,j}\right), \tag{3.54}$$

$$\begin{aligned} N_{tr}^{CH} = \sum_{n=1}^{N} n_{tr,n}^{CH} &= \frac{1}{2}\sum_{n=1}^{N}\left(n_n^D + \sum_{j=1}^{N} w_{n,j}\right) \\ &= \frac{1}{2}\left(\sum_{n=1}^{N} n_n^D + \sum_{n=1}^{N}\sum_{j=1}^{N} w_{n,j}\right) \\ &= \frac{D_1 + 2W}{2}, \end{aligned} \tag{3.55}$$

$$\langle n_{tr}^{CH}\rangle = \frac{\langle d\rangle + \langle\delta\rangle\langle w\rangle}{2}. \tag{3.56}$$

Obviously, considering our example network we obtain $\langle n_{tr}^{CH}\rangle = 4$. The average cost per OXC is obtained with

$$\langle c_{tr}^{OXC}\rangle = \gamma^{OXC} + \langle n_{tr}^{CH}\rangle\gamma^{SW}. \tag{3.57}$$

3.5.2.3 Cost of OXCs in Translucent Transport Mode

In translucent mode, we have to consider the number of demands that need regeneration. Each regeneration requires one additional capacity for switching, because the demand has to be dropped through an OXC tributary port and re-added through another OXC tributary port. The number of regenerations that a demand d has to suffer can be calculated with

$$n_d^R = \left\lceil \frac{P_d}{\Lambda} \right\rceil - 1, \tag{3.58}$$

where P_d is the path length of demand d, and Λ is the MTL. Considering all demands we obtain the number of regenerators in the network with

$$N^R = \sum_{d=1}^{D} n_d^R = \sum_{n=1}^{N} n_n^{DR}, \tag{3.59}$$

where n_n^{DR} is the number of demands that need regeneration at node n. Dividing (3.59) by N we obtain the average number of regenerators per node, then we have

$$\langle n^R \rangle = \frac{N^R}{N}. \tag{3.60}$$

We can calculate the cost of a translucent OXC with

$$c_{tl,n}^{OXC} = \gamma^{OXC} + n_{tl,n}^{CH} \gamma^{SW}. \tag{3.61}$$

where $n_{tl,n}^{CH}$ is the number of channels that are processed in the node n. Notice the "tl" index to indicate translucent mode configuration. We can obtain $n_{tl,n}^{CH}$ with

$$n_{tl,n}^{CH} = \frac{1}{2}\left(n_n^D + 2n_n^{DR} + \sum_{j=1}^{N} w_{n,j}\right), \tag{3.62}$$

In order to illustrate the calculation of (3.62), let's consider our example network, in Figure 3.1, and three bidirectional demands. Figure 3.3 illustrates the routing of the three demands. One demand interconnects nodes 1-2 (represented as a blue line), one interconnects nodes 1-3 (as a green line), and one interconnects nodes 3-4 (the orange line). Notice the demand {3-4} was not routed through the shortest path (it is just to show the regeneration). Considering the Maximum Transparency Length as $\Lambda = 600$ the demand {3-4} has to suffer one regeneration in the node 1, since its length is 724 km (notice the regenerator as a triangle shape above the node 1).

Now let's calculate the number of channels processed in node 1, with (3.62). We have $n_1^D = 2$, $n_1^{DR} = 1$ and $w_{1,1} = 0$, $w_{1,2} = 1$, $w_{1,3} = 2$, and $w_{1,4} = 1$. Thus, can write

$$n_{tl,1}^{CH} = \frac{1}{2}\left(2 + 2 + (0 + 1 + 2 + 1)\right) = 4.$$

This result can also be obtained by counting the number of channels directly in the

node 1 of Figure 3.3.

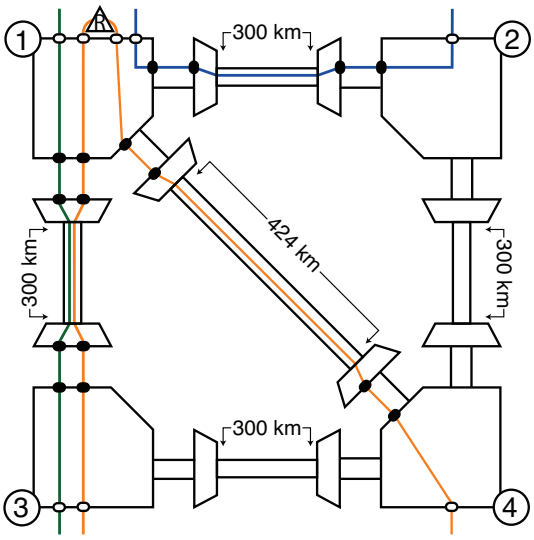

Figure 3.3: The example network in translucent mode and with three demands.

Considering all nodes we obtain the total number of channels in translucent OXCs, which can be written as

$$\begin{aligned} N_{tl}^{CH} = \sum_{n=1}^{N} n_{tl,n}^{CH} &= \frac{1}{2}\sum_{n=1}^{N}\left(n_n^D + 2n_n^{DR} + \sum_{j=1}^{N} w_{n,j}\right) \\ &= \frac{1}{2}\left(\sum_{n=1}^{N} n_n^D + \sum_{n=1}^{N} 2n_n^{DR} + \sum_{n=1}^{N}\sum_{j=1}^{N} w_{n,j}\right) \\ &= \frac{D_1 + 2N^R + 2W}{2}, \end{aligned} \tag{3.63}$$

Dividing (3.63) by N we obtain the average number of channels per translucent OXC, which is

$$\begin{aligned} \langle n_{tl}^{CH} \rangle = \frac{N_{tl}^{CH}}{N} &= \frac{D_1 + 2N^R + 2W}{2N} \\ &= \frac{D_1}{2N} + \frac{2N^R}{2N} + \frac{L}{L}\frac{2W}{2N} \\ &= \frac{\langle d \rangle + 2\langle n^R \rangle}{2} + \langle \delta \rangle \frac{W}{2L} \\ &= \frac{\langle d \rangle + 2\langle n^R \rangle + \langle \delta \rangle \langle w \rangle}{2}. \end{aligned} \tag{3.64}$$

Considering our example network, in Figure 3.1, and the demand matrix in (3.5) we have $\langle n^R \rangle = 0$ and $\langle n_{tl}^{CH} \rangle = 4$. From (3.61) and (3.64) we obtain the average cost of a translucent OXC with

$$\langle c_{tl}^{OXC} \rangle = \gamma^{OXC} + \langle n_{tl}^{CH} \rangle \gamma^{SW}. \tag{3.65}$$

3.5.3 Cost of Transponders

The number of transponders per node also depends on the traffic and the transport mode. In the next three sections we show how to obtain the cost of transponders in networks with opaque, transparent and translucent transport mode.

3.5.3.1 Cost of Transponders in Opaque Transport Mode

In order to provide an interface to signals coming from the client equipment, opaque networks may use short-reach transponders at the tributary ports of the OXC. One long-reach transponder is used at each OXC trunk port. Therefore, the cost of transponders for a node n in opaque networks is given by

$$c_{op,n}^{TSP} = n_n^{SR} \gamma^{SR} + n_n^{LR} \gamma^{LR}, \tag{3.66}$$

where n_n^{SR} is the number of short-reach transponders in the node n, γ^{SR} is the cost of a short-reach transponder, n_n^{LR} is the number of long-reach transponders in the node n and γ^{LR} is the cost of a long-reach transponder.

Since each add/drop channel uses a short-reach transponder we can write

$$n_n^{SR} = n_n^{D}, \tag{3.67}$$

and summing over all the nodes we obtain the total number of short-reach transponders in the network with

$$N^{SR} = \sum_{n=1}^{N} n_n^{SR} = D_1. \tag{3.68}$$

Dividing (3.68) by the number of nodes we obtain the average number of short-reach transponders per node, which can be written as

$$\langle n^{SR} \rangle = \frac{N^{SR}}{N} = \frac{D_1}{N} = \langle d \rangle. \tag{3.69}$$

Notice that, if the EXC trunk cards have the capability to interface directly with the OXC, short-reach transponders are not necessary. Considering our example network, Figure 3.1, and the demand matrix in (3.5) we obtain $\langle n^{SR} \rangle = 3.5$.

In order to calculate the number of long-reach transponders, we have to know the number of channels per node. Since long-reach transponders are used only on the trunk ports, using (3.48) we can obtain the number of long-reach transponders for an opaque node n with

$$n_{op,n}^{LR} = 2n_{op,n}^{CH} - n_n^D = \sum_{j=1}^{N} w_{n,j}. \tag{3.70}$$

Notice that we have to multiply the first term by two because each channel uses one input and one output ports. Considering all nodes we have

$$N_{op}^{LR} = \sum_{n=1}^{N} n_{op,n}^{LR} = \sum_{n=1}^{N} \sum_{j=1}^{N} w_{n,j} = 2W, \tag{3.71}$$

and dividing (3.71) by the number of nodes we obtain the average number of transponders per node,

$$\langle n_{op}^{LR} \rangle = \frac{N_{op}^{LR}}{N} = \frac{L}{L} \frac{2W}{N} = \langle \delta \rangle \langle w \rangle. \tag{3.72}$$

Considering our example network, Figure 3.1 and traffic matrix (3.5) we have an average of $\langle n_{op}^{LR} \rangle = 4.5$ long-reach transponders per node. From (3.66), (3.69) and (3.72) we obtain the average cost with transponders per node, in opaque networks, with

$$\langle c_{op}^{TSP} \rangle = \langle n^{SR} \rangle \gamma^{SR} + \langle n_{op}^{LR} \rangle \gamma^{LR}. \tag{3.73}$$

3.5.3.2 Cost of Transponders in Transparent Transport Mode

Short-reach transponders are not used in transparent mode. Long-reach transponders are placed at the tributary ports of OXCs, where they guide the signal into the network. Therefore, for transparent networks have

$$n_{tr,n}^{LR} = n_n^D, \tag{3.74}$$

and summing over all the nodes we obtain the total number of long-reach transponders in the network with

$$N_{tr}^{LR} = \sum_{n=1}^{N} n_{tr,n}^{LR} = N\langle d \rangle. \tag{3.75}$$

Considering the averages we obtain the average number of long-reach transponders per node, in transparent networks, with

$$\langle n_{tr}^{LR} \rangle = \frac{N_{tr}^{LR}}{N} = \langle d \rangle. \tag{3.76}$$

For our example network, Figure 3.1, and demand matrix (3.5) we obtain $\langle n_{tr}^{LR} \rangle = 3.5$, and from (3.76) we can obtain the average cost of transponders per node, in transparent networks, with

$$\langle c_{tr}^{TSP} \rangle = \langle n_{tr}^{LR} \rangle \gamma^{LR}. \tag{3.77}$$

3.5.3.3 Cost of Transponders in Translucent Transport Mode

In translucent networks, the number of long-reach transponders is calculated as in transparent networks. Therefore we have

$$n_{tl,n}^{LR} = n_n^D = \langle d \rangle, \tag{3.78}$$

Summing over all the nodes we obtain the total number of long-reach transponders in the network with

$$N_{tl}^{LR} = \sum_{n=1}^{N} n_{tl,n}^{LR} = N\langle d \rangle. \tag{3.79}$$

Considering the averages we obtain the average number of long-reach transponders per node, in translucent network, with

$$\langle n_{tl}^{LR} \rangle = \frac{N_{tl}^{LR}}{N} = \langle d \rangle. \tag{3.80}$$

And the average cost of transponders per node, in translucent networks, can be written as

$$\langle c_{tl}^{TSP} \rangle = \langle n_{tl}^{LR} \rangle \gamma^{LR}. \tag{3.81}$$

3.5.4 Cost of Regenerators

In opaque networks the signal is regenerated at every nodes. In transparent networks there is no regeneration, and in translucent networks the signal is regenerated only when necessary, i.e., when the length of a demand is longer than an Λ. The cost of regenerators for a node n in translucent networks is given by

$$c_n^{REG} = n_n^{DR} \gamma^{REG}, \tag{3.82}$$

where n_n^{DR} is the number of demands that need regeneration in node n, and γ^{REG} is the cost of a bidirectional regenerator. The total number of regenerators in a network can be calculated with (3.59), and using (3.60) we can obtain the average cost of regenerators per node with

$$\langle c^{REG} \rangle = \langle n^R \rangle \gamma^{REG}. \tag{3.83}$$

3.6 Number of Channels per Link

In order to evaluate the costs in a network, we need firstly to calculate the number of channels per link, which we denoted by W. Diviging W by the number of links L we obtain the average number of channels per link. In this section we show how to obtain the values for these variables.

The demands are routed across the network according to a routing algorithm (such as shortest path). Each demand occupies a unit of transmission capacity on each of the links interconnecting the source and destination nodes, i.e., if a source node is three hops away from the destination, a demand needs three units of capacity (one for each link). In this thesis a unit of transmission capacity is also called a channel. Because several solutions may exist for the same routing strategy, the number of channels in a specific link may differ from solution to solution [6, 7]. Therefore, as a preliminary evaluation, it makes sense to calculate the average number of channels per link.

One way to obtain the average number of channels per link is starting by obtaining the number of different routing solutions R for a given demand matrix $[d]$, which can be obtained by using the matrix $[d]$ and a routes matrix $[r]$. The routes matrix $[r]$ is an $N \times N$ matrix being each element ($r_{i,j}$) the number of different candidate routes (paths) to interconnect the nodes i and j. The matrix $[r]$ can be obtained from a

searching algorithm. In (3.84) we show a routes matrix for the network presented in Figure 3.1. The searching for the routes follow the shortest path strategy in number of hops.

$$[r] = \begin{bmatrix} 0 & 1 & 1 & 1 \\ 1 & 0 & 2 & 1 \\ 1 & 2 & 0 & 1 \\ 1 & 1 & 1 & 0 \end{bmatrix} \tag{3.84}$$

Given the matrices $[r]$ and $[d]$ we can obtain the number of different routing solutions with

$$R = \prod_{i=1}^{N-1} \prod_{j=i+1}^{N} d_{i,j} r_{i,j}, \quad \forall\, d_{i,j} \neq 0. \tag{3.85}$$

For our example network, Figure 3.1, we obtain $R = 4$.
Giving an integer number to represent each single demand presented in (3.5), as in

Node pair	1-2	1-3	1-4	2-3	2-3	2-4	3-4
Demand label	1	2	3	4	5	6	7

we can show the possible routings in Figure 3.4. Notice that the node pair $(2-3)$ appears twice, since there exist two single demands between them.

Each routing solution, χ_r, may be represented by L unidimensional vectors (one for each link l). Each unidimensional vector l_l holds D binary values (one for each demand, d), in which the value is 1 for a demand d that is carried through the link l_l or 0 otherwise. The structure of each routing solution χ_r may be defined as

$$\chi_r \begin{cases} l_1 & \rightarrow & d_1 & d_2 & \dots & d_D \\ l_2 & \rightarrow & d_1 & d_2 & \dots & d_D \\ \dots & \rightarrow & d_1 & d_2 & \dots & d_D \\ l_L & \rightarrow & d_1 & d_2 & \dots & d_D \end{cases}$$

and each element of the routing solution is defined as $\chi_{r,l,d}$, that is, $\chi_{r,l,d} = 1$ if the demand d is carried through the link l at the routing solution r.

Considering the routings presented in Figure 3.4 and the link order presented in Figure 3.5, we have the following four possible routing solutions:

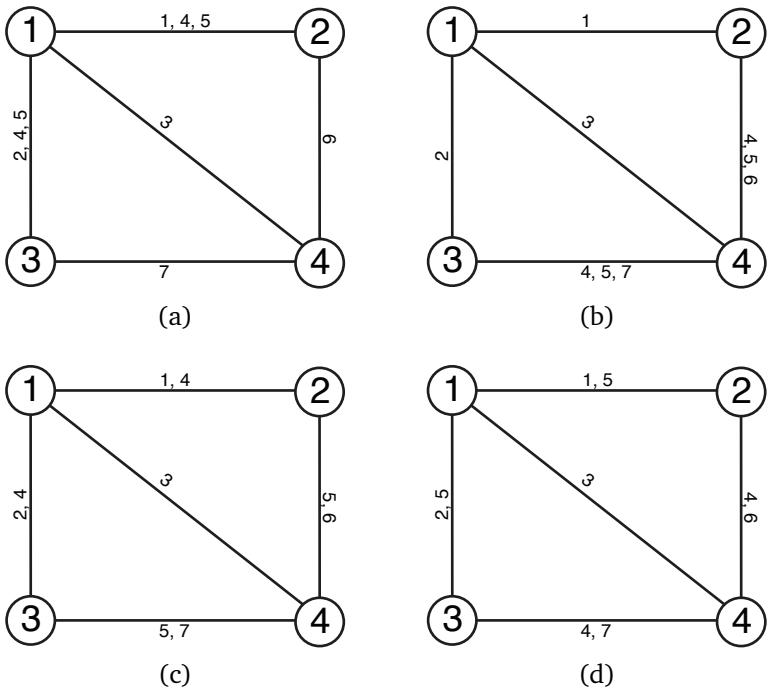

Figure 3.4: The four possible routing solutions for the network in Figure 3.1 and demand matrix in (3.5). The numbers close to the links are the demands routed through the links.

$$\chi_1 \left\{ \begin{array}{lcccccccc} l_1 & \rightarrow & 1 & 0 & 0 & 1 & 1 & 0 & 0 \\ l_2 & \rightarrow & 0 & 0 & 0 & 0 & 0 & 1 & 0 \\ l_3 & \rightarrow & 0 & 0 & 0 & 0 & 0 & 0 & 1 \\ l_4 & \rightarrow & 0 & 1 & 0 & 1 & 1 & 0 & 0 \\ l_5 & \rightarrow & 0 & 0 & 1 & 0 & 0 & 0 & 0 \end{array} \right. \qquad \chi_3 \left\{ \begin{array}{lcccccccc} l_1 & \rightarrow & 1 & 0 & 0 & 1 & 0 & 0 & 0 \\ l_2 & \rightarrow & 0 & 0 & 0 & 0 & 1 & 1 & 0 \\ l_3 & \rightarrow & 0 & 0 & 0 & 0 & 1 & 0 & 1 \\ l_4 & \rightarrow & 0 & 1 & 0 & 1 & 0 & 0 & 0 \\ l_5 & \rightarrow & 0 & 0 & 1 & 0 & 0 & 0 & 0 \end{array} \right.$$

$$\chi_2 \left\{ \begin{array}{lcccccccc} l_1 & \rightarrow & 1 & 0 & 0 & 0 & 0 & 0 & 0 \\ l_2 & \rightarrow & 0 & 0 & 0 & 1 & 1 & 1 & 0 \\ l_3 & \rightarrow & 0 & 0 & 0 & 1 & 1 & 0 & 1 \\ l_4 & \rightarrow & 0 & 1 & 0 & 0 & 0 & 0 & 0 \\ l_5 & \rightarrow & 0 & 0 & 1 & 0 & 0 & 0 & 0 \end{array} \right. \qquad \chi_4 \left\{ \begin{array}{lcccccccc} l_1 & \rightarrow & 1 & 0 & 0 & 0 & 1 & 0 & 0 \\ l_2 & \rightarrow & 0 & 0 & 0 & 1 & 0 & 1 & 0 \\ l_3 & \rightarrow & 0 & 0 & 0 & 1 & 0 & 0 & 1 \\ l_4 & \rightarrow & 0 & 1 & 0 & 0 & 1 & 0 & 0 \\ l_5 & \rightarrow & 0 & 0 & 1 & 0 & 0 & 0 & 1 \end{array} \right.$$

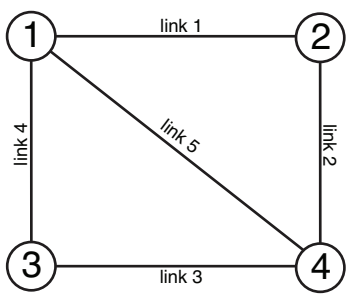

Figure 3.5: Labels of links in the network.

In order to obtain the number of channels in a link l, at a specific routing r, $w_{r,l}$, we may add the elements $\chi_{r,l,d} = 1$ for the given l and r, this may be represented as

$$w_{r,l} = \sum_{d=1}^{D} \chi_{r,l,d}. \tag{3.86}$$

From that, the average number of channels in a link (e.g. link 1) is obtained by the summation over $w_{r,l}$ divided by the number of different routing solutions, R. This can be written as

$$\langle w_l \rangle = \frac{1}{R} \sum_{r=1}^{R} \sum_{d=1}^{D} \chi_{r,l,d} = \frac{1}{R} \sum_{r=1}^{R} w_{l,r}. \tag{3.87}$$

Considering the link 1 (l_1) of our example network and the four possible routings we obtain $w_{1,1} = 3$, $w_{1,2} = 1$, $w_{1,3} = 2$ and $w_{1,4} = 2$. Then, using (3.87) we obtain $\langle w_1 \rangle = 2$.

In order to calculate the number of channels in a network, we do not need to consider each different routing possibility. To show this, we note that the number of channels on a link looking only the first routing is

$$w_l = \sum_{d=1}^{D} \chi_{1,l,d}. \tag{3.88}$$

Summing (3.88) over all links we obtain the total number of channels in the network, which can be written as

$$W = \sum_{l=1}^{L} w_l, \tag{3.89}$$

Similarly we can use $w_{i,j}$ instead of w_l to specify the end-points of the link l. Dividing the result from (3.89) by the number of links, L, we obtain the average number of channels per link, which can be written as [1]

$$\langle w \rangle = \frac{1}{L} \sum_{l=1}^{L} w_l = \frac{1}{L} \sum_{i=1}^{N-1} \sum_{j=i+1}^{N} 1 \times h_{i,j} = \frac{1}{L} \frac{D}{D} \sum_{i=1}^{N-1} \sum_{j=i+1}^{N} h_{i,j} = \frac{D\langle h \rangle}{L}. \tag{3.90}$$

Considering the expressions (3.11) (for the number of demands) and (3.4) (for the nodal degree) we can rewrite the expression (3.90) as

$$\langle w \rangle = \frac{N\langle d \rangle \langle h \rangle}{2L} = \frac{\langle d \rangle \langle h \rangle}{\langle \delta \rangle}. \tag{3.91}$$

For the network in Figure 3.1, and the demand matrix (3.5), we obtain $\langle d \rangle = 3.5$, $\langle h \rangle = 1.29$ and $\langle \delta \rangle = 2.5$, so it is estimated to have $\langle w \rangle = 1.8$ channels per link.

3.7 Number of Hops per Demand

As we observed in the previous section, the calculation of the average number of channels per link requires the average number of hops per demand. Thus, in this section we show how to obtain this variable.

In order to interconnect a node pair, it is required a route through the network that traverses one or more links. The set of links to that interconnect a node pair is also called a path and each traversed link represents a hop.

From the network topology we can obtain the hops matrix $[h]$, being each element ($h_{i,j}$) the path length (in number of hops) from the node i to the node j. Considering the shortest path, in number of hops, the hops matrix for the example network presented in Figure 3.1 is:

$$[h] = \begin{bmatrix} 0 & 1 & 1 & 1 \\ 1 & 0 & 2 & 1 \\ 1 & 2 & 0 & 1 \\ 1 & 1 & 1 & 0 \end{bmatrix} \tag{3.92}$$

This hops matrix can be obtained from the Dijkstra's shortest path algorithm [8]. Notice that in this case the traffic load is not considered. From the h and d matrices we can obtain the average number of hops for a given traffic load with

$$\langle h \rangle = \frac{1}{D} \sum_{i=1}^{N-1} \sum_{j=i+1}^{N} h_{i,j} d_{i,j}. \tag{3.93}$$

If the network topology and traffic demand are known, then we can calculate the exact value of $\langle h \rangle$. However, in the case of uncertainties about the traffic we may consider approximations. This issue is discussed in Chapter 5. For our sample network presented in Figure 3.1, and considering the hops matrix in (3.92) and the traffic demand presented in (3.5), the average number of hops per demand is $\langle h \rangle = 1.29$.

3.7.1 Number of Hops for Backup Paths

Depending on survivability scheme, the number of hops for backup may be required. Usually a backup path is a failure-disjoint path between itself and the working path. We might define the backup path as the second shortest path between a given pair of nodes, being the first shortest path the working path. This can be achieved by using an algorithm that finds the shortest cycle between the source and destination nodes, such as the Suurballe algorithm [9]. Considering the four-node network presented in Figure 3.1, the hops matrix for backup paths $[h']$ is given by

$$[h'] = \begin{bmatrix} 0 & 2 & 2 & 2 \\ 2 & 0 & 2 & 2 \\ 2 & 2 & 0 & 2 \\ 2 & 2 & 2 & 0 \end{bmatrix}. \tag{3.94}$$

From the matrices $[h']$ and $[d]$ we can obtain the average number of hops for the backup paths with,

$$\langle h' \rangle = \frac{1}{D} \sum_{i=1}^{N-1} \sum_{j=i+1}^{N} h'_{i,j} d_{i,j}. \tag{3.95}$$

As in $\langle h \rangle$, $\langle h' \rangle$ may be calculated exactly or approximated in the case of uncertainties. For our sample network presented in Figure 3.1, and considering the hops matrix in (3.94) and the traffic demand presented in (3.5), the average number of hops that each single connection request has to perform in its backup path is $\langle h' \rangle = 2$.

3.7.2 Number of Hops in Ring Topologies

Ring and mesh-based topologies have different characteristics in terms of the number of paths between the end-nodes. Rings have only two possible paths between the source and destination nodes (i.e., one path following the clockwise direction and another following the counter-clockwise). On the other hand, mesh-based topologies may have several paths between each node pair. In this section we present a mathematical derivation of the number of hops in ring network topologies.

We assume bidirectional rings with nodes labeled $\{1, \ldots, N\}$ in a clockwise direction. Node i, which is $1 < i < N$, is connected to nodes $i-1$ and $i+1$, node N is connected to node $N-1$ and node 1. Node 1 is connected to the node $i+1$ and

node N. Figure 3.6 shows a general example of two cases in a ring topology.

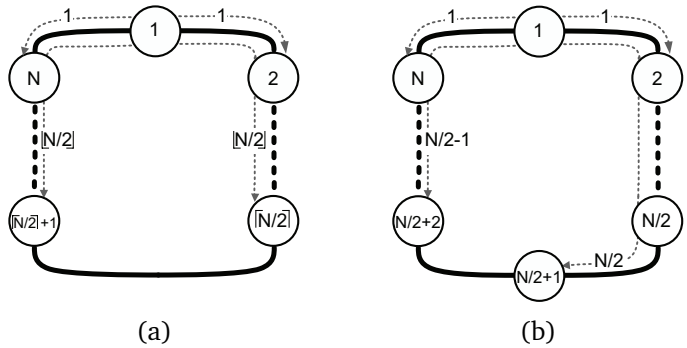

Figure 3.6: General ring topology with: (a) odd number of nodes and (b) even number of nodes. A demand is routed in a clockwise direction if the distance to the destination node is smaller than or equal to $\lfloor N/2 \rfloor$, otherwise the demand is routed counter-clockwise.

Considering Figure 3.6a, which is a ring with an odd number of nodes, a demand between nodes i and j is routed clockwise if $j - i \leq \lfloor N/2 \rfloor$, otherwise the demand is routed counter-clockwise. For the case of rings with even number of nodes, as in Figure 3.6b, the demand goes in a clockwise direction if $j - i \leq N/2$, otherwise the demand goes counter-clockwise. Then, the elements of the hops matrix for rings ($h_{r_{i,j}}$) with N nodes can be written as,

$$h_{r_{i,j}} = \begin{cases} j - i, & \text{for } j - i \leq \left\lfloor \frac{N}{2} \right\rfloor \\ \\ (i + N) - j, & \text{for } j - i > \left\lfloor \frac{N}{2} \right\rfloor \end{cases} . \tag{3.96}$$

For example, the hops matrix for the ring with $N = 5$, as in Figure 3.6a, is given by

$$[h_5] = \begin{bmatrix} 0 & 1 & 2 & 2 & 1 \\ 1 & 0 & 1 & 2 & 2 \\ 2 & 1 & 0 & 1 & 2 \\ 2 & 2 & 1 & 0 & 1 \\ 1 & 2 & 2 & 1 & 0 \end{bmatrix} , \tag{3.97}$$

and the hops matrix for a ring with $N = 6$, as in Figure 3.6b, is given by

$$[h_6] = \begin{bmatrix} 0 & 1 & 2 & 3 & 2 & 1 \\ 1 & 0 & 1 & 2 & 3 & 2 \\ 2 & 1 & 0 & 1 & 2 & 3 \\ 3 & 2 & 1 & 0 & 1 & 2 \\ 2 & 3 & 2 & 1 & 0 & 1 \\ 1 & 2 & 3 & 2 & 1 & 0 \end{bmatrix}. \tag{3.98}$$

The upper triangular (or lower) of the hops matrix has $N - 1$ diagonals that can be divided into two sets. Starting from the main diagonal, the first $\lfloor N/2 \rfloor$ diagonals correspond to the demands routed in a clockwise direction, and the other $\lceil N/2 \rceil - 1$ diagonals to the demands routed in a counter-clockwise direction. The expression for the number of paths with a certain number of hops is different for ring with odd and even number of nodes. Thus, each case was investigated separately.

Rings with odd number of nodes have $(N - x)$ paths with x number of hops in each diagonal, for $x = 1, \ \ldots, \ \lfloor N/2 \rfloor$. This corresponds to demands that are routed in a clockwise direction. Thus, we can calculate the total number of hops performed by demands routed in a clockwise direction for rings, h_{r_c}, using

$$h_{r_c} = \sum_{x=1}^{\lfloor N/2 \rfloor} x(N - x). \tag{3.99}$$

Considering the hops matrix in (3.97) we can find four paths with one hop in the first diagonal and then three paths with two hops in the second diagonal, therefore $h_{r_c} = 10$. For the demands going in a counter-clockwise direction there are $(\lfloor N/2 \rfloor - x)$ paths with length $(\lfloor N/2 \rfloor - x)$, for $x = 0, \ \ldots, \ \lfloor N/2 \rfloor - 1$. The total number of hops for demands routed in a counter-clockwise direction for ring topologies, $h_{r_{cc}}$, is given by,

$$h_{r_{cc}} = \sum_{x=0}^{\lfloor N/2 \rfloor - 1} \left(\left\lfloor \frac{N}{2} \right\rfloor - x \right)^2. \tag{3.100}$$

Looking at the two last diagonals of the matrix in (3.97), we observe two paths with two hops in the first diagonal of the second set and one path with one hop in the last diagonal, therefore $h_{r_{cc}} = 5$.

The total number of hops in ring topologies, h_r, with odd number of nodes is equal to the sum of (3.99) with (3.100),

$$h_r = \sum_{x=1}^{\lfloor N/2 \rfloor} x(N-x) + \sum_{x=0}^{\lfloor N/2 \rfloor - 1} \left(\left\lfloor \frac{N}{2} \right\rfloor - x \right)^2 . \tag{3.101}$$

For rings with even number of nodes there are $(N-x)$ paths with length x for $x = 1, \ldots, N/2$, corresponding to demands routed in a clockwise direction. In a counter-clockwise direction there are $(N/2 - x)$ paths with $(N/2 - x)$ hops, for $x = 1, \ldots, N/2 - 1$. Therefore, we can calculate the total number of hops by,

$$h_r = \sum_{x=1}^{N/2} x(N-x) + \sum_{x=1}^{N/2-1} \left(\frac{N}{2} - x \right)^2 . \tag{3.102}$$

For instance, considering the matrix in (3.98) and observing the diagonals, we can find five paths with one hop, four paths with two hops and three paths with three hops. Besides this, there are also two paths with two hops and one path with one hop.

Adding all the path lengths, i.e., solving expressions (3.101) and (3.102) we found that the total number of hops in a ring topology with N nodes is given by,

$$h_r = \begin{cases} \left(\left\lfloor \frac{N}{2} \right\rfloor\right)^3 - \left(\left\lfloor \frac{N}{2} \right\rfloor\right)^2 + \left\lfloor \frac{N}{2} \right\rfloor N \\ \quad + \dfrac{\left(\left\lfloor \frac{N}{2} \right\rfloor\right)^2 - \left(\left\lfloor \frac{N}{2} \right\rfloor\right)}{2}, & \text{for N odd} \\ \\ \left(\frac{N}{2}\right)^3, & \text{for N even} \end{cases} . \tag{3.103}$$

The average number of hops for ring topologies, considering the traffic load may be calculated with the expression (3.93).

3.7.3 Number of Hops of Backup Paths in Ring Topologies

In a ring topology with dedicated protection, the backup path traverses the ring in the opposite direction to the working path. Then, we can obtain the number of hops of

the backup path between i and j with,

$$h'_{r_{i,j}} = N - h_{r_{i,j}}, \tag{3.104}$$

that is the number of nodes minus the number of hops for the working path. From (3.104) we can find the matrix $[h']$ for the five-node ring,

$$[h'_5] = \begin{bmatrix} 0 & 4 & 3 & 3 & 4 \\ 4 & 0 & 4 & 3 & 3 \\ 3 & 4 & 0 & 4 & 3 \\ 3 & 3 & 4 & 0 & 4 \\ 4 & 3 & 3 & 4 & 0 \end{bmatrix}, \tag{3.105}$$

and for the six-node ring,

$$[h'_6] = \begin{bmatrix} 0 & 5 & 4 & 3 & 4 & 5 \\ 5 & 0 & 5 & 4 & 3 & 4 \\ 4 & 5 & 0 & 5 & 4 & 3 \\ 3 & 4 & 5 & 0 & 5 & 4 \\ 4 & 3 & 4 & 5 & 0 & 5 \\ 5 & 4 & 3 & 4 & 5 & 0 \end{bmatrix}. \tag{3.106}$$

Using (3.101), (3.102) and (3.104) the total number of backup hops can be obtained. In rings with odd number of nodes there are $(N - x)$ backup paths with $(N - x)$ number of hops, for $x = 1, \ldots, \lfloor N/2 \rfloor$, in the counter-clockwise direction and $(\lfloor N/2 \rfloor - x)$ paths with $N - (\lfloor N/2 \rfloor - x)$ hops, for $x = 0, \ldots, \lfloor N/2 \rfloor - 1$ in the clockwise direction. Therefore, we can write

$$h'_r = \sum_{x=1}^{\lfloor N/2 \rfloor} (N - x)^2 + \sum_{x=0}^{\lfloor N/2 \rfloor - 1} \left(\left\lfloor \frac{N}{2} \right\rfloor - x \right) \left(N - \left(\left\lfloor \frac{N}{2} \right\rfloor - x \right) \right). \tag{3.107}$$

In the same way, the total number of backup paths for rings with even number of nodes can be obtained by

$$h'_r = \sum_{x=1}^{N/2} (N - x)^2 + \sum_{x=1}^{N/2-1} \left(\frac{N}{2} - x \right)^2. \tag{3.108}$$

Considering the matrix in (3.106) we have five paths with five hops, four paths with four hops and three paths with three hops. Besides that there are two paths with four hops and one path with five hops.

Solving (3.107) and (3.108) results in the exact value of the total backup hops in ring topologies, h'_r,

$$h'_r = \begin{cases} \left(\lfloor \frac{N}{2} \rfloor - 1\right)\left(N^2 + \lceil \frac{N}{2} \rceil \lfloor \frac{N}{2} \rfloor\right) + \lceil \frac{N}{2} \rceil N + \frac{\left(\lfloor \frac{N}{2} \rfloor\right)^3 - \left(\lfloor \frac{N}{2} \rfloor\right)^2}{2} \\ \qquad - \lceil \frac{N}{2} \rceil \left(\frac{\left(\lfloor \frac{N}{2} \rfloor - 1\right)\lfloor \frac{N}{2} \rfloor}{2}\right) - N\left(\left(\lfloor \frac{N}{2} \rfloor - 1\right)\lfloor \frac{N}{2} \rfloor\right), & \text{for N odd} \\ \frac{3N^3 - 4N^2}{8}, & \text{for N even} \end{cases} . \quad (3.109)$$

From (3.103) and (3.109), we obtain for the five-node ring a total of 15 hops in working paths and 35 hops in backup paths. The ring with six nodes has 27 hops in working paths and 63 hops in backup paths.

3.8 Survivability Coefficients

Transport networks have to be tolerant to failures to allow high availability of connections. In order for a network being able to recover from a failure, operators employ a fraction of spare capacity over the working capacity. However, employing too much spare capacity will represent a waste of resources and money while employing less than the required spare capacity may represent loss of revenues (e.g. due to violations of service level agreements). In this section we discuss how to calculate the spare capacity necessary for a network to survive against a single link failure, considering dedicated path protection and shared path restoration.

3.8.1 Protection Capacity Coefficient

In dedicated path protection a dedicated disjoint backup path is pre-established to protect each working path. In order to differentiate the number of hops for working paths from the ones required for the backup paths, we consider two matrices, $[h]$ and $[h']$, for the working and backup number of hops, respectively. The average number of hops for backup paths, $\langle h' \rangle$, can be obtained using the expression (3.93), but replacing $h_{i,j}$ by $h'_{i,j}$, which is the number of hops for the second shortest path between the nodes i and j. Similarly, the average number of backup channels per link, $\langle w' \rangle$, can be obtained using the expression (3.91), but replacing $\langle h \rangle$ by $\langle h' \rangle$. From $\langle w \rangle$ and $\langle w' \rangle$, we can calculate the fractional amount of additional capacity required to implement path dedicated protection against single link failures [1, 10], which we call protection coefficient,

$$\langle k_p \rangle = \frac{\langle w' \rangle}{\langle w \rangle} = \frac{\frac{\langle d \rangle \langle h' \rangle}{\langle \delta \rangle}}{\frac{\langle d \rangle \langle h \rangle}{\langle \delta \rangle}} = \frac{\langle h' \rangle}{\langle h \rangle}. \tag{3.110}$$

Expression (3.110) is valid for any traffic model considering dedicated path protection. Nevertheless, the values of $\langle h \rangle$ and $\langle h' \rangle$ are dependent on the traffic model. When $\langle h' \rangle$ is the average value for the second shortest path, $\langle h' \rangle$ is traditionally equal or higher than $\langle h \rangle$. Furthermore, $\langle k_p \rangle$ is always greater or equal to one.

Considering the four-node and five-link example network presented in Figure 3.1 and the traffic demand presented in (3.5) we obtain $\langle k_p \rangle = 2/1.29 = 1.55$, which means that the network needs 155% of extra capacity to guarantee survivability against single link failures. The value of $\langle k_p \rangle$ can be calculated exactly when the demand matrix $[d]$ and the network topology is given. However, in the lack of information, approximations can be obtained. Notice that the approximation for $\langle k_p \rangle$ is dependent on the approximation of $\langle h' \rangle$ and $\langle h \rangle$.

3.8.2 Restoration Capacity Coefficient

A network with N nodes and L links may be arranged in many different topologies. Each topology may have a different average number of hops, $\langle h \rangle$, variance of nodal

degree, $\sigma^2(\delta)$, and resource sharing. All those parameters affect the required needed spare capacity in order to guarantee survivability. In this thesis we consider the spare capacity of a link, ψ_l, as the ensemble of channels available to restore services. The summation of ψ_l over all links yields the spare capacity of the network, Ψ (in number of channels). The survivability coefficient of a link, k_l, is the fractional increase above the average number of channels on links, $\langle w \rangle$, (which is also known as the working capacity) and it is defined as

$$k_l = \frac{\psi_l}{\langle w \rangle}. \tag{3.111}$$

The survivability coefficient for a network is defined as a mean over the number of links

$$\langle k \rangle = \frac{1}{L} \sum_{l=1}^{L} k_l. \tag{3.112}$$

Using (3.111) in (3.112) we obtain

$$\langle k \rangle = \frac{1}{L} \sum_{l=1}^{L} \frac{\psi_l}{\langle w \rangle} = \frac{1}{L\langle w \rangle} \sum_{l=1}^{L} \psi_l = \frac{\Psi}{W}. \tag{3.113}$$

The average number of channels on links, $\langle w \rangle$, and needed spare capacity for restoration, Ψ_{min}, can be exactly calculated (for a given routing and restoration scheme) when the network topology and traffic is known. Adding W and Ψ_{min} we obtain the overall capacity of the network in order to achieve survivability,

$$W_{min}^{k_r} = W + \Psi_{min}. \tag{3.114}$$

The restoration coefficient of a network, $\langle k_r \rangle$, is defined as

$$\langle k_r \rangle = \frac{\Psi_{min}}{W}. \tag{3.115}$$

Both W and Ψ_{min} depend on the network topology and the traffic demand model, however we have analyzed networks with uniform and random traffic models and found that there is not a significant difference in terms of restoration coefficient [11].

Notice that W also depends on the routing scheme while Ψ_{min} also depends on the restoration scheme. The value of $\langle k_r \rangle$ depends on the network topology.

In the following we present the steps necessary to obtain the $\langle k_r \rangle$ from a given topology and traffic demand.

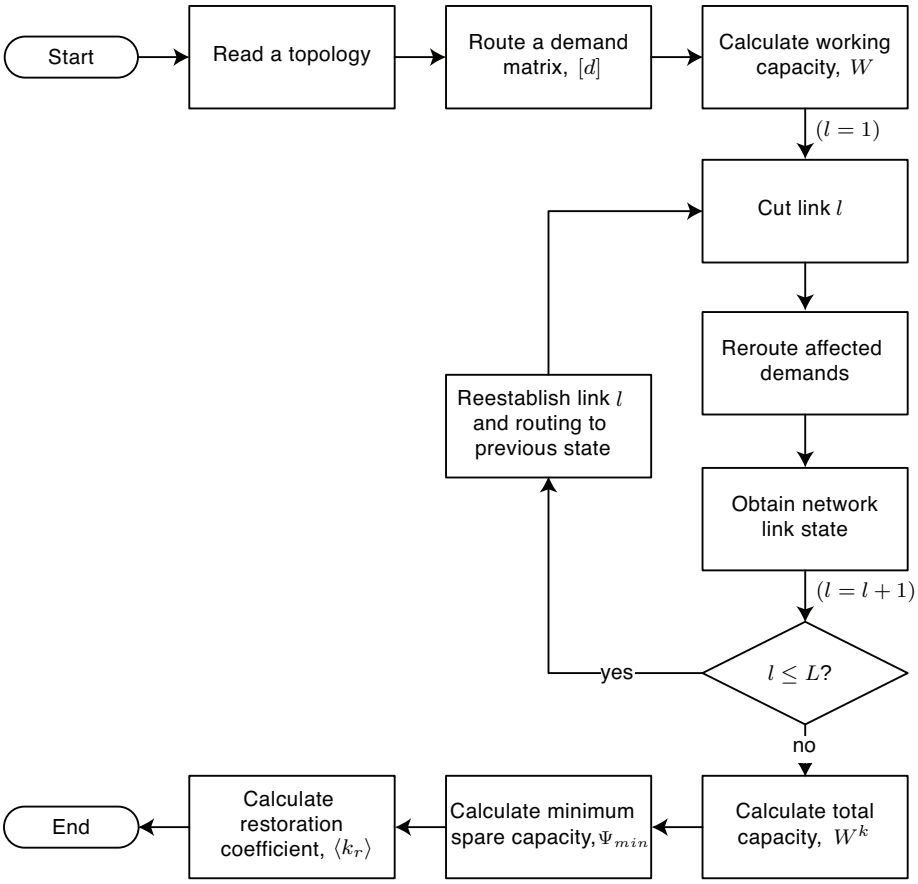

Figure 3.7: From a network topology and after routing the traffic, the working capacity is calculated. Next in order to calculate the spare capacity, a failure is generated in each link. In order to recover from the failure, the affected traffic must be rerouted, which adds and tears down capacity in some other links. After performing this procedure for all the links, the total capacity, the needed spare capacity and the restoration coefficient are calculated.

As shown on the flowchart in Figure 3.7, given a survivable network topology with no link capacity constraints, the demands in a matrix $[d]$ are routed through the network. After routing all demands each link holds the number of optical channels necessary to support the traffic, without considering survivability (i.e., the working capacity for the links).

The total number of optical channels in the network is given by

$$W = \sum_{i=1}^{N-1} \sum_{j=i+1}^{N} w_{i,j}. \tag{3.116}$$

in which $w_{i,j}$ is the number of channels in the link that connects the nodes i and j. The elements $w_{i,j}$ are members of an optical channels matrix $[o]$.

To calculate the capacity for the network recover from single link failures, links are removed from the topology (simulation of a fiber cut), one-by-one with replacement, see Figure 3.8b to 3.8g. For each link cut, a new $[o^f]$ matrix is generated, which stores the number of channels on every link after a single link failure. Each $[o^f]$ matrix represents the link state after recovering from a failure on link f, which imposes either extra or tear down capacity in some links. After all possible link cut are simulated, an optical channels matrix that considers survivability, $[o^{k_r}]$, is generated from

$$w_{i,j}^{k_r} = max_f\{w_{i,j}^{k_r,f}\} \ , i,j = \{1,...,N\} \ , f = \{1,...,L\}. \tag{3.117}$$

The summation of the $w_{i,j}^{k_r}$ elements (with $i < j$) yields the total capacity required, considering survivability, which can be expressed as

$$W^{k_r} = \sum_{i=1}^{N-1} \sum_{j=i+1}^{N} w_{i,j}^{k_r}. \tag{3.118}$$

Subtracting from (3.118) the working capacity, (3.116), we obtain an amount of extra capacity enough to guarantee restoration. Some optimization can be made on the computation of the $[o^k]$ matrix, which leads eventually to a smaller W^{k_r}. However, based on extensive simulations we observed that its effect on the accuracy of the prediction for the restoration coefficient is negligible. Thus we assume that from (3.116) and (3.118) we obtain

$$\Psi_{min} = W^{k_r} - W. \tag{3.119}$$

Thereafter the $\langle k_r \rangle$ value is calculated from (3.115).

3.8.2.1 Illustrative Example

Let's assume a network with five nodes, $N = 5$, and six links, $L = 6$, and a uniform and unitary demand matrix to illustrate the procedure described in Figure 3.7. Figure 3.8a shows a survivable topology with the traffic matrix routed through it. The numbers close to the links are the bidirectional demands that cross the links. After the

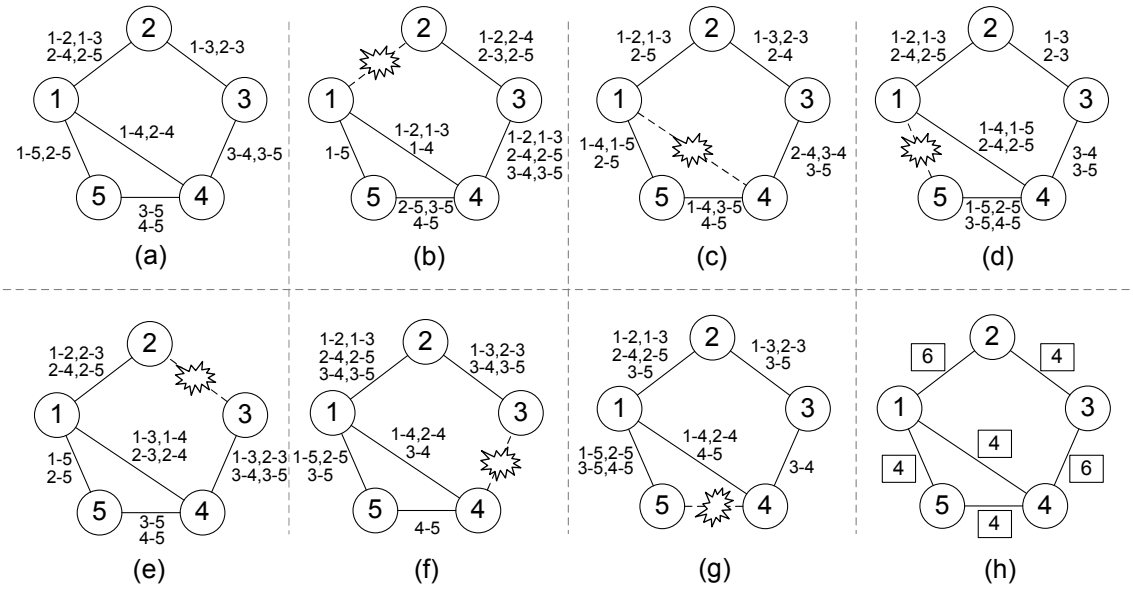

Figure 3.8: Over a survivable mesh network topology, traffic is routed following the shortest path scheme, (a). In order to calculate the spare capacity required to recover from any single link failure, from (b) to (g), the affected demands are released from the network and rerouted again. Finally, the maximum number of channels on each link is calculated, see (h), i.e., the working capacity plus the needed spare capacity.

first routing procedure, the number of optical channels on links can be represented as a symmetrical matrix, $[o]$, which for our example holds the following values,

$$[o] = \begin{bmatrix} 0 & 4 & 0 & 2 & 2 \\ 4 & 0 & 2 & 0 & 0 \\ 0 & 2 & 0 & 2 & 0 \\ 2 & 0 & 2 & 0 & 2 \\ 2 & 0 & 0 & 2 & 0 \end{bmatrix}. \tag{3.120}$$

This matrix is used to calculate the total number of channels without survivability, W, which is the capacity required to transport the demands. Thus, using (3.116) we obtain $W = 14$. Afterwards, it is simulated a failure on link 1 which connects the nodes $(1, 2)$, see Figure 3.8b. The affected demands are {1-2, 1-3, 2-4, 2-5}, and they should be released from all the links where they are assigned, i.e., from the links between the nodes $(2, 3)$, $(1, 4)$ and $(1, 5)$. Table 3.1 shows the restoration result in case of a link cut between the nodes $(1, 2)$. In the third column, the added demands for each link are shown. The fourth column shows the released demands for each link. Finally, the last column holds the required spare capacity on each link in the event of a failure, which is the subtraction between the number of added and released demands.

Table 3.1: Added/Released demands and the required spare capacity for each link in the event of a failure on link $(1, 2)$.

Link N^o	Nodes	Added Demands	Released	Added-Released
1	(1, 2)	x	x	x
2	(1, 4)	1-2, 1-3	2-4	1
3	(1, 5)		2-5	-1
4	(2, 3)	1-2, 2-4, 2-5	1-3	2
5	(3, 4)	1-2, 1-3, 2-4, 2-5		4
6	(4, 5)	2-5		1

The negative number, -1, on link $(1, 5)$ means that an affected demand was released, {2-5}, but no one was rerouted through that link. After the affected demands are rerouted through the restoration path, the $[o^1]$ matrix holds the following values,

$$[o^1] = \begin{bmatrix} 0 & x & 0 & 3 & 1 \\ x & 0 & 4 & 0 & 0 \\ 0 & 4 & 0 & 6 & 0 \\ 3 & 0 & 6 & 0 & 3 \\ 1 & 0 & 0 & 3 & 0 \end{bmatrix}, \tag{3.121}$$

which is a copy of the $[o]$ matrix with its elements updated with the values presented in the fifth column of the Table 3.1. The symbol "x" on the $o^1_{1,2}$ element indicates that the

link $(1,2)$ is down. After performing the link cut for all the links, we can use (3.117) to obtain the $[o^{k_r}]$ matrix. For our example, the $[o^{k_r}]$ matrix holds the following values,

$$[o^{k_r}] = \begin{bmatrix} 0 & 6 & 0 & 4 & 4 \\ 6 & 0 & 4 & 0 & 0 \\ 0 & 4 & 0 & 6 & 0 \\ 4 & 0 & 6 & 0 & 4 \\ 4 & 0 & 0 & 4 & 0 \end{bmatrix}. \tag{3.122}$$

From $[o^{k_r}]$ and using (3.118), we obtain $W^{k_r} = 28$, see Figure 3.8h, and using (3.119) we obtain $\Psi_{min} = 14$. Finally we can obtain the fractional increase for survivability with (3.115), which for our example is $\langle k_r \rangle = 1$. This concludes the illustration of the use of flowchart presented in Figure 3.7. In the following paragraphs we illustrate the calculation of the resource sharing for the same five-node network scenario.

In case of restoration the spare capacity of a network may be shared by a number of demands, and its use depends on the place where a failure occurs and on the restoration scheme. As we assume the shortest path restoration scheme [12] with stub release [13], in case of a link failure, all the channels of the affected demands should be released from their original paths and rerouted. These released channels may be reused, in the restoration process, to improve the resource utilization.

We define link sharing, denoting by ϕ_l, as the ratio between the number of distinct demands that could cross a link l, w_l^* (considering single link failures), and the capacity (in terms of number of channels) of the link l, considering restoration, $w_l^{k_r}$. Therefore, the ϕ_l can be written as

$$\phi_l = \frac{w_l^*}{w_l^{k_r}}, \tag{3.123}$$

We can obtain w_l^* with

$$w_l^* = \sum_{f=1, f \neq l}^{L} w_{lf}^*, \tag{3.124}$$

where w_{lf}^* denotes the number of distinct demands that could cross the link l in the

event of failure on link f. As we can notice from (3.123), link sharing equal to one means that there is no sharing at all, because each available capacity is used by only one demand. On the other hand, if link sharing is equal or greater than two, it means that each unit of capacity available can be used by two or more demands (one at a time, of course).

Considering the mean value of ϕ_l over all links, we obtain the network resource sharing, $\langle\phi\rangle$, which can be written as

$$\langle\phi\rangle = \frac{1}{L}\sum_{l=1}^{L}\phi_l. \tag{3.125}$$

In order to calculate the resource sharing, $\langle\phi\rangle$, we need first to calculate the link sharing, ϕ_l, for all the links. In the first row of Table 3.2 we can see the demands that use link 1, which connects the nodes $1-2$, in a failure free scenario, see Figure 3.8a.

Table 3.2: Demands that could cross the link 1.

Cut in link N^o	nodes	Demands crossing the link 1
none	none	<u>1-2</u>, <u>1-3</u>, <u>2-4</u>, <u>2-5</u>
1	(1, 2)	
2	(1, 4)	1-2, 1-3, 2-5
3	(1, 5)	1-2, 1-3, 2-4, 2-5
4	(2, 3)	1-2, <u>2-3</u>, 2-4, 2-5
5	(3, 4)	1-2, 1-3, 2-4, 2-5, <u>3-4</u>, <u>3-5</u>
6	(4, 5)	1-2, 1-3, 2-4, 2-5, 3-5
Total		7 distinct demands (as underlined text)

If a link cut occurs in link 1 all these demands have to be rerouted using other links, this situation is presented in the second row of Table 3.2. In third row is considered a cut in link 2. After restoration we can see that link 1 is only used by the following demands: $\{1-2\}$, $\{1-3\}$ and $\{2-5\}$. In the other rows of the table are presented the results obtained when a cut occurs in any other link. The distinct demands on link 1 are shown as underlined text. The summation of the distinct demands yields $w_1^* = 7$. Figure 3.8h shows that the link $(1,2)$ has capacity to support six optical channels, $w_1^{k_r} = 6$. Therefore, using (3.123), we have $\phi_1 = 1.17$. Calculating ϕ_l for all the links

and using (3.125) we obtain the network resource sharing, $\langle\phi\rangle$. Table 3.3 shows both the link and the resource sharing for our five-node example network.

Table 3.3: Link and resource sharing.

Link N^o	Nodes	w_l^*	$w_l^{k_r}$	ϕ_l
1	(1, 2)	7	6	1.17
2	(1, 4)	9	4	2.25
3	(1, 5)	5	4	1.25
4	(2, 3)	7	4	1.75
5	(3, 4)	7	6	1.17
6	(4, 5)	5	4	1.25
Resource sharing, $\langle\phi\rangle$				1.47

3.9 Cost of Links with Survivability

In case of a link failure, the affected demands have to be rerouted through alternative paths. This means that the network has to be dimensioned to support the working channels and a number of additional channels (also called backup channels). We can obtain the number of channels on a link, considering survivability, with

$$w_l^k = w_l + \psi_l. \tag{3.126}$$

Using the averages we can write

$$\langle w^k\rangle = \langle w\rangle + \langle w\rangle\frac{1}{L}\sum_{l=1}^{L} k_l = \langle w\rangle + \langle w\rangle\langle k\rangle = \langle w\rangle(1+\langle k\rangle). \tag{3.127}$$

Notice that $\langle k\rangle$ represents a general case for survivability, we must use $\langle k_p\rangle$ if dedicated protection survivability is chosen, or $\langle k_r\rangle$ for shared path restoration. Therefore, to consider survivability in the model, we have to add the protection or restoration capacity, using the protection coefficient, $\langle k_p\rangle$, or restoration coefficient, $\langle k_r\rangle$, and the average number of channels per link, $\langle w\rangle$, which will result in $\langle w^{k_p}\rangle$ and $\langle w^{k_r}\rangle$. As a consequence, the calculation of the number of network components will consider the

number of working and backup channels.

A key expression for survivability in links is the one that calculates the number of transmission systems. Therefore, from (3.23) we have

$$n_l^{S,k} = \left\lceil \frac{w_l^k}{S} \right\rceil . \tag{3.128}$$

Dividing (3.128) by the number of links we obtain the average number of transmission systems per link,

$$\langle n^{S,k} \rangle = \frac{1}{L} \sum_{l=1}^{L} n_l^{S,k}. \tag{3.129}$$

From (3.129) we can calculate the average number of OLTs per link, considering survivability as

$$\langle n^{OLT,k} \rangle = 2 \langle n^{S,k} \rangle. \tag{3.130}$$

Using (3.130) we can calculate the average cost of OLTs per link, considering survivability, as

$$\langle c^{OLT,k} \rangle = \langle n^{OLT,k} \rangle \gamma^{OLT}. \tag{3.131}$$

From (3.30) and (3.128) we can calculate the total number of optical amplifiers, in the network, considering survivability with

$$N^{A,k} = \sum_{l=1}^{L} n_l^{A,k}, \tag{3.132}$$

where $n_l^{A,k}$ is the number of optical amplifiers in a link l, considering survivability, which can be obtained using (3.128) in (3.29), which is:

$$n_l^{A,k} = \left(\left\lceil \frac{\nu_l}{\partial} \right\rceil - 1 \right) n_l^{S,k}. \tag{3.133}$$

Dividing (3.132) by the number of links we obtain the average number of optical amplifiers per link considering survivability, which can be written as

$$\langle n^{A,k} \rangle = \frac{N^{A,k}}{L}, \tag{3.134}$$

and the cost of OAs considering survivability is

$$\langle c^{A,k} \rangle = \langle n^{A,k} \rangle \gamma^{A}. \tag{3.135}$$

Similarly, we can calculate the number of optical fibers considering survivability. From (3.34) and (3.128) we can obtain the total quantity of optical fibers in the network as

$$N^{F,k} = \sum_{l=1}^{L} 2\nu_l n_l^{S,k}, \tag{3.136}$$

and considering the averages we have

$$\langle n^{F,k} \rangle = \frac{N^{F,k}}{L}. \tag{3.137}$$

Therefore, the cost with optical fibers considering survivability is

$$\langle c^{F,k} \rangle = \langle n^{F,k} \rangle \gamma^{F}. \tag{3.138}$$

Using (3.131), (3.135) and (3.138) we can obtain the total cost of links with

$$C_L^k = L\Big(\langle c^{OLT,k} \rangle + \langle c^{A,k} \rangle + \langle c^{F,k} \rangle \Big), \tag{3.139}$$

and the average cost per link with

$$\langle c_l^k \rangle = \langle c^{OLT,k} \rangle + \langle c^{A,k} \rangle + \langle c^{F,k} \rangle. \tag{3.140}$$

Notice that we can use $\langle c_l^{k_p} \rangle$ and $\langle c_l^{k_r} \rangle$ to indicate that the survivability is based on dedicated path protection or shared path restoration, respectively.

3.10 Cost of Nodes with Survivability

Since we consider survivability at optical layer, EXCs are not affected by survivability schemes. The OXCs, however, have to be equipped with larger switching capability. The number of channels that an OXC has to deal with increases when survivability is required. Moreover, it depends on the traffic, survivability scheme and transport mode. Regarding the transponders, only long-reach transponders are affected in opaque transport mode. Regenerators are affected in translucent transport mode. Therefore, the average cost of nodes, considering survivability can be written as

$$\langle c_n^k \rangle = \langle c^{EXC} \rangle + \langle c_{tm}^{OXC} \rangle + \langle c_{tm}^{TSP,k} \rangle + \langle c_{tm}^{REG,k} \rangle, \tag{3.141}$$

where “tm” indicates the transport mode. Multiplying (3.141) by the number of nodes we obtain the total cost of nodes considering survivability,

$$C_N^k = N \langle c_n^k \rangle. \tag{3.142}$$

In this section we show how to obtain the cost of nodes considering dedicated path protection and shared path restoration schemes, for opaque, transparent and translucent networks.

3.10.1 Cost of OXCs with Dedicated Path Protection in Opaque and Transparent Networks

The calculation of the costs of OXCs for opaque and transparent networks does not differ. We assume dedicated path protection using single-ended switching, which protection transponders are used to perform the switching. A protection transponder splits the input signal into a working and protection path, and these paths feed two tributary OXC ports [14]. The OXC switches the working and protection signals to the appropriated trunk ports. At the receiver end, the better signal is selected and forwarded to EXC. This mechanism is called single-ended switching because one

switching action is sufficient to recover the affected signal [13]. Thus, it is required two OXC tributary ports for each add/drop channel. The cost of an OXC, considering survivability is:

$$c_{op,n}^{OXC,k_p} = \gamma^{OXC} + n_{op,n}^{CH,k_p}\gamma^{SW}, \tag{3.143}$$

where $n_{op,n}^{CH,k_p}$ is the number of bidirectional channels, including protection capacity, that are processed in the opaque node n, which can be obtained with

$$n_{op,n}^{CH,k_p} = \frac{1}{2}\left(2n_n^D + \sum_{j=1}^{N} w_{n,j}^{k_p}\right), \tag{3.144}$$

where $w_{n,j}^{k_p}$ is the number of channels connecting nodes n, j, including protection.

In order to illustrate the calculation of (3.144), let's consider our example network, in Figure 3.1, and three bidirectional demands with dedicated path protection: one demand interconnecting nodes 1-2, one interconnecting nodes 1-3, and one interconnecting nodes 2-3. Figure 3.9 illustrates the routing of that demands.

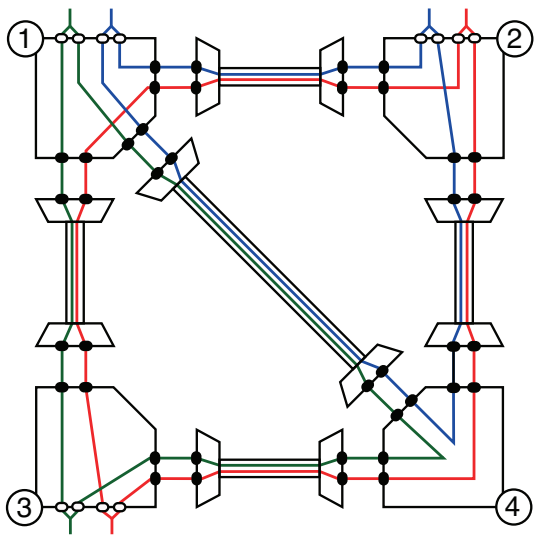

Figure 3.9: The example network in opaque mode, with three demands and dedicated protection. Routing is performed through the shortest path for working and through the second shortest path for protection.

The blue line represents the demand {1-2}, the green line the demand {1-3} and the red line the demand {2-3}. The shortest path between the end nodes is the working

path and the second shortest path the backup path. For instance, the demand {1-2} is routed through nodes 1-2 for working and through nodes 1-4-2 for backup. Now let's calculate the number of channels processed in node 1, with (3.144). We have $n_1^D = 2$ and $w_{1,1}^{k_p} = 0$, $w_{1,2}^{k_p} = 2$, $w_{1,3}^{k_p} = 2$, and $w_{1,4}^{k_p} = 2$. Thus, can write

$$n_{op,1}^{CH,k_p} = \frac{1}{2}\Big(2 \times 2 + \Big(0 + 2 + 2 + 2\Big)\Big) = 5.$$

This result can also be obtained by counting the number of channels (colored lines) directly in the node 1 of Figure 3.9. Considering all nodes we obtain

$$\begin{aligned} N_{op}^{CH,k_p} = \sum_{n=1}^{N} n_{op,n}^{CH,k_p} &= \frac{1}{2}\sum_{n=1}^{N}\left(2n_n^D + \sum_{j=1}^{N} w_{n,j}^{k_p}\right) \\ &= \frac{1}{2}\left(\sum_{n=1}^{N} 2n_n^D + \sum_{n=1}^{N}\sum_{j=1}^{N} w_{n,j}^{k_p}\right) \\ &= D_1 + W^{k_p}, \end{aligned} \tag{3.145}$$

where W^{k_p} is the total number of channels on links, including protection capacity. Dividing (3.145) by the number of nodes we obtain the average number of channels processed per OXC, including protection capacity, which can be written as

$$\begin{aligned} \langle n_{op}^{CH,k_p} \rangle = \frac{N_{op}^{CH,k_p}}{N} &= \frac{2D_1 + 2W^{k_p}}{2N} \\ &= \frac{2D_1}{2N} + \frac{L}{L}\frac{2W^{k_p}}{2N} \\ &= \langle d \rangle + \langle \delta \rangle \frac{W^{k_p}}{2L}, \end{aligned} \tag{3.146}$$

where W^{k_p}/L is the average number of channels per link including protection capacity, $\langle w^{k_p} \rangle$. Therefore, we can rewrite (3.146) as

$$\langle n_{op}^{CH,k_p} \rangle = \langle d \rangle + \frac{\langle \delta \rangle \langle w^{k_p} \rangle}{2}. \tag{3.147}$$

From (3.143) and (3.147) we obtain the average cost per opaque OXC, including

protection capacity with

$$\langle c_{op}^{OXC,k_p} \rangle = \gamma^{OXC} + \langle n_{op}^{CH,k_p} \rangle \gamma^{SW}. \tag{3.148}$$

In order to consider transparent mode we can just replace the index "op" by "tr".

3.10.2 Cost of OXCs with Shared Path Restoration in Opaque and Transparent Networks

The calculation of the cost of OXCs in opaque and transparent networks with shared path restoration does not differ. We assume shared path restoration using dual-ended switching, which is done by the OXCs. In this case a switching protocol is needed to coordinate the switching action at both ends. This mechanism is called dual-ended because the switching has to be done at both the sending and receiving end [13]. The OXC needs only one tributary port for each add/drop channel. This is the difference from dedicated path protection in terms of tributary ports. Furthermore, one OXC trunk port is used for the working channel and another is used for restoration, which may be shared with a number of demands.

The cost of an opaque OXC, considering shared path restoration is, therefore:

$$c_{op,n}^{OXC,k_r} = \gamma^{OXC} + n_{op,n}^{CH,k_r} \gamma^{SW}, \tag{3.149}$$

where $n_{op,n}^{CH,k_r}$ is the number of bidirectional channels, including restoration capacity, that are processed in the opaque node n, which can be obtained with

$$n_{op,n}^{CH,k_r} = \frac{1}{2} \left(n_n^D + \sum_{j=1}^{N} w_{n,j}^{k_r} \right), \tag{3.150}$$

where $w_{n,j}^{k_r}$ is the number of channels connecting node n to node j, including restoration capacity.

In order to illustrate the calculation of (3.150), let's consider our example network, in Figure 3.1, and three bidirectional demands with shared path restoration:

one demand interconnecting nodes 1-2, one interconnecting nodes 1-3, and one interconnecting nodes 2-3. Figure 3.10 illustrates the routing of the three demands. The blue line represents the demand {1-2}, the green line the demand {1-3} and the red line the demand {2-3}. The shortest path between the source and destination nodes is the working path (represented as a solid line) and the second shortest path the backup path (represented as a dashed line). For instance, the demand {1-2} is routed through nodes 1-2 for working and through nodes 1-4-2 for backup. The working path of demand {1-3} uses the nodes 1-3 and its backup path uses the nodes 1-4-3. The demands {1-2} and {1-3} are failure-disjoint, i.e., a link failure that affects the demand {1-2} does not affect the demand {1-3} and vice-versa), so they can share the capacity for survivability in the link between the nodes 1-4 (represented as a gray dashed line).

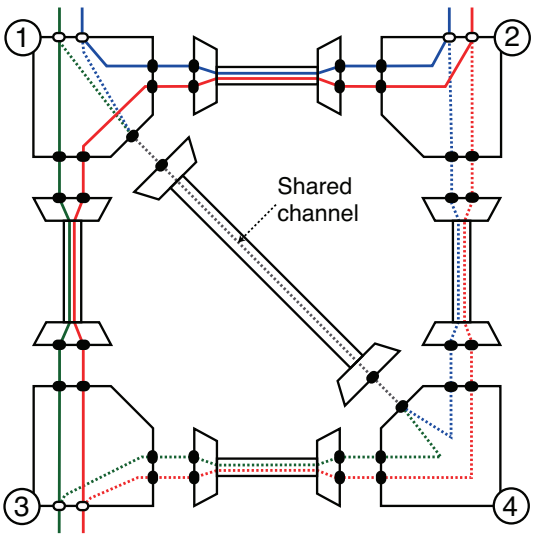

Figure 3.10: The example network in opaque mode, with three demands and shared path restoration. Dashed lines represent the backup paths.

Now let's calculate the number of channels in node 1, with (3.150). We have $n_1^D = 2$ and $w_{1,1}^{k_r} = 0$, $w_{1,2}^{k_r} = 2$, $w_{1,3}^{k_r} = 2$, and $w_{1,4}^{k_r} = 1$. Thus, can write

$$n_{op,1}^{CH,k_r} = \frac{1}{2}\Big(2 + \big(0 + 2 + 2 + 1\big)\Big) = 3.5.$$

Notice that the result is not an integer because some trunk ports may be shared with a number of demands. Since a channel requires two ports to traverse an OXC we can also

count the number of ports in the node 1 of Figure 3.10, and divide it by two to obtain the number of channels in the OXC.

Considering all nodes we obtain

$$\begin{aligned} N_{op}^{CH,k_r} = \sum_{n=1}^{N} n_{op,n}^{CH,k_r} &= \frac{1}{2}\sum_{n=1}^{N}\left(n_n^D + \sum_{j=1}^{N} w_{n,j}^{k_r}\right) \\ &= \frac{1}{2}\left(\sum_{n=1}^{N} n_n^D + \sum_{n=1}^{N}\sum_{j=1}^{N} w_{n,j}^{k_r}\right) \\ &= \frac{D_1 + 2W^{k_r}}{2}, \end{aligned} \tag{3.151}$$

where W^{k_r} is the total number of channels on links, including restoration capacity. Dividing (3.151) by the number of nodes we obtain the average number of channels per opaque OXC, including restoration capacity, which can be written as

$$\begin{aligned} \langle n_{op}^{CH,k_r}\rangle = \frac{N_{op}^{CH,k_r}}{N} &= \frac{D_1 + 2W^{k_r}}{2N} \\ &= \frac{D_1}{2N} + \frac{L}{L}\frac{2W^{k_r}}{2N} \\ &= \frac{\langle d\rangle}{2} + \langle\delta\rangle\frac{W^{k_r}}{2L}, \end{aligned} \tag{3.152}$$

where W^{k_r}/L is the average number of channels per link including restoration capacity, $\langle w^{k_r}\rangle$. Therefore, from (3.152) we obtain

$$\langle n_{op}^{CH,k_r}\rangle = \frac{\langle d\rangle + \langle\delta\rangle\langle w^{k_r}\rangle}{2}. \tag{3.153}$$

From (3.149) and (3.153) we obtain the average cost per OXC, including restoration capacity with

$$\langle c_{op}^{OXC,k_r}\rangle = \gamma^{OXC} + \langle n_{op}^{CH,k_r}\rangle\gamma^{SW}. \tag{3.154}$$

In order to consider transparent mode we can just replace the index “op” by “tr”.

3.10.3 Cost of OXCs with Dedicated Path Protection in Translucent Networks

When calculating the cost of OXCs in translucent networks we have to consider regeneration. We have seen how to obtain the number of regenerators per demand, without considering survivability, in (3.58). However, in dedicated path protection we have also to calculate the number of regenerators required per backup demand. Therefore, from (3.58) and denoting l'_d as the length of a backup demand, we can obtain the number of regenerators per backup demand with

$$n_d^{r'} = \left\lceil \frac{l'_d}{\Lambda} \right\rceil - 1, \tag{3.155}$$

As regeneration is performed in-node (see Figure 3.11), we have $n_n^{DR'}$ regenerators per node. Considering all backup demands we obtain the number of regenerators in the network, for backup demands, with

$$N^{r'} = \sum_{d=1}^{D} n_d^{r'} = \sum_{n=1}^{N} n_n^{DR'}, \tag{3.156}$$

where $n_n^{DR'}$ is the number of backup demands that need regeneration at node n. Dividing (3.156) by the number of nodes we obtain the average number of regenerators per node for backup demands, which can be written as

$$\langle n^{r'} \rangle = \frac{N^{r'}}{N}. \tag{3.157}$$

The number of regenerators per node, considering dedicated protection can be obtained with

$$n_n^{r,k_p} = n_n^{DR} + n_n^{DR'}. \tag{3.158}$$

Considering all nodes we obtain the total number of regenerators in a network, which can be written as

$$N^{r,k_p} = \sum_{d=1}^{D} n_d^{R} + \sum_{d=1}^{D} n_d^{r'} = \sum_{n=1}^{N} n_n^{r,k_p}. \tag{3.159}$$

Dividing (3.159) by the number of nodes we obtain the average number of regenerators per OXC, considering dedicated path protection, which is:

$$\langle n^{r,k_p} \rangle = \frac{N^{r,k_p}}{N} = \langle n^R \rangle + \langle n^{r'} \rangle. \tag{3.160}$$

The cost of a translucent OXC, considering dedicated path protection is obtained with

$$c_{tl,n}^{OXC,k_p} = \gamma^{OXC} + n_{tl,n}^{CH,k_p} \gamma^{SW}, \tag{3.161}$$

where $n_{tl,n}^{CH,k_p}$ is the number of bidirectional channels, including protection capacity, that are processed in the translucent OXC n, which can be obtained with

$$n_{tl,n}^{CH,k_p} = \frac{1}{2} \left(2n_n^D + 2n_n^{r,k_p} + \sum_{j=1}^{N} w_{n,j}^{k_p} \right). \tag{3.162}$$

In order to illustrate the calculation of (3.162), let's consider our example network, in Figure 3.1, and three bidirectional demands with dedicated path protection: one demand interconnecting nodes 1-2, one interconnecting nodes 1-3, and one interconnecting nodes 2-3. Figure 3.11 illustrates the routing of the three demands. The blue line represents the demand {1-2}, the green line the demand {1-3} and the red line the demand {2-3}. The shortest path between the source and destination nodes is the working path and the second shortest path the backup path. For instance, the demand {1-2} is routed through nodes 1-2 for working and through nodes 1-4-2 for backup. Notice that the length of backup path for the demand {1-2} is longer than the Maximum Transparency Length so it needs to be regenerated at node 4. The same occurs for the demand {1-3}.

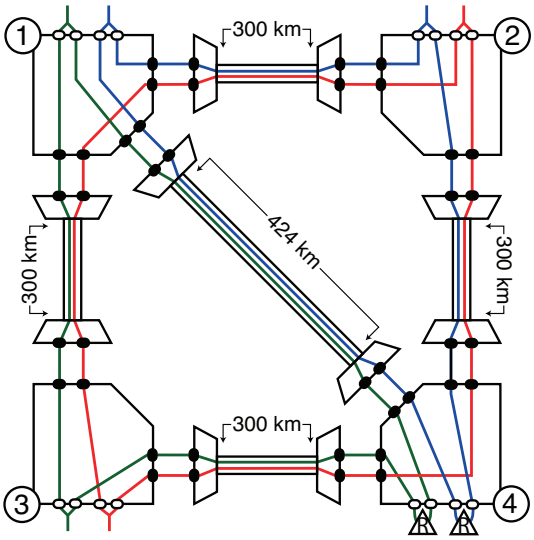

Figure 3.11: The example network in translucent transport mode, with three demands and dedicated path protection.

Now let's calculate the number of channels in node 1, with (3.162). We have $n_1^D = 2$, $n^{r,k_p} = 0$ and $w_{1,1}^{k_p} = 0$, $w_{1,2}^{k_p} = 2$, $w_{1,3}^{k_p} = 2$, and $w_{1,4}^{k_p} = 2$. Thus, we can write

$$n_{tl,1}^{CH,k_p} = \frac{1}{2}\Big(2 \times 2 + 2 \times 0 + \big(0 + 2 + 2 + 2\big)\Big) = 5.$$

Now let's consider the number of channels in node 4, with (3.162). Then we have $n_4^D = 0$, $n^{r,k_p} = 2$ and $w_{4,1}^{k_p} = 2$, $w_{4,2}^{k_p} = 2$, $w_{4,3}^{k_p} = 2$, and $w_{4,4}^{k_p} = 0$. Thus, we can write

$$n_{tl,4}^{CH,k_p} = \frac{1}{2}\Big(2 \times 0 + 2 \times 2 + \big(2 + 2 + 2 + 0\big)\Big) = 5.$$

Considering all nodes we obtain

$$\begin{aligned} N_{tl}^{CH,k_p} = \sum_{n=1}^{N} n_{tl,n}^{CH,k_p} &= \frac{1}{2}\sum_{n=1}^{N}\left(2n_n^D + 2n_n^{r,k_p} + \sum_{j=1}^{N} w_{n,j}^{k_p}\right) \\ &= \frac{1}{2}\left(\sum_{n=1}^{N} 2n_n^D + \sum_{n=1}^{N} 2n_n^{r,k_p} + \sum_{n=1}^{N}\sum_{j=1}^{N} w_{n,j}^{k_p}\right) \\ &= D_1 + N^{r,k_p} + W^{k_p}, \end{aligned} \tag{3.163}$$

Dividing (3.163) by the number of nodes we obtain the average number of channels

per OXC, including dedicated protection with

$$\begin{aligned}\langle n_{tl}^{CH,k_p}\rangle = \frac{N_{tl}^{CH,k_p}}{N} &= \frac{2D_1 + 2N^{r,k_p} + 2W^{k_p}}{2N} \\ &= \frac{2D_1}{2N} + \frac{2N^{r,k_p}}{2N} + \frac{L}{L}\frac{2W^{k_p}}{2N} \\ &= \langle d\rangle + \langle n^{r,k_p}\rangle + \langle\delta\rangle\frac{W^{k_p}}{2L},\end{aligned} \tag{3.164}$$

where W^{k_p}/L is the average number of channels per link including dedicated protection, $\langle w^{k_p}\rangle$. Therefore, we can rewrite (3.164) as

$$\langle n_{tl}^{CH,k_p}\rangle = \langle d\rangle + \langle n^{r,k_p}\rangle + \frac{\langle\delta\rangle\langle w^{k_p}\rangle}{2}. \tag{3.165}$$

Considering our example network, Figure 3.1, with the demand matrix (3.5), we obtain $\langle n_{tl}^{CH,k_p}\rangle = 10.25$. From (3.161) and (3.165) we obtain the average cost per OXC, including dedicated protection with

$$\langle c_{tl}^{OXC,k_p}\rangle = \gamma^{OXC} + \langle n_{tl}^{CH,k_p}\rangle\gamma^{SW}. \tag{3.166}$$

3.10.4 Cost of OXCs with Shared Path Restoration in Translucent Networks

The cost of a translucent OXC, considering shared path restoration is given by

$$c_{tl,n}^{OXC,k_r} = \gamma^{OXC} + n_{tl,n}^{CH,k_r}\gamma^{SW}. \tag{3.167}$$

where $n_{tl,n}^{CH,k_r}$ is the number of channels, including restoration capacity, that are processed in the node n, which can be obtained with

$$n_{tl,n}^{CH,k_r} = \frac{1}{2}\left(n_n^D + 2n_n^{r,k_r} + \sum_{j=1}^{N} w_{n,j}^{k_r}\right), \tag{3.168}$$

where n_n^{r,k_r} is the number of demands that need regeneration in the node n, considering restoration. The value of n_n^{r,k_r} can be obtained with

$$n_n^{r,k_r} = max_f\{n_n^{r,k_r,f}\}\ , n = \{1, ..., N\}\ , f = \{1, ..., L\}, \tag{3.169}$$

where $n_n^{r,k_r,f}$ is the number of demands that need regeneration at node n, in the case of a failure in the link f. Considering all nodes we have

$$N^{r,k_r} = \sum_{n=1}^{N} n_n^{r,k_r}, \tag{3.170}$$

and dividing (3.170) by the number of nodes we obtain the average number of regeneration per translucent OXC, considering restoration, which can be written as

$$\langle n^{r,k_r} \rangle = \frac{N^{r,k_r}}{N}. \tag{3.171}$$

In order to illustrate the calculation of (3.168), let's consider our example network, in Figure 3.1, and three bidirectional demands: one demand interconnecting nodes 1-2, one interconnecting nodes 1-3, and one interconnecting nodes 2-3. Figure 3.12 illustrates the routing of the three demands.

The blue line represents the demand {1-2}, the green line the demand {1-3} and the red line the demand {2-3}. The shortest path between the source and destination nodes is the working path (represented as a solid line) and the second shortest path the backup path (represented as a dashed line). For instance, the demand {1-2} is routed through nodes 1-2 for working and through nodes 1-4-2 for backup. The working path of demand {1-3} uses the nodes 1-3 and its backup path uses the nodes 1-4-3. Considering $\Lambda = 600$ the backup demand {1-2} has to suffer one regeneration at node 4, since its length is 724 km. Moreover, the backup demand {1-3} also has to suffer one regeneration at node 4. The demands {1-2} and {1-3} are failure-disjoint, so they can share the capacity for survivability in the link between the nodes 1-4 (represented as a gray dashed line) and also the regenerator at node 4.

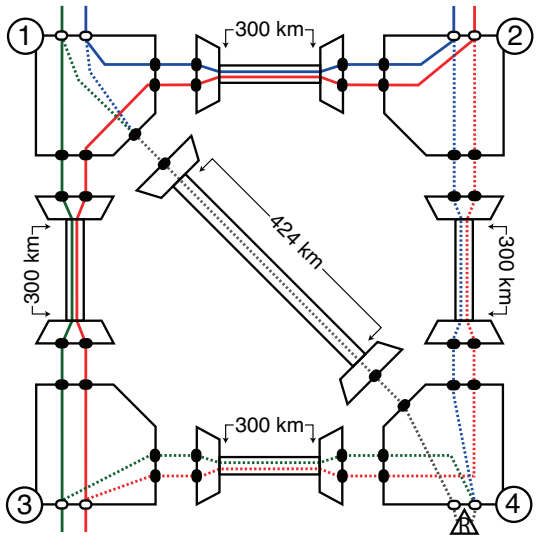

Figure 3.12: The example network in translucent mode, with three demands and considering shared path restoration.

Now let's calculate the number of channels in node 1, with (3.169). We have $n_1^D = 2$, $n_1^{r,k_r} = 0$ and $w_{1,1}^{k_r} = 0$, $w_{1,2}^{k_r} = 2$, $w_{1,3}^{k_r} = 2$, and $w_{1,4}^{k_r} = 1$. Thus, can write

$$n_{tl,1}^{CH,k_r} = \frac{1}{2}\Big(2 + 2 \times 0 + \big(0 + 2 + 2 + 1\big)\Big) = 3.5.$$

Considering node 4, we have $n_4^D = 0$, $n_4^{r,k_r} = 1$ and $w_{4,1}^{k_r} = 1$, $w_{4,2}^{k_r} = 2$, $w_{4,3}^{k_r} = 2$, and $w_{4,4}^{k_r} = 0$. Thus, can write

$$n_{tl,4}^{CH,k_r} = \frac{1}{2}\Big(0 + 2 \times 1 + \big(1 + 2 + 2 + 0\big)\Big) = 3.5.$$

Considering all nodes we obtain the total number of channels in a translucent OXCs, considering restoration, which can be written as

$$\begin{aligned} N_{tl}^{CH,k_r} = \sum_{n=1}^{N} n_{tl,n}^{CH,k_r} &= \frac{1}{2}\sum_{n=1}^{N}\left(n_n^D + 2n_n^{r,k_r} + \sum_{j=1}^{N} w_{n,j}^{k_r}\right) \\ &= \frac{1}{2}\left(\sum_{n=1}^{N} n_n^D + \sum_{n=1}^{N} 2n_n^{r,k_r} + \sum_{n=1}^{N}\sum_{j=1}^{N} w_{n,j}^{k_r}\right) \\ &= \frac{D_1 + 2N^{r,k_r} + 2W^{k_r}}{2}, \end{aligned} \tag{3.172}$$

Dividing (3.172) by N we obtain the average number of channels per translucent OXC, considering restoration, which is

$$\begin{aligned}\langle n_{tl}^{CH,k_r}\rangle = \frac{N_{tl}^{CH,k_r}}{N} &= \frac{D_1 + 2N^{r,k_r} + 2W}{2N} \\ &= \frac{D_1}{2N} + \frac{2N^{r,k_r}}{2N} + \frac{L}{L}\frac{2W^{k_r}}{2N} \\ &= \frac{\langle d\rangle + 2\langle n^{r,k_r}\rangle}{2} + \langle\delta\rangle\frac{W^{k_r}}{2L} \\ &= \frac{\langle d\rangle + 2\langle n^{r,k_r}\rangle + \langle\delta\rangle\langle w^{k_r}\rangle}{2}.\end{aligned} \tag{3.173}$$

From (3.167) and (3.173) we obtain the average cost of a translucent OXC with

$$\langle c_{tl}^{OXC,k_r}\rangle = \gamma^{OXC} + \langle n_{tl}^{CH,k_r}\rangle\gamma^{SW}. \tag{3.174}$$

3.10.5 Cost of Transponders considering Survivability

In opaque networks, the number of short-reach transponders are not affected by the survivability schemes considered in this thesis. The number of long-reach transponders, considering survivability, can be calculated by including the survivability coefficient. Therefore, from (3.72) we have

$$\langle n_{op}^{LR,k}\rangle = \langle\delta\rangle\langle w^o\rangle(1 + \langle k\rangle) = \langle\delta\rangle\langle w^k\rangle, \tag{3.175}$$

where k has to be k_p or k_r according to the survivability scheme. From (3.175) we can obtain the cost of long-reach transponders, considering survivability with

$$\langle c_{op}^{TSP,k}\rangle = \langle n^{SR}\rangle\gamma^{SR} + \langle n_{op}^{LR,k}\rangle\gamma^{LR}. \tag{3.176}$$

Since in transparent and translucent networks the long-reach transponders are installed between EXCs and OXCs, transponders are not affected by the survivability schemes considered in this thesis.

3.10.6 Cost of Regenerators considering Survivability

In translucent networks with dedicated path protection, the cost of regenerators is given by

$$c_n^{REG,k_p} = n_n^{r,k_p}\gamma^{REG}, \tag{3.177}$$

and considering the averages we obtain

$$\langle c^{REG,k_p}\rangle = \langle n^{r,k_p}\rangle\gamma^{REG}. \tag{3.178}$$

In order to consider translucent networks with shared path restoration, we can use (3.177) and (3.178), replacing the index "k_p" by "k_r".

3.11 A Case Study

In this section we present the costs related to the nodes and links of an optical transport network. Let's consider the network topology presented in Figure 3.1, implemented as a SONET/SDH-over-WDM multilayer network. Each EXC basic node provides 16 bidirectional slots of 40 Gbps. The slots may be equipped with a variety of tributary and trunk port cards differing in granularity and interface technology. Nonetheless, here we consider only the cost of trunk ports. Each trunk port (also known as EXC trunk interface) is assumed to be a gray interface STS-192/STM-64 (10 Gbps). Each OXC provides a number of fiber ports (degrees), and each degree has capacity to support a transmission system with 40 channels (e.g., an OXC with degree four, $\delta_n = 4$, supports four bidirectional transmission systems of 40 channels each. Therefore the switching matrix should have at least $4 \times 40 = 160$ bidirectional ports (usually represented in "number of ingress ports" x "number of egress ports" like 160 x 160) [15]. Figure 3.13a shows an example of an OXC with four degrees, in which each degree is connected to a transmission system that supports one bidirectional channel. Notice that all channels from the trunk sides may be dropped on the tributary side. The node has eight input ports and eight output ports. Therefore, it requires a 8 x 8 switching matrix. Figure 3.13b shows the dimension of the required matrix.

In fact, the cost of an OXC basic includes a fixed cost and a cost that scales with the nodal degree, which is $\gamma^{OXC} = 8.33 \times \delta_n + 2.5$ [16]. In this thesis we calculate the cost of each OXC using the average nodal degree, which for our example network is $\langle\delta\rangle = 2.5$. Each link comprises one transmission system with capacity to deal with forty WDM channels, ($S = 40$), at bit rate of 10 Gbps each, and is equipped with an OA every 100 km ($\partial = 100$ km). The traffic to be considered is the one presented in the matrix (3.5), the page 44. Each demand represents an STS-192/STM-64.

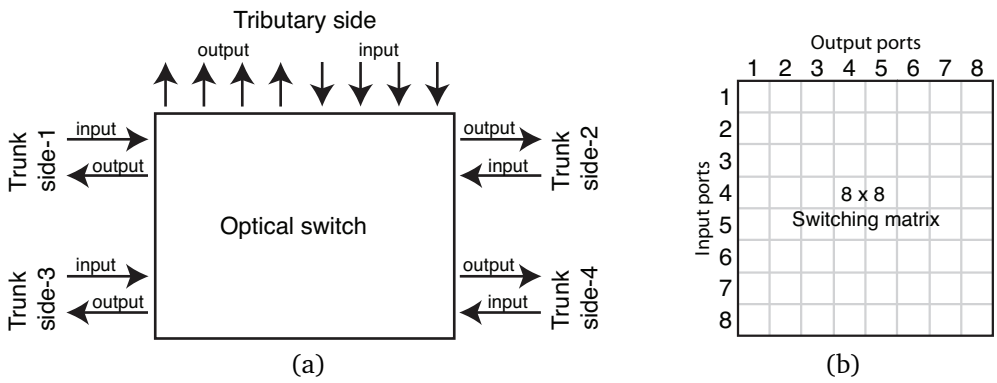

Figure 3.13: Schematic representation of a non-blocking OXC: (a) the OXC input and output ports. (b) the dimension of its switching matrix.

The cost model still depends on a set of variables that represent the monetary cost of each network component. We are going to use the normalized cost values shown in Table 3.4, which is based on the work presented in [17].

Table 3.4: Cost of network components.

Component	Variable	Cost	Relation
EXC basic (640 Gbps - 16 slots)	γ^{EXC}	13.33	node
OXC basic (40 channel system)*	γ^{OXC}	23.32	node
Switching per channel	γ^{SW}	0.67	node
EXC trunk port	γ^{TP}_{exc}	0.67	node
Short-reach transponder	γ^{SR}	0.67	node
Long-reach transponder	γ^{LR}	1.00	node
Regenerator	γ^{REG}	2.00	node
Optical Line Terminal	γ^{OLT}	4.17	link
Optical Amplifier (100 km span)	γ^{OA}	1.92	link
Optical Fiber (1 km)	γ^{F}	0.80	link

* - Obtained from $\gamma^{OXC} = 8.33 \times \langle\delta\rangle + 2.5$, with $\langle\delta\rangle = 2.5$.

In Table 3.5 shows the values of the variables presented throughout this Chapter, for opaque, translucent and transparent transport modes. Moreover, the values are calculated in three ways: 1) considering a network without survivability, 2) with dedicated path protection and 3) with shared path restoration. Notice that, since a transmission system has sufficient capacity to support the optical channels crossing the link, even considering survivability, the number of optical line terminals, optical amplifiers and fiber does not increase with survivability.

In Table 3.6 we present the CAPEX for the network with opaque transport mode and dedicated path protection. The second column shows the average cost of components, separated by costs of links and nodes. For instance, the average cost of OLTs per link is $\langle c^{OLT,k_p} \rangle = 8.34$ monetary units (see the first line and second column in Table 3.6). Multiplying that value by the number of links we obtain the total cost with OLTs in the network. The third column shows the average number of components (per link or node) and the fourth column the total number of components in the network. For instance, we can see that it is needed an average of 2.4 optical amplifiers per link, which results in 12 for the network (see the second line in Table 3.6). Notice that in lines of the cost of EXCs and OXCs the number of components is related to EXC trunk ports and channels processed in OXC, respectively. Moreover, in the number of transponders we sum the short- and long-reach transponders (see the ninth line, third column), i.e., $3.5 + 11.5 = 15$, the values for this addition were taken from Table 3.5. The last row shows the total CAPEX for the network. All quantities shown on the second to the last column of Table 3.6 were also obtained by counting the components directly on Figure 3.15. This validates our calculation procedure. Notice that the network is configured as single-ended switching, so each short-reach transponder duplicates the traffic and feed it two tributary ports of the OXC.

Similarly we present a table and a figure to show CAPEX of every transport modes and survivability schemes studied in this thesis. Table 3.7 shows CAPEX for our example network, considering opaque transport mode and shared path restoration. The quantities shown on the table were confirmed by counting directly on Figure 3.16. Notice that the network is configured as dual-ended switching, so each short-reach

transponder feeds only one tributary port of the OXC, and the OXCs at both ends of the affected optical channel performs the switching from the working path to the backup path, in case of a link failure. Since this method saves OXC tributary ports and switching capacity, the cost of OXCs is lower than the previous configuration. Moreover, since each long-reach transponders is shared among a number optical channels we need less transponders. Therefore, this configuration tends to be more cost-efficient than the previous one.

Table 3.8 shows CAPEX for our example network, considering translucent transport mode with dedicated path protection. The quantities were confirmed by counting directly on Figure 3.17. Notice that this configuration has single-ended switching, but here we use long-reach transponders to feed the signal to two tributary ports of the OXCs, and transponders are not used between the OXC and the transmission system. Additionally, in this transport mode regenerators were taken into account. Considering $\Lambda = 600$, four backup demands {1-2, 1-3, 2-4, 3-4} need one regeneration each, therefore we obtain $\langle n^{r'} \rangle = 1$. Table 3.9 shows results for translucent transport mode with shared path restoration, and Figure 3.18 shows the network configuration for component number checking. Although this configuration has the additional cost of regenerators, the number of transponders is greatly reduced when compared with opaque configurations. Therefore, the cost of nodes tends to be lower.

Table 3.10 shows the results for transparent transport mode with dedicated path protection. The quantities of components were confirmed by counting directly on Figure 3.19. Notice that in this case the network does not make use of short-reach transponders. Therefore, the cost and number of transponders is related to long-reach transponders. Table 3.11 shows the results for transparent transport mode with shared path restoration, and Figure 3.20 shows the network configuration for component number checking. Since this configuration does not use regenerator, short-reach transponders, and long-reach transponders between OXCs and transmission systems, it tends to be the most cost-efficient. Figure 3.14 shows a comparative chart of the CAPEX for all analyzed transport modes and survivability strategies.

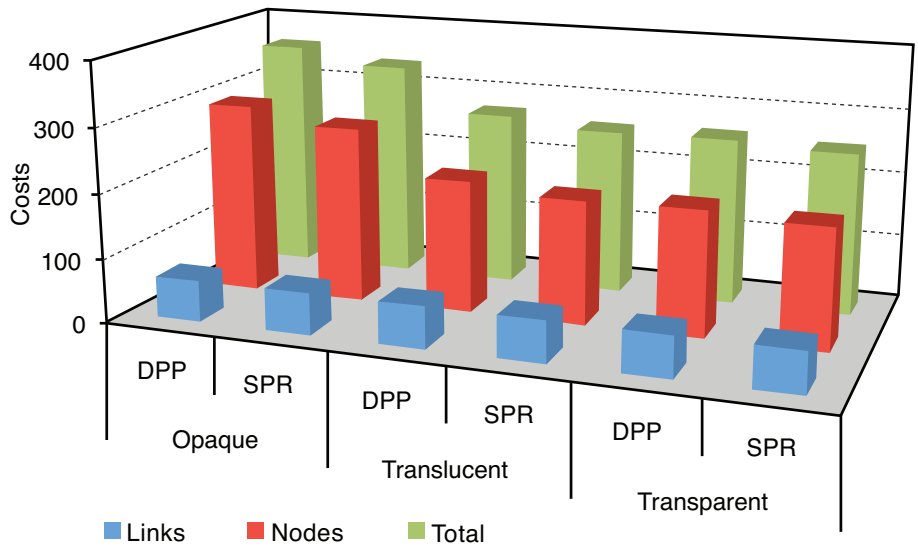

Figure 3.14: Comparative of CAPEX for the four-node network under different transport mode and survivability strategy. DPP stands for dedicated path protection, and SPR for shared path restoration.

According to our model, the cost of links is the same for all transport modes and survivability strategies. The cost of nodes tends to decrease as we configure the network with opaque to translucent to transparent. However, the survivability strategy may change this tendency. For instance, for the network considered in Figure 3.14, the configuration with translucent transport mode and shared path restoration is more cost-effective than the configuration with transparent transport mode and dedicated path protection.

Table 3.5: Quantities of network components.

	Without Survivability		With Protection		With Restoration	
	Variable	Value	Variable	Value	Variable	Value
Number of Nodes	N	4	N	4	N	4
Number of Links	L	5	L	5	L	5
Number of bidirectional demands	D	7	D	7	D	7
Average number of demands	$\langle d \rangle$	3.5	$\langle d \rangle$	3.5	$\langle d \rangle$	3.5
Average nodal degree	$\langle \delta \rangle$	2.5	$\langle \delta \rangle$	2.5	$\langle \delta \rangle$	2.5
Average number of hops	$\langle h \rangle$	1.3	$\langle h \rangle$	1.3	$\langle h \rangle$	1.3
Average number of hops for backup	$\langle h' \rangle$	2.0	$\langle h' \rangle$	2.0	$\langle h' \rangle$	2.0
Average number of channels on links	$\langle w \rangle$	1.8	$\langle w \rangle$	1.8	$\langle w \rangle$	1.8
Survivability coefficients			$\langle k_p \rangle$	1.6	$\langle k_r \rangle$	1.0
Average number of channels on links, with survivability			$\langle w^{k_p} \rangle$	4.6	$\langle w^{k_r} \rangle$	3.6
Capacity of transmission system	$\langle S \rangle$	40	$\langle S \rangle$	40	$\langle S \rangle$	40
Average number of transmission system	$\langle n^S \rangle$	1.0	$\langle n^{S,k_p} \rangle$	1.0	$\langle n^{S,k_r} \rangle$	1.0
Average number of OLTs	$\langle n^{OLT} \rangle$	2.0	$\langle n^{OLT,k_p} \rangle$	2.0	$\langle n^{OLT,k_r} \rangle$	2.0
Average number of optical amplifiers	$\langle n^A \rangle$	2.4	$\langle n^{A,k_p} \rangle$	2.4	$\langle n^{A,k_r} \rangle$	2.4
Average quantity of fiber	$\langle n^F \rangle$	649.6	$\langle n^{F,k_p} \rangle$	649.6	$\langle n^{F,k_p} \rangle$	649.6
Average number of EXC trunk ports	$\langle n^{TP}_{exc} \rangle$	3.5	$\langle n^{TP}_{exc} \rangle$	3.5	$\langle n^{TP}_{exc} \rangle$	3.5
Average number of channels on OXC for opaque networks	$\langle n^{CH}_{op} \rangle$	4.0	$\langle n^{CH,k_p}_{op} \rangle$	9.3	$\langle n^{CH,k_r}_{op} \rangle$	6.3
Average number of channels on OXC for transparent networks	$\langle n^{CH}_{tr} \rangle$	4.0	$\langle n^{CH,k_p}_{tr} \rangle$	9.3	$\langle n^{CH,k_r}_{tr} \rangle$	6.3
Average number of regenerators per OXC			$\langle n^R \rangle$	0.0		
Average number of regenerators per OXC, for backup			$\langle n^{r'} \rangle$	1.0		
Average number of regenerators per OXC, considering survivability			$\langle n^{r,k_p} \rangle$	1.0	$\langle n^{r,k_r} \rangle$	0.5
Average number of channels on OXC for translucent networks	$\langle n^{CH}_{tl} \rangle$	4.0	$\langle n^{CH,k_p}_{tl} \rangle$	10.3	$\langle n^{CH,k_r}_{tl} \rangle$	6.8
Average number of short-reach transponders	$\langle n^{SR} \rangle$	3.5	$\langle n^{SR} \rangle$	3.5	$\langle n^{SR} \rangle$	3.5
Average number of long-reach transponders in opaque networks	$\langle n^{LR}_{op} \rangle$	4.5	$\langle n^{LR,k_p}_{op} \rangle$	11.5	$\langle n^{LR,k_r}_{op} \rangle$	9.0
Average number of long-reach transponders in transparent networks	$\langle n^{LR}_{tr} \rangle$	3.5	$\langle n^{LR}_{tr} \rangle$	3.5	$\langle n^{LR}_{tr} \rangle$	3.5
Average number of long-reach transponders in translucent networks	$\langle n^{LR}_{tl} \rangle$	3.5	$\langle n^{LR}_{tl} \rangle$	3.5	$\langle n^{LR}_{tl} \rangle$	3.5

Table 3.6: CAPEX for the opaque network with dedicated path protection.

	Variable	Cost	Avg. # components	# total	Equation
Cost of links	$\langle c^{OLT,k_p} \rangle$	8.34	2.00	10	(3.131)
	$\langle c^{A,k_p} \rangle$	4.61	2.40	12	(3.135)
	$\langle c^{F,k_p} \rangle$	0.00	649.60	3248	(3.138)
	$\langle c_l^{k_p} \rangle$	12.95			(3.140)
	$C_L^{k_p}$	64.74			(3.139)
Cost of nodes	$\langle c^{EXC} \rangle$	15.68	3.50	14	(3.46)
	$\langle c_{op}^{OXC,k_p} \rangle$	29.52	9.25	37	(3.148)
	$\langle c_{op}^{TSP,k_p} \rangle$	13.84	15.00	60	(3.176)
	$\langle c_n^{k_p} \rangle$	59.03			(3.141)
	$C_N^{k_p}$	295.17			(3.142)
		$C_T = 359.91$			(3.12)

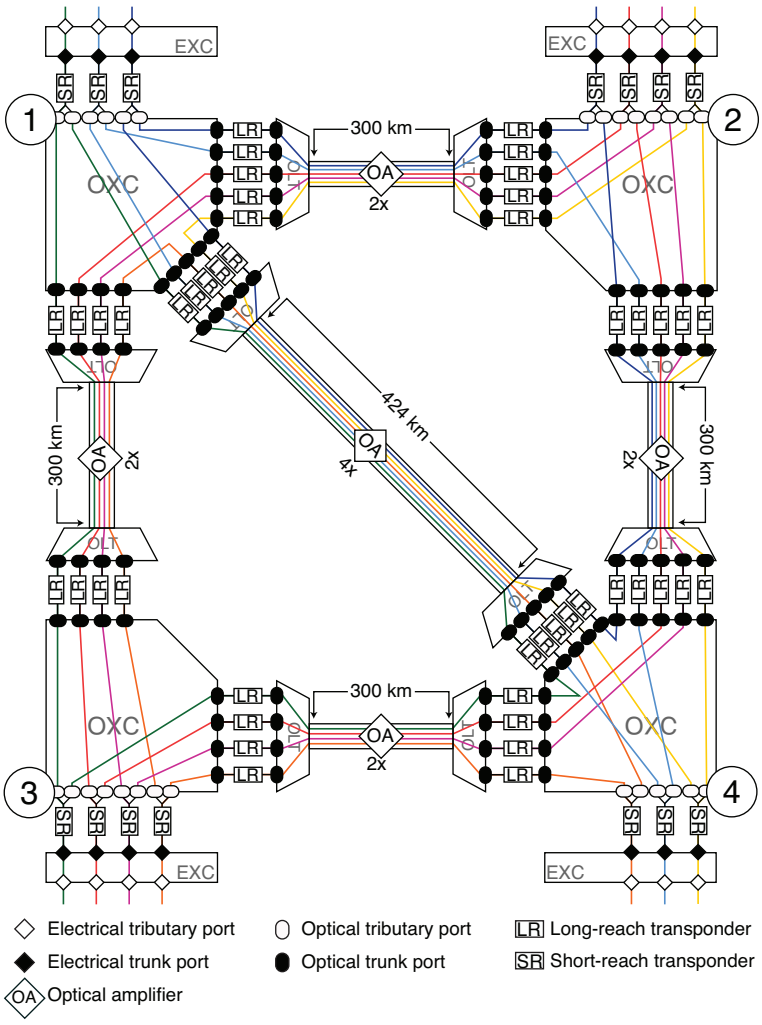

Figure 3.15: Opaque network with dedicated path protection.

Table 3.7: CAPEX for the opaque network with shared path restoration.

	Variable	Cost	Avg. # components	# total	Equation
Cost of links	$\langle c^{OLT,k_r} \rangle$	8.34	2.00	10	(3.131)
	$\langle c^{A,k_r} \rangle$	4.61	2.40	12	(3.135)
	$\langle c^{F,k_r} \rangle$	0.00	649.60	3248	(3.138)
	$\langle c_l^{k_r} \rangle$	12.95			(3.140)
	$C_L^{k_r}$	64.74			(3.139)
Cost of nodes	$\langle c^{EXC} \rangle$	15.68	3.50	14	(3.46)
	$\langle c_{op}^{OXC,k_r} \rangle$	27.51	6.25	25	(3.154)
	$\langle c_{op}^{TSP,k_r} \rangle$	11.34	12.50	50	(3.176)
	$\langle c_n^{k_r} \rangle$	54.52			(3.141)
	$C_N^{k_r}$	272.60			(3.142)
		$C_T = 337.34$			(3.12)

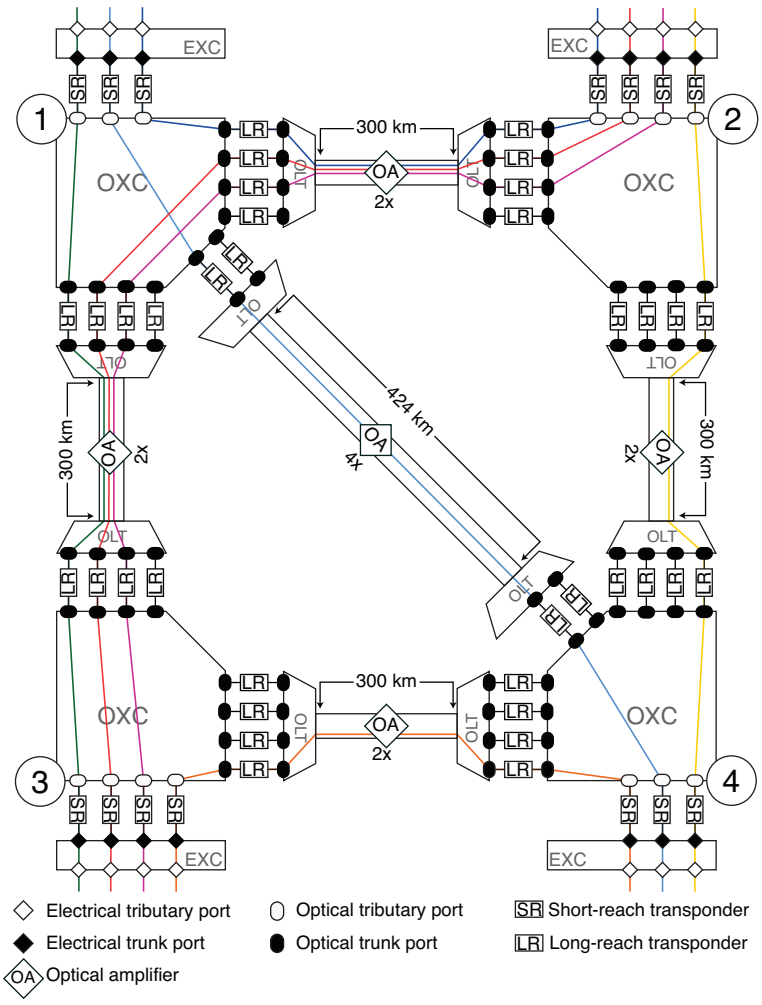

Figure 3.16: Opaque network with shared path restoration.

Table 3.8: CAPEX for the translucent network with dedicated path protection.

	Variable	Cost	Avg. # components	# total	Equation
Cost of links	$\langle c^{OLT,k_p} \rangle$	8.34	2.00	10	(3.131)
	$\langle c^{A,k_p} \rangle$	4.61	2.40	12	(3.135)
	$\langle c^{F,k_p} \rangle$	0.00	649.60	3248	(3.138)
	$\langle c_l^{k_p} \rangle$	12.95			(3.140)
	$C_L^{k_p}$	64.74			(3.139)
Cost of nodes	$\langle c^{EXC} \rangle$	15.68	3.50	14	(3.46)
	$\langle c_{tl}^{OXC,k_p} \rangle$	30.19	10.25	41	(3.166)
	$\langle c_{tl}^{TSP} \rangle$	3.50	3.50	14	(3.81)
	$\langle c^{REG,k_p} \rangle$	2.00	1.00	4	(3.178)
	$\langle c_n^{k_p} \rangle$	51.36			(3.141)
	$C_N^{k_p}$	205.45			(3.142)
		$C_T = 270.19$			(3.12)

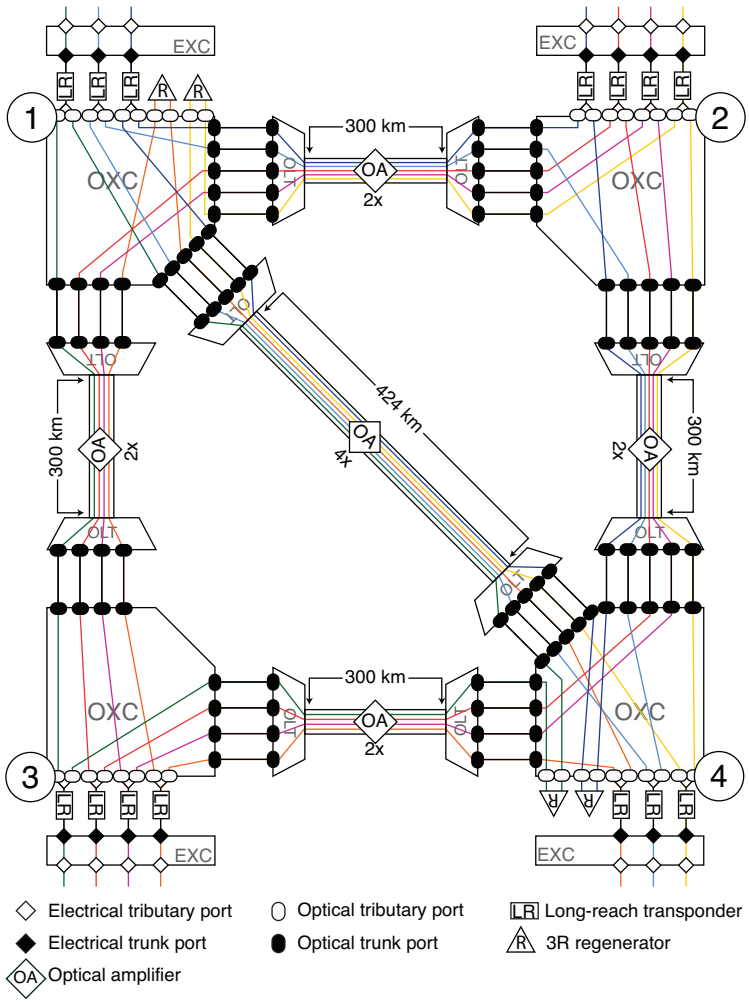

Figure 3.17: Translucent network with dedicated path protection.

Table 3.9: CAPEX for the translucent network with shared path restoration.

	Variable	Cost	Avg. # components	# total	Equation
Cost of links	$\langle c^{OLT,k_r} \rangle$	8.34	2.00	10	(3.131)
	$\langle c^{A,k_r} \rangle$	4.61	2.40	12	(3.135)
	$\langle c^{F,k_r} \rangle$	0.00	649.60	3248	(3.138)
	$\langle c_l^{k_r} \rangle$	12.95			(3.140)
	$C_L^{k_r}$	64.74			(3.139)
Cost of nodes	$\langle c^{EXC} \rangle$	15.68	3.50	14	(3.46)
	$\langle c_{tl}^{OXC,k_r} \rangle$	27.84	6.75	27	(3.174)
	$\langle c_{tl}^{TSP} \rangle$	3.50	3.50	14	(3.81)
	$\langle c^{REG,k_r} \rangle$	1.00	0.5	2	(3.178)
	$\langle c_n^{k_r} \rangle$	48.02			(3.141)
	$C_N^{k_r}$	192.06			(3.142)
		$C_T = 256.80$			(3.12)

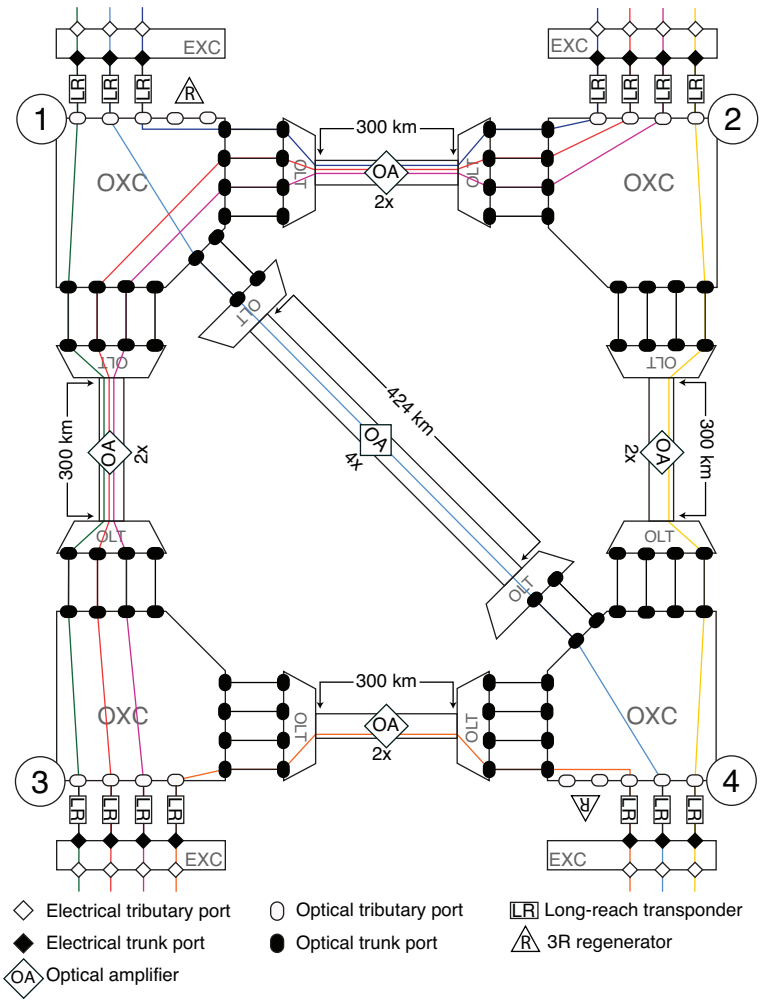

Figure 3.18: Translucent network with shared path restoration.

Table 3.10: CAPEX for the transparent network with dedicated path protection.

	Variable	Cost	Avg. # components	# total	Equation
Cost of links	$\langle c^{OLT,k_p} \rangle$	8.34	2.00	10	(3.131)
	$\langle c^{A,k_p} \rangle$	4.61	2.40	12	(3.135)
	$\langle c^{F,k_p} \rangle$	0.00	649.60	3248	(3.138)
	$\langle c_l^{k_p} \rangle$	12.95			(3.140)
	$C_L^{k_p}$	64.74			(3.139)
Cost of nodes	$\langle c^{EXC} \rangle$	15.68	3.50	14	(3.46)
	$\langle c_{tr}^{OXC,k_p} \rangle$	29.52	9.25	37	(3.148)
	$\langle c_{tr}^{TSP} \rangle$	3.50	3.50	14	(3.77)
	$\langle c_n^{k_p} \rangle$	48.69			(3.141)
	$C_N^{k_p}$	194.77			(3.142)
		$C_T = 259.51$			(3.12)

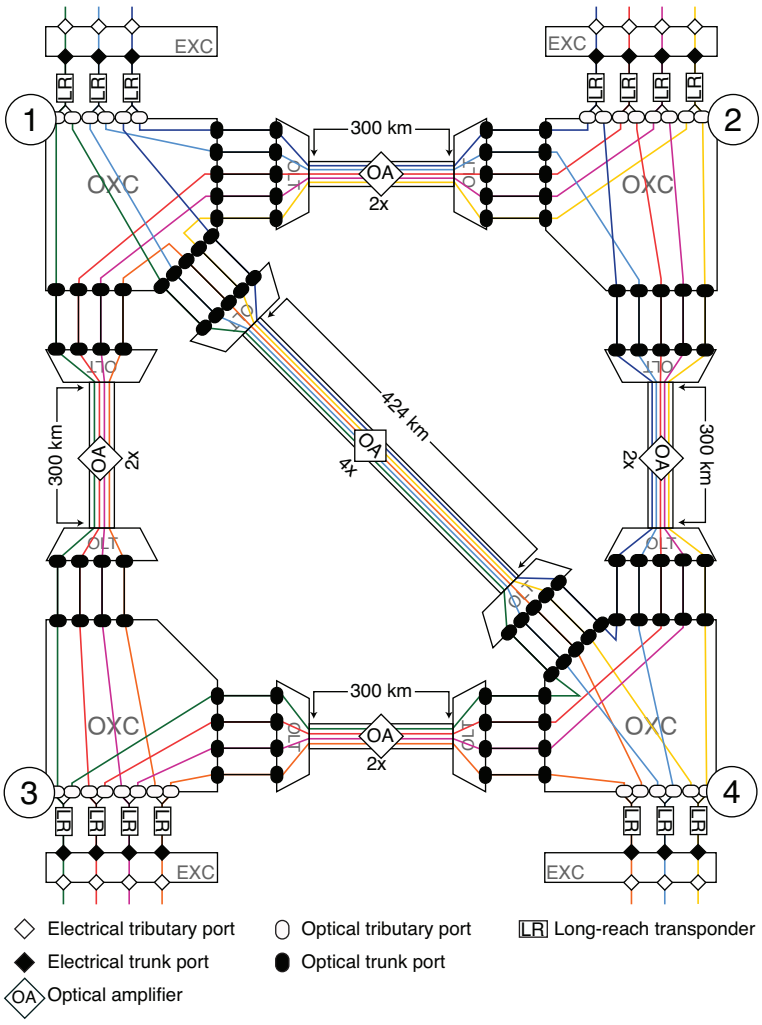

Figure 3.19: Transparent network with dedicated path protection.

Table 3.11: CAPEX for the transparent network with shared path restoration.

	Variable	Cost	Avg. # components	# total	Equation
Cost of links	$\langle c^{OLT,k_r} \rangle$	8.34	2.00	10	(3.131)
	$\langle c^{A,k_r} \rangle$	4.61	2.40	12	(3.135)
	$\langle c^{F,k_r} \rangle$	0.00	649.60	3248	(3.138)
	$\langle c_l^{k_r} \rangle$	12.95			(3.140)
	$C_L^{k_r}$	64.74			(3.139)
Cost of nodes	$\langle c^{EXC} \rangle$	15.68	3.50	14	(3.46)
	$\langle c_{tr}^{OXC,k_r} \rangle$	27.51	6.25	25	(3.154)
	$\langle c_{tr}^{TSP} \rangle$	3.50	3.50	14	(3.77)
	$\langle c_n^{k_r} \rangle$	46.68			(3.141)
	$C_N^{k_r}$	186.72			(3.142)
		$C_T = 251.46$			(3.12)

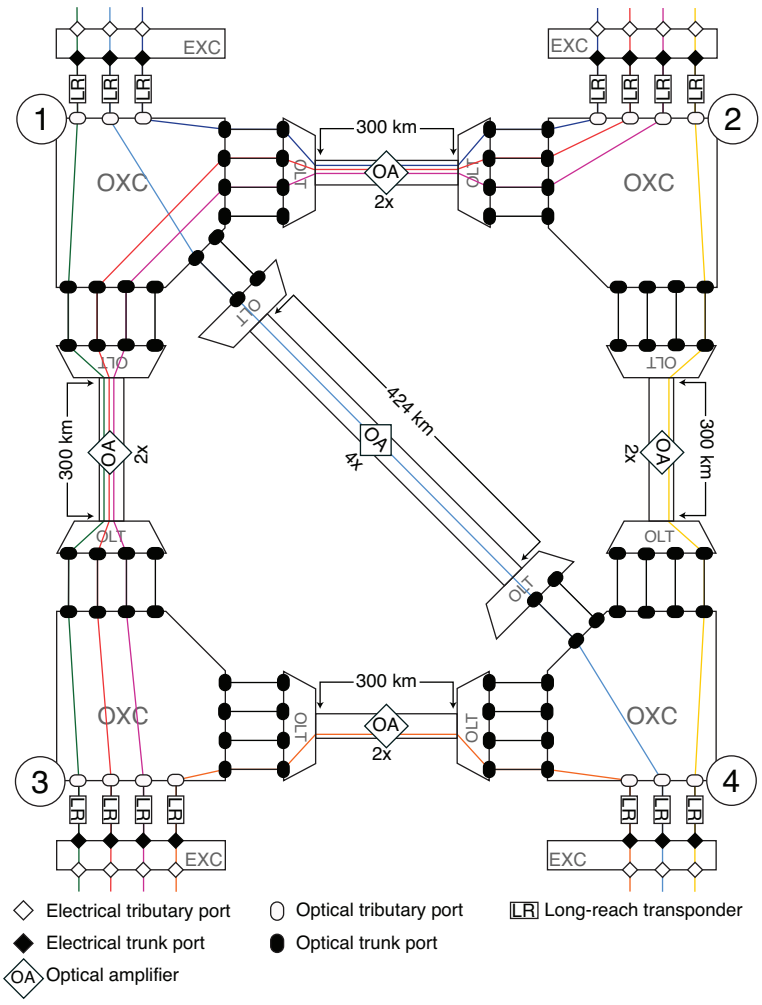

Figure 3.20: Transparent network with shared path restoration.

3.12 Chapter Summary

In this Chapter, the network cost model for networks operating in opaque, transparent and translucent transport mode was introduced. The model can be used to calculate the quantities and costs of the main components into a network.

However, notice that some information may be computational intensive to obtain, such as the average number of hops and survivability coefficients, specially for larger networks. In order to obtain the exact values for those variables we have to route the traffic demand, and compute backup paths for the demands affected in case of failures.

Furthermore, it is assumed that all information about the network is available. In order to overcome the absence of some information about the network, we can use statistics to estimate that information. We noticed that in order to estimate the CAPEX of a network with a given number of nodes and links, but without the knowledge on the network topology and traffic matrix, we need to estimate just five parameters: the total traffic, the average number of hops for working and backup paths, survivability coefficient and average link length. The specific case of translucent networks with shared path restoration also requires an estimation for the sharing of regenerators. The estimation of the required parameters will be studied in Chapter 5.

References

[1] S. K. Korotky, "Network global expectation model: A statistical formalism for quickly quantifying network needs and costs," *IEEE Journal of Lightwave Technology*, vol. 22, no. 3, pp. 703–722, Mar. 2004.

[2] M. Bhardwaj, L. McCaughan, S. K. Korotky, and I. Sanniee, "Analytical description of shared restoration capacity for mesh networks," *OSA Journal of Optical Networking*, vol. 4, no. 3, pp. 130–141, Mar. 2005.

[3] R. Sedgewick, *Algorithms in C++ Part 5: Graph Algorithms*, 3rd ed. Addison-Wesley, 2002, vol. 2.

[4] A. R. Correia, "Planeamento e dimensionamento de redes ópticas com encaminhamento ao nível da camada óptica," Master thesis, Universidade de Aveiro, Aveiro, Portugal, 2008.

[5] S. De Maesschalck, "How the asymmetric nature of IP traffic influences the cost of the underlying optical layer," *Fiber and Integrated Optics*, vol. 22, no. 2, pp. 63–77, March 2003.

[6] A. R. Correia, C. Pavan, and A. N. Pinto, "A probabilistic model for the demands on link on mesh optical networks," in *Proceedings of the 4th Symposium on Enabling Optical Networks and Sensors, SEON'06*, Porto, Portugal, Jun. 2006, pp. 43–44.

[7] M. Guerreiro, C. Pavan, A. L. Barradas, A. N. Pinto, and M. C. Medeiros, "Path selection strategy for consumer grid over obs networks," in *Proceedings of the 10th International Conference on Transparent Optical Networks, ICTON'08*, vol. 3. Athens, Greece: IEEE, June 2008, pp. 138–141.

[8] E. W. Dijkstra, "A note on two problems in connexion with graphs," *Numerische Mathematik*, vol. 1, pp. 269 –271, 1959.

[9] J. W. Suurballe and R. E. Tarjan, "A quick method for finding shortest pairs of disjoint paths," *Networks*, vol. 14, no. 2, pp. 325–336, October 1984. [Online]. Available: http://dx.doi.org/10.1002/net.3230140209

[10] J. F. Labourdette, E. Bouillet, R. Ramamurthy, and A. A. Akyama, "Fast approximate dimensioning and performance analysis of mesh optical networks," *IEEE/ACM Journal of Transactions on Networking*, vol. 3, no. 4, pp. 906–917, Aug. 2005.

[11] C. Pavan, R. M. Morais, and A. N. Pinto, "Impact of the traffic model on the restoration coefficient in optical transport networks," in *Proceedings of the 8th International Conference on Decision Support for Telecommunications and Information Society, DSTIS'09*, Coimbra, Portugal, September 2009.

[12] B. Ramamurthy, H. Feng, D. Datta, J. Heritage, and B. Mukherjee, "Transparent vs. opaque vs. translucent wavelength-routed optical networks," *Optical Fiber Communication Conference, 1999, and the International Conference on Integrated Optics and Optical Fiber Communication. OFC/IOOC '99. Technical Digest*, vol. 1, pp. 59–61 vol.1, 1999.

[13] J.-P. Vasseur, M. Pickavet, and P. Demeester, *Network Recovery: Protection and Restoration of Optical, SONET-SDH, IP, and MPLS*. San Francisco, CA, USA: Morgan Kaufmann, 2004.

[14] *SP Guru Transport Planner Documentation Set*, 16th ed., OPNET Technologies, Bethesda, MD, USA, February 2010.

[15] A. Devarajan, K. Sandesha, R. Gowrishankar, B. Kishore, G. Prasanna, R. Johnson, and P. Voruganti, "Colorless, directionless and contentionless multi-degree roadm architecture for mesh optical networks," in *Proceedings of the 2nd International Conference on Communication Systems and Networks, COMSNETS'10*. Bangalore, India: IEEE, 2010, pp. 1 –10.

[16] R. Hulsermann, A. Betker, M. Jager, S. Bodamer, M. Barry, J. Spath, C. Gauger, and M. Kohn, "A set of typical transport network scenarios for network modelling," *ITG FACHBERICHT*, no. 182, pp. 65–72, 2004.

[17] R. Huelsermann, M. Gunkel, C. Meusburger, and D. A. Schupke, "Cost modeling and evaluation of capital expenditures in optical multilayer networks," *J. Opt. Netw.*, vol. 7, no. 9, pp. 814–833, Aug. 2008.

Chapter 4

Generation of Transport Network Topologies

4.1 Introduction

Computer generated network topologies are often employed to perform simulations and analysis of algorithms in telecommunications networks. The reason for using computer generated (CG) topologies is due to the lack of available real-world networks in a large number for extensive studies [1]. Usually, completely random topologies do not have the required characteristics [2]. Therefore, their use can lead to incorrect decision making, such as underestimation of the impact of failures in a network. Thus, it is crucial to have a method to generate network topologies that resemble real-world transport networks.

Network topology generators [3–11] are extensively available in the literature. In [3], the author presents a model for generating random graphs in which the nodes are distributed over a plane, and links are added to the graph using a probability function based on the Euclidean distance between the nodes. In [4] and [5], the multi-level hierarchy found in the Internet is used to generate Internet-like topologies. In [6], the authors extract the autonomous system and router level topologies from the Internet and from that realistic core, topologies are generated. In [7], the authors show that the nodal degree distribution of the autonomous system level topologies follow a power-law. From that, several topology generators have been built based on power laws [8–11]. However, previous efforts have been focused on topologies resembling the Internet, which is a scale-free network [12]. Scale-free networks contain a few nodes with a very high number of links, while most nodes have just a few links. The nodal

degree distribution tends to follow a power law [12].

In this thesis, we are concerned with optical transport networks with survivable topologies. The characteristics of this kind of networks differs from scale-free networks. For instance, it is extremely rare to find nodes that have significantly more or fewer links than the average. Thus, topologies that resemble the Internet or topologies based on power laws are not suitable for optical transport network analysis. The starting point of our work is an extensive analysis of real-world transport networks to identify their relevant characteristics, presented in section 4.2. Next, in section 4.3 a model to generate topologies that resemble optical transport networks is proposed, and in section 4.4 we validate the model. In section 4.5 we study how to obtain a survivable physical topology that satisfies the traffic requirements and minimizes CAPEX, using a genetic algorithm.

4.2 Transport Network Topology Characteristics

In order to identify and study the key variables of real transport networks, we have collected a set of twenty nine topologies of real survivable transport networks (all that we have found). The number of nodes ranges from nine to one hundred, see Table 4.1. Next we analyze the characteristics of these network topologies, with the aim of identifying the relevant variables for the adequate characterization of transport networks.

In general, a real-world transport network topology can be seen as a graph over a two-dimensional plane. The nodes are distributed according to the expected traffic demand in each geographic area. Thereby, we can often identify regions with more nodes than the others. Here a region stands for a number of cities or countries (it depends on the geographic area). Figure 4.1 shows a possible set of regions on the European Optical Network topology. Although regions without any or very few nodes are pretty likely to be found, we can frequently find a set of nodes that form a closed cycle when the region hosts a set of at least three nodes. Closed cycles of nodes allow for the survivability because each pair of nodes has two disjoint interconnecting

Table 4.1: Real-world reference networks.

Number	Network [13]	N	L	$\langle\delta\rangle$
1	VIA NETWORK	9	12	2.67
2	BREN	10	11	2.20
3	RNP	10	12	2.40
4	vBNS	12	17	2.83
5	CESNET	12	19	3.17
6	NSFNET	14	21	3.00
7	ITALY	14	29	4.14
8	AUSTRIA	15	22	2.93
9	MZIMA	15	19	2.53
10	ARNES	17	20	2.35
11	GERMANY	17	26	3.06
12	SPAIN	17	28	3.29
13	LAMBDARAIL	19	23	2.42
14	MEMOREX	19	24	2.53
15	CANARIE	19	26	2.74
16	EON	19	37	3.89
17	ARPANET	20	32	3.20
18	PIONIER	21	25	2.38
19	COX	24	40	3.33
20	SANET	25	28	2.24
21	NEWNET	26	31	2.38
22	PORTUGAL	26	36	2.77
23	RENATER	27	35	2.59
24	GEANT2	32	52	3.25
25	LONI	33	37	2.24
26	METRONA	33	41	2.48
27	OMNICOM	38	54	2.84
28	INTERNET 2	56	61	2.18
29	USA 100	100	171	3.42

paths. When a node is unique within a region the survivability tends to be provided by connecting the node to at least two nodes in neighbor regions; in the case of regions with two nodes, the nodes tend to be directly connected and each one tends to be directly connected to at least a single node in a neighbor region. This way a transport network can also be seen as a set of smaller networks (one for each region).

Besides this holistic view, we were able to identify a few variables that characterize transport network topologies. The most relevant are the nodal degree, δ; the number

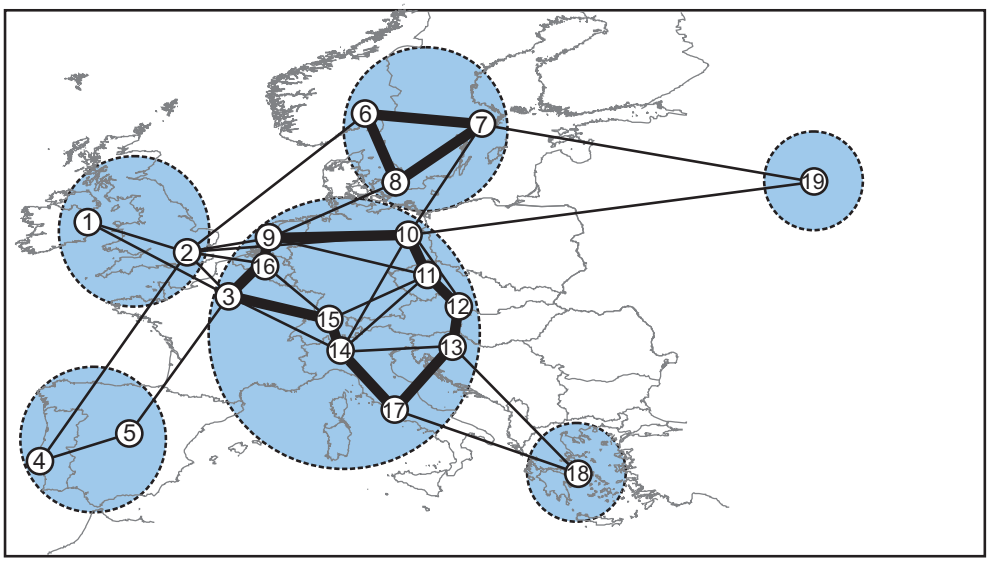

Figure 4.1: Physical topology of the European Optical Network (EON). The nodes, numbered from 1 through 19, are interconnected with optical cables and distributed across a geographic area. Some regions are more densely populated with nodes and links than others. Regions with a cluster of nodes often present cycles (see the stronger links).

of hops, h; link-disjoint pairwise connectivity, ω; node-disjoint pairwise connectivity, θ; and clustering coefficient, c. In the following we define and present each variable in more detail, and relate them to the real-world transport networks shown in Table 4.1.

In order to determine the distribution of δ, h, ω, θ and c, we performed a variety of goodness-of-fit statistical tests. A goodness-of-fit test is a special kind of hypothesis test, which is used to verify how well a model describe the data. Moreover, it lies on parametric or nonparametric statistic test [14]. Parametric statistical tests require that a sample analyzed is taken from a population that meets the normality assumption. On the other hand, non-parametric tests are used when assumptions about the population distribution are not made or are questionable [15]. Thus, because we did not know the distribution that describe our data in advance, we conducted non-parametric statistics (also called distribution-free statistics). There exist a number of non-parametric tests, including Wilcoxon, Mann-Whitney, Kruskal-Wallis and Kolmogorov-Smirnov tests. Kolmogorov-Smirnov test tends to be more powerful when the sample size is smal [14], therefore, this test was chosen for our analysis since our data set comes from 29 networks. The Kolmogorov-Smirnov goodness-of-

fit test for one sample is used to compare the observed frequencies of the values of a variable against a given theoretical distribution. Then it determines the statistical significance of the largest difference between them. We have tested our data against normal, uniform, Poisson and exponential distributions, using a software for statistical analysis called SPSS [16].

Using the one-sample Kolmogorov-Smirnov test, we verified that the nodal degrees of 21 networks out from 29 from Table 4.1 follow a Poisson distribution at 0.05 significance level, and the remaining 4 networks (18, 21, 23, 27) follow a Poisson distribution at 0.01 significance level. In Figure 4.2, it is presented the nodal degree relative frequency distribution for the USA100 network and the Poisson probability function, with mean $\langle\delta\rangle = 3.42$. We have noticed that the networks failing the test at

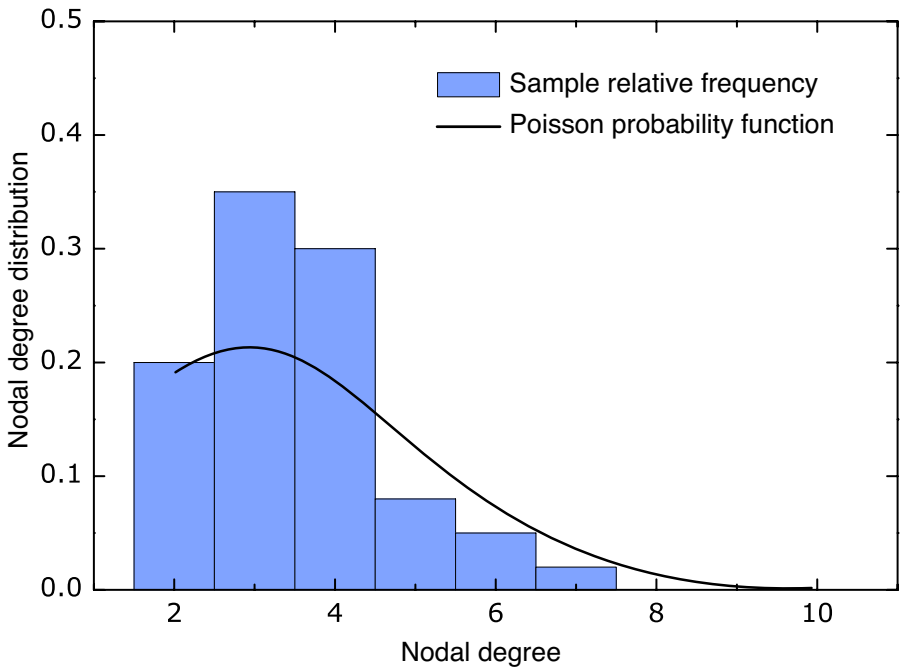

Figure 4.2: Nodal degree relative frequency and the Poisson probability function, with mean $\langle\delta\rangle = 3.42$, for the USA100 network. We verified that real transport networks tend to follow a Poisson distribution for the nodal degree.

both significance levels (networks 17, 25, 26, 28), are quasi-regular, i.e., the nodal degree is almost the same for all nodes and the variance is small. The above results confirm the results obtained in [12] and [17]. According to [17], the nodal degree of optical transport networks tends to follow a Poisson distribution. These networks are

also called exponential networks because the probability that a node is connected to k other nodes tends to decrease exponentially for larger k.

In survivable topologies, the minimum nodal degree is required to be two, i.e., $\delta_{min} \geq 2$. Note that this condition is necessary but not sufficient for survivability purposes. The nodal degree in our reference networks ranges from 2 to 10, and the average nodal degree ranges from $\langle\delta\rangle = 2.18$ to $\langle\delta\rangle = 4.14$, as shown in Figure 4.3. Considering all networks we have obtained $\langle\delta\rangle^* = 2.8$. We use the asterisk index to indicate that the value of the parameter is obtained from the set of networks rather than a particular one. The standard deviation for nodal degree ranges from 0.4 to 2.

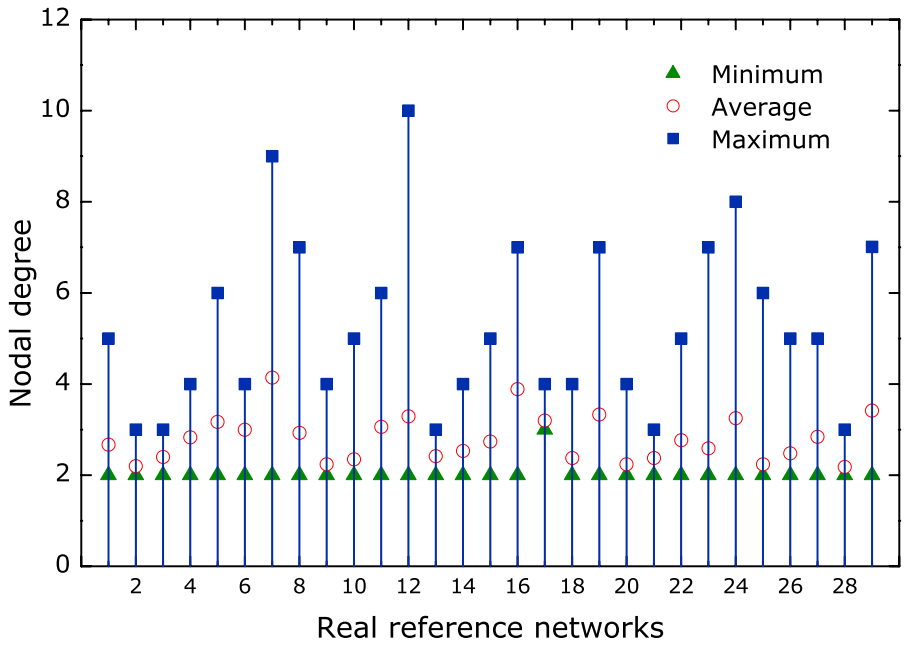

Figure 4.3: The minimum, average and maximum values of nodal degree for the twenty nine real-world network topologies of Table 4.1.

In Chapter 3 we have defined the average number of hops, expression (3.93), depending on the demands matrix. In this Chapter we intend to obtain the number of hops between a node pair, and the number of demands between them are not considered. Thus, we may consider a uniform demands matrix, i.e., a matrix where

all $d_{i,j}$ elements are 1. This allow to rewrite the expression (3.93) as

$$\langle h \rangle = \frac{2}{N(N-1)} \sum_{i=1}^{N-1} \sum_{j=i+1}^{N} h_{i,j}. \tag{4.1}$$

In Figure 4.4 we can see that the number of hops vary between 1 and 21. Regarding the average number of hops, $\langle h \rangle$, the values range from 2 to 8.5 and the standard deviation is in the range of 0.7 to 4.6. Considering all networks we have $\langle h \rangle^* = 3.4$. We observed that larger networks are sparser, which tends to lead to higher average number of hops.

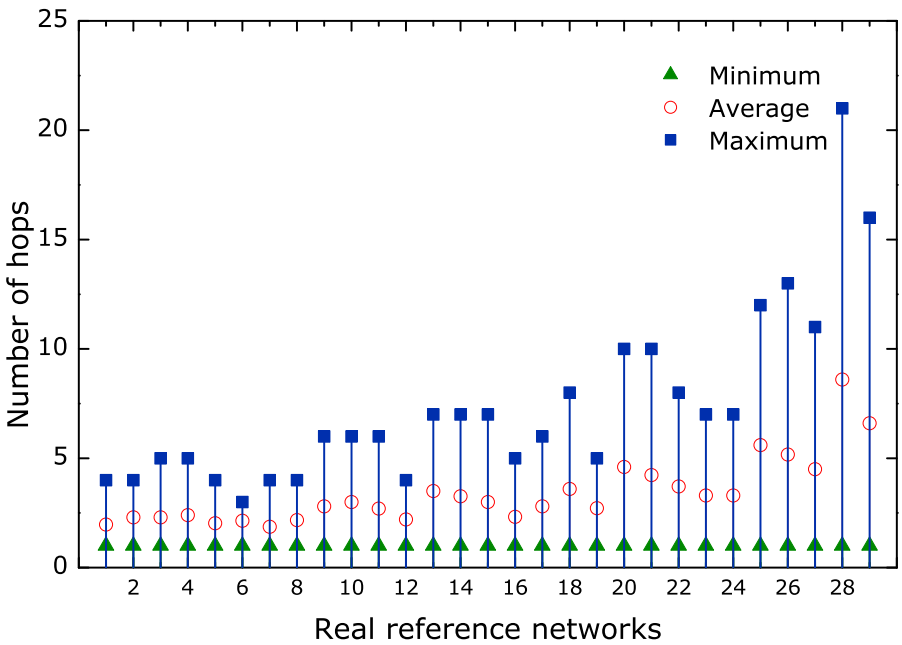

Figure 4.4: The minimum, average and maximum values of number of hops for twenty nine real-world network topologies.

Since a failure may affect various shared resources, the connectivity must be sufficient to allow recovery techniques to be employed. Recovery techniques usually rely on node and/or link-disjoint paths to ensure that both the working and backup paths will not be affected by the same single failure [18]. Connectivity is a measure that depends on the number of disjoint paths. Link-disjoint pairwise connectivity, $\omega_{i,j}$, is the number of link-disjoint paths between the node pair i, j. That is, between the nodes i and j there are $\omega_{i,j}$ paths in which the intermediary links are not shared. The value of $\omega_{i,j}$ also indicates the allowed number of link failures. For instance, a network

with $\omega_{i,j} = 2$ for all pairs of nodes tolerates single link failures [4, 19]. For $\omega_{i,j} = 3$ at most two link failures are tolerated and so forth. Adding the link-disjoint pairwise connectivity of all node pairs and dividing by the number of possible bidirectional node pairs we obtain the average link-disjoint pairwise connectivity, $\langle\omega\rangle$, for a network,

$$\langle\omega\rangle = \frac{2}{N(N-1)} \sum_{i=1}^{N-1} \sum_{j=i+1}^{N} \omega_{i,j}. \tag{4.2}$$

Referring to Figure 4.5 we can see that survivable networks have at least two link-disjoint paths between each pair of nodes, $\omega_{i,j} \geq 2$. Furthermore, this value goes up to 7 in our sample, $\omega_{i,j} \leq 7$. The standard deviation obtained is in the range of 0 to 0.9. The average link-disjoint pairwise connectivity, $\langle\omega\rangle$, increases with $\langle\delta\rangle$. Considering all networks we have $\langle\omega\rangle^* = 2.25$.

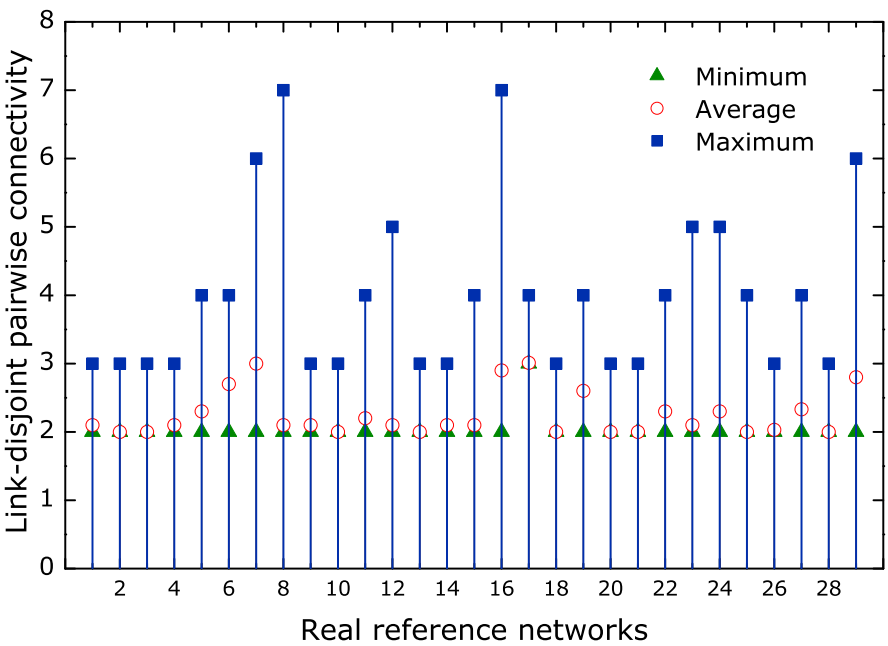

Figure 4.5: The minimum, average and maximum values of link connectivity for twenty nine real-world network topologies.

Two paths are node-disjoint if they have no nodes in common other than the source and destination. Node-disjoint pairwise connectivity, $\theta_{i,j}$, is the number of node-disjoint paths between the node pair i, j. The value of $\theta_{i,j}$ also indicates the tolerance to node failures. Since a node-disjoint path also implies link-disjoint path, a network with

$\theta_{i,j} \geq 2$ for all node pairs allows survivability against both node and link failures [20]. We can obtain the average node-disjoint pairwise connectivity, $\langle\theta\rangle$, for a network with,

$$\langle\theta\rangle = \frac{2}{N(N-1)} \sum_{i=1}^{N-1} \sum_{j=i+1}^{N} \theta_{i,j}. \tag{4.3}$$

Node-disjoint pairwise connectivity, $\langle\theta\rangle$, tends to increase with $\langle\delta\rangle$. As can be seen in Figure 4.6, some of our real-world reference topologies do not tolerate node failures, see the networks in which the minimum node-disjoint pairwise connectivity is 1. For our reference networks, the values of node-disjoint pairwise connectivity satisfies $1 \leq \theta_{i,j} \leq 7$, with standard deviation in the range of 0 to 1. The average node-disjoint pairwise connectivity, $\langle\theta\rangle$, for survivable topologies against single node failures ranges between 2 and 3. Considering all networks we have $\langle\theta\rangle^* = 2.21$.

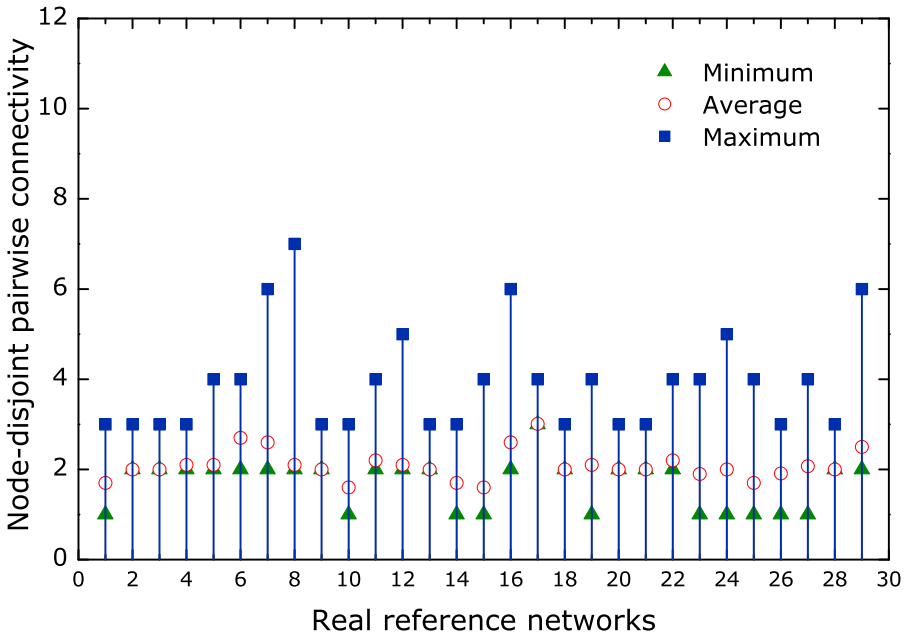

Figure 4.6: The minimum, average and maximum values of node connectivity for twenty nine real-world network topologies.

The clustering coefficient of a node, c_i, quantifies how close its neighbors are to being a full mesh. The neighborhood of a node, n_i, is the set of nodes which are directly connected to the node i. The value of c_i vary from 0 to 1, being 1 if the neighborhood forms a full mesh and 0 if none of the neighbors are directly connected [21]. For

undirected and connected graphs, the clustering coefficient of a node is defined as

$$c_i = \frac{2t_i}{\delta_i(\delta_i - 1)}, \tag{4.4}$$

where t_i is the number of existing triangles involving the node i and its n_i neighbors, and δ_i is the nodal degree of the node i. The clustering coefficient of the network, $\langle c \rangle$, is the average clustering coefficient of all nodes in the network,

$$\langle c \rangle = \frac{1}{N} \sum_{i=1}^{N} c_i. \tag{4.5}$$

The clustering coefficient of the network ranges from 0 to 0.69, with standard deviation in the range of 0 and 0.4. Considering all networks we have obtained $\langle c \rangle^* = 0.19$.

4.3 Generating Realistic Transport Network Topologies

The proposed method is based on the Waxman model [3]. This choice was made because topologies generated with the Waxman model tend to follow a Poisson distribution for the nodal degree [22, 23] (the same trend of real-world transport networks). However, in order to more accurately satisfy the characteristics of survivable networks, our method differs from the Waxman model in the following: a) the plane is divided into regions; b) nodes placement and connectivity obey certain constraints.

In the Waxman approach the probability of a node pair to be directly connected is

$$P_{i,j} = \beta \, exp^{\frac{-\iota_{i,j}}{\zeta\alpha}}, \tag{4.6}$$

where $\iota_{i,j}$ is the Euclidean distance between the nodes i and j, ζ is the maximum distance between any two nodes and α and β are parameters in the range of $(0, 1]$. Increasing the value of α leads to a larger ratio of long links to short links, whereas the probability of links between any pair of nodes increases with β. Figure 4.7 shows a network topology generated with the Waxman model. As can be seen in Figure 4.7, the Waxman model produces topologies with nodes of degree one. Also, it does not

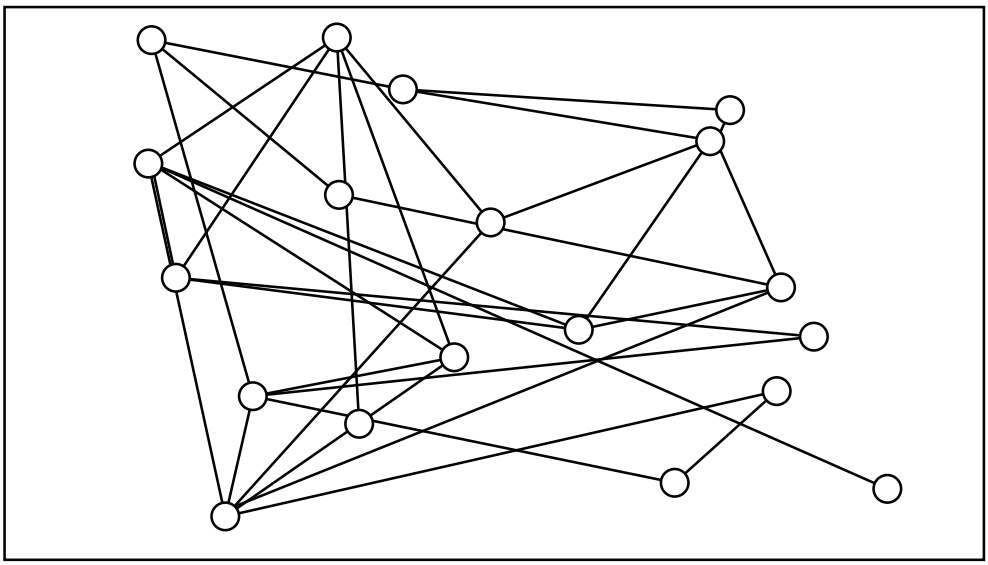

Figure 4.7: A network generated by the Waxman model, with $\alpha = 0.4$ and $\beta = 0.4$.

guarantee a connected topology [4,5]. Moreover, as the Waxman model distributes the nodes randomly over the whole plane, links crossing the whole plane tend to appear. Therefore, the networks generated do not have the connectivity characteristics of real-world survivable transport networks.

Our proposed method models a survivable transport network according to our observations on real networks, which is a set of interconnected smaller sub-networks, and introduces constraints to guarantee the characteristics showed in the previous section. As presented in Table 4.2, our method requires a set of nine inputs. The number of nodes, N. Minimum and maximum mean nodal degrees, $\langle\delta\rangle_{min}$ and $\langle\delta\rangle_{max}$, used to specify the minimum and maximum number of links. The area of the plane, A. The plane is assumed to be a square with side $X = \sqrt{A}$. The number of regions, $\mathring{R}$, used as part of the strategy to resemble the connectivity of transport networks. The minimum distance between the nodes, d, which restricts the distance between the nodes. The α and β are parameters of the embedded Waxman link probability [3]. The number of simulations is specified by φ.

The method consists of the following five major steps:

- divide the plane into $\mathring{R}$ regions;
- assign and place the N nodes into the regions;

- interconnect the nodes inside each region;
- interconnect nodes between different regions;
- add links to satisfy the mean nodal degree criterion.

Table 4.2: Input variables for the proposed method.

Variable	Description
N	number of nodes
$\langle\delta\rangle_{min}$	minimum average nodal degree
$\langle\delta\rangle_{max}$	maximum average nodal degree
A	area of the plane in arbitrary units
$\mathring{R}$	number of regions
ι	minimum distance between two nodes
α	Waxman link probability parameter
β	Waxman link probability parameter
φ	number of simulations

The plane is partitioned into $\mathring{R}$ equal area regions. Each region has an area of

$$A_r = \Delta X_r^x \Delta X_r^y, \tag{4.7}$$

where ΔX_r^x and ΔX_r^y are the dimensions of the region r. The number of horizontal and vertical divisions on the plane depends on the given $\mathring{R}$, which is firstly decomposed into two numbers ($p1,\ p2$). The $p1$ is the largest prime number such that $\mathring{R}$ is divisible by $p1$. The number $p2$ is the ratio between $\mathring{R}$ and $p1$. Then $\Delta X_r^x = X/p2$ and $\Delta X_r^y = X/p1$. Thus, the plane is divided into $p1$ rows and $p2$ columns, as illustrated in Figure 4.8, where $\mathring{R} = 6$. In case of $\mathring{R}$ being a prime number, one is added to $\mathring{R}$ to allow this plane division strategy. The extra region remains without nodes.

Given the area of a region, A_r, and the minimum distance between two nodes, ι, the maximum number of nodes that can be placed into a region is roughly

$$n_{max} = \frac{A_r}{\iota^2}. \tag{4.8}$$

In order to distribute the nodes the regions are chosen at random and the nodes are assigned to them, obeying the limit n_{max}. Thereafter, the nodes are randomly placed

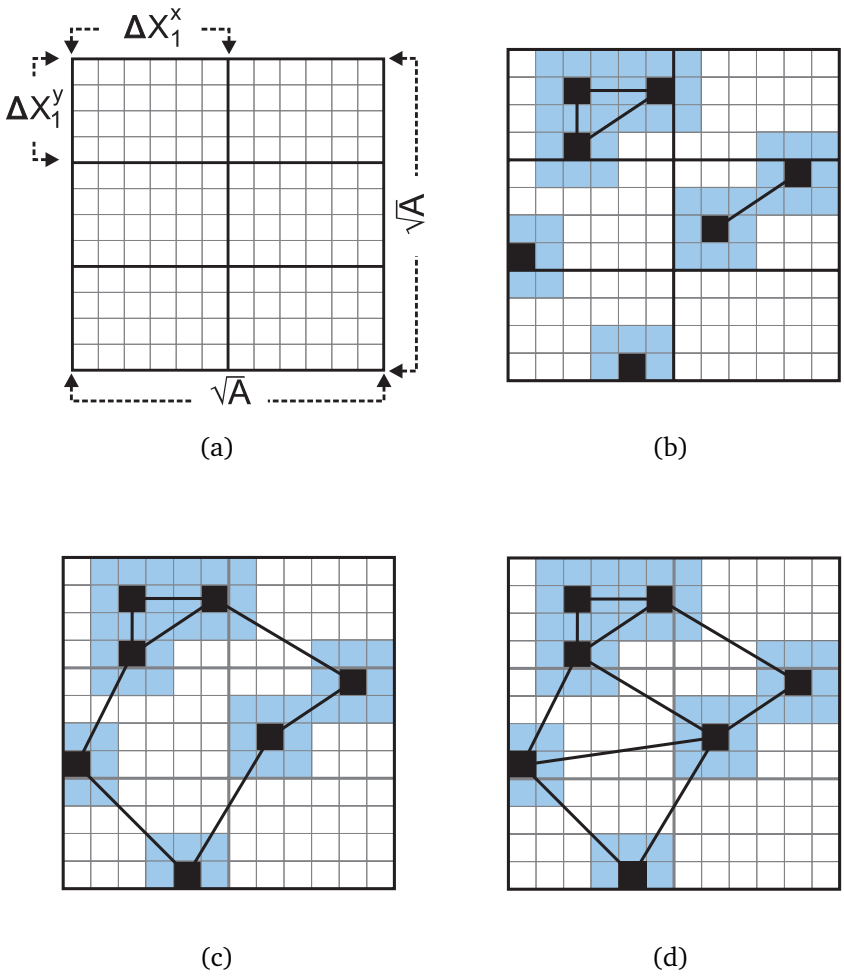

Figure 4.8: (a) The plane and regions. (b) Node placing, connection and blocked areas. (c) Region interconnection. (d) A possible network topology over a six-region plane.

over the respective regions, obeying the given minimum distance between the nodes, ι (which represents a blocked area around the nodes). In Figure 4.8b, the placed nodes are shown as black squares whereas the light blue squares represent the blocked area.

After the above procedure, we may have regions without nodes, with one, two or more than two nodes. If a region has two or more nodes an additional procedure is required, that is, if there are two nodes they are directly connected; if there are more than two nodes they are connected as a cycle. For regions with more than three nodes, the way the nodes are directly connected follows the Waxman link probability [3]. See a scenario for this phase in Figure 4.8b.

Once the nodes inside each region are interconnected, new links should be added to interconnect the regions. This process also follows the Waxman link probability, however, each node of the selected pair belongs to different regions. In order to guarantee that the generated topology will be survivable, some precautions should be taken into account: if a region has only one node, this node must be connected to at least two nodes of neighbor regions; if the region has only two nodes, each one must be connected to a node in neighbor regions; if a region has more than two nodes, at least two nodes must be connected to nodes of neighbor regions. Two nodes of a region can be connected to the same destination node in a neighbor region only if node-disjoint paths are not required.

At this phase we have a connected and survivable network topology (at least against single link failures). However, new links should be added until the given minimum mean nodal degree, $\langle\delta\rangle_{min}$, is reached. This procedure is done following the Waxman link probability. Afterwards, a new topology is stored for each new link between $\langle\delta\rangle_{min}$ and $\langle\delta\rangle_{max}$. This procedure will generate several network topologies with the same node distribution, but with different average nodal degrees, $\langle\delta\rangle$. If the number of simulations, φ, is more than one, the nodes and links should be cleared from the plane and all procedures from the node distribution are done again with the same inputs.

The number of topologies that are generated during the algorithm run, T, depends on $\langle\delta\rangle_{min}$, $\langle\delta\rangle_{max}$, φ and N, and it is given by

$$T = \varphi\left\lfloor\left(\frac{\langle\delta\rangle_{max}N - \langle\delta\rangle_{min}N}{2}\right) + 1\right\rfloor. \tag{4.9}$$

Given the minimum average nodal degree, $\langle\delta\rangle_{min}$, maximum average nodal degree, $\langle\delta\rangle_{max}$, and total number of nodes, N, we achieve the number of different topologies that are generated during the algorithm run. The expression $(\langle\delta\rangle_{max}N - \langle\delta\rangle_{min}N)/2$ gives the number of bidirectional links that remains to be included in an initial topology in order to go from $\langle\delta\rangle = \langle\delta\rangle_{min}$ until $\langle\delta\rangle = \langle\delta\rangle_{max}$. The φ is the number of algorithm runs. The floor function is applied because it is not always possible to obtain topologies with the given $\langle\delta\rangle_{min}$ and $\langle\delta\rangle_{max}$, with N nodes. Figure 4.8d shows an example of a

network topology, and Figure 4.9 shows the flowchart of the algorithm.

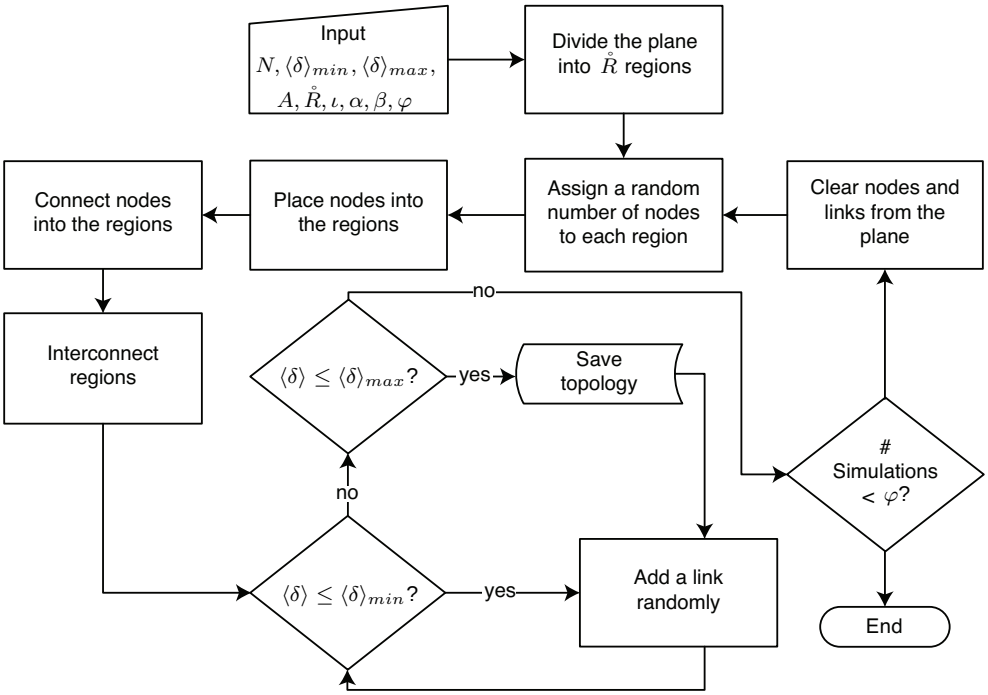

Figure 4.9: Flowchart of the generation algorithm. A plane is divided into $\mathring{R}$ regions, and a number of nodes is assigned and placed to each region. After the nodes are interconnected, new links are added while the mean nodal degree is between $\langle\delta\rangle_{min}$ and $\langle\delta\rangle_{max}$.

4.4 Experiments and Results

In order to validate the method, we implemented a program following the flowchart in Figure 4.9. Before starting the topology generation we have to calibrate the generator, which means to find out adequate values for the input parameters.

For transport network topologies, the number of nodes N varies from 10 to 100 nodes. The mean nodal degree is $2 \leq \langle\delta\rangle \leq 4$ as can be seen in Figure 4.3. The area of the plane, A, must be large enough to accommodate N nodes. Using the number of nodes, N, and the minimum distance between the nodes, ι, the value of A must be larger than $N\iota^2$. The number of regions, $\mathring{R}$, depends on the size of the plane and the number of nodes. A plan with more regions leads to more cycles and higher $\langle h\rangle$. We performed several simulations varying the value of $\mathring{R}$ from 1 to 40 using the number

of nodes of our reference networks, and noticed that for transport networks with a number of nodes under a hundred, a suitable range of values is between $4 \leq \mathring{R} \leq 20$. For larger networks, a higher $\mathring{R}$ may be used.

For the experiments conducted in this work we have assumed the same N and $\langle\delta\rangle$ of the real-world reference networks. The plane was assumed to be $A = 100^2$. The plane was partitioned into twelve regions, $\mathring{R} = 12$, and the minimum distance between the nodes was considered to be two, $\iota = 2$. In [3], the author used $\alpha = 0.4$ and $\beta = 0.4$. In order to verify whether these values are appropriate for our method, we used the one-sample Kolmogorov-Smirnov test to obtain the best-fit curve to the link length distribution over all real-world topologies.

Figure 4.10 shows that the curve fits well with the same values originally used by Waxman in [3], with mean error less than 2%. Therefore we use $\alpha = 0.4$ and $\beta = 0.4$. The minimum, average and maximum values for the nodal degree, δ, number of hops, h, link-disjoint pairwise connectivity, ω, and node-disjoint pairwise connectivity, θ, for the generated networks have been calculated and are graphically represented in Figures 4.11, 4.13, 4.14 and 4.15.

In order to identify whether the variables of computer generated topologies follow the same distribution of the real-world ones, we have conducted the two-independent-sample Kolmogorov-Smirnov test [15]. We take one sample of computer generated networks and a sample of real-world networks, with the same number of nodes and links. Then we test the hypothesis that they follow the same distribution. Regarding nodal degree, the tests have revealed that all computer generated topologies follow the same distribution of the respective real-world topologies at 0.05 significance level.

Referring Figure 4.11, we can see that the network topologies have $\delta_{min} \geq 2$ and $\delta_{max} \leq 8$ and $\langle\delta\rangle$ ranges from 2 to 4 with standard deviation in range of 0.6 to 2.6. Considering all networks we have $\langle\delta\rangle^* = 2.8$. Figure 4.12 shows the nodal degree relative frequency and the Poisson probability function, with mean $\langle\delta\rangle = 3.42$, for a computer generated topology with $N = 100$, $L = 171$ (these values correspond to the ones of the network presented in Figure 4.2). As we can see, the degree distribution of the computer generated network tends to follow a Poisson probability function.

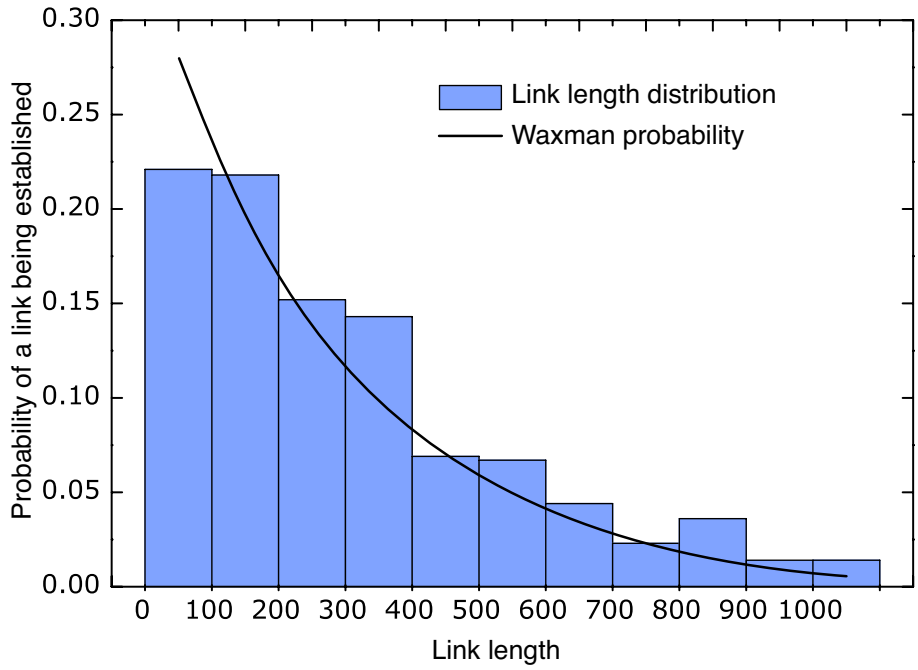

Figure 4.10: Waxman link probability (expression 4.6) with $\alpha = 0.4$ and $\beta = 0.4$ over a link length distribution. We have considered 950 links of networks presented in Table 4.1.

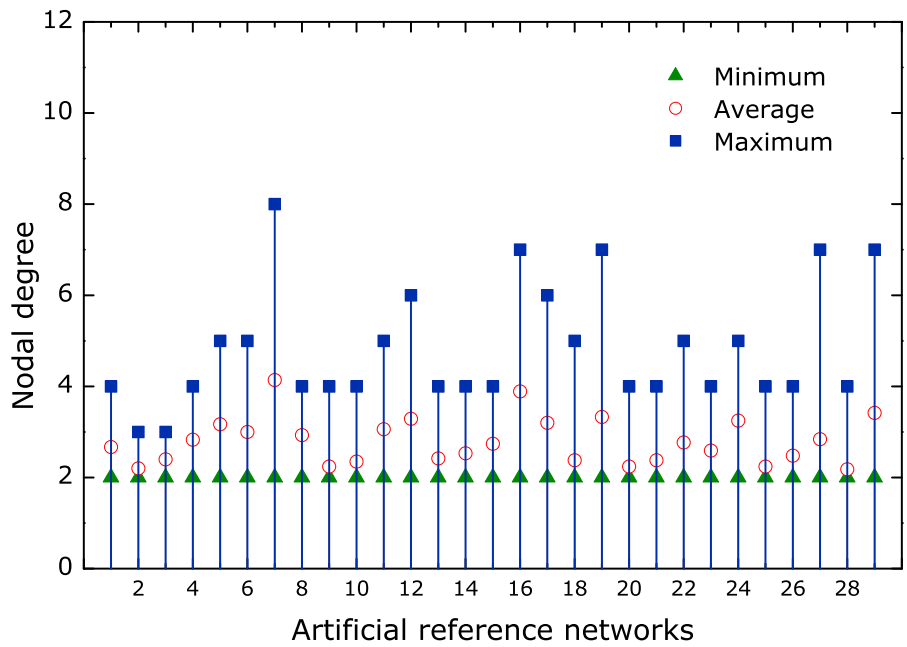

Figure 4.11: The minimum, average and maximum values of nodal degree for twenty nine computer generated network topologies.

Figure 4.13 shows that the number of hops range from 1 to 20. The average number of hops, $\langle h \rangle$, ranges from 2 to 8.3 with a standard deviation in range of 0.7 to 4.3.

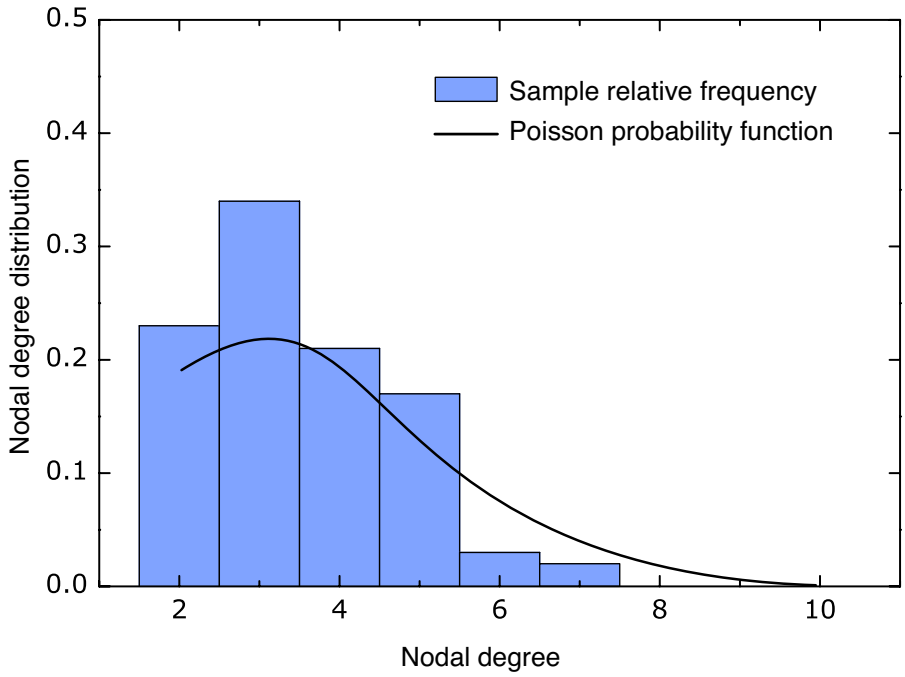

Figure 4.12: Nodal degree relative frequency and the Poisson probability function, with mean $\langle\delta\rangle = 3.42$, for a computer generated topology with $N = 100$, $L = 171$ (these values are identical to the USA100 topology, see Figure 4.2).

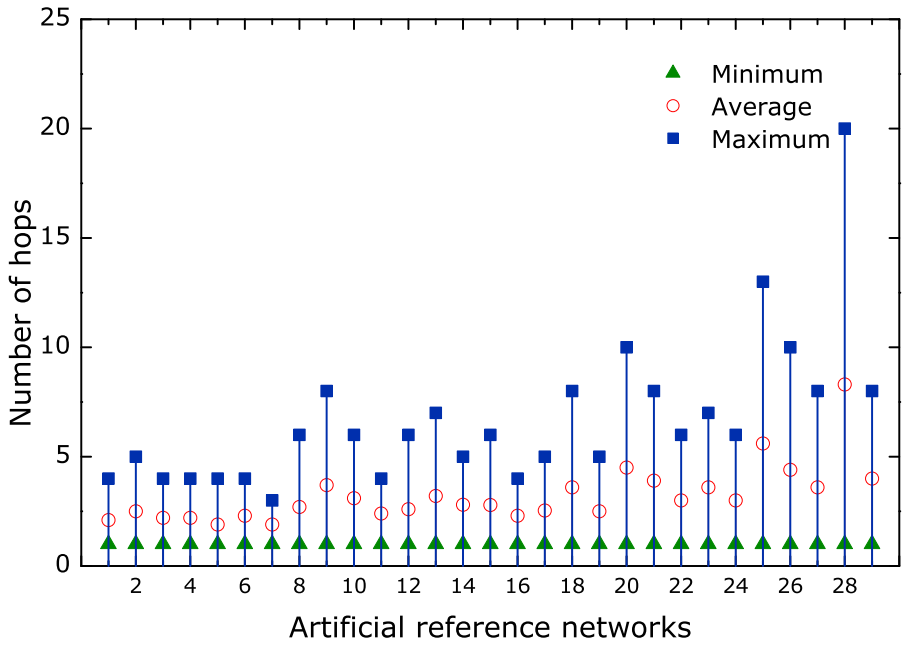

Figure 4.13: The minimum, average and maximum values of number of hops for twenty nine computer generated network topologies.

Considering all networks we have $\langle h \rangle^* = 3.2$. These results closely agree with the observations obtained from real-networks.

Figure 4.14 shows that all computer generated network topologies have at least two link-disjoint paths between each pair of nodes, $\omega_{i,j} \geq 2$, and at most six, $\omega_{i,j} \leq 6$. The average link-disjoint pairwise connectivity, $\langle \omega \rangle$, ranges from 2 to 3 independently of the network size and present a standard deviation in range of 0.1 to 1. Considering all networks we have $\langle \omega \rangle^* = 2.3$.

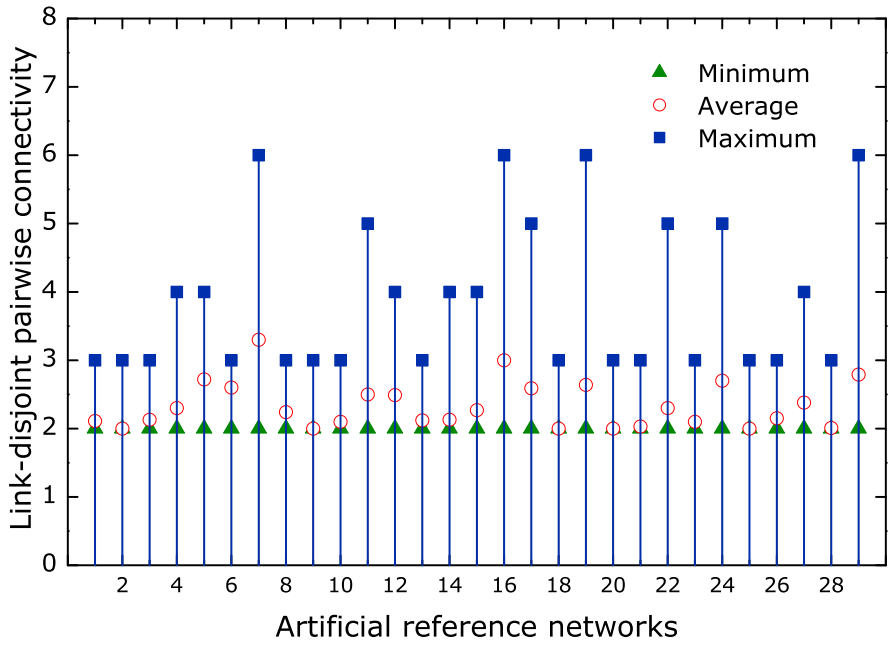

Figure 4.14: The minimum, average and maximum values of link-disjoint pairwise connectivity for twenty nine computer generated network topologies.

The node-disjoint pairwise connectivity satisfies $1 \leq \theta_{i,j} \leq 6$, see Figure 4.15. The average node-disjoint pairwise connectivity, $\langle \theta \rangle$, for survivable topologies against single node failures ranges between 2 and 3 with a standard deviation in range of 0 to 1.1. Considering all networks we have $\langle \theta \rangle^* = 2.26$. In terms of both link and node-disjoint pairwise connectivity, all the computer generated topologies follow the same distribution of the respective real-world topologies at 0.05 significance level.

In terms of clustering coefficient of the network, all the computer generated topologies follow the same distribution of the respective real-world topologies at 0.05 significance level. The clustering coefficient of the networks ranges from 0 to 0.65 with

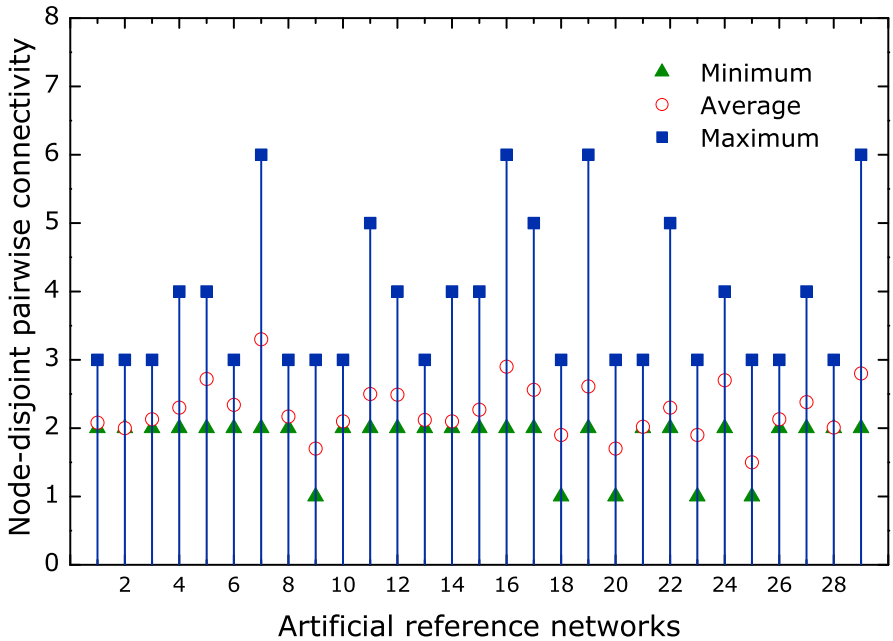

Figure 4.15: The minimum, average and maximum values of node-disjoint pairwise connectivity for twenty nine computer generated network topologies.

standard deviation in the range of 0 to 0.4. Considering all networks we have obtained $\langle c \rangle^* = 0.16$. Figure 4.16 shows a comparison between the clustering coefficient of real and computer generated networks. The average deviation is 0.07.

Table 4.3: Summary of the values of key variables.

Var	Minimum		Average*		Maximum		Std.Deviation	
	Real	CG	Real	CG	Real	CG	Real	CG
δ	2	2	2.80	2.80	10	8	0.4-2.0	0.6-2.6
h	1	1	3.40	3.20	21	20	0.7-4.6	0.7-4.3
ω	2	2	2.25	2.30	7	6	0.0-0.9	0.1-1.0
θ	1	1	2.21	2.26	7	6	0.0-1.0	0.0-1.1
c	0	0	0.19	0.16	1	1	0.0-0.4	0.0-0.4

In Table 4.3 we summarize the values of key variables obtained from both real and computer generated (CG) network topologies. We can see that, although a given number of nodes and links may produce a huge number of topologies, the computer generated topologies effectively shows statistics similar to the real-world optical transport networks. Table 4.4 shows a comparison between a real-world transport network and a computer generated one.

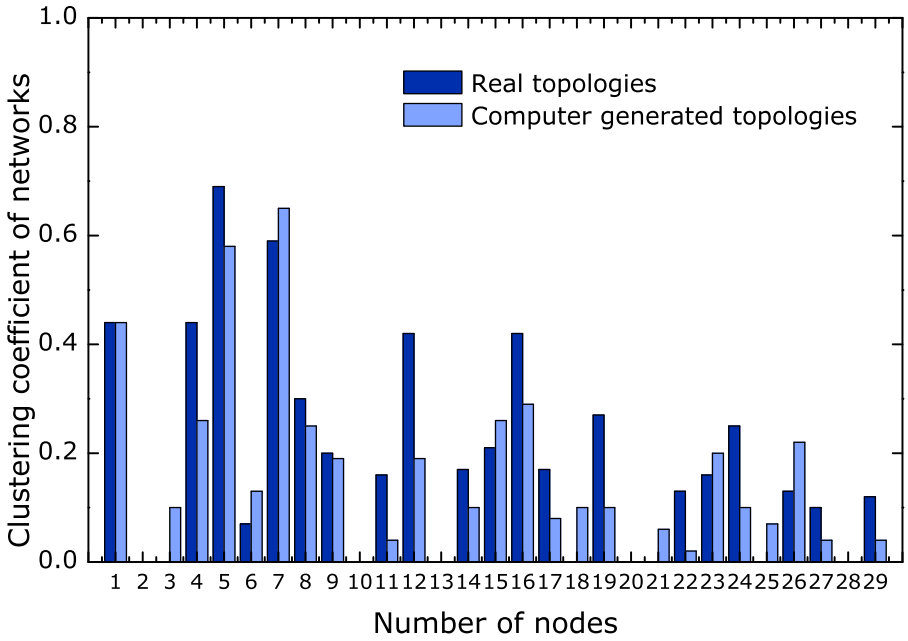

Figure 4.16: Comparison between the clustering coefficient of real and computer generated networks. The minimum and maximum deviation between each pair of networks (real and computer generated) is 0 and 0.23, respectively. The average deviation is 0.07.

Table 4.4: Comparative between a real and a computer generated topology. The topologies has the same number of nodes and links as the EON topology.

Var	Real EON Topology		CG EON topology	
	Range	Average	Range	Average
δ	1-7	3.89	1-6	3.89
h	1-5	2.30	1-5	2.40
ω	2-7	2.90	2-6	3.00
θ	2-6	2.6	2-6	2.8

Therefore, the statistics are similar to the ones presented in the EON network. Similar results were obtained with more than fifty thousand computer generated network topologies, when compared with the real-world network statistics. Figure 4.17 shows an example of a computer generated network.

4.5 Topological Design using a Genetic Algorithm

In this section we study how to obtain a survivable physical topology that satisfies the traffic requirements and minimizes CAPEX, i.e., the most cost efficient network

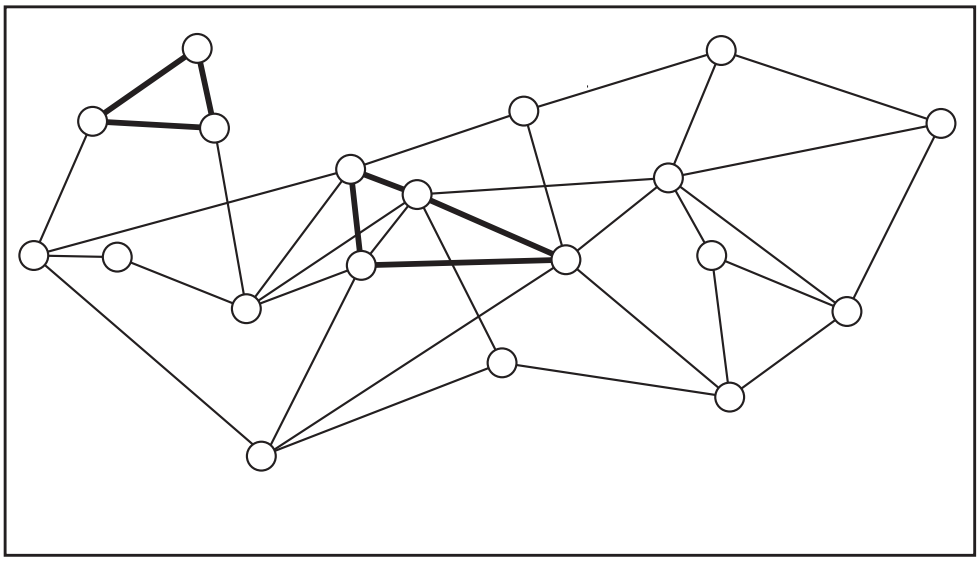

Figure 4.17: Example of a computer generated network topology for $N=19$, $L=37$, $A=100$, $\mathring{R}=12$, $\iota=2$, $\zeta=71$, $\alpha=0.4$, $\beta=0.4$. Possible cycles inside regions are shown as stronger links.

topology. In practice, several traffic scenarios are defined and evaluated, then the lowest cost network which will remain feasible for the majority of the scenarios is implemented [24]. However, this method is time consuming so it is crucial to design physical topologies, ensuring the routing of the required traffic and guaranteeing the network survivability at minimum cost.

In this section we consider networks with opaque transport mode and dedicated path protection. For ease of modeling, the cost of long-reach transponders is calculated as part of the links cost. Moreover, we consider that the network should be survivable against any single link failure. Thus, the underlying topology is a 2-connected graph. The topological design of minimum cost 2-connected graphs, not allowing the use of parallel edges, is strongly NP-hard [25], thus Integer Linear Programming (ILP) models only lead to optimal solutions, within reasonable time and computational effort, for small size networks. Consequently, heuristics are commonly used to search near optimal solutions. Here we address the problem of design the physical topology, ensuring survivability and minimizing the network CAPEX in optical transport networks. In order to deal with this problem we propose a genetic algorithm [26].

As the convergence of the genetic algorithm depends on the used genetic operators,

we analyze their impact on the quality of the obtained solutions. We also compare the performance of different generators of initial population, selection methods, crossover operators and population sizes. The performance of the proposed heuristic is evaluated using an ILP model. We use a simplified cost model to calculate the CAPEX of an optical network to obtain exact results that can be compared with the heuristic solutions. The computational results are obtained using the node location of nine real telecommunications networks.

4.5.1 Simplified Model

Let's represent a transport network as a weighted graph, $G(V, E)$, in which the set of vertices, $V = \{1, \ldots, N\}$, correspond to the nodes and the set of edges, $E = \{(i, j) : i, j \in V, i < j\}$, represents all possible bidirectional links. The weight of an edge (link) (i, j) is assumed to be proportional to its length and is denoted by $\nu_{i,j}$.

The demand between the origin node, a, and destination node, b, is denoted by $\{a, b\}$ and the set of all demands by $D = \{\{a, b\} : a, b \in V\}$. The number of optical channels needed in each link to support the demands from a to b is denoted by $B_{a,b}$.

We denote the total cost of a link by $c_{i,j}$, which can be calculated with

$$c_{i,j} = \left(c_{i,j}^{OLT} + c_{i,j}^{A} + c_{i,j}^{F}\right). \tag{4.10}$$

Notice that expression (4.10) is the same presented in (3.21). Here we just replace the index "l" by "i, j" to indicate the nodes connected to the link.

We can calculate the cost of long-reach transponders with

$$c_{i,j}^{TSP} = 2\gamma^{TSP} w_{i,j}^{k_p}, \tag{4.11}$$

where $w_{i,j}^{k_p}$ is calculated using

$$w_{i,j}^{k_p} = \sum_{(a,b)\in D} B_{a,b} Z_{i,j}^{a,b}, \tag{4.12}$$

where $Z_{i,j}^{a,b}$ is a binary variable that indicates whether the demand $\{a, b\}$ is routed through the link (i, j) or not. Using (4.10) and (4.11) the total cost of links is given by

$$C_L = \sum_{\{i,j\} \in E} (c_{i,j} + c_{i,j}^{TSP}). \tag{4.13}$$

We assume that the node location and the traffic are inputs of the model. We are also assuming that the EXC and the OXC switching matrices are able to process all the required traffic, so the cost of nodes is fixed. Now the main goal is to find the physical topology that minimizes C_L. Since addressing topological design problems via ILP models is prohibitive for larger networks, we propose a genetic algorithm to minimize the expression (4.13). In order to evaluate the performance of our proposed genetic algorithm, in terms of accuracy, time consumption and memory requirements, we compare its results with an ILP model and a set of realistic transport networks.

4.5.2 Genetic Algorithm

A genetic algorithm is a heuristic based on the theory of natural evolution and has the following steps: generation of an initial population, encoding, evaluation, selection, crossover, mutation and decoding [26, 27]. After generating a set of initial feasible solutions of the problem (also called individuals), the genetic algorithm modifies that population repeatedly. A pair of individuals is chosen under selection rules and is combined under crossover rules. This gives rise to another pair of individuals (also called offsprings). To increase the population diversity, mutations can be also applied.

For our proposed genetic algorithm, a feasible solution is a network topology with at least two link-disjoint paths between any pair of nodes. We consider two topology generators to create the initial population set. One generates completely random topologies and is based on the work presented in [28]. The other is our generator presented in Chapter 4. The random topology generator starts by designing a ring topology connecting all nodes of the network, thus, guaranteeing that all initial solutions are feasible (they have at least link-disjoint paths between any pair of nodes).

Afterwards, links are added to the ring topology to connect pairs of nodes randomly selected. The number of additional links is randomly generated and ranges from 0 to $(N^2 - 3N)/2$, i.e., from a ring to a full mesh network.

The encoding corresponds to the creation of a genetic code which uniquely represent a solution. To encode the solutions we used the concatenation of the rows of the upper triangular of the adjacency matrix, $[g]$. As the network links are bidirectional the adjacency matrix is symmetric. Given the genetic code of the solutions, the decoding performs the inverse operation. As an example, considering the adjacency matrix presented in (3.1) (see page 42), which represents our example network presented in Figure 3.1, the respective genetic code is

$$1\ 1\ 1 \mid 0\ 1 \mid 1.$$

The evaluation consists of determining the Capital Expenditures of each individual, i.e., the CAPEX of each feasible topology. In the selection phase, pairs of individuals are chosen for crossover. Usually, individuals are selected based on their fitness, i.e., the CAPEX of the respective solution, emphasizing the fitter individuals and expecting that their offsprings will have higher fitness. However, a rigid selection may reduce the diversity of the population leading to suboptimal solutions; contrariwise a flexible selection may result in slow evolution. We have implemented two different selection methods, that differ in the selection rigidness. The methods are the roulette wheel and the tournament method [29].

In the roulette wheel method, after all solutions are evaluated, the total cost of the generation is determined by adding the cost of all solutions. The next step is the calculation of the fitness of each solution. The fitness of each solution is the difference between the total cost of the generation and the cost of the solution. Thus, the solutions with lower cost will have higher fitness than the solutions with higher cost. Finally, the selection probability is calculated making the ratio between the fitness of each solution and the sum of the fitness of all individuals. In this way solutions with lower cost have greater probability of being selected for crossover.

In the tournament method, four individuals are randomly selected from the population and then they are grouped into sets of two. Afterwards, two random numbers, r_1 and r_2, ranging between 0 and 1 are generated. If $r_1 < 0.75$, the solution with the lowest cost (highest fit) in the first set is selected for crossover. Otherwise, the less fit solution is selected. The same process occurs in the second set, allowing the selection of the lowest cost solution from one set and the highest from the other.

In the crossover operation pairs of individuals, previously selected, are combined giving rise to another pair of new individuals. Two crossover operators are implemented, the single point crossover and the uniform crossover [29].

In the single point crossover, a border between two elements of the genetic code is randomly selected. Then, the left side code part of Progenitor 1 and Progenitor 2 is copied to the Offspring 1 and Offspring 2, respectively. The right side code parts are exchanged, i.e., the right side code part of the Progenitor 1 is copied to the Offspring 2 and the right side code part of the Progenitor 2 to the Offspring 1. Table 4.5 shows an example of single point crossover. Using the border between the fourth and the fifth element of the genetic code for both progenitors we obtain the two offsprings.

Table 4.5: Example of the single point crossover.

Individual	Genetic Code					
Progenitor 1	1	1	1	1	**0**	**1**
Progenitor 2	1	0	1	1	**1**	**1**
Offspring 1	1	1	1	1	**1**	**1**
Offspring 2	1	0	1	1	**0**	**1**

In the uniform crossover, a binary mask is randomly generated. If the crossover mask bit i is 1, the Offspring 1 receives the bit i from the Progenitor 1 and the Offspring 2 the bit i from the Progenitor 2. If the mask bit i is 0, the Offspring 1 inherit the bit i from the Progenitor 2 and the Offspring 2 from the Progenitor 1. The example in Table 4.6 illustrates the process.

The mutation operation consists in a simple exchange of 0's to 1's, or vice versa, at random locations of the genetic code, for a random number of selected individuals. The goal of this operation is to increase the diversity of the population.

Table 4.6: Example of the uniform crossover.

Individual	Genetic Code					
Progenitor 1	1	**1**	1	1	**0**	1
Progenitor 2	1	**0**	1	1	**1**	1
Mask	0	**1**	1	0	**0**	1
Offspring 1	1	**1**	1	1	**1**	1
Offspring 2	1	**0**	1	1	**0**	1

After the individuals are evaluated, selected and reproduced, the next generation is created. The selection of the individuals to form the next generation is made from the current generation and the generated Offsprings. In this work we consider that a maximum of 20% of individuals are selected from the current generation, and the remaining 80% are generated Offsprings.

4.5.3 Integer Linear Programming Model

In this section, we present an ILP model to minimize the transmission cost a survivable optical transport network. In order to formulate the flow conservation constraints the binary variable $Z_{i,j}^{a,b}$ is divided into two variables $Y_{i,j}^{a,b}$ and $Y_{j,i}^{a,b}$, where the former indicates that the demand $\{a,b\}$ is routed through the link (i,j) and flows from node i to j. The latter indicates that the demand flows is in the opposite direction. The ILP model is the following [30],

$$minimize \quad C_L = \sum_{\{i,j\}\in E} (c_{i,j} + c_{i,j}^{TSP})$$

$$subject\ to$$

$$\sum_{j\in V\setminus\{a\}} Y_{i,j}^{a,b} - \sum_{j\in V\setminus\{b\}} Y_{j,i}^{a,b} = \begin{cases} 2, & i = a \\ 0, & i \neq a,b \\ -2, & i = b \end{cases} \quad \forall (a,b)\in D, \forall i \in V \tag{4.14}$$

$$\sum_{(a,b)\in D} B_{a,b}(Y_{i,j}^{a,b} + Y_{j,i}^{a,b}) \leq S_{i,j} n_{i,j}^{S} \quad \forall \{i,j\}\in E \tag{4.15}$$

$$n_{i,j}^{S} \in \mathbb{N}_0 \quad \forall \{i,j\}\in E \tag{4.16}$$

$$Y_{i,j}^{a,b} \in \{0,1\} \quad \forall (a,b)\in D \tag{4.17}$$

$$\forall \{i,j\},\{j,i\}\in E$$

Constraints set (4.14) are the usual flow conservation constraints and ensure that, for each $\{a, b\}$ pair, we route two units of flow from node a to node b, i.e., one flow as the working path and one as the backup. Constraints set (4.15) connects the variables $n^S_{i,j}$ and $Y^{a,b}_{i,j}$, guaranteeing that the total number of optical channels crossing the link (i, j), in both directions, does not exceeds the maximum capacity, $S_{i,j}$, of the number of transmission systems, $n^S_{i,j}$. Constraints set (4.16) define the variables $n^S_{i,j}$ as natural numbers (zero is also included), allowing the installation of more than one pair of transmission systems in each connection. The disjointness of the two flows, to ensure survivability, is enforced by constraints (4.17). As the variables $Y^{a,b}_{i,j}$ are binary, the two flows cannot traverse the same edges.

4.5.4 Computational Experiments

In the following the computational results obtained using the genetic algorithm and the ILP model are presented. The genetic algorithm is implemented in C++. Using the genetic algorithm feasible solutions, corresponding to upper bounds for the optimal value, are obtained. The ILP model is used to obtain lower bounds and is solved using the branch and bound method from the commercial optimization software Xpress IVE 1.18. The results are obtained using a PC Intel Core 2 at 1.83 GHz and 1 GB RAM. The halting criteria used for the ILP model is the obtention of the optimal solution or 10 hours of processing time. In the genetic algorithm we performed 100 iterations, which required less than four minutes for the largest network. We observed marginal improvements in the solutions obtained when increasing this number of iterations.

To evaluate the quality of the obtained solutions the gap between the upper, b_u, and the lower, b_l, bound is calculated as follows

$$gap = \frac{100(b_u - b_l)}{b_u}, \tag{4.18}$$

where b_u is obtained using the genetic algorithm and b_l using the ILP model.

The computational results are obtained for the node location of nine real transport networks. We assume that all links can be implemented. The maximum number of

optical channels supported by each transmission system is 40, i.e., $S_{i,j} = S = 40$, and the interval between OAs is 100 km, i.e., $\partial = 100$. The cost of the equipments is shown in Table 3.4. To assess the impact of the initial population, selection method, crossover operator and number of individuals in the population, we perform five runs for each combination:

- 100 individuals, roulette wheel selection, single point crossover;
- 100 individuals, tournament selection, single point crossover;
- 100 individuals, roulette wheel selection, uniform crossover;
- 100 individuals, tournament selection, uniform crossover;
- 500 individuals, roulette wheel selection, single point crossover;
- 500 individuals, tournament selection, single point crossover;
- 500 individuals, roulette wheel selection, uniform crossover;
- 500 individuals, tournament selection, uniform crossover.

4.5.4.1 The Impact of the Initial Population

We start by assessing and comparing the quality of the obtained solutions when using different initial population generators. The presented results are obtained using a uniform demand matrix. The initial populations are randomly generated as described in [28] and following our proposed generator presented in Chapter 4. The number of nodes, regions, and nodes placed in each region are presented in Table 4.7, for all considered networks. Notice that the regions and nodes per region are features of our topology generator only.

Table 4.7: Real-world reference networks.

Network	Nodes	Regions	Nodes per Region
VIA	9	2	5 - 4
RNP	10	4	0 - 8 - 1 - 1
vBNS	12	3	3 - 4 - 5
CESNET	12	3	4 - 7 - 1
ITALY	14	2	12 - 2
NFSNET	14	2	7 - 7
AUSTRIA	15	3	3 - 4 - 8
GERMANY	17	4	8 - 2 - 5 - 2
SPAIN	17	4	8 - 2 - 7 - 0

Figure 4.18 shows the evolution of the gap for the best solution obtained, among all combinations, for initial populations generated using the random topology generator (Figure 4.18a) and using our topology generator (Figure 4.18b). As we can see in Figure 4.18a, for initial populations generated using the random topology generator, the optimal solution is obtained for VIA, RNP and vBNS networks. With the increase in the number of nodes the gap also increases reaching almost 15%.

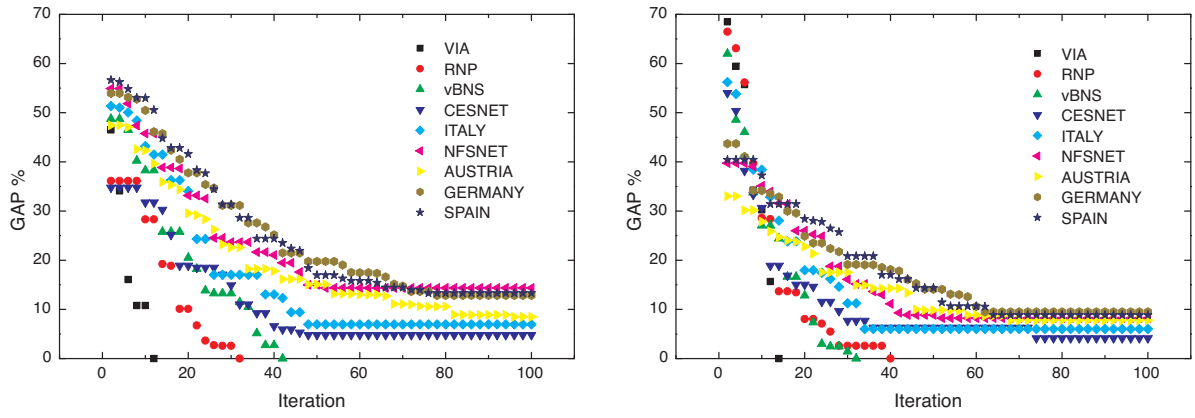

(a) (b)

Figure 4.18: Evolution of the gap for nine reference networks. Each shape mark represents the best solution of each iteration. Initial populations are generated with: (a) random topology generator and (b) our proposed topology generator.

For initial populations generated using our topology generator, see Figure 4.18b, the genetic algorithm also obtains the optimal solution for VIA, RNP and vBNS networks.

Increasing the number of nodes the gap also increases. However, the solutions obtained within 100 iterations have gaps always smaller than 10%.

Considering our results, only for the networks in which the optimal solution is obtained, an initial population randomly generated obtains a solution as good as the one obtained using our proposed topology generator. In all the other networks the solutions obtained using our topology generator have smaller cost. The improvements range between 1% and 10%. One reason for this is that in the random topology generator all the links have the same probability to be chosen. Contrariwise, in our topology generator longer links have smaller probability than shorter ones.

4.5.4.2 The Impact of the Combinations

In this section, the eight combinations are compared and analyzed. The results are obtained using an initial population generated using our topology generator and a uniform demand model. Figure 4.19 shows the best solutions obtained in each iteration by the genetic algorithm, for each combination. Results for the vBNS network are presented in Figure 4.19a and for SPAIN network in Figure Figure 4.19b. The lower bound was obtained using the ILP model and is presented as a solid line.

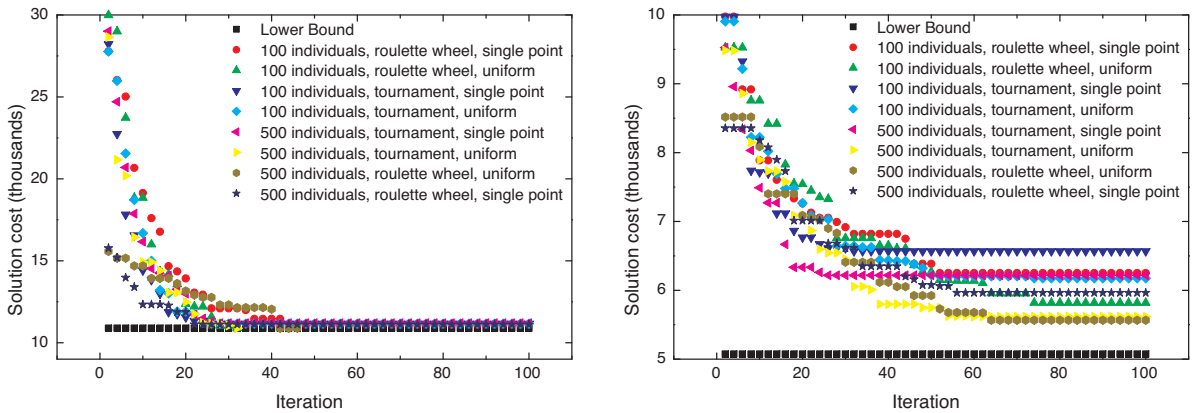

(a) vBNS Network (b) SPAIN Network

Figure 4.19: Evolution of the best solution obtained in each iteration using our topology generator for the eight combinations. The lower bound was obtained with the ILP model (solid black line). Experiments were performed with (a) vBNS and (b) SPAIN networks.

Figure 4.19a shows that, for the 12-node network, the convergence to a solution is

fast for all combinations. As the number of nodes increases, the convergence is slower. Figure 4.19b shows that the convergence to a solution is only visible after the 60th iteration. The difference between the quality of the solutions increases as well.

To compare the eight combinations the gap of the best solution obtained for each method, among the five runs, is presented in Table 4.8. The best solution obtained is marked as bold. The genetic algorithm with a population of 500 individuals, roulette wheel selection and uniform crossover obtains the best solution for eight networks. Moreover, a population of 500 individuals, tournament selection and uniform crossover equals the best solution in six networks. The second best solution is also always obtained by another combination. The difference between the solutions tends to increase with increasing of the number of nodes.

Table 4.8: Gap of the best solution with eight combinations for initial populations.

	100 individuals				500 individuals			
	Single Point		Uniform		Single Point		Uniform	
Network	R. Wheel	Tourn.	R. Wheel	Tourn.	R. Wheel	Tourn.	R. Wheel	Tourn.
VIA	**0.0**	**0.0**	**0.0**	**0.0**	**0.0**	**0.0**	**0.0**	**0.0**
RNP	2.6	7.9	3.5	2.7	1.9	1.9	**0.0**	**0.0**
vBNS	1.9	2.5	0.0	2.7	2.1	2.7	**0.0**	**0.0**
CESNET	6.0	8.9	4.1	6.0	7.0	7.3	4.8	**4.1**
ITALY	15.6	16.3	8.5	10.1	21.1	10.4	**6.0**	**6.0**
NFSNET	13.2	22.2	9.7	11.3	10.5	13.1	**8.2**	8.7
AUSTRIA	17.6	14.8	9.8	11.3	13.9	13.7	**7.8**	8.4
GERMANY	19.6	22.4	13.9	13.9	16.8	14.9	**9.5**	**9.5**
SPAIN	18.8	22.7	12.8	17.8	14.9	18.4	**8.8**	9.7

Making a comparison among the combinations, the uniform crossover obtains better solutions than the single point crossover, independently of the number of individuals and selection method, see Table 4.8. In the uniform crossover, offsprings do not preserve large blocks of genetic code from their progenitors, therefore it increases the population diversity and allows the genetic algorithm to obtain better solutions. On the other hand, with the crossover operator fixed, the solutions obtained using the roulette wheel method for selection are quite similar to the ones obtained using the tournament method. Comparing the results obtained with the different sizes of population, with the selection method and crossover operator fixed, large populations

(e.g., 500 individuals) result better solutions than smaller ones (e.g., 100 individuals). However, runs were also done with populations of 1000 individuals and only residual improvements were obtained, when compared to solutions with 500 individuals. In spite of the individuals generation and the crossover operators being random, the difference between the solutions obtained by each run is not significant. Moreover, as the size of the network increases such difference decreases.

4.5.4.3 The Impact of the Traffic Model

In the following, we analyze the best results obtained using the genetic algorithm and the results obtained using the ILP model, for uniform and non-uniform demand matrices. The non-uniform demand matrices are randomly generated with $0 \leq B_{a,b} \leq 5$. The gap and the processing time for the solutions obtained using the ILP model and the genetic algorithm are presented in Table 4.9.

Table 4.9: Computational results using the ILP model and the Genetic Algorithm for uniform and non-uniform demand matrices.

		Uniform Demand Model				Non-uniform Demand Model			
		ILP		GA		ILP		GA	
Network	Nodes	Time	gap	Time	gap	Time	gap	Time	gap
VIA	9	1 s	0.0	8 s	0.0	4 s	0.0	8 s	0.0
RNP	10	42 s	0.0	27 s	0.0	24 m	0.0	27 s	3.2
vBNS	12	2 m	0.0	32 s	0.0	10 h	1.8	32 s	4.6
CESNET	12	7 h	0.0	01 m	4.1	10 h	0.3	01 m	5.7
ITALY	14	10 h	4.4	02 m	6.0	10 h	3.2	02 m	9.3
NFSNET	14	10 h	3.0	02 m	8.2	10 h	5.7	02 m	9.6
AUSTRIA	15	10 h	4.4	02 m	7.7	10 h	8.0	02 m	10.8
GERMANY	17	10 h	6.7	04 m	9.5	8 h*	8.6	04 m	12.2
SPAIN	17	10 h	8.3	04 m	8.8	10 h	8.4	04 m	13.0

* Overloaded memory

Considering uniform demand matrices, the ILP model obtained the optimal solution for networks with less than 12 nodes. Considering the vBNS and CESNET networks, note that in spite of having the same number of nodes the processing time required using the ILP model to achieve the optimum solution is substantially different, see

Table 4.9. A reason for this may be found in the difference of the geographical area where the networks are implemented. The vBNS network, with 12 nodes, is in the USA and the CESNET network, also with 12 nodes, is in the Czech Republic. Due to the large area that the USA network has to cover, the majority of its links are fixed since the beginning due to the distance. For networks with more than 12 nodes the ILP model obtains a solution with a gap smaller than 8.3% within 10 hours.

The genetic algorithm is much faster than the ILP model and obtains near optimal solutions. For networks with less than 12 nodes the genetic algorithm obtains either the optimal solution or a solution with a gap of 4% within 1 minute. For networks with more than 12 nodes the genetic algorithm obtains solutions with gaps smaller than 10% within 4 minutes. A solution was obtained in approximately 45 minutes for a network with 100 nodes. In this case, the gap was not calculated as this problem cannot be addressed using the ILP model within a reasonable time and computational effort.

The results obtained using the ILP model and the genetic algorithm for GERMANY network and a uniform demand matrix is shown in Figure 4.20a. Dashed links are the ones that differ in both solutions. Black dashed lines represent the links obtained using the genetic algorithm, and red dashed lines the links using the ILP model. The black solid lines represent the common links to both solutions. None of the topologies is optimal, see Table 4.9. However, the majority of the optimal links are already present in both solutions.

Considering non-uniform demand matrices, the complexity increases. In this case the ILP model obtained the optimal solution, within the time limit, only for network VIA and RNP. However, solutions with a gap smaller than 8.6% can still be obtained in 10 hours. We noticed that the ILP model obtains solutions with gaps smaller than 10% within 3 hours of processing time. With GERMANY network, the computer runs out of memory before the given time limit.

The genetic algorithm maintains the processing time, although the results obtained show an increased gap. We observed that such increase is due to the routing algorithm. The optimal routing is not always the shortest path, sometimes longer routes can

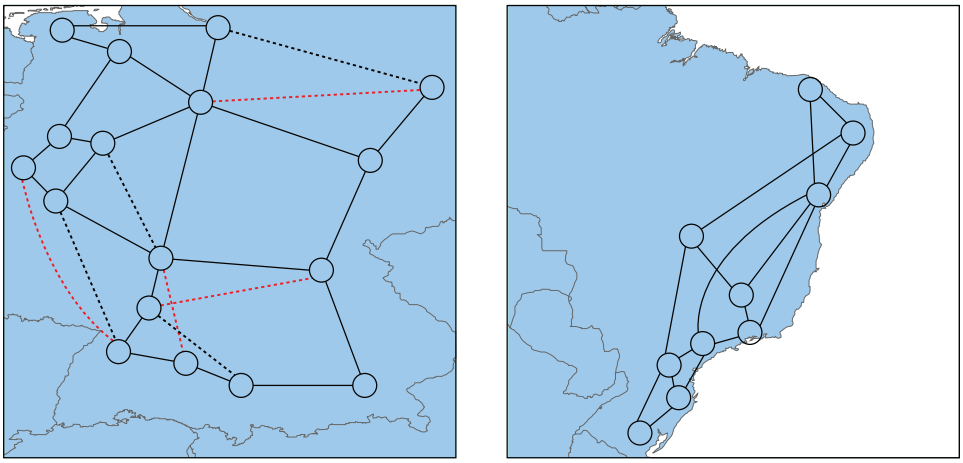

(a) GERMANY (b) RNP

Figure 4.20: Topologies obtained using the ILP model and the genetic algorithm for the node location of (a) GERMANY network with uniform demand matrix and (b) RNP network with non-uniform demand matrix. The dashed links differ in both solutions and the solid links are common.

optimize the network available resources. For instance, when a transmission system along the shortest path of a channel does not have available capacity, it may be preferable to route that channel through a longer path to avoid the installation of an additional transmission system. Figure 4.20b depicts the best result obtained with the node location of the RNP network, using the ILP model and the genetic algorithm with a non-uniform demand matrix. As we can see in Table 4.9, the genetic algorithm obtained a solution with a gap of 3.2%. Nevertheless, the physical topology obtained is optimal, see Figure 4.20b. The gap is only due to suboptimal routing.

4.5.4.4 Discussion

The ratio between the gap (of the order of 10%) and the processing time obtained, using the genetic algorithm, encourage the use of this kind of heuristic within the survivable optical network design problem. We shown that providing initial populations generated using a method that preserves the main characteristics of real optical networks improves the quality of the obtained solutions. Moreover, crossover operators that do not preserve large blocks of the genetic code increase the diversity of the population and the probability of finding better solutions.

4.6 Chapter Summary

This Chapter described the work that we developed in order to generate transport network topologies, that resemble the characteristics of real-transport networks. The Chapter starts by analyzing relevant characteristics, that were obtained from a set of twenty nine real-world reference networks. After analyzing available methods for generating network topologies, we proposed a new one including decisions and constraints to guarantee that the observed characteristics are present when network topologies are generated. In order to validate the proposed method, we generated a set of network topologies with the same size (number of nodes and links) of real-world networks, and over this set we performed the same analysis of the relevant characteristics, which was also compared with the real-world topologies characteristics. Experiments have shown that our proposed model produces network topologies that resemble the characteristics of the transport networks. Thereafter we presented a study about the topological design using a genetic algorithm. We have shown that it is possible to obtain accurate results in less processing time, when compared with ILP based approaches.

References

[1] M. H. Gunes and K. Sarac, "Inferring subnets in router-level topology collection studies," in *Proceedings of the 7th ACM SIGCOMM conference on Internet measurement, IMC '07*. New York, NY, USA: ACM, October 2007, pp. 203–208.

[2] M. Naldi, "Connectivity of waxman topology models," *Journal of Computer Communications*, vol. 29, no. 1, pp. 24–31, February 2005.

[3] B. Waxman, "Routing of multipoint connections," *IEEE Journal on Selected Areas in Communications*, vol. 6, no. 9, pp. 1617–1622, Dec. 1988.

[4] M. Doar, "A better model for generating test networks," in *Proceedings of the IEEE Global Telecommunications Conference, GLOBECOM '96*. IEEE, November 1996, pp. 86–93.

[5] E. Zegura, K. Calvert, and S. Bhattacharjee, "How to model an internetwork," in *Proceedings of the 15th Annual Joint Conference of the IEEE Computer Societies. Networking the Next Generation. INFOCOM '96*, vol. 2, March 1996, pp. 594–602.

[6] L. Cheng, N. Hutchinson, and M. Ito, "Realnet: A topology generator based on real internet topology," in *Proceedings of the 22nd International Conference on Advanced Information Networking and Applications, AINAW '08*, March 2008, pp. 526–532.

[7] M. Faloutsos, P. Faloutsos, and C. Faloutsos, "On power-law relationships of the internet topology," in *Proceedings of the Conference on Applications, Technologies, Architectures, and Protocols for Computer Communication, SIGCOMM '99*. New York, NY, USA: ACM, 1999, pp. 251–262.

[8] C. Jin, C. J. Qian, and S. Jamin, "Inet: Internet topology generator," Technical Report CSE-TR-433-00, EECS Department, University of Michigan, 2000.

[9] D. Magoni, "Nem: A software for network topology analysis and modeling," in *Proceedings of the 10th IEEE International Symposium on Modeling, Analysis and Simulation of Computer and Telecommunications Systems, MASCOTS '02*. IEEE Computer Society, October 2002, pp. 364–371.

[10] C. Palmer and J. Steffan, "Generating network topologies that obey power laws," in *Proceedings of the Global Telecommunications Conference, GLOBECOM '00*, vol. 1. IEEE, November 2000, pp. 434–438.

[11] A. Medina, A. Lakhina, I. Matta, and J. Byers, "Brite: An approach to universal topology generation," in *Proceedings of the 9th International Symposium on Modeling, Analysis and Simulation of Computer and Telecommunication Systems, MASCOTS '01*. IEEE Computer Society, August 2001, pp. 346–353.

[12] A.-L. Barabasi and E. Bonabeau, "Scale-free networks," *Scientific American Magazine*, pp. 60–69, May 2003.

[13] C. Pavan, R. M. Morais, J. R. F. da Rocha, and A. N. Pinto, "Generating realistic optical transport network topologies," *IEEE/OSA Journal of Optical Communications and Networking*, vol. 2, no. 1, pp. 80–90, January 2010.

[14] D. J. Sheskin, *Handbook of parametric and nonparametric statistical procedures*, 3rd ed. Chapman & Hall/CRC, 2004.

[15] J. H. Stapleton, *Models for probability and statistical inference: theory and applications*, ser. Probability and Statistics. Wiley-Interscience, 2008.

[16] SPSS Inc., "SPSS for Windows, Rel. 14.0.1." Chicago, USA, 2008.

[17] A.-L. Barabasi, "The architecture of complexity," *Control Systems Magazine, IEEE*, vol. 27, no. 4, pp. 33–42, August 2007.

[18] J.-P. Vasseur, M. Pickavet, and P. Demeester, *Network Recovery: Protection and Restoration of Optical, SONET-SDH, IP, and MPLS*. San Francisco, CA, USA: Morgan Kaufmann, 2004.

[19] W. D. Grover, *Mesh-Based Survivable Networks: options and strategies for optical, MPLS, SONET, and ATM networking*. NJ: Prentice Hall, 2004.

[20] S. Ramamurthy, L. Sahasrabuddhe, and B. Mukherjee, "Survivable WDM mesh networks," *IEEE/OSA Journal of Lightwave Technology*, vol. 21, no. 4, pp. 870–883, April 2003.

[21] N. Takahashi, "On clustering coefficients of graphs with the fixed numbers of vertices and edges," in *Circuit Theory and Design, 2009. ECCTD 2009. European Conference on*, August 2009, pp. 814–817.

[22] H. Tangmunarunkit, R. Govindan, S. Jamin, S. Shenker, and W. Willinger, "Network topology generators: Degree-based vs. structural," in *Proceedings of the Conference on Applications, Technologies, Architectures, and Protocols for Computer Communication, SIGCOMM '02*, vol. 32, no. 4. New York, NY, USA: ACM, August 2002, pp. 147–159.

[23] G. Siganos, M. Faloutsos, P. Faloutsos, and C. Faloutsos, "Power laws and the as-level internet topology," *IEEE/ACM Transactions on Networking*, vol. 11, no. 4, pp. 514–524, August 2003.

[24] O. Klopfenstein, "Access network dimensioning with uncertain traffic forecasts," in *The 13th International Telecommunications Network Strategy and Planning Symposium, 2008. Networks 2008.*, Budapest, September 2008, pp. 1 –52.

[25] H. Kerivin and A. R. Mahjoub, "Design of survivable networks: A survey," *Journal of Network*, vol. 46, no. 1, pp. 1–21, June 2005.

[26] R. M. Morais, "Desenho topológico de redes ópticas," Master's thesis, Universidade de Aveiro, Aveiro, Portugal, 2008.

[27] R. M. Morais, C. Pavan, A. N. Pinto, and C. Requejo, "Genetic algorithm for the topological design of survivable optical transport networks," *IEEE/OSA Journal of Optical Communications and Networking*, vol. 3, no. 1, pp. 17–26, January 2011.

[28] J. F. Labourdette, E. Bouillet, R. Ramamurthy, and A. A. Akyama, "Fast approximate dimensioning and performance analysis of mesh optical networks," *IEEE/ACM Journal of Transactions on Networking*, vol. 3, no. 4, pp. 906–917, Aug. 2005.

[29] D. Goldberg, *Genetic algorithms in search, optimization and machine learning*. Boston, MA, USA: Addison-Wesley, 1989.

[30] A. Balakrishnan, T. L. Magnanti, and P. Mirchandani, “Connectivity–splitting models for survivable network design,” *Networks*, vol. 43, no. 1, pp. 10–27, November 2004.

Chapter 5

Modeling Survivability in Optical Networks

5.1 Introduction

As detailed in Chapter 3, the exact CAPEX of an optical transport network can be obtained when the values of all key variables are available. Network operators, however, do not always have all information about the network and, in such a situation, the unknown values should be estimated. Two important estimations are for protection coefficient and restoration coefficient. Both estimations are required even in the absence of information such as network topology and traffic demand. To estimate protection coefficient it is necessary to estimate the average number of hops for working and backup paths, which besides being useful to calculate the spare capacity for protection, it is also useful to calculate other variables including the average number of demands per link.

For estimations purposes, we need a collection of networks to perform numerical processing using search and routing algorithms and generate a meaningful data set. To generate the appropriate set of networks we use the topology generator presented in the previous Chapter. In section 5.2 we present a study on estimating the average number of hops for working and protection paths. In section 5.3 we present a similar study for the restoration coefficient. We also compare the performance of our proposed protection and restoration coefficients with previous work. In section 5.4 we study the impact of the traffic model on the coefficients, and in section 5.5 we calculate the CAPEX of a network, using the approximations, and considering different survivability schemes and transport modes.

5.2 Estimation of Protection Coefficient

The dimensioning of an optical network involves the determination of a fractional amount of extra capacity to allow recovery from failures. The extra capacity is usually calculated over the capacity needed to transport a given traffic in a failure-free scenario. As we have discussed in Chapter 3 the protection coefficient, $\langle k_p \rangle$, is obtained from the average number of hops in the working paths, $\langle h \rangle$, and the average number of hops in the backup paths, $\langle h' \rangle$, see equation (3.110). Therefore, in order to estimate the protection coefficient we need approximations for $\langle h \rangle$ and $\langle h' \rangle$.

5.2.1 Previous Work

In [1], Labourdette et al. present expressions to calculate protection coefficient in mesh networks, without requiring complete knowledge about the network topology. The approximation for the average number of hops in working paths, $\langle h \rangle$, was derived from the Moore bound [2, 3]. The Moore bound is an upper limit on the number of nodes of a regular graph of a given degree and diameter, $N_{\langle\delta\rangle,H}$. Trivially, if average nodal degree is $\langle \delta \rangle = 1$ then diameter is $H = 1$ and $N_{\langle\delta\rangle,H} = 2$. For survivable networks the interest falls on $\langle \delta \rangle \geq 2$, and the Moore bound for $\langle \delta \rangle \geq 2$ is given by

$$N_{\langle\delta\rangle,H} = \begin{cases} 1 + \langle\delta\rangle \frac{(\langle\delta\rangle-1)^H-1}{\langle\delta\rangle-2} & \text{if } \langle\delta\rangle > 2 \\ 2H+1 & \text{if } \langle\delta\rangle = 2 \end{cases}. \tag{5.1}$$

The obtained result was

$$\langle h \rangle \approx \frac{\ln\left[(N-1)\frac{\langle\delta\rangle-2}{\langle\delta\rangle}+1\right]}{\ln(\langle\delta\rangle-1)}. \tag{5.2}$$

To calculate the average number of hops for the backup paths, $\langle h' \rangle$, the following

expression was proposed,

$$\langle h' \rangle \approx \frac{\ln\left[(N-2)\frac{\langle \delta' \rangle - 2}{\langle \delta \rangle - 1} + 1\right]}{\ln(\langle \delta' \rangle - 1)} + 1, \tag{5.3}$$

in which $\langle \delta' \rangle$ is the average nodal degree obtained from a graph transformation,

$$\langle \delta' \rangle = \frac{2(L - (\langle \delta \rangle + \langle h \rangle) + 1)}{N-1}. \tag{5.4}$$

Using (3.110), (5.2) and (5.3) the $\langle k_p \rangle$ can be obtained with

$$\langle k_p \rangle \approx \frac{\frac{\ln\left[(N-2)\frac{\langle \delta' \rangle - 2}{\langle \delta \rangle - 1} + 1\right]}{\ln(\langle \delta' \rangle - 1)} + 1}{\frac{\ln\left[(N-1)\frac{\langle \delta \rangle - 2}{\langle \delta \rangle} + 1\right]}{\ln(\langle \delta \rangle - 1)}}. \tag{5.5}$$

The experiments performed by the authors demonstrated, however, that expression (5.5) is only valid for networks with average nodal degree equal to or larger than three. For smaller averages the expressions become inaccurate. This occurs because as the average nodal degree converges to two, the average path length converges to a linear function of the number of nodes, instead of following the logarithmic form of their model. The degree constraint of expression (5.5) is limitative for transport networks since the average nodal degree in these networks sits around $\langle \delta \rangle = 3$. Therefore, as presented in the next subsection, we decided to study how to obtain an expression that is also suitable for networks with nodal degree in the range of $\langle \delta \rangle = 2$ and $\langle \delta \rangle = 3$.

In [4], it is presented an approximation for the average number of hops in working paths,

$$\langle h \rangle = \begin{cases} 0.66 - 0.011N + \frac{1.23 + 0.31N - 0.002N^2}{\langle \delta \rangle}, & \text{if } N < 60 \\ 0.31 - 0.006N + \frac{-9.67 + 5.37ln(N)}{\langle \delta \rangle}, & \text{if } N \geq 60 \end{cases}. \tag{5.6}$$

The expression was obtained from statistical methods. However, the network topologies used in that study were randomly generated, which may not preserve the characteristics of real transport networks.

5.2.2 Our Proposed Approach

In this section we present a statistical approach to develop an analytical expression for the average number of hops. In order to obtain a meaningful data set of average number of hops from realistic survivable transport network topologies, we used our proposed topology generator presented in Chapter 4. First of all we generated a data set with about fifty thousands realistic survivable networks. In fact, we performed twenty runs with the topology generator for each N, ranging from $N = 15$ to $N = 100$, with increments of five. Furthermore, we define the minimum average nodal degree as $\langle\delta\rangle_{min} = 2.1$ and maximum as $\langle\delta\rangle_{max} = 5$. Notice that, because the number of possible topologies for each N with a given nodal degree interval is different, the data set is composed of a different number of networks for each N. For instance, in our data set there exist about 3700 networks with $N = 50$ and about 25000 with $N = 100$.

For each example network we stored $N, L, \langle\delta\rangle, \langle h\rangle$ and $\langle h'\rangle$. In order to obtain $\langle h\rangle$ and $\langle h'\rangle$ we calculate the shortest cycle between each pair of nodes. Then, the first shortest path is accounted to $\langle h\rangle$ and the second shortest path is accounted to $\langle h'\rangle$. Next, to obtain one single expression that depends on the number of nodes N and average nodal degree $\langle\delta\rangle$, two kinds of regressions were performed. Firstly, we grouped the overall $\langle h\rangle$ and $\langle h'\rangle$ data set based on N, obtaining one subset for each of the eighteen N considered (from 15 to 100).

Afterwards, in each subset we performed linear, polynomial, logarithmic, inverse, power, S-curve and exponential regressions where $\langle\delta\rangle$ was the independent variable and $\langle h\rangle$ or $\langle h'\rangle$ the dependent. In principle the use of L as independent variable brings similar results. Nevertheless, as L is incorporated in $\langle\delta\rangle$ we decided to use the latter as independent variable. Regressions were performed by using a software called SPSS [5]. The criterion to assess the accuracy of regressions was the coefficient of determination, R^2 [6]. This methodology leads to eighteen expressions of the same type, dependent on $\langle\delta\rangle$, to estimate $\langle h\rangle$ and further eighteen expressions to estimate $\langle h'\rangle$.

The type of expression with the highest R^2 for the most of subsets was the S-curve function, $\exp\{b_0 + (b_1/\langle\delta\rangle)\}$, for both $\langle h\rangle$ and $\langle h'\rangle$, in which b_0 and b_1 are constants

depending on N. Table 5.1 shows the values of constants b_0 and b_1 for $\langle h \rangle$ and $\langle h' \rangle$. In order to achieve one single expression we then considered the two sets of

Table 5.1: Values of constants b_0 and b_1 for $\langle h \rangle$ and $\langle h' \rangle$.

	$\langle h \rangle$		$\langle h' \rangle$	
# of Nodes	b_0	b_1	b_0	b_1
15	0.14	2.19	0.15	3.61
20	0.20	2.39	0.14	4.07
25	0.24	2.58	0.15	4.33
30	0.24	2.84	0.15	4.59
35	0.34	2.65	0.34	4.02
40	0.36	2.75	0.30	4.32
45	0.34	2.97	0.27	4.60
50	0.37	3.02	0.30	4.60
55	0.29	3.35	0.19	5.03
60	0.30	3.44	0.19	5.10
65	0.42	3.09	0.32	4.71
70	0.34	3.44	0.24	5.08
75	0.38	3.38	0.27	5.00
80	0.37	3.48	0.26	5.10
85	0.38	3.50	0.26	5.16
90	0.32	3.72	0.20	5.34
95	0.37	3.63	0.26	5.24
100	0.62	3.27	0.55	4.72

eighteen values of constants b_0 and b_1 and, using the same methodology, we performed regressions over the two sets using N as independent variable. For $\langle h \rangle$, we obtained $b_0 = 0.14\ln(N) - 0.22$ and $b_1 = 0.75\ln(N) + 0.2$ as expressions with the highest R^2. Figure 5.1 illustrates the fit of the function to b_0 (Figure 5.1a) and b_1 (Figure 5.1b).

Thus, we achieve one single expression that depends on N and $\langle \delta \rangle$. For the average number of hops in the working paths we obtained,

$$\begin{aligned} \langle h \rangle &\approx \exp\left\{0.14\ln(N) - 0.22 + \frac{0.75\ln(N) + 0.2}{\langle \delta \rangle}\right\} \\ &= \exp\left\{-0.22 + \frac{0.2}{\langle \delta \rangle}\right\} N^{0.14 + \frac{0.75}{\langle \delta \rangle}}. \end{aligned} \tag{5.7}$$

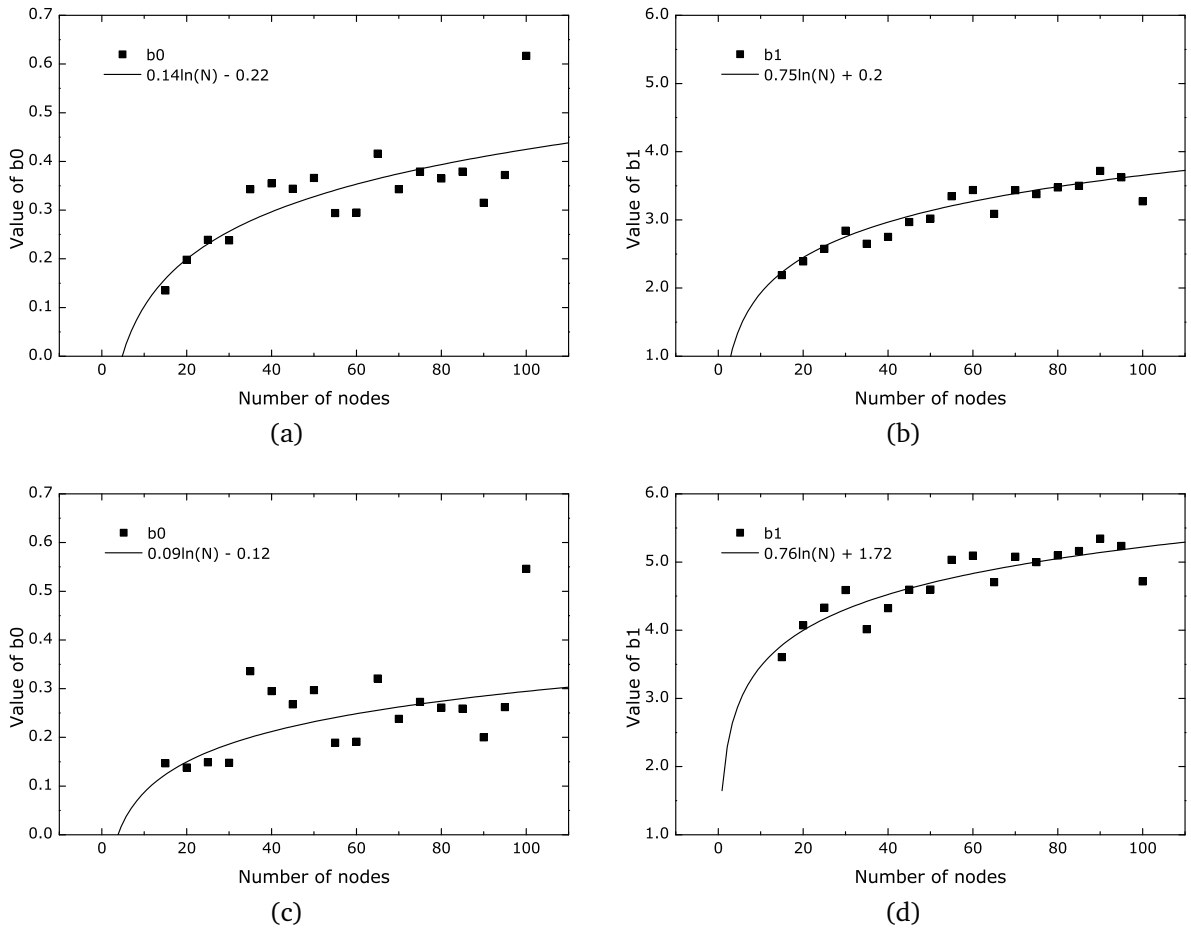

Figure 5.1: Curve fitting considering $\langle h \rangle$: (a) for constants b_0 with $R^2 = 0.60$ and (b) for constants b_1 with $R^2 = 0.89$, and considering $\langle h' \rangle$: (c) for constants b_0 with $R^2 = 0.30$ and (d) for constants b_1 with $R^2 = 0.78$.

The same methodology was used to obtain the constants for the mean number of hops for backup paths. We have obtained $b_0 = 0.09\ln(N) - 0.12$ and $b_1 = 0.76\ln(N) + 1.72$. Figure 5.1 illustrates the fit of the function to b_0 (Figure 5.1c) and b_1 (Figure 5.1d), thus we have

$$\begin{aligned} \langle h' \rangle &\approx \exp\left\{0.09\ln(N) - 0.12 + \frac{0.76\ln(N) + 1.72}{\langle \delta \rangle}\right\} \\ &= \exp\left\{-0.12 + \frac{1.72}{\langle \delta \rangle}\right\} N^{0.09 + \frac{0.76}{\langle \delta \rangle}}. \end{aligned} \tag{5.8}$$

The equations for the average number of hops in the working paths, (5.7), and average number of hops in the backup paths, (5.8), show that the mean

number of hops increases as $f_1(\langle\delta\rangle)N^{f_2(\langle\delta\rangle)}$ and $f_3(\langle\delta\rangle)N^{f_4(\langle\delta\rangle)}$, respectively, where $f_1(\langle\delta\rangle), f_2(\langle\delta\rangle), f_3(\langle\delta\rangle), f_4(\langle\delta\rangle) < 1$, since in our case $\langle\delta\rangle$ is always larger than 2. The growth with N^v, with v positive and smaller than one, for $\langle h\rangle$ and $\langle h'\rangle$, can be explained by the fact that for a given $\langle\delta\rangle$ the addition of extra nodes in large networks has a small impact on the network structure. The opposite is expected in smaller networks, where the impact will be larger. With $\langle\delta\rangle$ fixed the derivative of $\langle h\rangle$ with respect to N is

$$\frac{d\langle h\rangle}{dN} = f_1(c)f_2(c)N^{f_2(c)-1} \tag{5.9}$$

where c is a constant value. Similarly, the derivative of $\langle h'\rangle$ with respect to N is

$$\frac{d\langle h'\rangle}{dN} = f_3(c)f_4(c)N^{f_4(c)-1} \tag{5.10}$$

With N constant, equations (5.7) and (5.8) also show that the mean number of hops decreases with $\langle\delta\rangle$. This behavior is also expectable, since as more links are added into the network it becomes more connected and the paths become shorter. Therefore, the impact of adding new nodes is higher for networks with lower $\langle\delta\rangle$.

In [7], it is shown that for certain families of random graphs the average distance between the nodes satisfies $\ln(N)/\ln(\langle\delta\rangle)$ with probability almost one. This expression is asymptotically exact for random graphs. However, in our investigations, we observed that for optical transport networks $\langle h\rangle$ does not decreases as $1/\ln(\langle\delta\rangle)$. This apparent contradiction, can be explained by the fact that real optical transport networks are far from being random graphs and the number of nodes and links tend to be quite small. We observed that a decrease as $1/\ln(\langle\delta\rangle)$ overestimates the average number of hops. Using (5.7) and (5.8) we can obtain the protection coefficient with

$$\begin{aligned}\langle k_p\rangle &\approx \exp\left\{-0.05\ln(N) + 0.1 + \frac{0.01\ln(N) + 1.52}{\langle\delta\rangle}\right\} \\ &= \exp\left\{\frac{0.1\langle\delta\rangle + 1.52}{\langle\delta\rangle}\right\} N^{\frac{-0.05\langle\delta\rangle+0.01}{\langle\delta\rangle}}.\end{aligned} \tag{5.11}$$

Figure 5.2 shows the performance of our proposed expressions and Labourdette's

expressions for $\langle h \rangle$ and $\langle h' \rangle$ as function of $\langle \delta \rangle$ for networks with $N = 30$ and $N = 80$. The expression for $\langle h \rangle$ proposed by Correia in [4] is plotted as well. The exact values of $\langle h \rangle$ and $\langle h' \rangle$ were obtained from numerical simulation. The square shape marks represent the exact $\langle h \rangle$ in Figures 5.2a and 5.2c, and the exact $\langle h' \rangle$ in Figures 5.2b and 5.2d. Solid lines refers to our proposed expressions, short-dashed lines to Labourdette's and long-dashed lines to Correia's expressions.

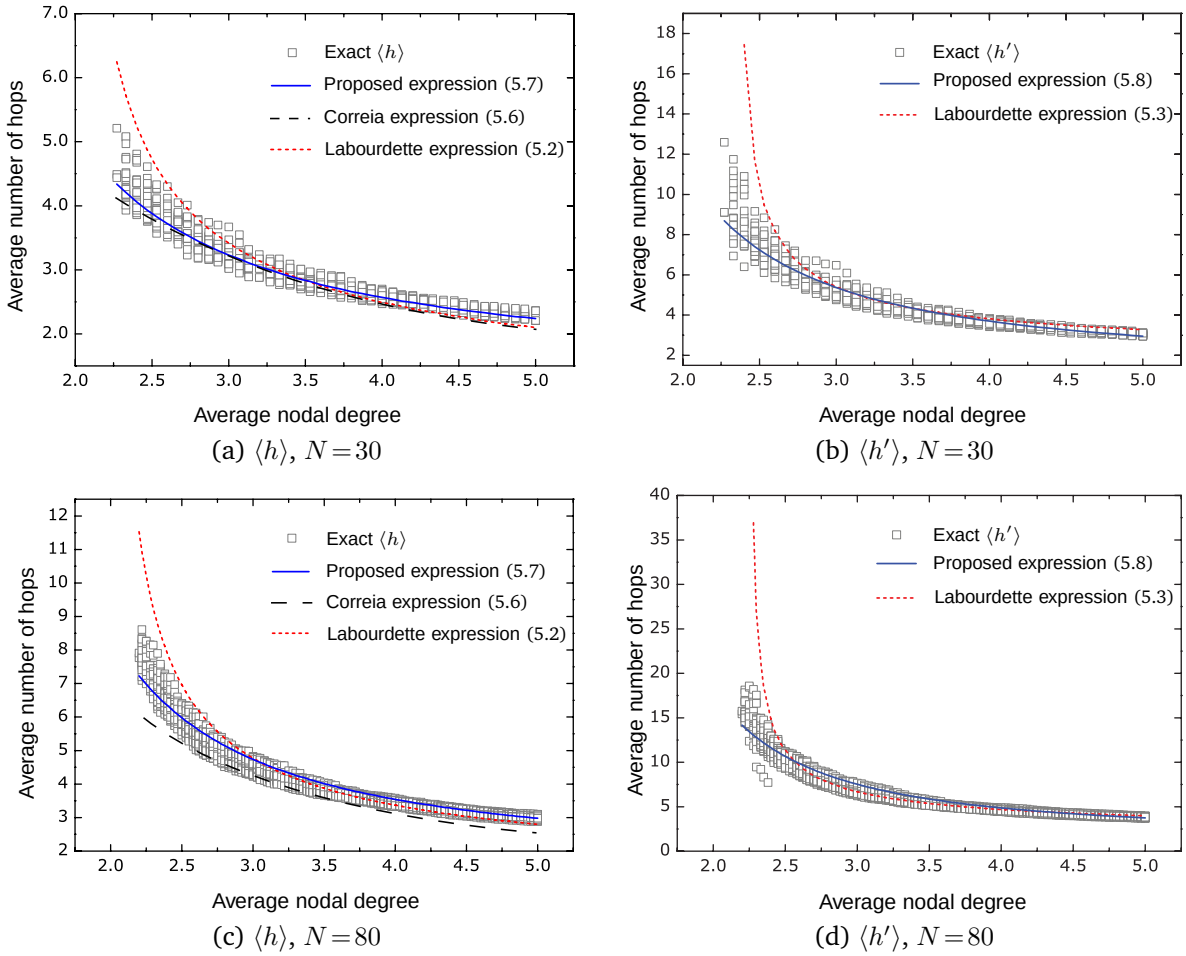

Figure 5.2: Comparative of approximations (5.2), (5.6) and (5.7) for $\langle h \rangle$ and approximations (5.3) and (5.8) for $\langle h' \rangle$ over topologies with $N = 30$ and $N = 80$.

In order to validate the accuracy of expressions, the relative error percentage between both approximations and exact values was calculated. For each generated

topology t with N nodes, the relative error percentage was calculated using

$$\epsilon_{t,N} = \left| \frac{V_{t,N} - V_N}{V_{t,N}} \right| \times 100, \tag{5.12}$$

in which $V_{t,N}$ is the exact value for a topology t with N nodes and V_N is the estimation obtained using the analytical expressions. The relative error percentage was calculated for the three parameters, $\langle h \rangle$, $\langle h' \rangle$ and $\langle k_p \rangle$.

As we can see in Figures 5.2a and 5.2c, Labourdette's expression to estimate $\langle h \rangle$ becomes inaccurate for degree smaller than 2.5. We can also see that the proposed expression agrees well with the numerical results for $\langle \delta \rangle$ ranging from 2.1 to 5.0. The Correia's expression presents similar results in smaller networks. However, it becomes inaccurate for larger networks. The reason for this behavior is because the topologies used to obtain that expression allow links with length equal to the network diameter, which results in a lower average number of hops. Calculating the average global error, i.e., the average of relative error percentage, equation (5.12), considering the whole data set, we obtained 7.1% for the expression (5.2), 6.4% for the expression (5.6), and 3.2% for the proposed expression (5.7). Our proposed approach for $\langle h' \rangle$ has good accuracy in the range $2 < \langle \delta \rangle \leq 5$, see Figures 5.2b and 5.2d. We obtained an average global error of 9.7% for Labourdette's expression (5.3) and 4.7% for proposed expression (5.8).

In order to analyze the error of expressions to estimate $\langle k_p \rangle$, expressions (5.5) and (5.11), as function of N, we calculated the average of relative error percentage for each N considered,

$$\langle \epsilon \rangle_N = \frac{1}{T_N} \sum_{t=1}^{T_N} \epsilon_{t,N} \tag{5.13}$$

where T_N is the total number of generated topologies with N nodes. The average error for $\langle k_p \rangle$ as function of N is presented in Figure 5.3. Our proposed expression (5.11) scales well with the increase of N. The estimation of $\langle k_p \rangle$ using our expression results an $\langle \epsilon \rangle_N$ of less than 3% for networks with N ranging between 15 and 100. Moreover, we can observe that the average error for the proposed expression (5.11) is almost

constant with N. This is a good improvement compared with Labourdette's expression (5.5) where the average error can be as high as 17% for smaller networks and is never lower than 7% for larger networks.

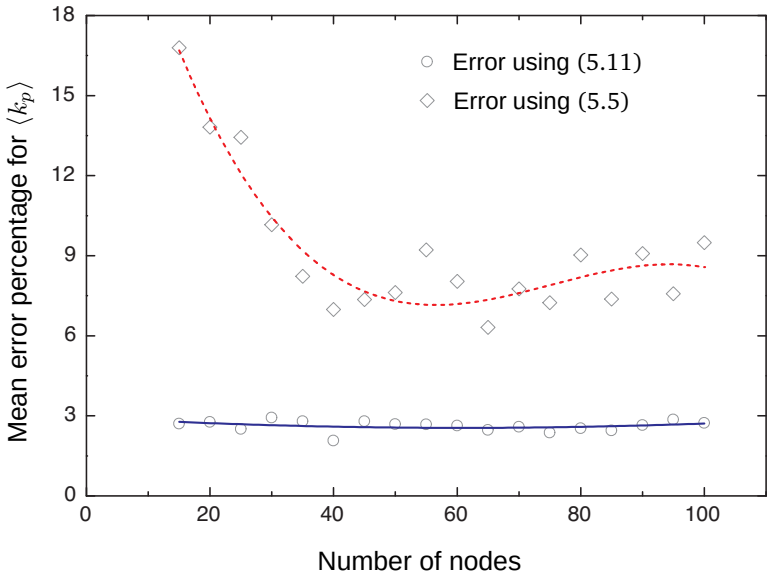

Figure 5.3: Average of relative error percentage for the protection coefficient, $\langle k_p \rangle$, considering fifty thousands computer generated topologies.

5.3 Estimation of Restoration Coefficient

In this section we first present a previous work to approximate the restoration coefficient. Next we propose an approximation to the restoration coefficient, which is useful to estimate the spare capacity required to a mesh network recover from any single link failure. The expression is based on statistical methods and does not requires knowledge of the network topology. We also provide experimental results evaluating the performance of the proposed approximation against the presented previous published and a network design tool.

5.3.1 Previous Work

In [8], the author presents an approximation for restoration coefficient, $\langle k_r \rangle$. He considered the results for the spare capacity for path-disjoint shared mesh restoration using a heuristic favoring a small differential path length between working and backup paths for eight mesh networks, i.e., quasi-regular networks, and also imposed the condition that $\langle k_r \rangle = 1$ for $\langle \delta \rangle = 2$. i.e., ring topologies requires 100% of spare capacity to tolerate single link failures.

The mesh networks that the author used had a number of nodes in the range of $4 \leq N \leq 100$, average nodal degree in the range of $2.5 \leq \langle \delta \rangle \leq 4.5$ and required a restoration coefficient in the range of $0.4 \leq \langle k_r \rangle \leq 0.9$. Based on this data he proposed the expression

$$\langle k_r \rangle \cong \frac{2}{\langle \delta \rangle}, \tag{5.14}$$

to estimate the restoration coefficient.

In [4], it is also presented an expression to estimate the restoration coefficient. The expression was obtained from statistical methods, using network topologies randomly generated,

$$\langle k_r \rangle = \begin{cases} 0.35 - 0.016N + 0.0001N^2 + \frac{1.85+0.024N-0.0002N^2}{\langle \delta \rangle}, & \text{if } N < 60 \\ 6 - 2.4\langle \delta \rangle + 0.28\langle \delta \rangle^2 - e^{-1.7+\frac{4}{\langle \delta \rangle}}, & \text{if } N \geq 60 \end{cases}. \tag{5.15}$$

5.3.2 Our Proposed Approach

To address the problem mentioned above, we needed a meaningful data set of restoration coefficients. For this purpose we first used the same approach that we used for the protection coefficient. That is, using our network topology generator presented in Chapter 4 we generated a set of fifty thousands realistic survivable network topologies. The number of nodes is in the range of $15 \leq N \leq 100$, the average nodal degree is in the range of $2 < \langle \delta \rangle \leq 5$. In this way, we guarantee that survivability against any single link failure is possible as long as enough additional capacity is available. Thereafter, for each network topology, we routed a uniform demand matrix

and the minimum amount of spare capacity required for survivability was found and the restoration coefficient, $\langle k_r \rangle$, was estimated as described in the flowchart presented in Figure 3.7 of Chapter 3. After obtaining these data, we analyzed the relation between the key variables of the network and the restoration coefficient. From this analysis we developed a new model to estimate the $\langle k_r \rangle$ without knowledge of the network topology.

From the analyzed data set we noticed that networks with the same number of nodes N and average nodal degree $\langle \delta \rangle$ may have a different restoration coefficient. As an example, Table 5.2 shows this behavior in more detail, for the three networks presented in Figure 5.4. The networks in Figure 5.4 have the same N, L and hence the same $\langle \delta \rangle$. However, each network has a different $\langle k_r \rangle$.

Table 5.2: Key variables for the networks presented in Figure 5.4.

Network	N	L	$\langle \delta \rangle$	W	ψ_{min}	$\langle k_r \rangle$	$\langle h \rangle$	$\langle \phi \rangle$	$\sigma^2(\delta)$
(a)	15	25	3.33	231	172	0.74	2.2	1.67	1.29
(b)	15	25	3.33	250	218	0.87	2.4	1.49	1.29
(c)	15	25	3.33	244	219	0.90	2.3	1.57	0.89

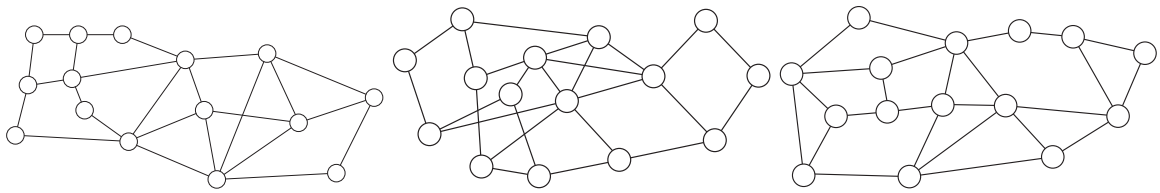

(a) (b) (c)

Figure 5.4: Three fifteen-node networks with $\langle \delta \rangle = 3.33$ (N=15, L=25). Distinct topologies yield different values for key variables such as that presented in the Table 5.2.

In Figure 5.5a, we present the most probable $\langle k_r \rangle$ for each N for $\langle \delta \rangle \approx 2.5$, $\langle \delta \rangle \approx 3.5$ and $\langle \delta \rangle \approx 4.5$. The most probable is value obtained from a histogram, where the more frequent value was chosen. We can see that for networks with $\langle \delta \rangle = 2.5$, the restoration coefficient is almost independent on the number of nodes. Networks with higher $\langle \delta \rangle$, on the other hand, show lower values for the restoration coefficient as the number of nodes increase. This behavior clearly indicates a dependence on N. Furthermore, the higher

the mean nodal degree, $\langle\delta\rangle$, the lower the restoration coefficient, $\langle k_r\rangle$. For instance, the restoration coefficient for a network with $N = 50$ and $\langle\delta\rangle \approx 3.5$ is about 0.6 while for a network with $N = 50$ and $\langle\delta\rangle \approx 4.5$ is about 0.5. This behavior is due to the resource sharing, $\langle\phi\rangle$, which tends to grow with the number of links and nodes. In Figure 5.5b we can see the trend of both the resource sharing and restoration coefficient as the N grows, for $\langle\delta\rangle \approx 3.5$.

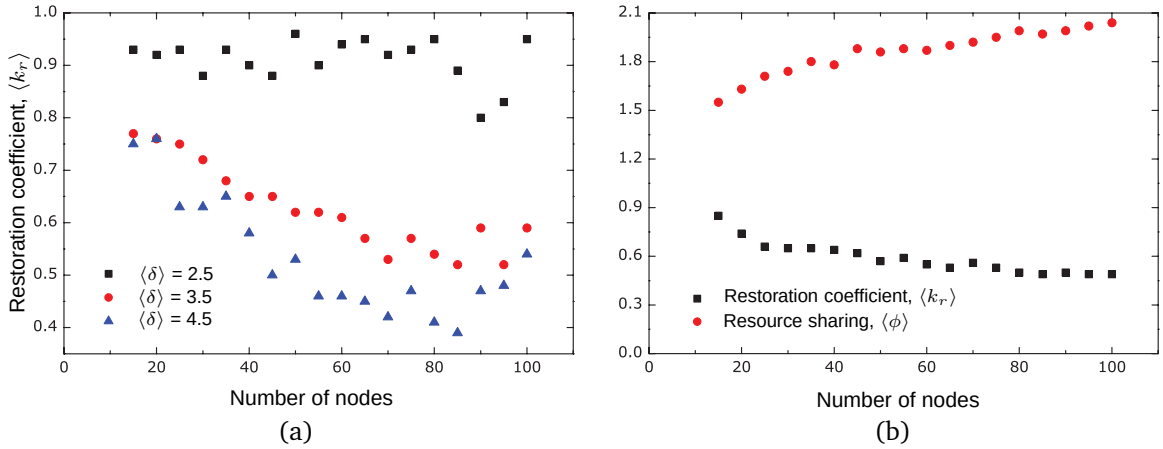

Figure 5.5: (a) Restoration coefficient vs. number of nodes and mean nodal degree. Shape marks represent the simulated restoration coefficient for three values of $\langle\delta\rangle$. (b) Resource sharing and restoration coefficient requirements as function of the number of nodes. The networks have $\langle\delta\rangle \approx 3.5$.

Our results show that N can have a significant impact on $\langle k_r\rangle$. These results are in agreement with the results obtained in [4], however this dependence was not considered in [8]. Networks with low $\langle h\rangle$ tend to have shorter path lengths, in terms of number of hops between any pair of nodes, hence these networks need less channels to support a given working capacity and tend to need less spare capacity to restore services in case of failures. An example of this behavior is also shown in Table 5.2. We can see that the network (a) has the smallest $\langle h\rangle$, and also the smallest W and ψ_{min}.

Notice also that, as the $\langle k_r\rangle$ is a fraction of W, the network with the lowest $\langle k_r\rangle$ does not represent necessarily the more cost-efficient solution. For instance, although the network (b) in Table 5.2 has a smaller $\langle k_r\rangle$ than network (c), it has a greater value for W. The most cost-efficient network is the one with the smallest W^k_{min} ($W^k_{min} = W + \psi_{min}$). Considering the networks in Table 5.2, the most cost-efficient

solution is the network (a) with $W^k_{min} = 403$, followed by networks (c) and (b), with $W^k_{min} = 463$ and $W^k_{min} = 468$, respectively. The influence of the variance of the nodal degree, $\sigma^2(\delta)$, was also evaluated and we concluded that it does not have a significant impact on $\langle k_r \rangle$.

In order to obtain a new model for the restoration coefficient we used a least-square method to perform linear and non-linear regressions from the results obtained for all considered networks, i.e., fifty thousand networks. First of all the analyzed networks were split by number of nodes and regressions were done for each set (networks with 15, 20, ..., 100 nodes). At this phase $\langle k_r \rangle$ and $\langle \delta \rangle$ were used as dependent and independent variables, respectively. In this way we obtained one expression for each N, which were the ones with the better coefficient of determination, R^2. The expressions with better R^2 follow an inverse function, $\langle k_r \rangle = b_0 + b_1/\langle \delta \rangle$, where b_0 and b_1 are constants that have a different value for each N. Table 5.3 shows the obtained values for b_0 and b_1.

In order to include the dependency on the number of nodes, N, in our expression we performed regressions over all b_0 and b_1, considering N as the independent variable. We have found that the constant b_0 vary with N following a logarithm function, $1.01 - 0.21ln(N)$, while the variable b_1 follows a power function, $0.45N^{0.32}$. Figure 5.6 shows the fit of these functions to the sets of b_0 and b_1 obtained above.

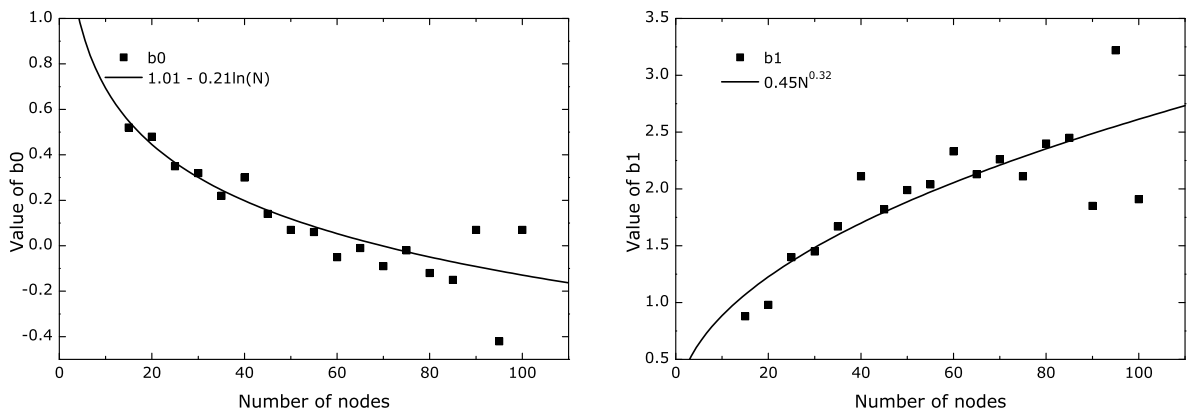

(a) (b)

Figure 5.6: Curve fitting (a) for constants b_0 with $R^2 = 0.69$ and (b) for constants b_1 with $R^2 = 0.83$.

Table 5.3: Values of constants b_0 and b_1 for $\langle k_r \rangle$.

# of Nodes	b_0	b_1
15	0.52	0.88
20	0.48	0.98
25	0.35	1.40
30	0.32	1.45
35	0.22	1.67
40	0.69	2.11
45	0.14	1.82
50	0.07	1.99
55	0.06	2.04
60	-0.05	2.33
65	-0.01	2.13
70	-0.09	2.26
75	-0.02	2.11
80	-0.12	2.40
85	-0.15	2.45
90	0.07	1.85
95	-0.42	3.22
100	0.07	1.91

Then we have obtained the expression

$$\langle k_r \rangle \approx 1.01 - 0.21 ln(N) + \frac{0.45 N^{0.32}}{\langle \delta \rangle} \tag{5.16}$$

to estimate the restoration coefficient in mesh-based networks.

We calculate the average of relative error percentage with the expression (5.13), for the Korotky's, the Correia's, and the proposed expressions for $\langle k_r \rangle$, using fifty thousands computer generated networks. Figure 5.7 shows the average of relative error percentage as a function of the number of nodes. Each diamond shape mark is the mean relative error percentage, obtained from Korotky's expression (5.14); triangle shape marks are for the Correia's expression (5.15), and circle shape marks are the errors obtained from our proposed expression (5.16), for a given N. As we can see, the average error of our proposed expression is less than 15% with N ranging from 15 and 100. Korotky's expression shows slightly better results in networks with N ranging

from 60 to 90. However, for networks with less than 40 nodes the error can be great. Correia's expression shows higher error in all considered networks.

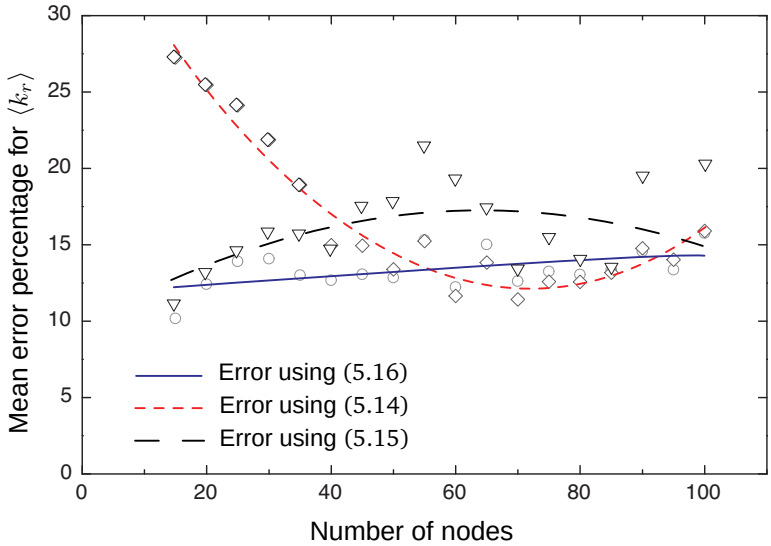

Figure 5.7: Average of relative error percentage for the restoration coefficient, $\langle k_r \rangle$, considering fifty thousands computer generated topologies.

5.4 Impact of Traffic Model on Survivability Coefficients

Traffic demand in optical transport networks exhibit a non-uniform statistical behavior [9]. In the dimensioning task, the expected traffic is usually taken into account in order to determine the working and spare capacities needed to transport such traffic and guarantee some level of survivability [10]. Typically the designers forecast the traffic volume considering parameters such as historical data or user population [11, 12]. The quantification of resources is often calculated by using software tools. However, the time required to obtain results increase with the network size and complexity. Indeed, the time required to calculate the spare capacity is often larger than for calculating the working capacity and eventually becomes prohibitive.

Moreover, the computational time to calculate the working, protection and restoration capacity may be quite different. It depends on the traffic matrix and the network size. Figure 5.8 shows the time consumed for calculating that variables for

the OMNICOM network. As we can see, for a low traffic load the time for calculating working, protection and restoration capacities do not differs so much. However, as the number of demands increase, the differences are clearly observed.

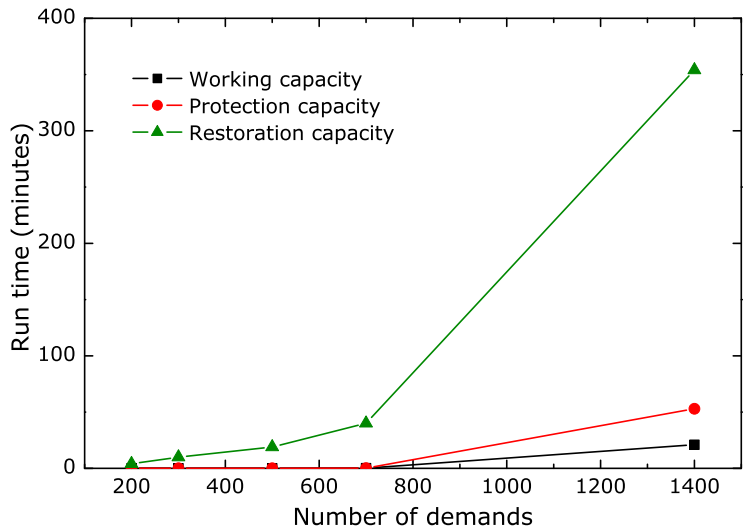

Figure 5.8: Run time for calculating the working, protection and restoration capacity for the OMNICOM network (N=38 and L=54), with different traffic loads. Simulations were run on the OPNET design tool [13], in a Pentium 4 2.8 GHz PC, with 1 GB of RAM.

It is clear that the amount of required resources for each demand is proportional to the hops count between the source and destination nodes. However, what happens with protection and restoration coefficient as the traffic changes? In this section we investigate how the protection and restoration coefficients vary, in optical transport networks, as a function of the traffic randomness. Analysis over real-world transport network topologies and a variety of traffic demand matrices are made for this purpose.

5.4.1 Experiments and Results

In order to assess the impact of traffic randomness in both protection and restoration coefficients, $\langle k_p \rangle$ and $\langle k_r \rangle$, we have considered the following real-world network topologies: RNP (N=10, L=12), EON (N=19, L=37), OMNICOM (N=38, L=54) and USA100 (N=100, L=171).

The topologies were set up on OPNET SP Guru Transport Planner software [13] and traffic matrices with different variances were routed through them. For each network

we have generated uniform and totally random matrices, as follow:

- Five uniform matrices, each with values 1, 5, 10, 20, or 50;
- Five random matrices with values between 0 and 5;
- Five random matrices with values between 0 and 10;
- Five random matrices with values between 0 and 20;
- Five random matrices with values between 0 and 50.

The variance of random demand matrices range from 0 to 270. The matrices were routed considering the shortest path, by hops count, path dedicated protection and shared path restoration. The resultant survivability coefficients of the four networks are plotted in Figure 5.9.

As we can see from Figure 5.9a, both protection and restoration coefficients differ significantly with random traffic in small networks. For instance, for the network under simulation (RNP), the protection and restoration coefficients vary up to 22% and 15%, respectively. As the network grows in size, the difference between the minimum and maximum survivability coefficients decrease. For instance, the difference between the minimum and maximum $\langle k_p \rangle$ and $\langle k_r \rangle$ for the EON network is 6% and 9% respectively, see Figure 5.9b. For the OMNICOM network the variation in $\langle k_p \rangle$ and $\langle k_r \rangle$ is smaller (just 5%), see Figure 5.9c. The last network, USA100, presents the lowest sensibility to traffic randomness, see Figure 5.9d, which the variations in $\langle k_p \rangle$ and $\langle k_r \rangle$ has a maximum value of about 2%. The reason for this decrease is because the length of backup paths tends to be smaller in larger mesh-based networks. We observed that for networks with more than twenty nodes, the traffic randomness does not impact significantly on $\langle k_p \rangle$ and $\langle k_r \rangle$. This indicates that approximations to spare capacity can be obtained without considering applicable traffic model, at least when all nodes are considered as central offices.

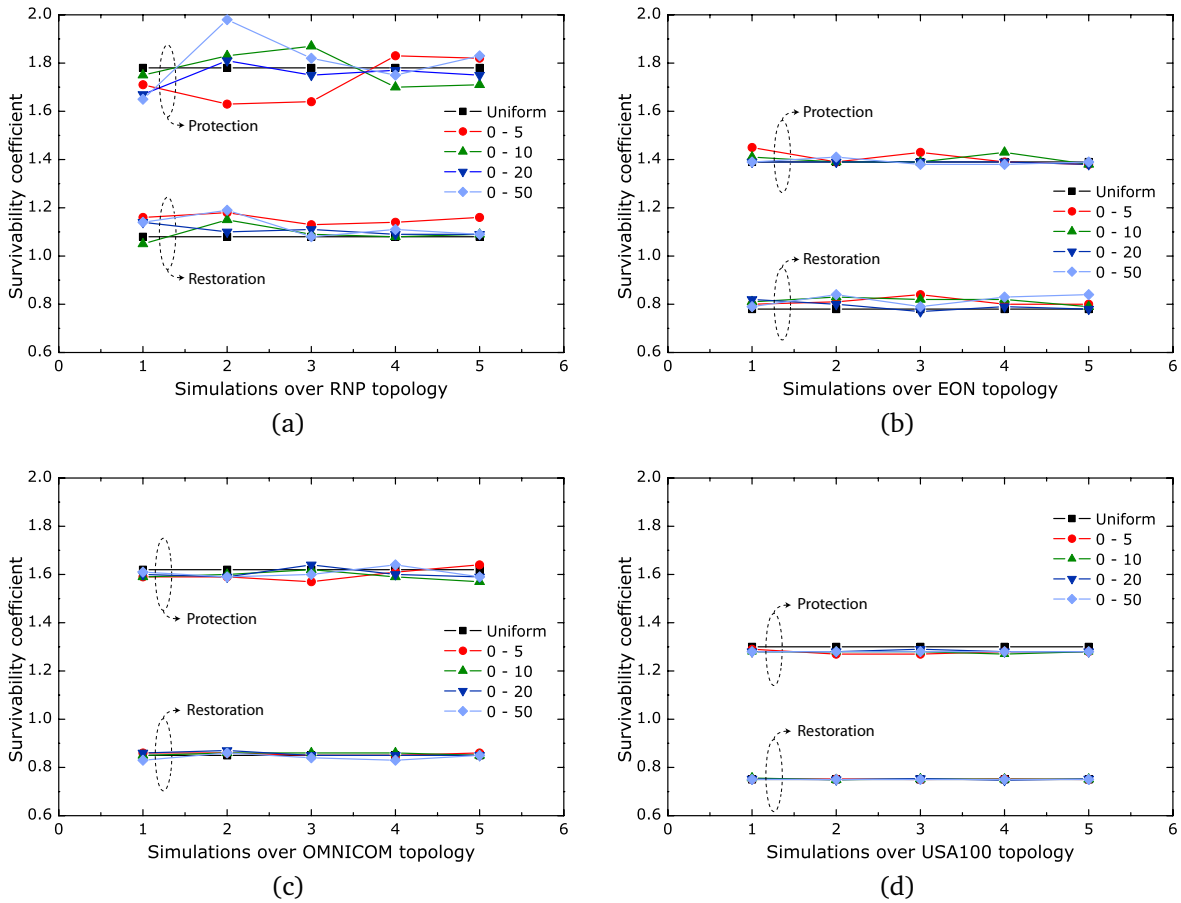

Figure 5.9: Protection and restoration coefficients of real-world topologies, under different traffic loads. Simulations with (a) RNP, (b) EON, (c) OMNICOM and (d) USA100 networks. We performed a simulation for each of five matrices considered, as indicated in the x-axis.

5.5 Estimating CAPEX in Optical Networks

In this section we study the impact of approximations in the model for calculating CAPEX in optical networks. We firstly calculate CAPEX for the EON topology, using the software OPNET SP Guru Transport Planner [13]. The EON network has 19 nodes (N=19) and 37 links (L=37). The results from OPNET are in agreement with the model presented in Chapter 3. Next, using the same network, we also consider that the topological information and traffic matrix are not available, and calculate CAPEX using approximations. Then, the results obtained from both methodologies were compared in order to evaluate the performance of the model using approximations.

In the absence of topological and traffic matrix information, we have to estimate the following variables:

1. average link length, $\langle \nu \rangle$;
2. average number of hops for working paths, $\langle h \rangle$;
3. average number of hops for backup paths, $\langle h' \rangle$;
4. protection coefficient, $\langle k_p \rangle$;
5. restoration coefficient, $\langle k_r \rangle$;
6. average number of transmission systems, $\langle n^S \rangle$;
7. average number of optical amplifiers, $\langle n^A \rangle$;
8. average quantity of fiber, $\langle n^F \rangle$;
9. average number of regenerators, $\langle n^R \rangle$.

However, with estimations for the items 1, 2, 3, and 5 we can approximate the remaining items. This is presented from now on.

The average link length, $\langle \nu \rangle$, can be approximated by using the geographic area, A, where the network is supposed to be built on [8]. It can be written as

$$\langle \nu \rangle \approx \frac{\sqrt{A}}{\sqrt{N} - 1}. \tag{5.17}$$

Approximations for items 2, 3, 4, and 5 were discussed in sections 5.2 and 5.3. Regarding the average number of transmission systems, since we do not have information of the amount of channels in each specific link, we can estimate its value by using the average number of channels per link, $\langle w \rangle$. Thus, we can write

$$\langle n^S \rangle \approx \left\lceil \frac{\langle w \rangle}{S} \right\rceil. \tag{5.18}$$

Similarly, considering survivability we can write

$$\langle n^{S,k} \rangle \approx \left\lceil \frac{\langle w^k \rangle}{S} \right\rceil. \tag{5.19}$$

Notice that the index "k" should be replaced by "k_p" or "k_r" according to the survivability strategy used in the network. Additionally, since the average number of

channels on links depends on the average number of hops, see equation (3.91) on page 63, we have to consider the approximation for the average number of hops, expression (5.7).

The number of optical amplifiers depends on the estimation for the number of transmission systems and the link length. Therefore, using the expressions (5.17) and (5.18) we can estimate the average number of OAs per link with

$$\langle n^A \rangle \approx \left(\left\lceil \frac{\langle \nu \rangle}{\partial} \right\rceil - 1 \right) \left\lceil \frac{\langle w \rangle}{S} \right\rceil . \tag{5.20}$$

Similarly, and considering survivability we can writte

$$\langle n^{A,k} \rangle \approx \left(\left\lceil \frac{\langle \nu \rangle}{\partial} \right\rceil - 1 \right) \left\lceil \frac{\langle w^k \rangle}{S} \right\rceil . \tag{5.21}$$

The quantity of optical fiber depends on estimations of link length and number of transmission systems. Therefore, it can be approximated by using the approximations (5.17) and (5.18), which can be written as

$$\langle n^F \rangle \approx 2 \frac{\sqrt{A}}{\sqrt{N} - 1} \left\lceil \frac{\langle w \rangle}{S} \right\rceil . \tag{5.22}$$

Similarly, considering survivability we have

$$\langle n^{F,k} \rangle \approx 2 \frac{\sqrt{A}}{\sqrt{N} - 1} \left\lceil \frac{\langle w^k \rangle}{S} \right\rceil . \tag{5.23}$$

The average number of regenerators per OXC depends on estimations for the average number of hops and link length. Using the total number of bidirectional

demands, D (see expression (3.11) on page 45), we can write

$$\begin{aligned}\langle n^R \rangle &\approx D\vartheta \frac{1}{N} \frac{\langle h \rangle \langle \nu \rangle}{\Lambda} \\ &\approx \frac{N\langle d \rangle}{2} \vartheta \frac{1}{N} \frac{\langle h \rangle \langle \nu \rangle}{\Lambda} \\ &\approx \frac{\langle d \rangle \langle h \rangle \langle \nu \rangle \vartheta}{2\Lambda}.\end{aligned} \tag{5.24}$$

where $\langle h \rangle$ is obtained from expression (5.7) and $\langle \nu \rangle$ from expression (5.17). The variable ϑ is the overall percentage of working channels that need regeneration.

Replacing $\langle h \rangle$ by $\langle h' \rangle$ we can estimate the average number of regenerators per OXC, for backup paths. Then we have

$$\langle n^{R'} \rangle \approx \frac{\langle d \rangle \langle h' \rangle \langle \nu \rangle \vartheta'}{2\Lambda}, \tag{5.25}$$

where ϑ' is the overall percentage of backup channels that need regeneration. In this thesis we do not address the problem of estimating ϑ and ϑ', so we assume $\vartheta = \vartheta' = 1$.

And adding expressions (5.24) and (5.25) we can estimate the average number of regenerators per OXC, considering protection. Thus, we can write

$$\langle n^{R,k_p} \rangle \approx \left(\frac{\langle d \rangle \langle h \rangle \langle \nu \rangle \vartheta}{2\Lambda} \right) + \left(\frac{\langle d \rangle \langle h' \rangle \langle \nu \rangle \vartheta'}{2\Lambda} \right), \tag{5.26}$$

In order to estimate the average number of regenerators per OXC, considering restoration, we can use the expression (5.26) and write

$$\langle n^{R,k_r} \rangle \approx \frac{1}{\langle \phi^R \rangle} \left(\left(\frac{\langle d \rangle \langle h \rangle \langle \nu \rangle \vartheta}{2\Lambda} \right) + \left(\frac{\langle d \rangle \langle h' \rangle \langle \nu \rangle \vartheta'}{2\Lambda} \right) \right). \tag{5.27}$$

where $\langle \phi^R \rangle$ is the sharing of regenerators in the network. Sharing of regenerators occurs when $\langle \phi^R \rangle > 1$. For instance, $\langle \phi^R \rangle = 2$ means that each regenerator is shared by two channels. The problem of estimating the value of $\langle \phi^R \rangle$ is not considered in this thesis. Therefore, we have used the $\langle n^{R,k_r} \rangle$ obtained from OPNET in our model.

The remaining variables of the model can be used as they are, but just using the approximations when topological and traffic matrix information is not available.

5.5.1 Experiments and Results

In this section we evaluate the performance of the approximations for calculating CAPEX in optical networks. We conducted experiments using the model presented in Chapter 3 and using the OPNET software tool for numerical processing. The EON topology was set up over a plane of area $A = 11,180,000$ km^2. The network was loaded with a demand matrix in which each source-destination node pair requires a demand of 10 Gpbs, corresponding to $D = 171$. The routing of demands was performed based on the shortest path strategy, calculated in number of hops. We assume that each transport system supports 40 channels, $S = 40$. Optical amplifiers were placed along the transmission systems every 100 km, $\partial = 100\ km$. The maximum transparency length is assumed to be 3000 km, $\Lambda = 3000$. Moreover, the dimensioning was performed considering opaque, translucent and transparent transport modes, and protection and restoration survivability strategies.

Table 5.4 shows the quantities obtained from the OPNET, for each variable. Rows in white background color show variables that are given (or obtained from the topology and traffic matrix). Rows in lighter gray background color shows the variables that can be calculated deterministically, and rows in darker gray background color are the ones that depends on numerical processing and, in the lack of information about the topology and traffic matrix, have to be estimated.

Similarly, Table 5.5 shows the quantities obtained from the model, but considering that the topology and traffic matrix are not available, i.e., using the estimations presented in this Chapter. In order to evaluate the performance of the approximated model, let's consider three scenarios with the EON topology.

1. Opaque network with dedicated path protection;
2. Transparent network with shared path restoration;
3. Translucent network with dedicated path protection.

Table 5.4: Quantities of components for the EON network.

	Without Survivability		With Protection		With Restoration	
	Variable	Value	Variable	Value	Variable	Value
Number of Nodes	N	19	N	19	N	19
Number of Links	L	37	L	37	L	37
Number of bidirectional demands	D	171	D	171	D	171
Capacity of transmission system	S	40	S	40	S	40
Distance between optical amplifiers	∂	100	∂	100	∂	100
Maximum transparency length	Λ	3000	Λ	3000	Λ	3000
Area (km^2)	A	4850000	A	4850000	A	4850000
Average number of demands	$\langle d \rangle$	18.00	$\langle d \rangle$	18.00	$\langle d \rangle$	18.00
Average nodal degree	$\langle \delta \rangle$	3.89	$\langle \delta \rangle$	3.89	$\langle \delta \rangle$	3.89
Average number of hops	$\langle h \rangle$	2.33	$\langle h \rangle$	2.33	$\langle h \rangle$	2.33
Average number of hops for backup		0.00	$\langle h' \rangle$	3.23	$\langle h' \rangle$	3.23
Average number of channels on links	$\langle w \rangle$	10.76	$\langle w^{k_p} \rangle$	25.68	$\langle w^{k_r} \rangle$	19.54
Survivability coefficients			$\langle k_p \rangle$	1.39	$\langle k_r \rangle$	0.82
Average number of transmission system	$\langle n^S \rangle$	1.00	$\langle n^{S,k_p} \rangle$	1.03	$\langle n^{S,k_r} \rangle$	1.00
Average number of OLTs	$\langle n^{OLT} \rangle$	2.00	$\langle n^{OLT,k_p} \rangle$	2.05	$\langle n^{OLT,k_r} \rangle$	2.00
Average number of optical amplifiers	$\langle n^A \rangle$	7.00	$\langle n^{A,k_p} \rangle$	7.08	$\langle n^{A,k_r} \rangle$	7.00
Average quantity of fiber (km)	$\langle n^F \rangle$	753.76	$\langle n^{F,k_p} \rangle$	763.89	$\langle n^{F,k_r} \rangle$	753.76
Average number of EXC trunk ports	$\langle n_{exc}^{TP} \rangle$	18.00	$\langle n_{exc}^{TP} \rangle$	18.00	$\langle n_{exc}^{TP} \rangle$	18.00
Average number of channels on OXC for opaque networks	$\langle n_{op}^{CH} \rangle$	29.95	$\langle n_{op}^{CH,k_p} \rangle$	68.00	$\langle n_{op}^{CH,k_r} \rangle$	47.05
Average number of channels on OXC for transparent networks	$\langle n_{tr}^{CH} \rangle$	29.95	$\langle n_{tr}^{CH,k_p} \rangle$	68.00	$\langle n_{tr}^{CH,k_r} \rangle$	47.05
Average number of regenerators per OXC	$\langle n^R \rangle$	1.21	$\langle n^{R,k_p} \rangle$	4.11	$\langle n^{R,k_r} \rangle$	2.42
Average number of regenerators per OXC, for backup paths			$\langle n^{R'} \rangle$	2.89	$\langle n^{R'} \rangle$	2.89
Average number of channels on OXC for translucent networks	$\langle n_{tl}^{CH} \rangle$	31.16	$\langle n_{tl}^{CH,k_p} \rangle$	72.11	$\langle n_{tl}^{CH,k_r} \rangle$	49.47
Average number of short-reach transponders	$\langle n^{SR} \rangle$	18.00	$\langle n^{SR} \rangle$	18.00	$\langle n^{SR} \rangle$	18.00
Average number of long-reach transponders in opaque networks	$\langle n_{op}^{LR} \rangle$	41.89	$\langle n_{op}^{LR,k_p} \rangle$	100.00	$\langle n_{op}^{LR,k_r} \rangle$	76.11
Average number of long-reach transponders in transparent networks	$\langle n_{tr}^{LR} \rangle$	18.00	$\langle n_{tr}^{LR} \rangle$	18.00	$\langle n_{tr}^{LR} \rangle$	18.00
Average number of long-reach transponders in translucent networks	$\langle n_{tl}^{LR} \rangle$	18.00	$\langle n_{tl}^{LR} \rangle$	18.00	$\langle n_{tl}^{LR} \rangle$	18.00

Table 5.5: Approximated quantities of components for the EON network.

	Without Survivability		With Protection		With Restoration	
	Variable	Value	Variable	Value	Variable	Value
Number of Nodes	N	19	N	19	N	19
Number of Links	L	37	L	37	L	37
Number of bidirectional demands	D	171	D	171	D	171
Capacity of transmission system	S	40	S	40	S	40
Distance between optical amplifiers	∂	100	∂	100	∂	100
Maximum transparency length	Λ	3000	Λ	3000	Λ	3000
Area (km^2)	A	4850000	A	4850000	A	4850000
Average number of demands	$\langle d \rangle$	18.00	$\langle d \rangle$	18.00	$\langle d \rangle$	18.00
Average nodal degree	$\langle \delta \rangle$	3.89	$\langle \delta \rangle$	3.89	$\langle \delta \rangle$	3.89
Average number of hops	$\langle h \rangle$	2.25	$\langle h \rangle$	2.25	$\langle h \rangle$	2.25
Average number of hops for backup			$\langle h' \rangle$	3.1	$\langle h' \rangle$	3.19
Average number of channels on links	$\langle w \rangle$	10.39	$\langle w^{k_p} \rangle$	25.16	$\langle w^{k_r} \rangle$	17.55
Survivability coefficients			$\langle k_p \rangle$	1.42	$\langle k_r \rangle$	0.69
Average length of links	$\langle \nu \rangle$	942.50	$\langle \nu \rangle$	942.50	$\langle \nu \rangle$	942.50
Average number of transmission systems	$\langle n^S \rangle$	1.00	$\langle n^{S,k_p} \rangle$	1.00	$\langle n^{S,k_r} \rangle$	1.00
Average number of OLTs	$\langle n^{OLT} \rangle$	2.00	$\langle n^{OLT,k_p} \rangle$	2.00	$\langle n^{OLT,k_r} \rangle$	2.00
Average number of optical amplifiers	$\langle n^A \rangle$	9.00	$\langle n^{A,k_p} \rangle$	9.00	$\langle n^{A,k_r} \rangle$	9.00
Average quantity of fiber (km)	$\langle n^F \rangle$	942.50	$\langle n^{F,k_p} \rangle$	942.50	$\langle n^{F,k_r} \rangle$	942.50
Average number of EXC trunk ports	$\langle n^{TP}_{exc} \rangle$	18.00	$\langle n^{TP}_{exc} \rangle$	18.00	$\langle n^{TP}_{exc} \rangle$	18.00
Average number of channels on OXC for opaque networks	$\langle n^{CH}_{op} \rangle$	29.24	$\langle n^{CH,k_p}_{op} \rangle$	66.99	$\langle n^{CH,k_r}_{op} \rangle$	43.17
Average number of channels on OXC for transparent networks	$\langle n^{CH}_{tr} \rangle$	29.24	$\langle n^{CH,k_p}_{tr} \rangle$	66.99	$\langle n^{CH,k_r}_{tr} \rangle$	43.17
Average number of regenerators per OXC	$\langle n^R \rangle$	4.42	$\langle n^{R,k_p} \rangle$	10.71	$\langle n^{R,k_r} \rangle$	2.42
Average number of regenerators per OXC, for backup paths			$\langle n^{R'} \rangle$	6.28	$\langle n^{R'} \rangle$	6.28
Average number of channels on OXC for translucent networks	$\langle n^{CH}_{tl} \rangle$	33.67	$\langle n^{CH,k_p}_{tl} \rangle$	77.69	$\langle n^{CH,k_r}_{tl} \rangle$	45.59
Average number of short-reach transponders	$\langle n^{SR} \rangle$	18.00	$\langle n^{SR} \rangle$	18.00	$\langle n^{SR} \rangle$	18.00
Average number of long-reach transponders in opaque networks	$\langle n^{LR}_{op} \rangle$	40.49	$\langle n^{LR,k_p}_{op} \rangle$	97.97	$\langle n^{LR,k_r}_{op} \rangle$	68.34
Average number of long-reach transponders in transparent networks	$\langle n^{LR}_{tr} \rangle$	18.00	$\langle n^{LR}_{tr} \rangle$	18.00	$\langle n^{LR}_{tr} \rangle$	18.00
Average number of long-reach transponders in translucent networks	$\langle n^{LR}_{tl} \rangle$	18.00	$\langle n^{LR}_{tl} \rangle$	18.00	$\langle n^{LR}_{tl} \rangle$	18.00

5.5.1.1 Opaque network with dedicated path protection scenario

Table 5.6 shows CAPEX, obtained from the OPNET, for the EON network configured in opaque transport mode and dedicated path protection. Table 5.7 presents the CAPEX obtained from the approximated model.

Table 5.6: CAPEX for EON in opaque mode and dedicated path protection.

	Variable	Cost	Avg. # components	# total	Equation
Cost of links	$\langle c^{OLT,k_p} \rangle$	8.57	2.05	76	(3.131)
	$\langle c^{A,k_p} \rangle$	13.60	7.08	262	(3.135)
	$\langle c^{F,k_p} \rangle$	0.00	763.89	28264	(3.138)
	$\langle c_l^{k_p} \rangle$	22.16			(3.140)
	$C_L^{k_p}$	819.96			(3.139)
Cost of nodes	$\langle c^{EXC} \rangle$	25.39	18.00	342	(3.46)
	$\langle c_{op}^{OXC,k_p} \rangle$	81.14	68.00	1292	(3.148)
	$\langle c_{op}^{TSP,k_p} \rangle$	112.06	118.00	2242	(3.176)
	$\langle c_n^{k_p} \rangle$	218.59			(3.141)
	$C_N^{k_p}$	4153.21			(3.142)
		$C_T = 4973.17$			(3.12)

Table 5.7: Approximated CAPEX for EON in opaque mode and dedicated path protection.

	Variable	Cost	Avg. # components	# total	Equation
Cost of links	$\langle c^{OLT,k_p} \rangle$	8.34	2.00	74	(3.131)
	$\langle c^{A,k_p} \rangle$	11.52	6.00	222	(3.135)
	$\langle c^{F,k_p} \rangle$	0.00	655.65	24259	(3.138)
	$\langle c_l^{k_p} \rangle$	19.86			(3.140)
	$C_L^{k_p}$	734.82			(3.139)
Cost of nodes	$\langle c^{EXC} \rangle$	25.39	18.00	342	(3.46)
	$\langle c_{op}^{OXC,k_p} \rangle$	80.45	67.00	1273	(3.148)
	$\langle c_{op}^{TSP,k_p} \rangle$	110.03	115.97	2203	(3.176)
	$\langle c_n^{k_p} \rangle$	215.87			(3.141)
	$C_N^{k_p}$	4101.59			(3.142)
		$C_T = 4836.41$			(3.12)

The cost of OLTs from the exact model refers to 76 OLTs in the network, corresponding to 38 transmission systems, and 2.05 OLTs per link. Notice that in this

case one link has to be equipped with two transmission systems. In the approximated model the cost of OLTs refers to 74 OLTs in the network. The difference is because we estimated 37 transmission systems when the exact number was 38.

In terms of optical amplifiers, the cost from the exact model refers to 262 OAs, corresponding to an average of 7.08 per link. In the approximated model the cost refers to 222 OAs, corresponding to an average of 6 per link. The main reason for this result is because the link length was underestimated. Using the exact model we obtain an average of 763.89 km of fiber-pair per link and using the approximated model we obtain an average of 655.65 km. Considering the costs of links, we obtained a relative error percentage of about $\epsilon = 10\%$.

Regarding the cost of nodes, the cost of EXC is the same in both models, as expected, since there are no approximations involved. The cost of OXCs from the exact model includes the cost of processing 1292 channels, corresponding to an average of 68 channels per node. The approximated model includes 1273 channels, corresponding to an average of 67 per node. The difference comes from the approximations for the average number of hops, and protection coefficient.

Concerning the cost of transponders, the cost from exact model refers to a total of 2242 transponders, being 342 short- and 1900 long-reach transponders, corresponding to an average of 118 per node. In this case, the number of short-reach transponders is the same in the approximated model, since no approximation is involved. From the approximated model we obtain 1861 long-reach transponders. This difference comes from the approximations for the average number of hops, and protection coefficient.

Considering the costs of nodes, we obtained a relative error percentage of about $\epsilon = 1.24\%$, and considering the total cost of the network we obtained $\epsilon = 2.75\%$.

Figure 5.10a shows a graphical comparative between the cost of components obtained from the exact and approximated models. From this figure we can see that the cost of transponders is dominant in this network configuration. Figure 5.10b shows a comparative between the number of components between exact and approximated models. Notice that in the latter we plotted the average number of EXC trunk ports, $\langle n_{exc}^{TP} \rangle$, and the average number of channels processed on OXCs, $\langle n^{CH,k_p} \rangle$, instead of the

number of EXCs and OXCs, which is obviously equal to the number of nodes.

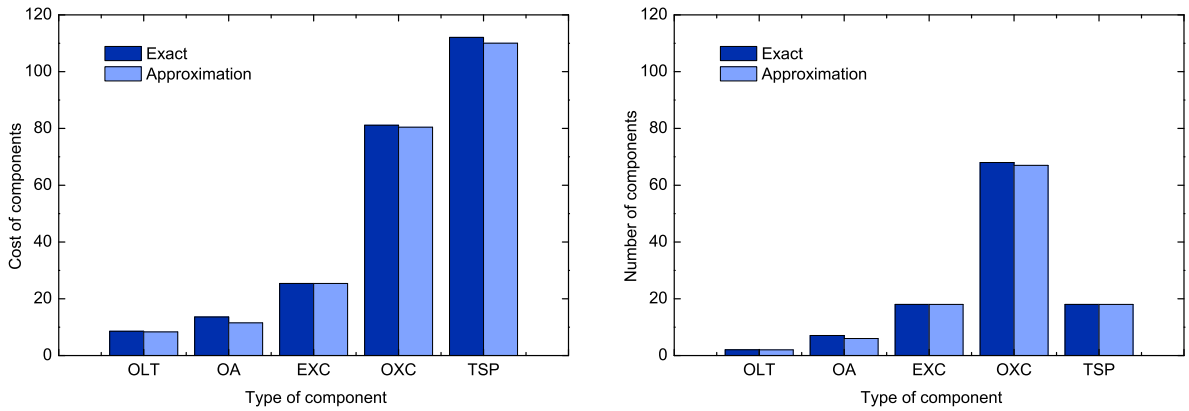

(a) (b)

Figure 5.10: Comparative between exact and approximated models for the EON network with opaque mode and protection. (a) cost of components, and (b) number of components.

5.5.1.2 Translucent network with dedicated path protection scenario

Table 5.8 shows CAPEX for the EON network configured in translucent transport mode and dedicated path protection. Similarly to the previous scenario, the results were obtained using the OPNET software tool. Table 5.9 presents the CAPEX obtained from the approximated model.

Table 5.8: CAPEX for EON in translucent mode and dedicated path protection.

	Variable	Cost	Avg. # components	# total	Equation
Cost of links	$\langle c^{OLT,k_p} \rangle$	8.57	2.05	76	(3.131)
	$\langle c^{A,k_p} \rangle$	13.60	7.08	262	(3.135)
	$\langle c^{F,k_p} \rangle$	0.00	763.89	28264	(3.138)
	$\langle c_l^{k_p} \rangle$	22.16			(3.140)
	$C_L^{k_p}$	819.96			(3.139)
Cost of nodes	$\langle c^{EXC} \rangle$	25.39	18.00	342	(3.46)
	$\langle c_{tl}^{OXC,k_p} \rangle$	83.93	72.11	1370	(3.166)
	$\langle c_{tl}^{TSP} \rangle$	18.00	18.00	342	(3.81)
	$\langle c^{REG,k_p} \rangle$	8.21	4.11	78	(3.178)
	$\langle c_n^{k_p} \rangle$	135.53			(3.141)
	$C_N^{k_p}$	2575.11			(3.142)
		$C_T = 3395.07$			(3.12)

Table 5.9: Approximated CAPEX for EON in translucent mode and dedicated path protection.

	Variable	Cost	Avg. # components	# total	Equation
Cost of links	$\langle c^{OLT,k_p} \rangle$	8.34	2.00	74	(3.131)
	$\langle c^{A,k_p} \rangle$	11.52	6.00	222	(3.135)
	$\langle c^{F,k_p} \rangle$	0.00	655.65	24259	(3.138)
	$\langle c_l^{k_p} \rangle$	19.86			(3.140)
	$C_L^{k_p}$	734.82			(3.139)
Cost of nodes	$\langle c^{EXC} \rangle$	25.39	18.00	342	(3.46)
	$\langle c_{tl}^{OXC,k_p} \rangle$	87.73	77.69	1476	(3.166)
	$\langle c_{tl}^{TSP} \rangle$	18.00	18.00	342	(3.81)
	$\langle c^{REG,k_p} \rangle$	21.41	10.71	203.41	(3.178)
	$\langle c_n^{k_p} \rangle$	152.53			(3.141)
	$C_N^{k_p}$	2898.12			(3.142)
		$C_T = 3632.94$			(3.12)

In this scenario, the cost of OLTs, OAs, and hence the cost of links, for both the exact and approximated models is the same as for the previous scenario.

Regarding the cost of nodes, the cost of EXC is also the same in both models, as expected, since there are no approximations involved. The cost of OXCs from the exact model includes the cost of processing 1370 channels, corresponding to an average of 72.11 channels per OXC. The approximated model includes 1476 channels, corresponding to an average of 77.69 per OXC. The difference comes from the approximations for the average number of hops, average number of regenerators per OXC and protection coefficient.

Since transponders are installed only at the ends of each demand, in translucent networks, there are no approximations involved. Therefore the result is the same for both exact and approximated models. The cost of transponders in this network refers to a total of 342 long-reach transponders, corresponding to an average of 18 per node.

The cost of regenerators in the exact model refers to 78 regenerators, corresponding to an average of 4.11 per node. In the approximated model the cost refers to 204 regenerators, corresponding to an average of 10.71 per node. Besides the expression for estimating the number of regenerators being an approximation, the difference also

comes from approximations for the average number of hops for working and backup paths, link length, and the percentage of demands that need regeneration.

Considering the costs of nodes, we obtained a relative error percentage of about $\epsilon = 12.5\%$, and considering the total cost of the network we obtained $\epsilon = 7\%$.

Figure 5.11a shows a graphical comparative between the cost of components obtained from the exact and approximated models. Figure 5.11b shows a comparative between the number of components between exact and approximated models.

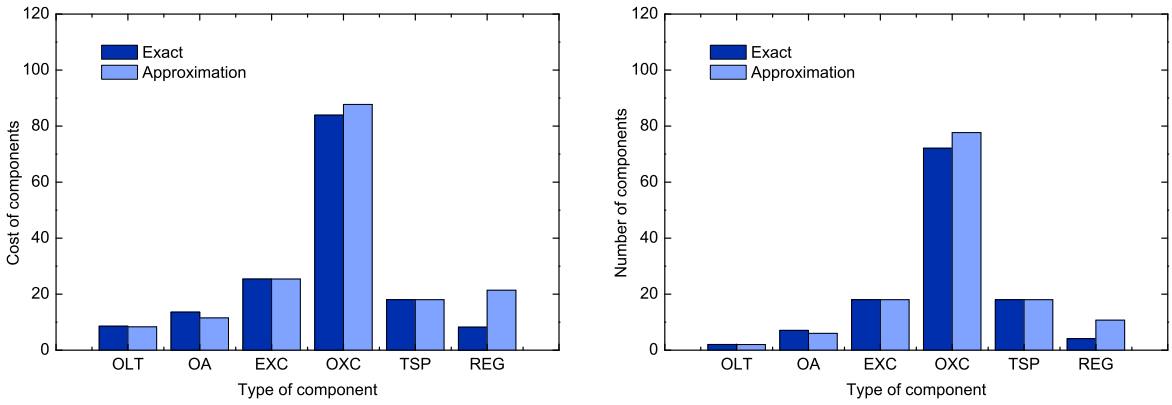

(a) (b)

Figure 5.11: Comparative between exact and approximated models for the EON network with translucent mode and protection. (a) cost of components, and (b) number of components.

The relative error percentage of the nodes may be reduced if we could estimate the percentage of channels that need regenerators, ϑ and ϑ'. In order to verify the impact of these variables, we obtained their exact values from the OPNET. The values are $\vartheta = 0.135$ and $\vartheta' = 0.315$. Using these values in the expression (5.26) the relative error percentage of nodes decreases from 12.5 to 3.5. Although the difference is large, the relative error percentage for the CAPEX of the network decreases from 7 to 5.2.

5.5.1.3 Transparent network with shared path restoration scenario

Table 5.10 shows CAPEX for the EON network configured in transparent transport mode and shared path restoration. Similarly to the previous scenario, the results were obtained using the OPNET software tool. Table 5.11 presents the CAPEX obtained from the approximated model.

Table 5.10: CAPEX for EON in transparent mode with shared path restoration.

	Variable	Cost	Avg. # components	# total	Equation
Cost of links	$\langle c^{OLT,k_r} \rangle$	8.34	2.00	74	(3.131)
	$\langle c^{A,k_r} \rangle$	13.44	7.00	259	(3.135)
	$\langle c^{F,k_r} \rangle$	0.00	753.76	27889	(3.138)
	$\langle c_l^{k_r} \rangle$	21.78			(3.140)
	$C_L^{k_r}$	805.86			(3.139)
Cost of nodes	$\langle c^{EXC} \rangle$	25.39	18.00	342	(3.46)
	$\langle c_{tr}^{OXC,k_r} \rangle$	66.90	47.05	894	(3.154)
	$\langle c_{tr}^{TSP} \rangle$	18.00	18.00	342	(3.77)
	$\langle c_n^{k_r} \rangle$	110.29			(3.141)
	$C_N^{k_r}$	2095.43			(3.142)
		$C_T = 2901.29$			(3.12)

Table 5.11: Approximated CAPEX for EON in transparent mode with shared path restoration.

	Variable	Cost	Avg. # components	# total	Equation
Cost of links	$\langle c^{OLT,k_r} \rangle$	8.34	2.00	74	(3.131)
	$\langle c^{A,k_r} \rangle$	11.52	6.00	222	(3.135)
	$\langle c^{F,k_r} \rangle$	0.00	655.65	24259	(3.138)
	$\langle c_l^{k_r} \rangle$	19.86			(3.140)
	$C_L^{k_r}$	734.82			(3.139)
Cost of nodes	$\langle c^{EXC} \rangle$	25.39	18.00	342	(3.46)
	$\langle c_{tr}^{OXC,k_r} \rangle$	64.26	43.17	820	(3.154)
	$\langle c_{tr}^{TSP} \rangle$	18.00	18.00	342	(3.77)
	$\langle c_n^{k_r} \rangle$	107.65			(3.141)
	$C_N^{k_r}$	2045.29			(3.142)
		$C_T = 2780.11$			(3.12)

In this scenario, the cost of OLTs from both the exact and approximated model refers to 74 OLTs in the network, corresponding to 37 transmission systems, and 2 OLTs per link. In terms of optical amplifiers, the cost from the exact model refers to 259 OAs, corresponding to an average of 7 per link. In the approximated model the cost refers to 222 OAs, corresponding to an average of 6 per link. Considering the costs of links, we obtained a relative error percentage of about $\epsilon = 8.8\%$.

Regarding the cost of nodes, the cost of EXC is the same in both models, as expected,

since there are no approximations involved. The cost of OXCs from the exact model includes the cost of processing 894 channels, corresponding to an average of 47.05 channels per OXC. Notice that the number of channels is expected to be smaller than the previous scenario, since network resources are shared in restoration survivability strategy. The approximated model includes 820 channels, corresponding to an average of 43.17 per OXC. The difference comes from the approximations for the average number of hops, and restoration coefficient.

Since transponders are installed only at the ends of each demand, in transparent network, there are no approximations involved. Therefore the result is the same. The cost of transponders in this network refers to a total of 342 long-reach transponders, corresponding to an average of 18 per node.

Considering the costs of nodes, we obtained a relative error percentage of about $\epsilon = 2.40\%$, and considering the total cost of the network we obtained $\epsilon = 4.18\%$.

Figure 5.12a shows a graphical comparative between the cost of components obtained from the exact and approximated models. Figure 5.12b shows a comparative between the number of components between exact and approximated models.

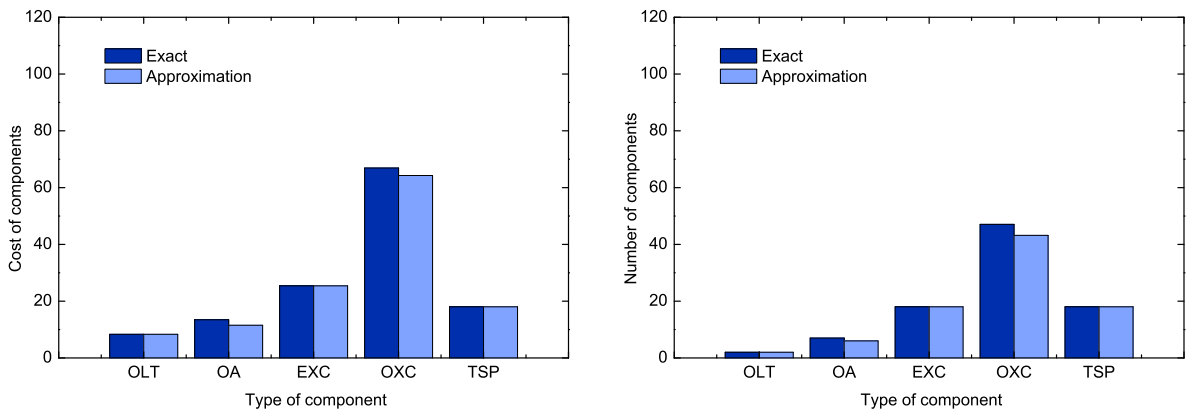

(a) (b)

Figure 5.12: Comparative between exact and approximated models for the EON network with transparent transport mode and restoration. (a) cost of components, and (b) number of components.

5.6 Chapter Summary

In this Chapter we presented expressions required to estimate the survivability coefficients, in the case of absence of topological and traffic matrix information. We proceeded with the evaluation of the impact of traffic randomness on those survivability coefficients, concluding that random traffic does not produce a significant impact, mainly in larger networks. Next we presented the estimation of CAPEX in optical transport networks, and analyzed its performance considering networks with different transport modes and survivability strategies. We have noticed, from extensive analysis with a variety of network topologies and sizes, that the approximated model usually estimates the cost of the networks with less than 10% of error.

References

[1] J. F. Labourdette, E. Bouillet, R. Ramamurthy, and A. A. Akyama, "Fast approximate dimensioning and performance analysis of mesh optical networks," *IEEE/ACM Journal of Transactions on Networking*, vol. 3, no. 4, pp. 906–917, Aug. 2005.

[2] N. Alon, S. Hoory, and N. Linial, "The moore bound for irregular graphs," *Graphs and Combinatorics*, vol. 18, no. 1, pp. 53–57, March 2002.

[3] M. Miller and J. Širáň, "Moore graphs and beyond: A survey of the degree/diameter problem," *Electronic Journal of Combinatorics, Dynamic survey*, vol. 14, pp. 1–61, December 2005.

[4] A. R. Correia, "Planeamento e dimensionamento de redes ópticas com encaminhamento ao nível da camada óptica," Master thesis, Universidade de Aveiro, Aveiro, Portugal, 2008.

[5] SPSS Inc., "SPSS for Windows, Rel. 14.0.1." Chicago, USA, 2008.

[6] R. A. Berk, *Statistical Learning from a Regression Perspective*, ser. Springer Series in Statistics. Springer New York, 2008.

[7] F. Chung and L. Lu, "The average distances in random graphs with given expected degrees," *Internet Mathematics*, vol. 1, pp. 15 879–15 882, 2002.

[8] S. K. Korotky, "Network global expectation model: A statistical formalism for quickly quantifying network needs and costs," *IEEE Journal of Lightwave Technology*, vol. 22, no. 3, pp. 703–722, Mar. 2004.

[9] H. Hassan, J. Garcia, and C. Bockstal, "Modeling internet traffic: Performance limits," in *International Conference on Internet Surveillance and Protection, 2006, (ICISP'06)*, August 2006, pp. 7–13.

[10] C. Pavan, R. Morais, A. Correia, and A. Pinto, "Dimensioning of optical networks with incomplete information," in *Proceedings of the 6th Advanced International Conference on Telecommunications, AICT'08*. Athens, Greece: IEEE, June 2008, pp. 261–264.

[11] W. Ben-Ameur and H. Kerivin, "Routing of uncertain traffic demands," *Optimization and Engineering*, vol. 6, no. 3, pp. 283–313, 2005.

[12] N. Benameur and J. W. Roberts, "Traffic matrix inference in ip networks," *Networks and Spatial Economics*, vol. 4, no. 1, pp. 103–114, 2004.

[13] Opnet Technologies Inc., "OPNET SP Guru Transport Planner," 2009.

Chapter 6

Conclusions and Future Directions

This Chapter summarizes the main conclusions of this work, along with suggestions for future directions.

6.1 Conclusions

We investigated the problem of dimensioning optical transport networks without complete information. The motivation for the work arises from the need to calculate the CAPEX of a network, without requiring extensive numerical processing and even without complete information. This is useful for a preliminary evaluation of the feasibility of a network.

In Chapter 3 we developed expressions to calculate network quantities and costs of optical transport networks. The set of expressions was divided according to the costs related to the links and nodes. Furthermore, we considered opaque, translucent and transparent transport modes. Survivability was considered being implemented as dedicated path protection or shared path restoration at the optical layer. Experiments showed that the results obtained from the developed models are in agreement with results obtained from a commercial numerical simulation tool, for all transport modes and survivability schemes studied in this thesis.

We also presented a case study of a network implemented as a SONET/SDH-over-WDM network. Considering that the cost of components is independent of the transport mode, and assuming the same survivability strategy, the total CAPEX of the network tends to decrease as we configure the network with an opaque, translucent or

transparent mode, respectively. The main reason for this result is the decreasing number of required transponders as the network becomes more transparent. On the other hand, comparing implementations with different survivability strategies, and the same traffic load, we observed that in some cases the CAPEX of a translucent network with shared path restoration may be more cost-effective than a transparent network with dedicated path protection. This occurs due to the higher number of network elements that are required by dedicated protection.

The models presented in Chapter 3 produce exact results, which depend on detailed information about the network and traffic demand. However, some information may be computational intensive to obtain, such as the average number of hops and survivability coefficients. Nonetheless, we found that, in order to estimate the CAPEX of a network with a given number of nodes and links, but without the knowledge on the network topology and traffic matrix, we need to estimate just a few parameters: the total traffic, the average number of hops for working and backup paths, survivability coefficient and average link length. The specific case of translucent networks with shared path restoration also requires the estimation for the sharing of regenerators.

In order to treat the non-deterministic variables and following a statistical approach, we had to obtain a meaningful number of network topologies. Then in Chapter 4 we presented a rigorous analysis of the main characteristics of real-world optical transport networks. We identified that the nodal degree, number of hops, link-disjoint pairwise connectivity, node-disjoint pairwise connectivity, and clustering coefficient are key variables of transport networks. The average value of nodal degree, in real-world networks, is around three, being two the minimum value for survivable networks. In terms of the number of hops, we observed that the average and maximum values tend to increase with the number of nodes of the network. This behavior is expected since larger networks tend to be sparser. Regarding the link-disjoint-pairwise connectivity, we observed that transport networks have a small number of link-disjoint paths between each pair of nodes, usually two or three. In terms of node-disjoint-pairwise connectivity, we observed that not all networks are tolerant to node failures. Some real-world transport networks do not have two node-disjoint paths between every pair of nodes.

Considering the clustering coefficient we observed that the transport networks are far from being full mesh networks. In fact we noticed that, in average, only about twenty percent of nodes forms a full mesh with their neighbor nodes. This result is in agreement with the average nodal degree, which is smaller than its possible maximum.

From that analysis, we proposed and implemented a network topology generator. The topology generator ensures that the generated networks are survivable against single link failures, since each pair of nodes has at least two-disjoint paths connecting them. In fact, comparing networks generated from our topology generator and real-world ones, using non-parametric statistical tests, we observed that all key variables present the same behavior, with similar values.

We also developed a genetic algorithm for finding the least-cost network topology for a given traffic. We found that the genetic algorithm produces better solutions when the initial population is generated using our topology generator, compared with a random topology generator. Moreover, it is possible to obtain accurate results in less processing time, when compared with ILP based approaches.

In Chapter 5 we studied the non-deterministic variables, which we addressed through statistical methods. The main contributions of this Chapter are the proposed expressions to estimate the average number of hops for working and backup paths, protection coefficient and restoration coefficient. These variables were obtained from statistical methods over a meaningful data set of realistic network topologies, generated by the generator presented in Chapter 4. For validation purpose, we compared the results obtained from the proposed expressions and results obtained from a commercial numerical tool. We found that our expressions usually have better performance than previous works. Using these expression in the approximated model, we have noticed, from extensive analysis with a variety of network topologies of different sizes, that the approximated model usually estimates the total CAPEX of the networks with less than 10% of relative error percentage.

We also presented a study about the impact of the demand model on survivability coefficients, i.e., the protection and restoration coefficients, considering that all nodes are central offices. We found that the traffic randomness does not influence significantly

the value of the survivability coefficients, specially for larger networks. This indicates that approximations for spare capacity can be obtained without considering applicable traffic model.

The proposed model can be used to assist network planners in assessing the impact of a variety of variables on CAPEX. We consider that it is possible to use the model to carry out "what-if" design and obtain fast results. Therefore, it may be seen as a decision-support tool in the network dimensioning. Moreover, as the model is quite generic, it may therefore be applied to a wide variety of scenarios.

6.2 Future Directions

We conclude this thesis with some suggestions for future works:

- Our model concerns with CAPEX. However, a network planning that optimizes CAPEX may penalize the OPEX, and vice versa. We propose to develop models to calculate OPEX and then performing the network planning for minimize both CAPEX and OPEX jointly.
- Currently, attention is being devoted towards energy consumption in information and communications technologies. Therefore, the model could also consider opportunities to minimize the energy consumption.
- A distinctive characteristic of optical networks is the presence of physical-layer impairments. This problem affects routing, which have to be done "intelligently" to avoid degradation of the optical signal. Moreover, as we move towards all-optical networks, this problem affects the signal quality with the increase of bit-rates and signal propagation distances. A future work could also develop an impairment-aware model, for routing.
- Another proposal is to extend the model to other types of networks, such as metro and access networks.